THE UNIVERSITY *of* EDINBURGH

Cerebral hypoperfusion in the rat and its consequences

Karim ben Amor Khallout BSc MSc

Doctor of Philosophy

The University of Edinburgh

2013

Table of Contents

Table of Contents…… **i**

Acknowledgements…… **vii**

Dedications…… **viii**

Declaration…… **ix**

List of Figures…… **x**

List of Tables…… **xv**

Abbreviations…… **xvi**

Preface…… **xix**

Abstract…… **xx**

CHAPTER 1: Introduction…… **1**

1.1 White matter…… **2**

1.1.1 Myelin…… **2**

1.1.2 Glial cells…… **4**

1.2 The Blood-Brain Barrier (BBB)…… **9**

1.2.1 History…… **10**

1.2.2 Structure…… **11**

1.2.2.1 Interendothelial cells junction..... **13**

1.2.2.1.1 Tight junctions..... **13**

1.2.2.1.2 Adherens junctions…… **15**

1.2.2.2 Pericytes…… **16**

1.2.2.3 Astrocytes…… 16

1.2.3 Functions and properties of the BBB…… 17

1.2.4 BBB permeability…… 18

1.3 Chronic cerebral hypoperfusion…… 21

1.3.1 The cerebrovascular autoregulation…… 21

1.3.2 The effects of chronic cerebral hypoperfusion on white (versus grey) matter integrity……. 22

1.3.3 Animal model of chronic cerebral hypoperfusion…… 26

1.3.4 The effects of BCCAo on neuropsychological indices …… 32

1.3.5 The effects of BCCAo on neurons and glial cells..... 32

1.3.6 The effects of BCCAo on white matter integrity…… 33

1.4 Objectives and aims of this thesis…….. 34

CHAPTER 2: Materials and Methods…… 36

2.1 Surgery…….. 36

2.1.1 Bilateral common carotid arteries occlusion (BCCAo)…… 36

2.1.1.1 CBF measurements in BCCAo model…… 37

2.1.1.2 Principle determinants of BCCAo outcome…… 41

2.1.1.2.1 Choice of the strain…… 43

2.1.1.2.2 Choice of the anaesthetic agent…… 43

2.1.2 Stereotaxic injection of N-methyl-D-Aspartate (NMDA) in the brain….. 44

2.1.3 Pose of femoral vein catheter……. 45

2.1.4 Perfusion and fixation…… 46

2.2 Histology…… 47

2.2.1 Paraffin processing and sectioning…… **47**

2.2.2 Haematoxylin and eosin staining…… **47**

2.2.3 Counter staining with haematoxylin…… **48**

2.2.4 Quantification of ischaemic damage following BCCAo in the rat… **48**

2.3 Immunohistochemistry…… **51**

2.3.1 General principles…… **51**

2.3.2 Protocol…… **51**

2.3.3 Quantification of axonal damage following BCCAo in the rat…… **53**

2.3.4 Quantification of myelin débris following BCCAo in the rat…… **55**

2.3.5 Quantification of pathological microglial activation following BCCAo in the rat …… **57**

2.3.6 Evaluation of axonal damage, myelin débris, damage to the perikarya and microglial activation…….. **59**

2.4 In vivo magnetic resonance imaging…… **60**

2.4.1 Principle…… **59**

2.4.2 Experimental design…… **64**

2.4.3 MRI scans…… **66**

2.4.4 Image analysis…….. **67**

2.4.5 Measurement of BBB permeability…….. **70**

2.5 Western Blotting…… **70**

2.6 Real-Time PCR…….. **72**

2.6.1 Preparation of PCR primers……. **73**

2.6.2 Reverse Transcription-PCR……. **73**

2.6.3 Real-Time PCR……. **75**

2.7 Statistical analyses……. **76**

2.7.1 Histopathology……. **76**

2.7.2 MRI analyses……. **76**

2.7.3 Western blots and RT-PCR analysis …… **77**

CHAPTER 3: Results…… **78**

3.1 Temporal sequence of pathological events after BCCAo…….. **78**

3.1.1 BCCAo-induced axonal damage……. **78**

3.1.2 BCCAo-induced myelin pathology……. **88**

3.1.3 BCCAo-induced enhancement of microglial activation…… **94**

3.1.4 BCCAo-induced damage to neuronal perikarya…… **103**

3.2 BBB integrity after BCCAo in the rat model using MRI…….. **112**

3.2.1 NMDA positive control for BBB permeability…… **112**

3.2.2 MRI acquisitions after BCCAo in the rat…… **116**

3.2.2.1 MTR measurements…… **117**

3.2.2.1.1 Regional MTR variations after three hours of BCCAo… **117**

3.2.2.1.2 Regional MTR variations after seven days of BCCAo…. **119**

3.2.2.2 MRI-T1 acquisitions related to the integrity of the BBB….. **121**

3.2.2.2.1 MRI-T1 acquisitions at three hours post BCCAo…… **121**

3.2.2.2.2 MRI-T1 acquisitions at seven days post BCCAo …… **121**

3.2.3 Histology and Immunohistochemistry assessment…… **124**

3.2.3.1 Axonal pathology after four hours post surgery…… **124**

3.2.3.2 Axonal pathology after seven days post surgery…… **126**

3.2.3.3 Enhancement of microglial activation after four hours post surgery……..... **128**

3.2.3.4 Enhancement of microglial activation following seven days post surgery..... **129**

3.2.3.5 Neuronal perikaryal damage after four hours post surgery…… **131**

3.2.3.6 Neuronal perikaryal damage after seven days post surgery…… **132**

3.3 Proteins implicated in the pathology of white matter in the rat model of chronic cerebral hypoperfusion…… **135**

3.3.1 Western blot analysis of protein levels following hypoperfusion…… **135**

3.3.1.1 HIF-1α Western blotting …… **135**

3.3.1.2 VEGF Western blotting …… **135**

3.3.1.3 Caspase-3 Western blotting …… **136**

3.3.1.4 MMP-2 Western blotting …… **136**

3.3.2 Gene expression of proteins which may be implicated in white and grey matter injury following hypoperfusion…… **144**

3.3.2.1 Expression of HIF-1α mRNA……. **144**

3.3.2.2 Expression of Caspase-3 mRNA …… **144**

3.3.2.3 Expression of VEGF mRNA …….. **144**

CHAPTER 4: Discussion…… **146**

4.1 Critics and limits of the studies…… **161**

4.2 Future studies…… **164**

4.3 Conclusion…… **167**

CHAPTER 5: References……..…… **168**

Appendix A: Quantification of damage following BCCAo in the rat model of chronic cerebral hypoperfusion in the rat…… **188**

Appendix B: Mean grey values obtained form ImageJ after MRI acquisitions…… **191**

Appendix C: Tables of values of % signal enhancement of Gd-DOTA in BCCAo and sham animal according to the regions……. **198**

Appendix D: T2 and T1 images acquistions with time…… **202**

Appendix E: Full runs of Western Blots…… **204**

Appendix F: Publications…… **210**

Aknowledgements

بسم الله الرحمن الرحيم

(In the name of Allah*, the Entirely Merciful, the Especially Merciful)

I would like to thank my supervisors, Prof James McCulloch and Dr Karen Horsburgh for their continued guidance, advice, expertise and most of all, for their support over the last three and a half years.

I'd like to thank a lot a lot a lot Dr Eric Thomson Mackenzie for all his great support, help and important advices, and great expertise, merci beaucoup Eric!!!!!!

I would like also to thank Dr Paul Kelly, Dr Henry Olverman for their constant support and great mood!! Also special thanks for Dr Linda Ferrington for her great support and help!!

During my Ph.D. I've been extremely happy to work with a great group of people in the McCulloch and Horsburgh labs. There is no one in the group who I couldn't turn to for help, advice or great laugh!! Thanks for Robin Coltman and Emma Bailey for their support and attention. I would like to thank the entire SINAPSE group, including Dr Mark Bastin for their kindness and I would like to thank specially Prof Joanna Wardlaw for her great support and attention during my poster presentation at the International Congress of Vascular Dementia 2011 at Riga (Latvia).

I'd also like to thank the BRR staff for technical support and good mood each time when heavy days of experiments were planned.

I also want to thank all the administration staffs of the University of Edinburgh, with a special thank to Dr Jane Haley, Audrey Kerr and Craig Masson for their kindness.

Dedications

I'd like to thank all my friends and Muslim brothers in Edinburgh for their support and kindness such as Luqman, Sheraz, Shamsu, Shezad, Bilal, Uthman, Tanveer, Asim, Aadil, Arif, Amru…As well as the above I would like to thank all my family: my mother Najet Khallout, my sisters Dr Karima Khallout for her huge support during my PhD, Chedia, Nahala and her husband Morad, my two little sisters Baya and Henneda, my brothers AbdelHamid, Amara and his wife Feten, and their two wee ones Wassim and Farah. I would like to give a special thank to my wife Marwa for her strength and patience being far from her family and also our sons Mohammed Yasin: el bnine el deb esmine, el weld papa wa mama and Anas: Annouss el gazgouzi. I would like also to thank my wife's parents: uncle Tahar, aunt Fathia and my wife's sisters: Ghofrane, Eya, and all my family in Tunisia.

Most of all I would like to dedicate my PhD to my father Amor Khallout (may Allah has mercy upon him) whose strength, seriouness, patience and determination during his lifetime have been a constant source of inspiration to me. My beloved father Amor Khallout (may Allah have mercy upon him) passed away on the 10th June 2011, before my submission, while I hoped he could have been present for that moment after 12 years of study at University, but as Allah The Most High says: "*And no soul perceives what it will earn tomorrow, and no soul perceives in what land it will die. Indeed, Allah is Knowing and Acquainted.*" (Surah 31 verse 34).

*Allah is a proper name belonging only to the one Almighty God, Creator and Sustainer of the heavens and the earth and all that is within them, the Eternal and Absolute, to whom alone all worship is due.

Declaration

I declare that this thesis comprises my own original work and has not been submitted previously for any degree. The work comprising this thesis was carried out by myself, except where acknowledged in the text. All sources of data and information have been specifically referenced.

Karim Khallout

List of Figures

Figure 1.1: Cell types and their relations in grey and white matter ……. **3**

Figure 1.2: Iba-1 staining showing interactions between microglia and neurons… **6**

Figure 1.3: Diagrammatic cross-section of a cerebral capillary to illustrates the components of the blood-brain barrier (BBB)…… **12**

Figure 1.4: BBB and the tight junction…...…… **14**

Figure 1.5: Astrocytes's end-feet covering a large surface of capillaries…… **17**

Figure 1.6: Basement membrane in ageing and in AD…… **25**

Figure 1.7: MRI showing enlarged ventricles and white matter changes with age…….. **25**

Figure 1.8: Models of chronic cerebral hypoperfusion in rodents…… **29**

Figure 1.9: CBF decrease in the mouse after bilateral common carotid artery stenosis.. **30**

Figure 1.10: Regional CBF decrease in the rat after permanent bilateral common carotid artery occlusion … **31**

Figure 2.1: Times of Sampling/(Value % of control) after BCCAo …… **38**

Figure 2.2: H&E staining grading scale…… **50**

Figure 2.3: APP immunostaining grading scale…… **54**

Figure 2.4: MAG immunostaining grading scale…… **56**

Figure 2.5: Iba-1 immunostaining grading scale…… **58**

Figure 2.6: Regions of interests of white and grey matter……..… **59**

Figure 2.7: Magnetic moment and its orientation in absence of magnetic fields… **60**

Figure 2.8: Orientation of the magnetic moment in the presence of magnetic fields… **61**

Figure 2.9: Relaxation times measurements…… **62**

Figure 2.10: The principle of Magnetisation Transfer Imaging…… **63**

Figure 2.11: Experimental design for MRI acquisition…… **65**

Figure 2.12: Coronal MRI images showing the selected ROIs…… **68**

Figure 2.13: First and second assessment of T2, MTR and T1 analyses …… **69**

Figure 3.1: APP immunostaining results after three hours of BCCAo compared to sham……. **82**

Figure 3.2: APP immunostaining results after three days of BCCAo compared to sham…… **83**

Figure 3.3: APP immunostaining results following seven days of BCCAo compared to sham..... **84**

Figure 3.4: APP immunostaining results after 14 days of BCCAo compared to sham... **85**

Figure 3.5: APP immunostaining results after 28 days of BCCAo compared to sham... **86**

Figure 3.6: Extent of axonal damage with time following BCCAo…… **87**

Figure 3.7: MAG immunostaining results following three hours of BCCAo compared to sham……. **90**

Figure 3.8: MAG immunostaining results following three days of BCCAo compared to sham…….. **91**

Figure 3.9: MAG immunostaining results following three days of BCCAo compared to sham.. **91**

Figure 3.10: MAG immunostaining results after 14 days of BCCAo compared to sham…… **92**

Figure 3.11: MAG immunostaining results after 28 days of BCCAo compared to sham…… **92**

Figure 3.12: Extent of myelin debris with time following BCCAo…… **93**

Figure 3.13: Iba-1 immunostaining results following three hours of BCCAo compared to sham…… **97**

Figure 3.14: Iba-1 immunostaining results following three days of BCCAo compared to sham……. **98**

Figure 3.15: Iba-1 immunostaining results following seven days of BCCAo compared to sham…….. **99**

Figure 3.16: Iba-1 immunostaining results after 14 days of BCCAo compared to sham…… **100**

Figure 3.17: Iba-1 immunostaining results after 28 days of BCCAo compared to sham…….. **101**

Figure 3.18: Extent of microglia activation with time following BCCAo…….. **102**

Figure 3.19: H&E staining results following three hours of BCCAo compared to sham..... **105**

Figure 3.20: H&E staining results following three days of BCCAo compared to sham..... **106**

Figure 3.21: H&E staining results following seven days of BCCAo compared to sham..... **107**

Figure 3.22: H&E staining results after 14 days of BCCAo compared to sham..... **108**

Figure 3.23: H&E staining after 28 days of BCCAo compared to sham…. **109**

Figure 3.24: Extent of neuronal perikaryal damage with time following BCCAo… **110**

Figure 3.25: T2-weighted structural images showing the injections of NMDA…… **112**

Figure 3.26: Positive control of BBB permeability…… **115**

Figure 3.27: MTR values BCCAo compared to sham rats following three hours intervention…… **118**

Figure 3.28: MTR values BCCAo compared to sham rats following seven days intervention …… **120**

Figure 3.29: Evolution of the gadolinium-induced increase in signal following three hours intervention…… **122**

Figure 3.30: Evolution of the gadolinium-induced increase in signal following seven days intervention …… **123**

Figure 3.31: Extent of axonal damage with time following four hours of BCCAo compared to sham…… **125**

Figure 3.32: APP immunostaining and extent of axonal damage following seven days of BCCAo compared to sham…… **127**

Figure 3.33: Extent of enhancement of microglial activation four hours following BCCAo compared to sham……..... **128**

Figure 3.34: Iba-1 immunostaining and extent of microglia activation following seven days of BCCAo compared to sham…… **130**

Figure 3.35: Extent of neuronal perikaryal damage four hours following BCCAo compared to sham……..... **131**

Figure 3.36: H&E staining and extent of neuronal perikaryal damage following seven days of BCCAo compared to sham…… **132**

Figure 3.37: HIF-1α Western blot analysis seven days following BCCAo compared to sham…….. **137**

Figure 3.38: VEGF Western blot analysis three hours following BCCAo compared to sham…… **138**

Figure 3.39: VEGF Western blot analysis seven days following BCCAo compared to sham……. **139**

Figure 3.40: Caspase-3 Western blot analysis three hours following BCCAo compared to sham…….. **140**

Figure 3.41: Caspase-3 Western blot analysis seven days following BCCAo compared to sham…….. **141**

Figure 3.42: MMP-2 Western blot analysis three hours following BCCAo compared to sham…….. **142**

Figure 3.43: MMP-2 Western blot analysis seven days following BCCAo compared to sham……. **143**

Figure 3.44: RT-PCR analysis of HIF-1α mRNA, Caspase3 mRNA and VEGF mRNA in selected regions seven days post BCCAo compared to sham…… **145**

Figure 4.1: Proposed pathway for the development of white matter pathology… **160**

Figure 4.2: Iba-1 satining of activated microglia in close contact with vessels… **166**

List of Tables

Table 2.1: CBF measurements in the rat model of BCCAo……...…… **40**

Table 2.2: Strains, anaesthetic agents and rate of mortality in the BCCAo model…. **42**

Table 2.3: Antibodies used in paraffin embedded tissue immunohistochemistry … **53**

Table 2.4: Antibodies used for western blots…… **72**

Table 2.5: Primers used for RT-PCR…… **75**

Table 3.1: Number of rats in which axonal damage was detected in selected regions ..**81**

Table 3.2: Number of rats in which presenting myelin débris was detected in selected regions…….. **89**

Table 3.3: Number of rats in which microglial activation was detected in selected regions…… **96**

Table 3.4: Number of rats in which ischaemic damage was detected in selected regions…… **104**

Table 3.5: Number of rats in which APP accumulation was detected in the selected regions following four hours of BCCAo.....…… **124**

Table 3.6: Number of rats in which APP accumulation was detected in the selected regions following seven days of BCCAo..... **126**

Abbreviations

AD: Alzheimer's disease

ABC: Avidin-biotin complex

APP: Amyloid Precursor Protein

BBB: Blood-Brain Barrier

BCCAo: Bilateral Common Carotid Arteries

BDNF: Brain-derived neurotrophic factor

bFGF: basic Fibroblast Growth Factor

BSA: Bovine Serum Albumin

CBF: Cerebral Blood Flow

$CMRO_2$: Cerebral Metabolic Rate of diOxygen

CNS: Central Nervous System

CPP: Cerebral Perfusion Pressure

CVR: Cerebrovascular Resistance

DAB: diaminobenzidene

DEPC: Diethylpyrocarbonate

dNTP: deoxyribonucleotide triphosphate

GAPDH: glyceraldehyde-3-phosphate dehydrogenase

Gd-DOTA: Gadolinium

GDNF: Glial cell-derived neurotrophic factor

H&E: Hematoxylin and Eosin

HIF-1α: hypoxia inducible factor 1

Iba-1: ionized calcium-binding adaptor molecule 1

ICP: Intracranial Pressure

IR: infrared

JAMs: Junction Adhesion Molecules

LPS: Lipopolysaccharide

MAG: Myelin Associated Glycoprotein

MBP: Myelin Basic Protein

MGH: Massachussets General Hospital

MMPs: Matrix Metalloproteinases

MMP-2: Matrix Metalloproteinase-2

MOG: Myelin Olygodendrocytre Glycoprotein

MRI: Magnetisation Resonance Imaging

MTI: Magnetisation Transfer Imaging

MTR: Magnetisation Transfer Resonance

NGF: Nerve Growth Factor

NMDA: N-methyl-D-Aspartate

OEF: Oxygen Extraction Fraction

PBS: Phosphate Buffered Saline

pCO_2: Partial Pressure of carbon dioxide

PCR: Polymerase Chain Reaction

PFA: paraformaldehyde

PLP: Proteolipid Protein

PO_2: Partial Pressure of Oxygen

PP: Perfusion Pressure

rCBF: Regional Cerebral Blood Flow

RNA: Ribonucleic acid

RNase H: Ribonuclease H

RNaseOUT: Recombinant Ribonuclease Inhibitor

ROI: regions-of-interest

RT-PCRq: Real time quantitative PCR

r-tPA: recombinant tissue plasminogen activator

SD: Sprague-Dawley

SVD: Small Vessel Diseases

TE: Echo Time

TGF-ß: Transforming Growth Factor ß

TNF-α: tumour necrosis factor

TR: Repetition Time

VEGF: vascular endothelial growth factor

ZO: Zonula Occludens

Preface

Chronic cerebral hypoperfusion is a characterized clinical situation which effects various neuropathological features such as small vessel disease. The widespread availability of magnetic resonance imaging has revealed extensive white matter abnormalities in man which are thought to be related to chronic cerebral hypoperfusion.

Bilateral common carotid artery occlusion in the rodent is widely considered to model chronic cerebral hypoperfusion in man. In this thesis, we used bilateral common carotid occlusion in an attempt to answer the following questions.

When are histology and functional imaging abnormalities evident after a long-lasting decrease in cerebral blood flow? What are the structures and cell types the most affected by the insult? What is the temporal sequence of these changes?

The aim of this thesis was, on the basis of our experimental results together with a critical reading of the available literature, to develop a credible and robust hypothesis to link chronic cerebral hypoperfusion to various neuropathological lesions. As with most scientific studies, the working hypothesis that was tested has given rise to even more questions.

Future research directions in this area are outlined in the discussion section to this thesis.

Abstract

Vascular, especially cerebrovascular, dysfunction may be a critical factor in ageing and dementia. Cerebrovascular impairment due to risk factors such as ageing, stroke, smoking, diabetes and cerebral hypoperfusion has a deterious impact on the normal supply of basic nutrients such as oxygen and glucose to the brain; their absence leads inevitably to neuronal death. The cerebral white matter lesions found in most forms of dementia are reportedly the result of chronic cerebral hypoperfusion. However the temporal and spatial evolution of damage remains unclear. Furthermore, any decrease in the integrity of the blood-brain barrier (BBB) has been hypothesised to be a precocious attack on white matter. The "*milieu interieure*" the most protected in the body, namely the extracellular fluid of the brain, is no longer maintained homeostatically. The cumulation of these various pathophysiological processes alters cerebral function and it has been postulated that, in the most extreme instances, the outcome of this cascade of nefarious events leads to dementia. This thesis examines the supposition that chronic cerebral hypoperfusion could be responsible for the time-related development of white and grey matter pathology and investigates the relationships between the disturbances in the integrity of the BBB and white matter pathology.

Three studies addressed these aims. In the first, chronic cerebral hypoperfusion, induced in male Wistar rats by bilateral common carotid artery occlusion (BCCAo), was chosen as the model to study changes in axons, myelin, perikarya as well as microglial activation. The groups of rats that underwent BCCAo were examined at three hours as well as three, seven, 14 and 28 days after the induction of chronic cerebral hypoperfusion. The microscopic examination revealed that, after three hours post BCCAo, damage was

detected only in axons and myelin. In contrast, no visible pathology to the neuronal perikarya or enhancement of activated microglia (compared to the sham group) was observable. Injury in both white and grey matter and enhancement of activated microglia was observed from three days post BCCAo and increased with time post BCCAo. The most severe damage to the white and grey matter and enhancement of microglial activation was detected at seven days post BCCAo. These results would indicate that white matter damage precedes grey matter pathology and the enhancement of activated microglia.

In the second study, the integrity of the BBB at three hours (when only white matter pathology was found according to the results of the first study) and seven days post BCCAo (when more severe damage to the white and grey matter was shown) was assessed by the use of MRI on T1-weighted image acquisitions with gadolinium as a tracer for BBB permeability. White matter integrity was measured by MTR maps from MTI acquisitions in four brain structures (corpus callosum, caudatoputamen, the external and internal capsules). No differences in white matter integrity were detected between the BCCAo and sham group at three hours and seven days. No differences in signal enhancement of gadolinium were detected three hours post BCCAo. However, a significant signal enhancement of gadolinium was detected at seven days post BCCAo in the caudatoputamen and in the external capsule. Furthermore, immunohistochemistry revealed a significant enhancement of activated microglia seven days post BCCAo compared to the sham group. This functional and immunohistochemical finding, when taken together, might indicate that chronic cerebral hypoperfusion is not in itself responsible for BBB permeability. Rather, the damage to the white matter caused by

cerebral hypoperfusion may be responsible for the dysfunction of the BBB over time. Another point of interest was the evidence that the enhancement of activated microglia may play a critical role in the increased permeability of the BBB.

The final study in this thesis aimed to investigate the possible pathway and proteins potentially implicated in white matter damage and BBB permeability. To address this question, protein levels and the expression of genes involved in the apoptotic and non-apoptotic hypoxic pathways were compared to the sham groups (at three hours and seven days after BCCAo), in three brain structures (cortex, corpus callosum and caudatoputamen). The levels of HIF-1α, MMP-2, Caspase-3 and VEGF were unchanged compared to the sham group after BCCAo. However, VEGF mRNA expression was found to be significantly different to the sham group seven days post BCCAo in all the three structures examined. An overexpression of HIF-1α and a significant level of Caspase-3 would indicate the activation of the apoptotic pathway. However, neither of these criteria were met and these negative results suggest that the apoptotic pathway is not implicated in the mechanisms that lead to white matter pathology after cerebral hypoperfusion. Finally, the significant expression of VEGF mRNA, compared to the sham group seven days post BCCAo, may contribute to the time-relate increased permeability of the BBB.

The results presented within this thesis provide a body of evidence to support the hypothesis that chronic cerebral hypoperfusion is - at least – causal to the damage to different components of the white matter which precedes either early ischaemic changes to the perikarya or enhancement of activated microglia following BCCAo. The increased permeability of the BBB, which can be related to the significant over-expression of

VEGF mRNA (compared to the sham group seven days post BCCAo), does not appear to be primarily responsible for white matter pathology, because the MRI investigations indicated that BBB integrity was not affected after three hours of BCCAo. The increased permeability of the BBB, observed seven days post BCCAo with MRI, seems to be the consequence of increased brain damage; thereafter, there is a time-dependent relationship between increasing BBB permeability and increasing brain pathology.

Overall, the studies reported herein, strengthen the initial working hypothesis. The conclusion – and direction for future studies – would be that minimising white matter pathology and protecting components of the BBB represent potential targets to decrease then incidence of neuropsychological function or to obtund the cerebral dysfunction in patients who suffer from chronic cerebral hypoperfusion.

CHAPTER 1: Introduction

The brain, devoid of any meaningful reservoir of nutrients, is entirely dependent on the cerebral circulation, and a failure in perfusion may be implicated in the pathogenesis of many neurological disorders and psychiatric illnesses. Even normal ageing may be related to cerebrovascular disease (Choi et al., 1998) due to structural changes in the major arteries which lead to increasing stiffness and greater sensitivity to changes in systemic arterial pressure (Levy, 2001). These changes, as a function of age, have been observed in vivo by the use of magnetic resonance imaging (MRI); explicitly, MRI has identified ventricular dilatation and white matter hyperintensities as characteristic of ageing when compared to the younger brain (Raz, 2001).

For many years, the importance of the white matter in the brain and its vulnerability to vascular changes has been neglected because of a focus on grey matter pathology. Specifically, the field of neurodegeneration caused by cerebral ischaemia and similar models concentrated on grey matter which might be one of the factors to explain the failure of pharmacotherapy in clinical trials. Importantly, some studies have demonstrated a considerable vulnerability of the white matter to ischaemia (Pantoni et al., 1996), and subsequent studies have shown that this vulnerability increases with age (Baltan et al., 2008; Raz, 2001).

Ischaemia, apoptosis, blood-brain barrier disturbances (Pantoni, 2002) and a long-lasting decrease in cerebral blood flow (CBF), now termed “chronic cerebral hypoperfusion” of the brain (Farkas et al., 2007), have all been hypothesised to be involved in cerebrovascular-related white matter lesions. Of interest, vascular pathology was also

observed in the original case of Alzheimer as "***moderate atherosclerosis*** *in the basal brain arteries of Auguste D*" (Kalaria, 1999) and it is that age-dependent cerebrovascular dysfunction that increases the risk of Alzheimer's disease (AD) (de la Torre, 2010).

1. White matter

The brain tissue is composed of grey and white matter. The grey matter contains the cells bodies (somata) of the neurons while the white matter consists of bundles of myelinated nerve fibres (axons) which convey the electrical signals between neurons. Both the somata and axons are in contact with glial cells (oligodendrocytes, astrocytes and microglia). All those components are in intimate contact with the cerebral blood vessels that supply the brain (Fig.1.1). Damage to any of these elements have functional consequences on the entire unit.

1.1.1 Myelin

The axons are of white appearance due to the myelin sheathing that contains about 80% lipids and 20% proteins. In the central nervous system (CNS), the oligodendrocytes fabricate the myelin as they do for peripheral nerves. Among the proteins present in the myelin sheath, the majority of them are specific for oligodendrocytes (Johnson et al., 1989), for instance: the myelin associated glycoprotein (MAG); the myelin basic protein (MBP); myelin oligodendrocyte glycoprotein (MOG); and the proteolipid protein (PLP).
MAG is a protein of 100 kilo Dalton (kDa). It is a transmembrane glycoprotein localised peri-axonally and is excluded from compact myelin (Quarles et al., 1983).

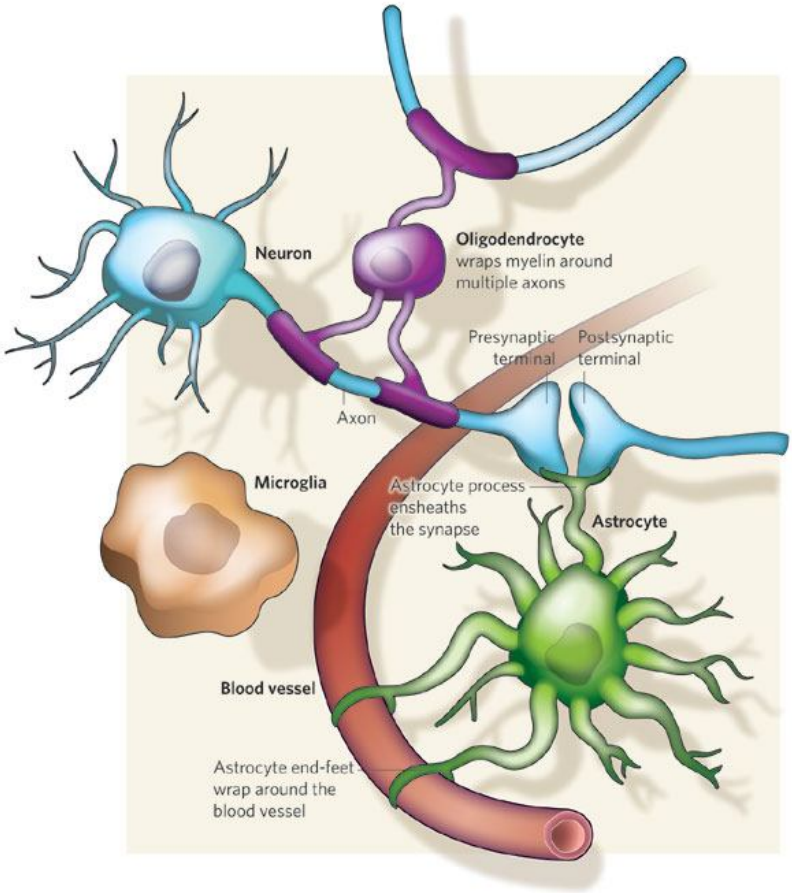

Fig.1.1: Cell types and their relations in grey and white matter (from Allen and Barres, 2009).

MAG is involved in cell-surface recognition and it has been shown that the adhesion of oligodendrocytes to neurons is mediated by MAG (Poltorak, 1987). MAG is also implicated in promoting neuritic outgrowth during embryonic development but it inhibits axonal regeneration in the adult nervous system (Johnson et al., 1989; Mukhopadhyay et al., 1994). Buss and Schwab (2003) have shown that, following damage to nerve fibres, the peri-axonal myelin membrane proteins (e.g. MAG) are degraded more rapidly than those in compact myelin (e.g. MBP and PLP) or those in the outer myelin membrane (e.g. MOG).

Myelination of the axons by the oligodendrocytes benefits the neurons in increasing the conduction velocity of the action potential and in decreasing the energy consumption by restricting ion currents and action potentials to less than 0.5% of the surface of the axon, while unmyelinated fibres need to consume a marked portion of ATP available for the re-establishment of the ion gradient (Nave, 2010).

1.1.2 Glial cells

Glial cells are the majority of cells present in the nervous system. Rudolf Virchow described that cells other than neurons were present in the brain, naming them neuroglia (Virchow, 1846). Ramon y Cajal identified astrocytes among the neuroglia (Ramon y Cajal, 1913) and it was in 1921 that Rio Hortega found two other non-neuronal cells: oligodendrocytes and microglia (Rio Hortega, 1921).

Glial cells are important for the normal function of the brain in general and in particular they are necessary for the correct development of neurons, for the function of mature

neurons by maintaining homeostasis, for producing the myelin and providing protection of, and support to, neurons.

Oligodendrocytes are specialised in producing the myelin responsible for the more efficient propagation of the electrical signal as decribed above (Baumann et al., 2001).

Microglia are the main mechanism for the active immune defense of the CNS, given that systemic antibodies cannot cross the blood-brain barrier (BBB). Microglia are smaller than oligodendrocytes and astrocytes but, after brain injury, they multiply rapidly around the lesion and migrate to the lesions site to initiate the immune response to the insult (Ransohoff and Perry, 2009). Ramified microglia (fig.1.2) react to pathological stimuli but do not have the morphology of macrophages (Kreutzberg, 1996; Stence et al., 2001; Petersen and Dailey, 2004; Davalos et al., 2005) because they fail to express the macrophage marker, CD 68 (Streit and Xue, 2012). Activated microglia express the CD 68 antigen ***only after*** being engaged in phagocytic activity and can therefore be considered as macrophages (Graeber et al., 1998).

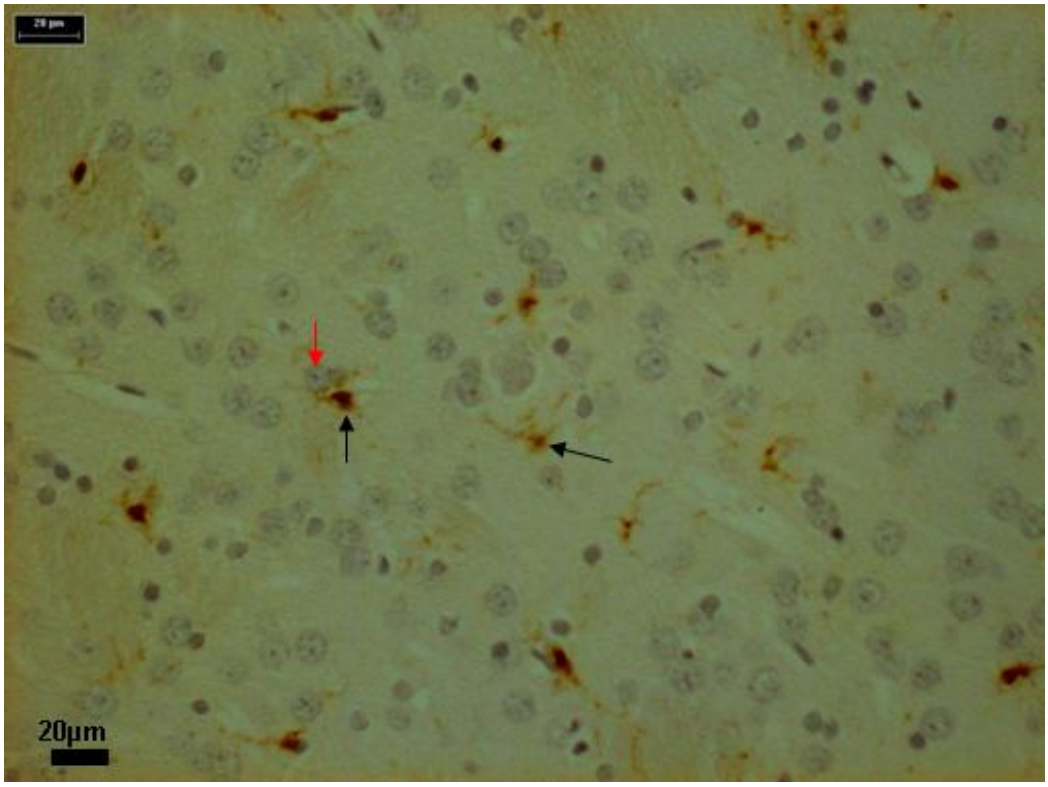

Fig.1.2: Iba-1 staining of microglia (brown) in the caudatoputamen of a rat control (from my own data) shows microglial cells (arrows) extending their processes around neurons, indicative of ongoing interactions between microglia and neurons. Neurons (red arrow) are stained with haematoxylin.

It is believed that, whatever the type of injury, microglia react in a stereotypic manner with a predetermined programme of executive functions. It has been shown that a phenotype (both inflammatory and cytotoxic) is acquired by microglia when activated in vitro by lipopolysaccharides (LPS) (Butovsky et al., 2005). Another interpretation might be that the microglial phenotype depends on the identity of the activating agent. Furthermore, the microglial responses are not inevitably neurotoxic.

Various neuroprotective effects of microglial activation have been demonstrated in an in vivo model of stroke (Lalancette-Hébert et al., 2007) and AD (El Khoury et al., 1998). Among the neuroprotective functions of microglial cells are the production and secretion of neurotrophic factors: BDNF (Brain-Derived Neurotrophic Factor) (Elkabes et al., 1996; Batchelor et al., 1999; Suzuki et al., 2001; Nakajima et al., 2002; Coull et al., 2005); NGF (Nerve Growth Factor) (Mallat et al., 1989; Heese et al., 1997; Frade and Barde, 1998); TGF-ß (Transforming Growth Factor ß) (Kiefer et al., 1993; Lehrmann et al., 1998); bFGF (basic Fibroblast Growth Factor) (Araujo and Cotman, 1992); and GDNF (Glial cell-Derived Neurotrophic Factor) (Brudin, 2002; Batchelor et al., 1999; Suzuki et al., 2001). In AD, it has been shown that microglia increase in size and number in proportion to the size of amyloid plaques (Wegiel et al., 2001; 2003; 2004) and play a role in amyloid clearance from the brain (Lee and Landreth, 2010).

Endogenous toxicity which might result from membrane breakdown products or aggregated proteins (e.g. beta-amyloid) lead to inflammation in the CNS, but if the concomitant microglial activation oversteps the threshold of tolerability, an exaggerated pathology rather than a defensive role might result (Schwartz et al., 2006).

To understand whether the CNS inflammatory response is protective or neurotoxic, it is essential to understand the control of the response (Carlson et al., 1998).

Astrocytes are the most predominant glial cell type in the adult brain and are associated with synapses and cerebral blood vessels (Fig.1.1). They interact with the metabolic activity of neurons (Haydon and Carmignoto, 2006) by regulating the concentrations of ions and recycling neurotransmitters released during synaptic transmission (Verkhratsky and Steinhäuser, 2000). As well as this role, astrocytes are in contact with neurons, oligodendrocytes, microglia and cerebral blood vessels; this multiplicity of anatomical relationships underlies the importance of the presence and homeostatic function of those glial cells, given that processes from a single astrocyte can envelop about 140,000 synapses (Bushong et al., 2002). Another important role of astrocytes is the coupling of CBF to neural activity. Indeed, Takano and collaborators (2006) have shown that electrical stimulation of cortical neural activity induced important Ca^{2+} increases in astrocytic endfeet, resulting in vasodilatation of cerebral blood vessel which, in turn, leads to an increase of CBF.

All those white matter components are interconnected, with an essential communication between all of them that is a function of the basic nutrients needed for normal function and supplied by the blood vessel: glucose and oxygen.

Cerebral blood vessels are highly specific and differ from those in the rest of the body by a unique structure termed: the blood-brain barrier.

1.2 The Blood-Brain Barrier

The brain is protected by many lines of defense. First, and one of the most important: the hepatic system, responsible of the metabolism, combination and detoxification of the large majority of harmful exogenous and endogenous molecules. A second line of defense includes all the interoceptor systems that are essential for maintaining the homeostasis of the internal milieu of the brain. Examples are: the chemoreceptors (for pO_2, pCO_2 and pH) that transduce a chemical signal into an action potential; the baroceptors that maintain a constant arterial pressure to the brain; the central osmoreceptors and thermoreceptors…The third line of defense of the brain is the blood-brain barrier (BBB).

In the brain, as in most organs and tissues, the capillary is that segment of the vasculature in which exchange occurs between blood and the extracellular fluids. The brain is, accordingly, protected from abnormal changes of its ionic composition which occur after exercise or a meal which – without the BBB – could disturb synaptic and axonal communication (Cserr and Bundgaard, 1984).

It is also important to underline the fact that some regions in the brain, the circumventricular organs, do not have a BBB: the area postrema, the median eminence, the neurohypophysis, the pineal gland, the subfornical organ, and the lamina terminalis (Ballabh et al., 2004). Blood vessels in those areas possess fenestrations that allow the diffusion of molecules (e.g. hormones) through their walls. Those brain areas without the BBB regulate certain effects of the autonomic nervous system and endocrine glands of the body (Ballabh et al., 2004).

1.2.1 History

In 1885, the German bacteriologist, Paul Ehrlich, noted that - following intravenous injections of aniline dyes - all of the organs would be stained except the brain. He made then the hypothesis of a difference of affinity of fixation of the dye between the CNS and the rest of the body.

In 1898, Bield and Kraus, as well as Lewandosky in 1900, described direct effects on the brain following intracerebroventricular injection of cholic acid and ferrocyanide, whereas no effects were noted after intravenous injection. Then, they postulated a presence of a vascular barrier, introducing the name of BBB to describe this phenomen.

In 1909, Edwin Goldman reproduced Ehrlich's experiment using trypan blue, demonstrating that only the CNS was stained after an injection below the arachnoid, which demonstrated the presence of a barrier between the cerebral parenchyma and the vascular compartment.

The hypothesis mentioning that the cerebral capillaries are the anatomic basis of the barrier was only confirmed in the late 1960s following the introduction of the scanning electron microscope.

1.2.2 Structure

The BBB is composed of endothelial cells joined by both tight (occludens) and adherens junctions, the capillary basement membrane, astrocyte end-feet ensheating the vessels and pericytes embedded within the basement membrane (Fig.1.3).

Electron microscopy demonstrated that the BBB is an endothelial barrier which is present in the cerebral capillaries and absent in the circumventricular organs.

Indeed, a functional neuropil depends on an intact endothelial BBB, which differs from the peripheral endothelial cells by morphological and functional characteristics:

- Abundance of mitochondria (8-11% of the cytoplasmic volume)
- Presence of tight junctions (most evident close to the luminal surface)
- Sparse pinocytotic intracellular vesicles (under normal conditions)
- Absence of transendothelial channels, absence of fenestrations

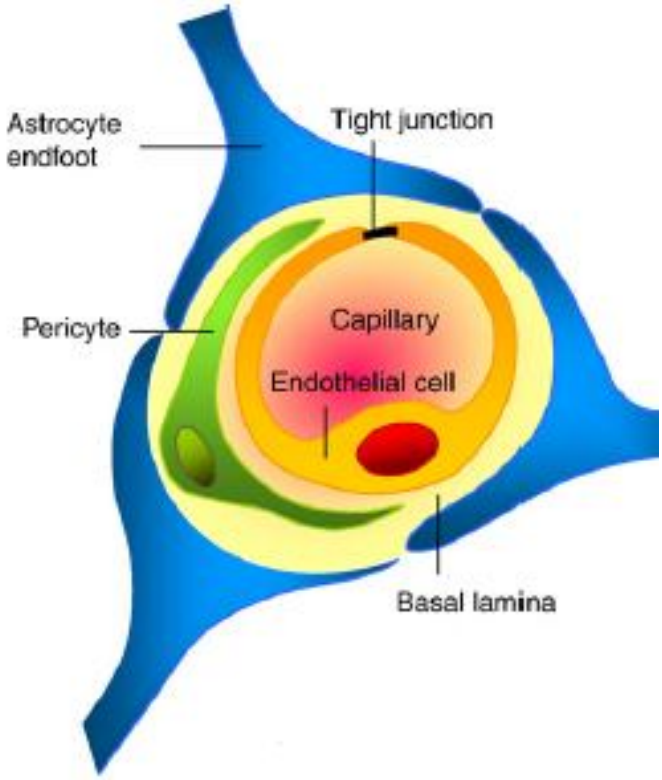

Fig.1.3: A Diagrammatic cross-section of a cerebral capillary to illustrates the components of the blood-brain barrier (BBB), as modified from Abbott and her colleagues (2010)

1.2.2.1 Interendothelial cells junction

1.2.2.1.1 Tight junctions

The tight junctions (zonluae occludentes) establish a selective barrier in the paracellular space between the endothelial cells and so form a structural and functional syncytium throughout the cerebrovascular system. One of the most obvious physiological roles of this syncitium is to limit the passage of both water and ions between blood and the extracellular fluids of the CNS. Tight junctions are, however, higly dynamic entities whose degree of sealing varies as a function of external stimuli as well as being modified according to differing physiological and pathological conditions (González-Mariscal et al., 2008; Deli et al., 2009).

The tight junctions were so named, following electron microscopic studies which incrorrectly supposed that they are static and impenetrable: in reality; they are highly dynamic structures which, for example, allow the migration of leukocytes into the brain, without any disruption of the BBB (Van Itallie et al., 2004). Another role for the tight junctions has been proposed in which they act as dynamic signalling complexes involved in the control of gene expression, cell proliferation and differentiation (González-Mariscal et al., 2008).

Electronic microscopy shows that the tight junctions appear as a series of discrete contacts between the plasma membranes of adjacent cells. By freeze-fracture electronic microscopy, tight junctions appear as proteins closely associated to each other as a series of anastomosing and branching fibrils (Abbott et al., 2006).

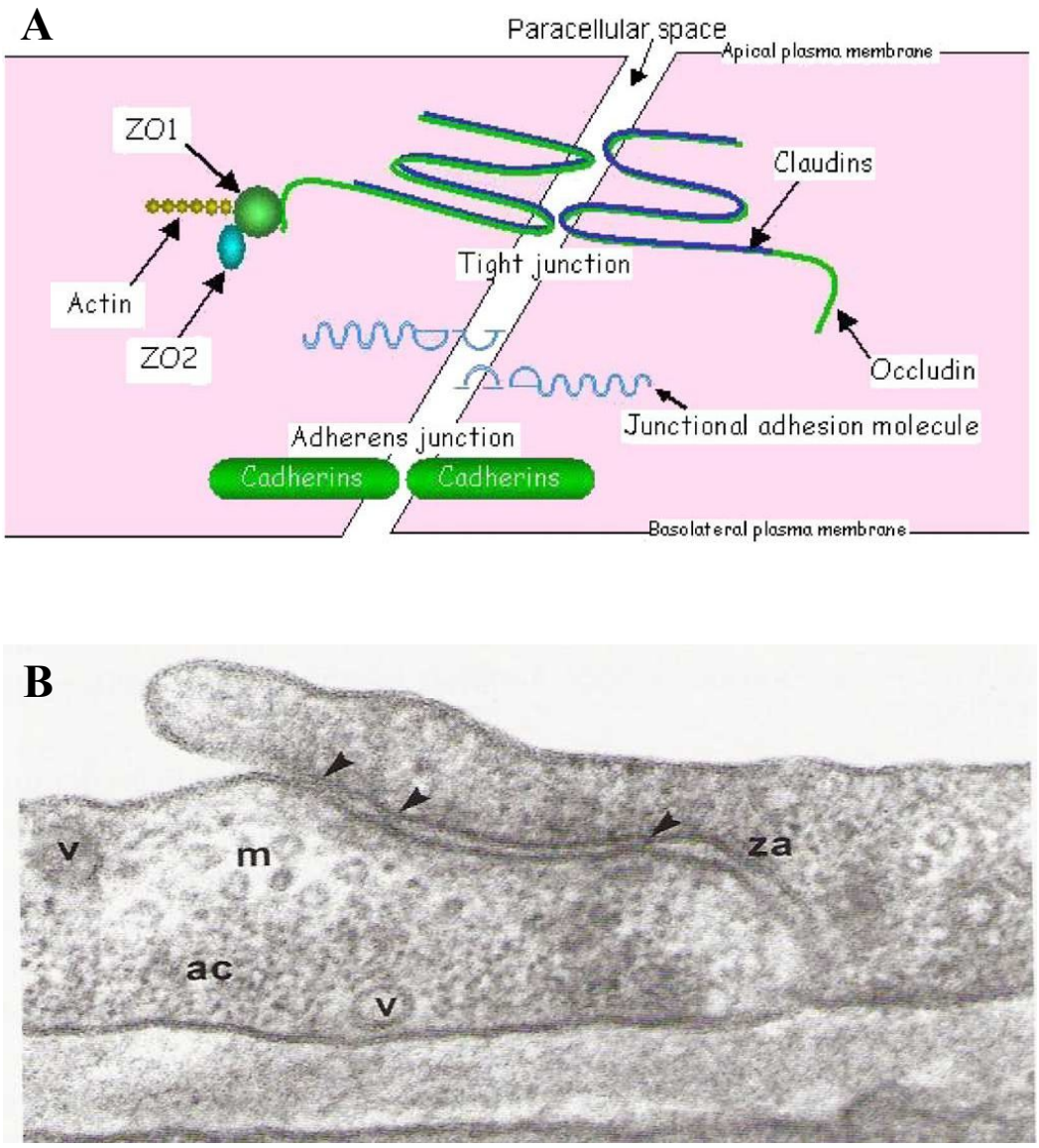

Fig.1.4: BBB and the tight junction. **A:** Schematic illustration of the tight junctions (Ballabh et al., 2004). **B:** Electronic microscopies of the endothelial cells link each other with the tight junctions (arrows) and adherens junctions (za). (m: microtubules; ac: actin filaments; v: plasmalemmal vesicules) (from Nag, 2003).

Three group of protein can be distinguished (fig. 1.4):

- Transmembrane proteins: claudins, occludin and JAMs (junctional adhesion molecules)
- Cytoplasmic accessory proteins: cingulin, zonula occludens 1, 2 and 3 (ZO-1, ZO-2 and ZO-3) (Hawkins et al., 2005)
- Cytoskeleton protein: actin

The transmembrane proteins are connected to the actin cytoskeleton by the tight junction accessory proteins: ZO-1, ZO-2, ZO-3.

The JAMs are involved in the formation and in the maintenance of the structure of the tight junctions (Vorbrodt and Dobrogowska, 2003; Abbott et al., 2006) and are involved in the regulation of the transendothelial migration of leukocytes (Del Maschio et al., 1999).

1.2.2.1.2 Adherens junctions

These junctions include the membrane protein, cadherin that joins the actin cytoskeleton via intermediary proteins, called the catenins, to form adhesive contacts between endothelial cells. Adherens junctions are calcium-dependent and essential for the formation of the tight junctions. A disruption of the adherens junction by the removal of extracellular calcium leads to a disruption of the tight junctions (Hirase et al., 1997), which ineluctably opens the BBB (Wolburg and Lippoldt, 2002).

1.2.2.2 Pericytes

Pericyte processes are present around cerebral capillaries, covering 22 to 32% of the capillaries (Cardoso et al., 2010) which they are invested by a duplication of the basement membrane to which they are directly apposed. Although the exact function of pericytes is unknown, some studies highlight their important role in the brain vasculature. Peppiatt et al. (2006) demonstrated that pericytes play a role in constricting the vessel wall. By stimulating electrically the somata of retinal pericytes, a capillary constriction was noted, consequent to an increase in intracellular [Ca^{2+}]. Moreover, pericytic degeneration in adult and ageing brain leads to a loss of integrity of the BBB prior to the phenomena of neurodegeneration or cerebral inflammation (Bell et al., 2010).

1.2.2.3 Astrocytes

Astrocytic end-feet are structurally the closest element to the endothelial cells of the brain capillaries, with the exception of the pericytes, by covering a large surface of the BBB endothelium and its associated basement membrane (fig.1.5).

A number of cell culture studies have suggested that the ability of CNS endothelial cells to establish a BBB is not specific to these cells; rather, it is the micro-environment to these cells that confers the barrier properties to brain capillaries. Indeed, cultured astrocytes, implanted into areas with normal leaky vessels, induced the formation of endothelial cells endowed with tight junctions (Janzer and Raff, 1987) and this by a modification of the phenotype of these cells (Fédérici et al., 1995; Wolburg et al., 1994).

Astrocytes are also integral to normal neuronal function and the close proximity of neuronal cell bodies to brain capillaries indicates that interactions among all those components are essential for the proper function of each of the components (Persidsky et al., 2006); a disturbance in one of them may induce changes in the functionality of the BBB.

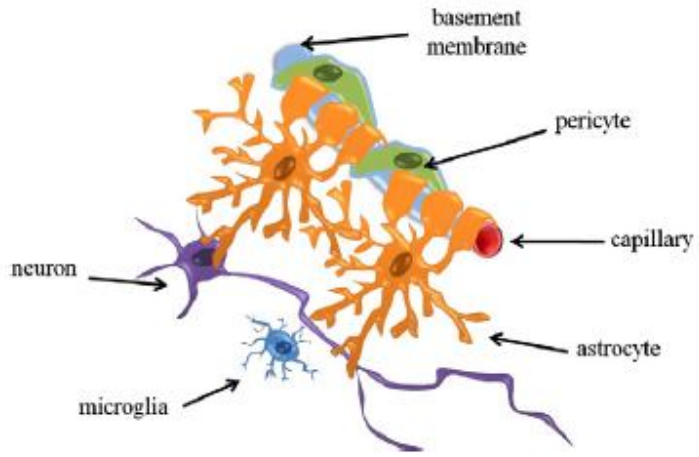

Fig.1.5: Astrocytic end-feet covering a large surface of the capillaries (from Cardoso et al., 2010)

1.2.3 Functions and properties of the BBB

The BBB exhibits specific functions and properties essential for the protection of the brain from peripheral changes.

The BBB is a selective barrier where lipid-soluble and small gaseous molecules such as O_2 and CO_2 can diffuse passively through the BBB. In contrast, the passage of most ions and protons as well as large molecules between the blood and the brain are restricted (Pardridge, 2003; Abbott et al., 2006). However, specific transport systems present on the

membrane surfaces of the endothelial cells allow the entry of essential nutrients including amino-acids and excludes any potentially harmful compounds (Begley and Brightman, 2003).

1.2.4 BBB permeability

Several mechanisms can modify BBB permeability: these adaptations include the separation of the interendothelial tight junctions, an increase of vesicular transport and the formation of transendothelial channels, or the biochemical and structural alterations of the endothelial membrane resulting in an increase in its permeability.

The opening of the tight junctions has not been observed in experimental simulations of conditions that lead to an increased BBB permeability. However, an increase in pinocytotic activity has been observed following intravenous injection of mercury or nickel salts in the rat (Joó, 1971). Godeau and Robert (1979) also observed a significant increase in the number of pinocytotic vesicles after the intravenous injection of collagenase or pronase to rats. Burns and collaborators (1981) noted a significant increase in the density of pinocytotic vesicles after the intravenous injection of clinically used contrast agents.

Those changes (i.e increased pinocytotic activity), occur after various pathological stimuli and are usually transient. Formation of open channels across the capillary endothelium has not been observed (Povlishock and Kontos, 1982; Balin et al., 1987). Other studies have suggested that, following brain damage, there may be a disturbation of the endothelial plasmalemma (Kawai et al., 1989; Maxwell et al., 1988).

Many studies have shown a disruption of the BBB after cerebral ischaemia/reperfusion. However, it is not the decrease of blood flow supply that leads to BBB permeability but, rather, the reperfusion of the brain with an elevated arterial pressure into already dilated cerebral vessels, dilated as the joint result of acidosis and an absence of autoregualtion, both induced ischaemia. The study of Yang and Betz (1994) clearly demonstrates this sequence of events. By comparing one group which was subjected to six hours of permanent middle cerebral artery occlusion (MCAo) to a group with three hours of occlusion followed by three hours of reperfusion, they found no increase of permeability of the BBB to the tracer used in the group of permanent MCAo, while the group which was subjected to 3 hours of reperfusion exhibited a disruption of the BBB.

It has been well established that two independent factors increase the permeability of the BBB (Kuroiwa et al., 1985). The first to increase the permeability of the BBB, the haemodynamic response, occurs just after recirculation in vasodilated vessels, whereas the second increase in BBB permeability is induced by unknown agents released from the damaged tissue, at a time when endothelial cells and tight junctions seems to be well preserved (Westergaard et al. 1976). This scenario explains the fact that, in several diseases that affect the CNS, an increase in permeability of the BBB is seen as a consequence of the pathology. This was the predominate view that prevailed to explain the sequence of events in models such as in cerebral ischaemia (Valable et al., 2005) or in traumatic brain injury (Readnower et al., 2010). A second view emerged seeing the increase of permeability of the BBB as being the cause – and not consequence - of brain damage in white matter diseases such as multiple sclerosis. Indeed, BBB permeability may be one of the initial events leading to the disease (De Keyser et al., 2008).

In ageing, an increase in permeability has been detected and it may be one of the leading causes of cerebral microvascular disease (Farrall and Wardlaw, 2009). Various histological changes in brain vasculature are described such as loss of capillary endothelial cells, a decreased capillary diameter in the rat cortex, a decrease in the number of mitochondria in endothelial cells in the monkey. Alterations in BBB transport have also been observed such as that of choline and a decrease in glucose influx to the brain (Kleine et al., 1993; Tang and Melethil, 1995; Mooradian et al., 1988). Wardlaw and collaborators hypothesized that, after an alteration in endothelial function, BBB disruption may be involved in the pathogenesis of lacunar stroke and the integrity of the BBB decreases with normal ageing (Wardlaw, 2008 and 2010).

As a function of the intensity and duration of hypoperfusion, damage to the brain can be the cause or the consequence of an increase in BBB permeability. To illustrate this point, Kuroiwa et al. (1985) demonstrated that a significant decrease of CBF (below 15ml/100g/min.) caused by transient cerebral ischaemia, and followed by an important hyperaemia lead to a disruption of the BBB, while a moderate decrease of CBF (above 15ml/100g/min.) fails to "open" the BBB.

Marked changes in CBF do not instantaneously lead to an increase in BBB permeability. Some authors (Tomimoto et al., 1996; Ueno et al., 2002) have hypothesized that a chronic decrease in the blood supply to the brain, such as hypoperfusion, may be responsible of the damage to the white matter, through a progressive breakdown of the BBB, and this cascade of events favourises cognitive impairments such as seen in Alzheimer's, leukoaraiosis or vascular dementia.

1.3 Chronic cerebral hypoperfusion

Local brain activity determines cerebral oxygen and glucose consumption as well as blood supply to the region specifically activated. These highly focalized relationships take place in the context of an unchanged global perfusion of the brain: the phenomenom of cerebral autoregulation.

1.3.1 Cerebrovascular autoregulation

The brain is dependent on a continuous supply of blood. CBF is qualified by cerebral perfusion pressure (CPP), which is defined as the difference between mean arterial pressure and intracranial pressure, and cerebrovascular resistance (CVR) (CPP divided by the CBF defines the CVR). The CPP, which, in most situations is identical to mean arterial pressure, is the net pressure driving blood flow to the brain.

Within physiological limits, any changes in CPP feedback negatively to change CVR, maintaining then a relatively constant CBF. If the CPP decreases, the CBF does not fall, because of the automatic compensatory decreases in CVR. Likewise, an increase in CPP does not produce an increase in CBF because of automatic compensatory increases in CVR (Aaslid et al, 1989). Beyond those limits in which this autoregulation of CBF operates: CPP range of 50 to 170mmHg (Harper, 1966; Berne et al., 1981), CBF will fall or rise as a function of CPP.

Furthermore, when the capacity for autoregulatory vasodilatation to maintain blood flow near normal limits is near exhausted, while arterioles continue to dilate, CBF falls with CPP but the oxygen extraction fraction (OEF) increases to maintain normal $CMRO_2$. The

brain enters then in a most severe stage of haemodynamic impairment called "misery perfusion" (Baron et al., 1981), also termed oligaemia or cerebral hypoperfusion.

An abrupt disruption of the blood supply to brain regions leads to stroke and whatever the type of stroke, there is an imbalance between blood supply and metabolism of the CNS, with, as consequence, severe neuronal damage located in the affected territory or territories. While a chronic but moderate decrease in regional CBF is not associated with a necrotic infarction it does affect memory processes (Sopala and Danysz, 2001; Tanaka et al., 1998; De Jong et al., 1999) and can be involved in the development of dementia (Farkas et al., 2007).

Chronic cerebral hypoperfusion has been identified in ageing, AD and other forms of dementias (Buée et al., 1997; Farkas and Luiten, 2001). Finally, it has been hypothesized that chronic cerebral hypoperfusion is the cause of the onset of AD (de la Torre, 2004).

1.3.2 The effects of chronic cerebral hypoperfusion on white (versus grey) matter integrity

The pathogenesis of white matter changes in the brains of subjects with AD has been attributed to chronic cerebral hypoperfusion and it has been shown that white matter is more susceptible to damage with chronic cerebral hypoperfusion than grey matter (Brun and Englund, 1986). However, in AD and other neurodegenerative processes, it has never been demonstrated that those lesions are unique to white matter, as atrophy of both grey and white matter has been observed (De la Monte, 1989). Moreover, this global cerebral hypoperfusion which occurs (Carmeliet et al., 1988) leads to a decrease in flow through the cerebral capillaries and hence will decrease the avaibility of nutrients for the brain,

culminating then in neuropathological features close to those of AD (Cho et al., 2006). The neuropathological changes in such cerebrovascular lesions are characterized by demyelination and axonal loss. During normal ageing, post-mortem studies have shown a breakdown in the structural integrity of myelin sheaths (Bartzokis et al., 2003) similar to the histopathological picture found in patients with AD (Terry et al., 1964). Discrete vascular changes have been noted in normal ageing and AD that include alterations in endothelial function (Levy, 2001) and a thickening of the basement membrane of the vessels (Buée et al., 1997) (fig.1.6). Any changes in vascular diameter lead to direct alterations in CVR and CBF (Farkas and Luiten, 2001). Moreover, in small vessel diseases (SVD), the microvascular degeneration is attributed to be the cause of white matter lesions in elderly people (Takebayashi and Kaneko, 1983). Vascular risk factor such as ageing, hypertension, diabetes, hypercholesterolemia, ischaemic heart diseases and smoking may be causal factors in the development of cerebral hypoperfusion of the brain which may lead to AD and white matter lesions (O'Brien et al., 2003). White matter hyperintensities - the radiological equivalent of demyelination - correspond to lower CBF in MRI (Mastrand et al., 2002) and in positron emission tomography (Turc et al., 1994). Following focal cerebral ischaemia in the rat model, it has been shown that white matter structures were sensitive to a decrease in CBF (Pantoni et al., 1996). Moreover, some studies indicate that this sensitivity increases with age (Baltan et al., 2008). In contrast, Falcao and collaborators (2004) stated *"the resistance to ischemia of white and gray matter after stroke"*, but their data presented, in patients after acute ischaemic stroke, indicated that both white and grey matter showed hypoxic injury on MRI but *"a potentially salvageable tissue in human white matter"* was observed, and this refers to the

penumbra which corresponds to the hypoxic tissue that can be saved through therapeutic treatment in a therapeutic window of 3 hours (The National Institute of Neurological Disorders and Stroke rt-PA Stroke Study Group, 1995). "*Thus, the limited 3 h therapeutic window only benefits 3% to 8.5% of all stroke admissions in individual centers*" (Zhan et al., 2011).

Some studies have lent support to the hypothesis that leukoaraiosis (rarefaction of the white matter detected in MRI (fig.1.7)) may be the result of an altered cerebrovascular autoregulation (Pantoni and Garcia, 1997). Histopathological studies in differing animal models provide evidence of damage to the white matter structures after a long-term decrease in CBF studied over a range of different animal models (Farkas et al., 2007).

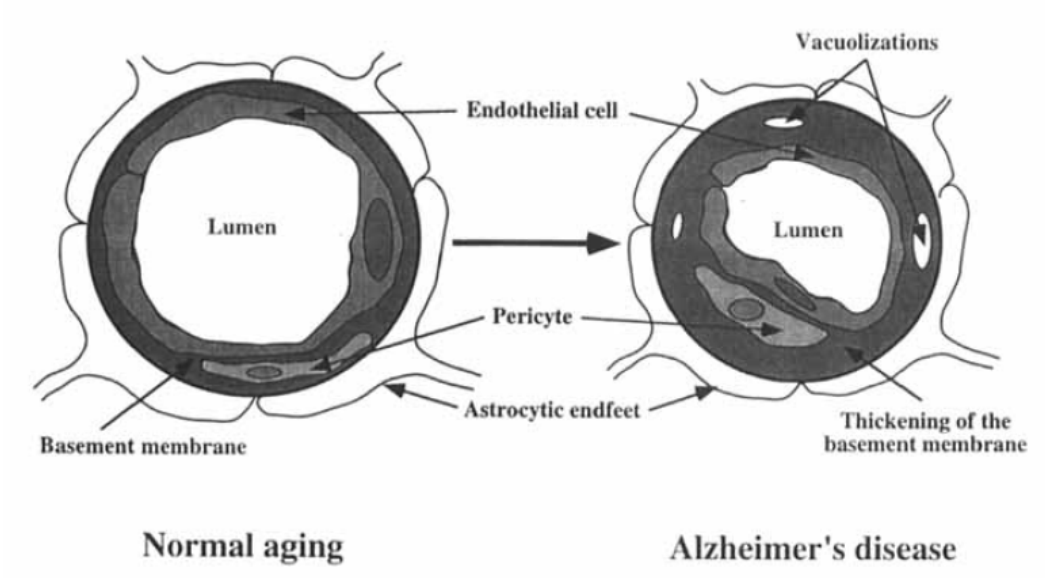

Fig.1.6: A thickening of the basement membrane is observed in ageing. In AD, this thickening is more important with the addition of vacuolisations within the basement membrane (from Buée et al., 1997)

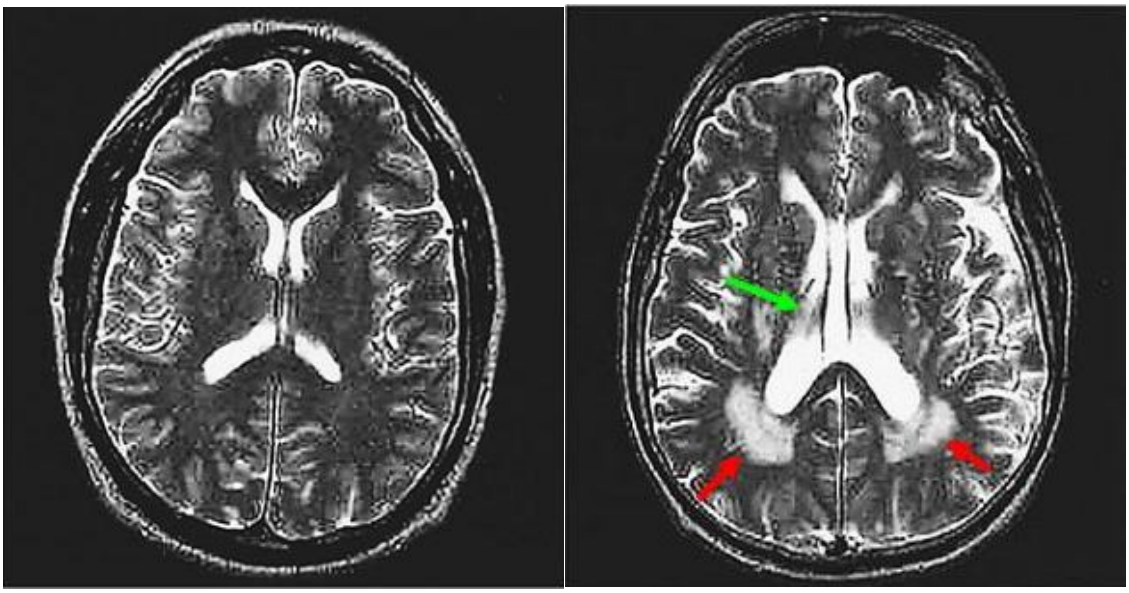

Fig.1.7: MRI showing enlarged ventricles (green arrows) and white matter hyperintensities (red arrows) in a 79-year-old man (right) which correspond to white matter rarefaction. On the left, a 24-year old male (normal). (Modified from Raz, 2001)

1.3.3 Animal models of chronic cerebral hypoperfusion

Various models have been advanced to study the effect of hypoperfusion on the brain. Stroke models have been used to investigate the short-term effects of vascular occlusion. Focal disruption of the blood supply to specific regions leads to an infarction, or pannecrosis, and neurological signs and signs and symptoms appropriate to the territory irrigated. Pannecrosis is the total loss of all cell elements (neurons, glia, vascular cells…) in the zone afflicted by the focal ischaemia. Two models of focal cerebral ischaemia have been proposed: a permanent (Tamura et al., 1981) and a transient (Longa et al., 1989) MCAo. In the commonly used model of transient MCAo, reperfusion is effected which engenders a damage more severe than that seen in the permanent MCAo model. The focal ischaemic lesion can be divided into a necrotic core and a region of penumbrae (Astrup et al., 1981). However, the severity of the ischaemic insult reduces considerably the opportunity to have a reserve of potentially salvageable penumbral tissue for rescue in man (Macrae, 2011). Hence, the interest for a novel model based on a moderate and chronic decrease in CBF.

In apposition to stroke experiments, the chronic cerebral hypoperfusion model aims to investigate an extended period of global CBF hypoperfusion without reperfusion where there is no ischaemic core and penumbral region, and the neuropathological outcome is less severe than that seen in “stroke” models (Farkas et al., 2007). In conclusion, chronic cerebral hypoperfusion, induced by a decrease in diameter of the conducting arteries, provokes clear white matter pathology without the necrotic infarction associated with stroke.

In the elderly, microvascular degeneration (SVD) (as discussed below) seems to provoke white matter lesions (Takebayashi and Kaneko, 1983) and vascular pathology was also observed in the white matter alterations in the original case of Alzheimer as "*moderate atherosclerosis in the basal brain arteries of Auguste D*" (Kalaria, 1999). Ueno and collaborators (2002) detected changes in the microvascular ultrastruture of the rat brain after chronic cerebral hypoperfusion which equally led to BBB damage. These characteristics indicate that, in reality, the induction of **chronic cerebral hypoperfusion modelizes SVD.** Four types of structural changes have been described in small vessel diseases affecting vessels of different size ranges:

- Atherosclerosis affecting distal vessels of diameter: 200-800 μm (Ferrer et al., 2008)
- Lipohyalinosis (also referred as complex SVD) describes fibrinoid deposition in the vessels walls of diameter: 40-300 μm (Fisher, 1972)
- Arteriolosclerosis with hyaline thickening in arterioles of 50-150 μm diameter (Lammie, 2000)
- Microaneurysms that occurs at branching sites in vessels of 100-300 μm diameter (Spangler et al., 1994)

It would appear from our analysis of the literature that the model of bilateral common carotid artery occlusion (BCCAo) replicates a state of atherosclerosis following a chronic decrease of CBF, with the proviso that both common carotid arteries are completely and permanently occluded.

Rodents have been commonly used as models for chronic cerebral hypoperfusion due to their economic and ethical acceptability (Ginsberg and Busto, 1989). Damage that occurs

in those hypoperfusion models is not exclusive to the white matter. In rodents, the white/grey matter ratio is much lower than in human (Hagberg et al., 2002).

In the gerbil model, microcoils have been introduced around both common carotid arteries without totally occluding the vessels. The microcoils are often placed in one carotid while a second is set after a certain time delay, because of the sensitivity of the gerbil to anaesthesia and surgery (Kudo et al., 1990; Hattori et al., 1992). These microcoils decrease the blood supply to the brain by producing a stenosis (fig.1.8a&b). This procedure induces a reduction of the CBF to less than 75% of the baseline levels in the gerbil. Hattori et al. (1992) noted that majority of the gerbils showed unilateral lesions was explained by the fact that the gerbil has an incomplete circle of Willis. One week after common carotid arterial stenosis, neuronal loss, dark neurons and neuronal degeneration were observed in selected grey matter regions.

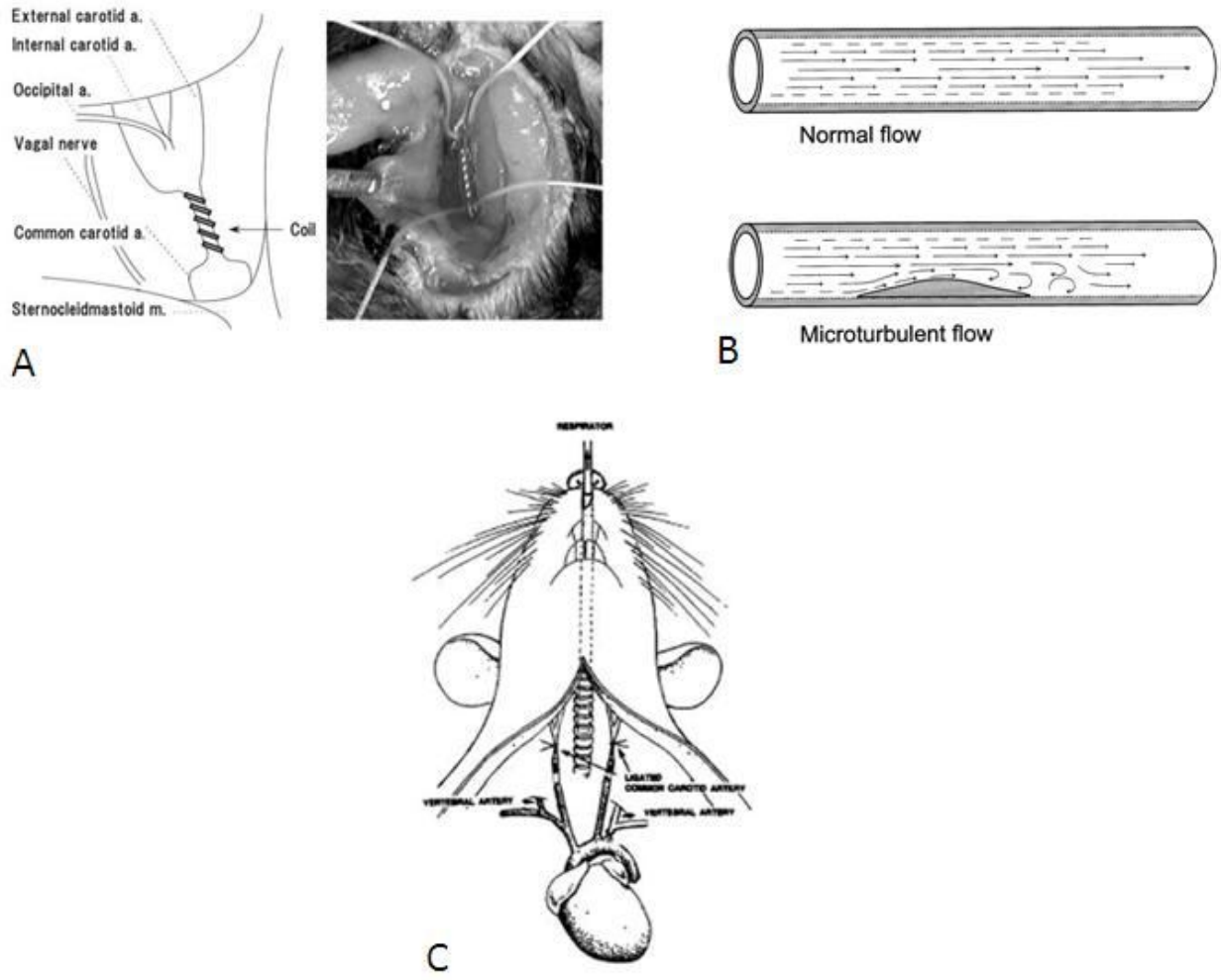

Fig.1.8: Models of chronic cerebral hypoperfusion in rodents. A: microcoil placed on the common carotid artery of the mouse (Shibata et al., 2004) which produces a stenosis of the vessel (Farkas and Luiten, 2001) (B). C: Bilateral common carotid artery occlusion in the rat (adapted from de la Torre et al., 1994)

In the mouse model (see fig.1.8a), the procedure developed recently by Shibata et al. (2004) is identical to that in gerbil and leads, for instance, to a decrease in CBF to 70% of control after 2 hours (with a coil diameter of 0.18mm) and recovery after 30 days to 90% of baseline values (fig.1.9). Shibata and collaborators (2004) found that the damage was specific for white matter, being more intense in the corpus callosum and less severe in the optic tract, when microcoils of 0.18 and 0.20 mm were used; there was a total absence of damage in the grey matter after 30 days of bilateral common carotid artery stenosis.

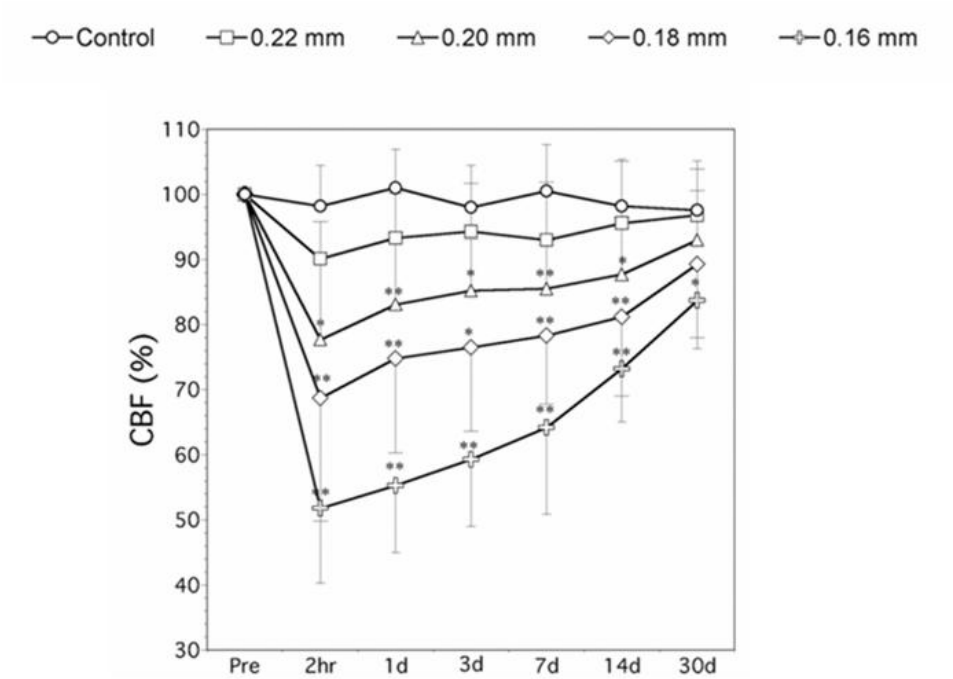

Fig.1.9: CBF decrease in the mouse after bilateral common carotid artery stenosis of varying severity (obtained by the placement of microcoils of graded diameter and as a function of time following the induction of hypoperfusion (Shibata et al. 2004).

A controversial result is that of Shibata et al. (2004) who found that the C57Black/6 strain of mouse exhibits a higher sensitivity to injury after chronic cerebral hypoperfusion or middle cerebral artery occlusion due to a *poorly* developed posterior communicating artery (Fujii et al., 1997; Kim et al., 2009).

In the rat model, the male Wistar rat presents a complete circle of Willis and the occlusion of both common carotid arteries engenders to a situation of cerebral hypoperfusion rather than ischaemia due to the compensatory flow from the vertebrobasilar system.

The male Wistar rat model (fig.1.8c) is commonly used to induce a chronic cerebral hypoperfusion, leading to a decrease of the regional CBF (rCBF) of 33 to 45% of the control level in the white matter and cortical areas after two days of BCCAo (Otori et al., 2003). rCBF begins to recover to 81.3 to 92.5% of baseline values after eight weeks of BCCAo (fig.1.10).

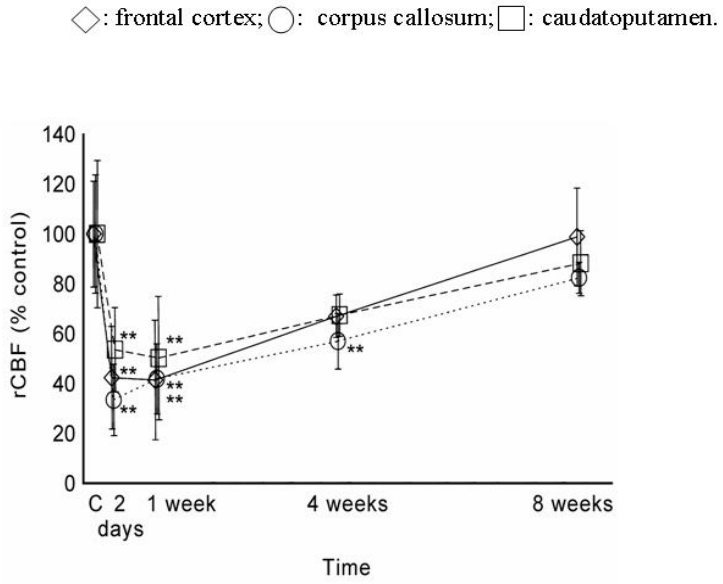

Fig.1.10: Regional CBF decrease in the rat after permanent bilateral common carotid artery occlusion and as a function of time following the induction of hypoperfusion (Otori et al., 2003).

1.3.4 The effects of BCCAo on neuropsychological indices

A number of studies have demonstrated that chronic cerebral hypoperfusion is one of the primary causes that contributes to memory impairment and vascular dementia (Farkas and Luiten, 2001; de la Torre, 1994; de la Torre, 2000). Most of the tests used to measure spatial learning memory after BCCAo in the rat have been based on the Morris water maze and the eight-arm radial maze (Ni et al., 1994; Farkas and Luiten, 2001; Farkas et al., 2004; Liu et al., 2005; Shang et al., 2005). Seven days after BCCAo, spatial memory was already significantly impaired in the BCCAo rats (de la Torre et al., 1997; Pappas et al., 1996) and learning and memory performances were significantly impaired with time compared to the sham-operated rats (Liu et al., 2005; Ni et al., 1994; Pappas et al., 1996). Those results indicate that chronic cerebral hypoperfusion leads to progressive cognitive impairement.

1.3.5 The effects of BCCAo on neurons and glial cells

In BCCAo rats, no damage to the neurons of the CA1 could be detected during the first week of BCCAo as evaluated by Haematoxylin and Eosin (H&E) staining (Ohtaki et al., 2006). However, another group who studied the effects of BCCAo in the rat from one hour to eight weeks post BCCAo found ischaemic neuronal damage two weeks after BCCAo (Schmidt-Kastner, 2001) while Bennett et al. (1998) detected necrotic pyramidial cells two weeks following BCCAo. Thirteen weeks post BCCAo, Sarti et al. (2002) failed to detect any neuronal damage in any grey matter structure examined. This latter study can be explained by the fact that macrophages may have removed any neuronal damage by this time and, hence, a false negative finding. Controversely, Farkas and collaborators

(2004) found total unilateral hippocampal lesions in four of six BCCAo rats, thirteen weeks post BCCAo. It has been proven that necrotic cell death occurrs before eight weeks of BCCAo due to low levels of ATP; by eight weeks post BCCAo, ATP levels returns to the control level (Briede and Duburs, 2007; Plaschke, 2005) which concord with the fact that necrosis is characterised by a lack of energetic substrate (Ueda and Fujita, 2004). Wakita and collaborators (1994) have investigated astrocytic reactions and microglial activation after BCCAo from 1h to 90 days and found that both parameters were significantly different but only after seven days post BCCAo. Others detected overt microglial activation after fourteen days post BCCAo (Farkas et al., 2007). Astriogliosis and microglial activation continue to increase at thirteen weeks post BCCAo (Farkas et al., 2004; 2005)

1.3.6 The effects of BCCAo on white matter integrity

White matter injury has been described in several studies which have identified the optic tract as being the more vulnerable white matter region in the rat brain due to its direct blood supply from the internal carotid artery (Takizawa et al., 2003, Wakita et al., 2002; Farkas et al., 2004, Ohta et al., 1997). Most of the studies have used the Kluver-Barrera staining to detect vacuolisations and rarefaction of the white matter from two days to four months post BCCAo; electron microscopy has shown that myelin sheaths were damaged, with an increase of oligodendrocyte density (Farkas et al., 2004; 2005; Wakita et al., 2002; Otori et al., 2003; Lee et al., 2006; Wakita et al., 2003; Ohta et al., 1997; Wakita et al., 1994; Cho et al., 2006).

Demyelination, axonal damage (Wakita et al., 2002), astrocytic proliferation, microglial activation, apoptic cell death of oligodenrocytes and astrocytes (Lee et al., 2006) and increased percentage of vacuoles in white matter tract (Tazikawa et al., 2003) indicate the pathological hallmarks in the white matter with time after BCCAo similar to those identified in post mortem human white matter lesions (Sheltens et al., 1995; Tomimoto et al., 1997; Kobayashi et al., 2002).

1.4 Objectives and aims of this thesis:

As stated in the introduction, chronic cerebral hypoperfusion could be at the origin of several pathological modifications in the brain and, hence, their dysfunctional and neurological corollaries. The field is vast but we have focused on three specific questions, detailed below.

1. **Characterising the effects of BCCAo on white and grey matter as well as microglial activation at early and later time end-points following BCCAo.**

To understand the possible pathway of pathophysiology after BCCAo, a detailed examination of axons, myelin, microglial activation and neuronal somata was undertaken at time points ranging from 3 hours to 28 days following BCCAo.

Numerous studies have shown the susceptibility of white matter to chronic cerebral hypoperfusion as manifested by: a rarefaction of both axonal and myelin components (Wakita et al., 2002; Kim et al., 2008; Cho et al., 2006; Takizawa et al., 2003); loss of oligodendrocytes (Taupin et al., 1997); gliosis (Wakita et al., 1994; Ritchie et al., 2004); and microglial activation (Farkas et al., 2004). However, none has compared temporal

sequences of each of these pathological processes and their underlying causes. White matter pathology, in the chronic cerebral hypoperfusion model, has become the object of attention but the link between white and grey matter pathology has been little detailed. It still remains unclear whether white matter damage occurs before, with, or after grey matter damage in the rat hypoperfusion model. Secondly the question remains as to whether enhancement of activated microglia matches white and/or grey matter damage with time, again in the same model.

2. **Is an increase of BBB permeability responsible for the pathology of the white matter?**

It was hypothesised that chronic cerebral hypoperfusion is a causal factor with respect to BBB damage. With the knowledge that no unequivocal evidence has been presented for the increased permeability of the BBB after BCCAo; it is therefore important and legitimate to know if the increase of permeability of the BBB is instrumental in the pathology of the white matter.

3. **Which proteins could be implicated in the pathology of the white matter?**

It has been postulated that chronic cerebral hypoperfusion provokes neuronal death and energy failure as a consequence of decreased blood flow and hypoxia. The final question that we have investigated in this thesis: is the degree of hypoxia sufficiently low to activate the pathway(s) of apoptosis and which pathway(s) could explain the differences between the pathological changes in grey and white matter in a model of chronic cerebral hypoperfusion?

CHAPTER 2: Materials and Methods

2.1 Surgery

All animal procedures were carried out under a UK Home Office project and personal licence and adhered to the regulations specified in the Animals (Scientific Procedure) Act (1986).

2.1.1 Bilateral common carotid arteries occlusion (BCCAo)

Adult male Wistar rats (280-320g, Charles River laboratories - UK) were deeply anaesthetized in an induction box with 5% isoflurane in 30% oxygen/70% nitrous oxide, intubated and mechanically ventilated with 2-2.5% isoflurane in 30% oxygen/70% nitrous oxide for the duration of the surgery. Via a small incision in the neck, both common carotid arteries were exposed, separated from the vagi and double ligated with a silk suture (see fig.1.8c) as described previously (Wakita et al., 1994). The control (sham) rats underwent the procedure without occlusion of the common carotid arteries. Rectal temperature was measured via a thermometer probes and controlled during surgery. Then the rats recovered from anaesthesia and food and water were provided *ad libitum* in their own cages and were monitored. At specific time points after the beginning eof chronic cerebral hypoperfusion, animals were perfused transcardially with 0.9% saline and 4% paraformaldehyde (PFA). Rat brains were then removed and processed for paraffin embedding and 6μm sections cut for histology and immunohistochemistry.

2.1.1.1 CBF measurements in the BCCAo model

We did not measure CBF after ligation of both common carotid arteries due to the number of concordant studies which have clearly described the pattern of CBF after the induction of BCCAo in the rat (see table 2.1). Immediately after the BCCAo procedure, the rCBF decreases to 34% of the control in the cortex, 58% of the control in the hippocampus, 70% of the control in the thalamus (Choy et al., 2006) and 48% of the control in the left temporal window (Watanabe et al., 2006). The greatest decrease in rCBF was recorded in the cortical and white matter areas immedialtely after BCCAo until 1 week after BCCAo, thereafter rCBF started to recover, but still significantly lower than the baseline. In the cortex rCBF values were 40 to 63% of the control and in the white matter rCBF was 42 to 72% of the control (Otori et al., 2003; Schmidt-Kastner et al., 2001; Tomimoto et al., 2003; Tsuchiya et al., 1992). After 4 weeks of BCCAo, the rCBF is still significantly lesser than control and from 2 to 6 months after BCCAo, either a slight decrease of rCBF or no change were recorded (Otori et al., 2003; Ohta et al., 1997; Choy et al., 2006).

These data explicitly indicate that a permanent ligation of both common carotid arteries leads to an immediately decrease in CBF which slowly recovers with time after a period of approximately 8 weeks post BCCAo.

The cortical CBF values, from the eleven available studies in the literature, are plotted as a function of time (minutes following BCCAo), the half-maximal recovery is achieved seven days after the intervention. The theoretical maximal decrease in CBF is – 80% from control values and – as stated above – full recovery is obtained 2-6 months after BCCAo. The various values for the CBF decrease immediately after the ligation of the

carotid arteries are somewhat scattered but this variation might be inherent to the time constant of the different methods employed to estimate CBF (fig. 2.1). From 24 hours and later after BCCAo, the numerous studies are highly concordant. Given the richness and coherence of the published cerebrovascular effects of BCCAo, the originality and ethical justification of future investigations could be questioned.

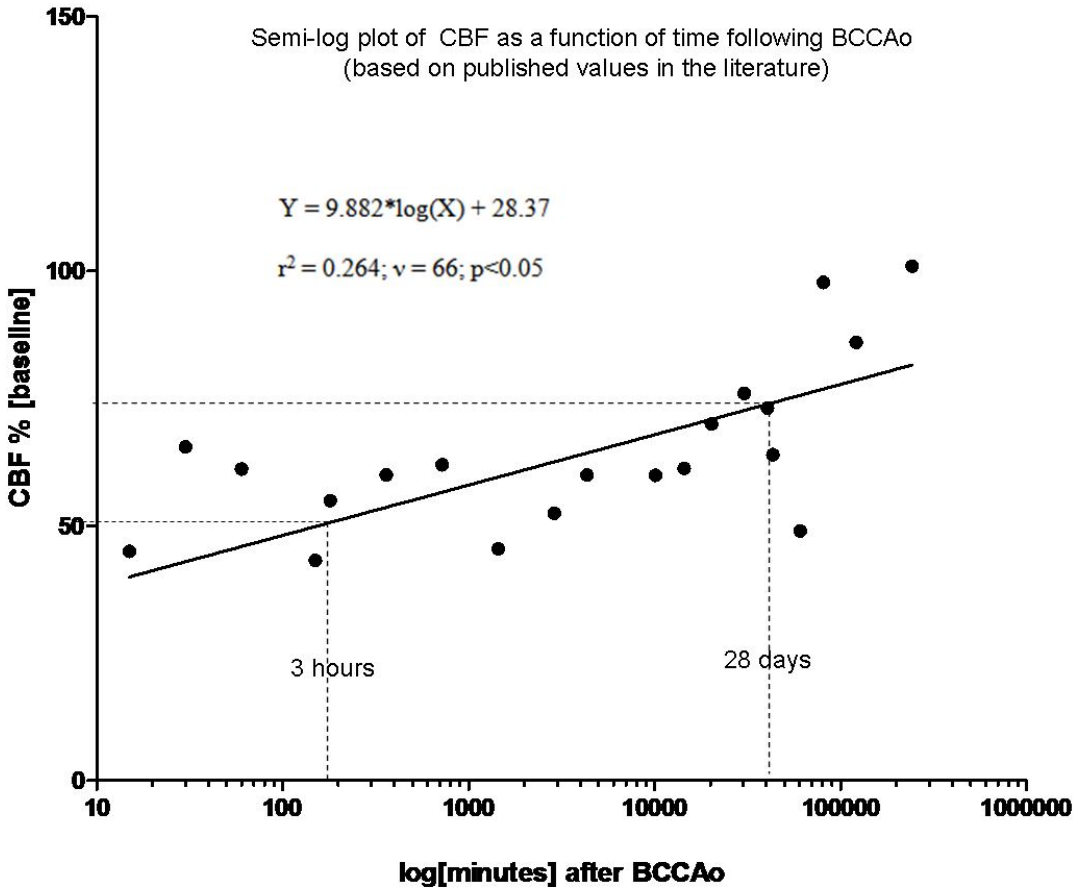

Fig.2.1: CBF (decrease from baseline or control values) as a function of log.time (in minutes) following BCCAo from the studies published in the literature as shown in table 2.1). The present investigations were performed between three and 28 days at which times one would expect a 50% and 25% decrease in CBF, respectively.

Methods	Regions	Times of Sampling/(Value % of control) after BCCAo	References
Continuous arterial spin labelling (CASL) method / spin-echo echoplanar imaging		**Immediately after BCCAo** / **6 Months**	Choy et al. (2006)
	Cortex	34 / 93	
	Hippocampus	58 / 103	
	Thalamus	69 / 107	
[I4C] iodoantipyrine		**60 minutes**	Dietrich et al. (1987)
	Medial cortex	33	
	Lateral cortex	29	
	Hippocampus	27	
	Thalamus	125	
	Caudatoputamen	91	
Laser Doppler Flowmetry	-	**12 hours**: 62	Guang et al. (2006)
Computed Tomography-angiography and measured by Laser speckle blood flow imager	Frontal cortices	**1 hour**: 62 / **3 hours**: 55 / **6 hours**: 60 / **1 day**: 59 / **3 days**: 68 / **14 days**: 76 / **28 days**: 87	Kitamura et al. (2012)
Hydrogen clearance method		**15 minutes**	Nagahori et a. (1994)
	Caudatoputamen	45	
[I4C] iodoantipyrine		**2 days** / **7 days** / **28 days** / **56 days**	Otori et al. (2003)
	Parietal cortex	46 / 45 / 70 / 93	
	Temporal cortex	36 / 40 / 79 / 105	
	Hippocampus	78 / 68 / 66 / 101	
	Thalamus	61 / 58 / 78 / 109	
	Corpus Callosum	33 / 42 / 56 / 81	
Colored microsphere method		**2 days** / **10 days** / **3 months**	Ohta et al. (1997)
	Anterior cortex	54 / 60 / 82	
	Posterior cortex	47 / 58 / 80	
	Hippocampus	65 / 66 / 96	

[I4C] iodoantipyrine		**7 days**	Schmidt-Kastner et al. (2001)
	Parietal cortex	63	
	Temporal cortex	57	
	Hippocampus	75	
	Thalamus	76	
Laser Doppler Flowmetry		**1-3 days** **7 days** **14 days** **30 days**	Tomimoto et al. (2003)
	Corpus callosum	32-34 52 59 64	
Laser Doppler Flowmetry		**30 minutes**	Ulrich et al. (1998)
	Cortex	62-69	
[I4C] iodoantipyrine		**2.5 hours** **7 days**	Tsuchiya et al. (1992)
	Frontal cortex	36 66	
	Parietal cortex	31 63	
	Hippocampus	51 74	
	Medial thalamus	49 80	
	Corpus callosum	49 72	
Hydrogen clearance method		**42 days**	Tanaka et al. (1996)
	Frontal cortex	49	
Laser Doppler Flowmetry		**Immediately after BCCAo** **3 days** **7 days** **14 days** **21 days** **28 days**	Watanabe et al. (2006)
	Left temporal window	48 52 70 75 76 76	

Table 2.1: CBF measurements in the rat model of BCCAo (p.39-40)

2.1.1.2 Principle determinants of BCCAo outcome

The outcome after bilateral common carotid ligation in rodents is dependent upon cerebral vascular anatomy, arterial pressure, age and anaesthetic agents. No coherent view of the relative importance of these factors emerges from a comprehensive review from the literature (see Table 2.2). The response (i.e. mortality and morbidity) to the procedure cannot be predicted from published work because of the disparity of results found in a model of chronic cerebral hypoperfusion as regards the rate of mortality, the severity of damage, the various anaesthetic agents used, the strain of rodent and the type of chronic hypoperfusion used. All these explain why our intervention was to select a model to minimise an important rate of mortality in particular related to the anaesthesia and strain. It should, however, be noted that in the four publications in which Spraque-Dawley rats were used, no usable figures for overall mortality are given.

References and rat strains	Age or weight	Anaesthetic agents	Mortality
de la Torre et al., 1994: male **Sprague Dawley (SD)**	**12 months**	**ketamine 100 mg/kg i.m.**	**olders rats are not recommended because of increased mortality**
Liu et al., 2005: male **Wistar**	**250 to 300 g (8 to 10 weeks)**	**10% chloral hydrate i.p.**	not stated
Miyamoto et al., 2001: **male Wistar**	**250 to 350 g**	**3% halothane**	**25% (2/8) died in group 1, 25% (2/8) died in group 2, 22.2% (2/9) died in group 3, 16.7% (1/6 died) in group 4**
Ni et al., 1994: male **Wistar**	**6-9 months old**	**pentobarbital 40 mg/kg i.p.**	**11.5% (3 of 26) died within 24h** after the BCCAO
Kasparova et al., 2005: male **Wistar**	**250-350 g (3-6 months old and 15-16 months** old were compared.)	**ketamine 50 mg/kg bw and xylazine 4mg/kg bw intraperitoneal**	not stated
Tanaka et al., 1996: male **Wistar**	**9 weeks**	**pentobarbital 50 mg/kg i.p.**	**22.2%**
Ohta et al., 1997: male **Wistar**	**9 weeks**	**pentobarbital 50 mg/kg i.p.**	not stated
Sopala and Danysz, 2001: male **SD**	**350-380 g (10 weeks old)**	**Hypnorm (fentanyl citrate 0.315 mg/ml; fluanisone 10 mg/ml)**	**3 controls and 2 occluded rats had died for unknown reasons within 16-month**
Pappas et al., 1996: male **SD**	**500-600 g (9 to 10 months of age)**	**Ketamine 100 mg/kg i.m. and methoxital sodium 40mg/kg i.p.**	not stated
Tanaka et al., 1998: male **Wistar**	**11 weeks**	**pentobarbital 35 mg/kg i.p.**	**36% (in 25 rats, 9 died)**
Davidson et al., 2000: male **SD**	**510-711 g (10 months old)**	**Ketamine hydrochlore 100 mg/kg i.m. and methohexitol sodium 40mg/kg**	not stated
Liu et al., 2006: male **Wistar**	**320-360 g**	**chloral hydrate 350mg/kg i.p.**	**10% (4/40) rats died after vessel occlusion**
Wakita et al., 1994: male **Wistar**	**150-200 g**	**sodium pentobarbital 25 mg/kg i.p.**	**13.7% (7/51) died 7 days after BCCAO**
de Wilde et al., 2002: male **Wistar**	**4 months**	**isoflurane**	**a week after surgery 21.7% of mortality**

Table 2.2: Strains, anaesthetic agents and rate of mortality in the model of BCCAo in the rat

2.1.1.2.1 Choice of strain

The Wistar rats present a complete circle of Willis which is important for the blood supply to the brain in a model of arterial occlusion. An incomplete circle of Willis may induce more pronounced ischaemic brain damage which may not "reproduce" the pattern of pathology observed in cerebrovascular diseases in patients who normally present a complete circle of Willis. The male Wistar rat is the strain most commonly used as the model of BCCAo; given the volume of ancillary data available in the Wistar rat publications, the strain was our obvious choice (table 2.2).

2.1.1.2.2 Choice of the anaesthetic agent

Wakita et al. (1994) used pentobarbital (an injectable barbituric) in their model of BCCAo (see table 2.2), however, this particular barbiturate leads to a significant respiratory depression and the duration of anaesthesia is extremely variable: from 10 minutes to several hours in the mouse and 1 to 2 hours in rats.

The combination of the injectable agents ketamine and xylazine induces anaesthesia; however, excessive doses of xylazine can provokes hypotension.

Isoflurane anaesthesia is easier to control in a stable manner. A further advantage of isoflurane is that it induces anaesthesia rapidly (within minutes) and recovery is equally and post anaesthesia monitoring is of short duration compared to pentobarbital.

This various elements led to the choice of a halogenated anaesthetic agent (isoflurane) in all the studies undertaken in this thesis.

2.1.2 Stereotaxic injection of N-methyl-D-Aspartate (NMDA) in the brain

Stereotaxic injections were performed to produce positive controls for MRI acquisition. From my master's project (Khallout et al., 2007 unpublished data), I had already observed an increase of BBB permeability to Evan's blue (960.82 Da), 24 hours after the injection of NMDA into the caudatoputamen. This extravasation increased at 48 hours. As it was essential to detect BBB permeability to Gadolinium (938 Da) during the T1-MRI acquisition (and that the MRI parameters were correct), I chose to inject NMDA into the caudoputamen. Two days later, in the male Wistar rat, was scanned as a positive control to observe an increase of BBB permeability to the tracer. Strbian et al. (2008) demonstrated that the pattern of BBB permeability to Gadolinium and Evan's blue in the ischaemic rat brain is similar.

The rats were anaesthetized initially in an induction box containing 5% isoflurane in a nitrous oxide and oxygen mixture (70:30), then transferred to a David Kopf stereotaxic frame (Clark, Electromedical). A face mask was fitted over the snout and isoflurane was reduced to 2-2.5% for the remainder of the surgical procedure. Rectal temperature was monitored and maintained close to 37°C with the aid of heating lamps.

A midline incision was made in the scalp which with the temporatis was retracted to reveal the surface of the skull, bregma and the interaural line. The muscles were retracted to reveal the right and left occipital bones, down to the base of the skull. A 2µl Hamilton syringe attached to the stereotaxic frame was aligned over bregma and then moved to the appropriate coordinates from the bregma. A burr hole was drilled over this area. The dura mater was incised by using a dural hook. Five minutes later, the needle was lowered 0.68 mm ventrally from the surface of the brain. NMDA (Sigma) made in PBS (10mM, pH

7.4) was injected (75 nmoles of NMDA in 1.7µl PBS) into the caudatoputamen, at the rate of 0.1µl per minute. A total volume of 2µl was injected, and then the needle was left in place for a further five minutes. Then a second injection in of PBS (10mM, pH7.4) was done in the second hemisphere (controlateral) in an identical manner. The scalp was then sutured, anaesthesia discontinued and rats were monitored in their own cages with food and water *ad libitum*.

Forty-eight hours later, the rats were re-anaesthetised and a catheter was introduced into the femoral vein for the injection of gadolinium prior to the MRI acquisitions.

2.1.3 Pose of femoral vein catheter

Following each specific time point after the onset of chronic cerebral hypoperfusion, the rats were anaesthetized in an induction box filled with 5% isoflurane in a 30% oxygen / 70% nitrous oxide mixture, 20 minutes prior to the MRI session. When completely anaesthetized, a facemask was apposed and where anaesthesia was maintained with 2.0-2.5% isoflurane. The right femoral vein was exposed and separated from the surrounding connective tissue and femoral artery. A small incision was made in the femoral vein compressed with silk thread to reduce flow. A polythene catheter (external diameter 0.96 mm, internal diameter 0.58 mm diameter; SIMS Portex Ltd; 1 m long) containing heparinised saline was inserted 1 cm into the vein and then secured with 2/0 silk suture. Local anaesthetic (xylocaine) was applied to the incision site which was then sutured. The rat was then introduced into the MRI, under anaesthesia (2% isoflurane in a 30% oxygen / 70% nitrous oxide mixture). The head was fixed to the coil through ears bar. A rectal probe was inserted to allow temperature to be monitored. Animals were maintained

between 36.8 and 37°C during the MRI examination. Ventilation was monitored to assure a constant respiration.

After the T2 sequence, MTI-MRI were acquired, 1 ml of Gadolinium (Gd-DOTA; gadoteric acid; DOTAREM; Guerbet) was administrated into intravenously, after the T1-MRI baseline signal was acquired.

The acquisition and analyses of the various MRI sequences are detailed later in sub-chapter 2.4.

2.1.4 Perfusion and fixation

Animal were deeply anaesthetised in an induction box containing 5% isoflurane in a 30% oxygen / 70% nitrogen mixture, and then transferred to a facemask and isoflurane levels were reduced to 2% until the end of the procedure. An abdominal incision was made to reveal the diaphragm which was excised. The rib cage was reflected to expose the heart. A blunt needle attached to the perfusion system was inserted into the ascending aorta via the right atrium was pierced to allow the drainage of the venous return. Between 200-300ml of heparinised saline (1ml heparin / 500ml saline) was administred until the perfusate ran clear. The rat then received 200-300 ml of 4% PFA until rigor. The head were removed and immersed in the PFA solution for 24 hours. The brain was then removed from the skull, and post-fixed in PFA for a further 24 hours.

2.2 Histology

2.2.1 Paraffin processing and sectioning

After post-fixation for 24 hours, the whole brains were placed in a rat brain matrix and were dissected coronally into slices of 3mm. The brain sections were dehydrated through a series of alcohols, cleared with xylene and then submerged in liquid paraffin at 60°C in an automated tissue processor. The brain sections were then embedded in small containers containing liquid paraffin, left to cool, then removed and mounted. Paraffin sections (6 μm thick) were cut on a microtome (Leica RM 2135) and mounted on poly-L-lysine coated slides. Sections were taken at two locations, 0.20 and -3.30 mm from the bregma, based on the atlas of Paxinos and Watson (Paxinos and Watson, 1998).

2.2.2 Haematoxylin and eosin staining

Paraffin sections were placed in an oven at 60°C for 30 minutes, then in xylene for 15 minutes to remove the wax, then the sections were rehydrated through a series of alcohols, 100% (2X 5mins) > 90% (2mins) > 70% (2mins) and then into tap water for 10 minutes.

Sections were immersed in haematoxylin (Thermo Scientific, Loughborough, UK) for 1 minute, rinsed and placed in acid alcohol solution (1% hydrochloric acid in 70% ethanol) for 8 to 10 seconds to destain to a grey colour, then placed in Scott's tap water (2% $MgSO_4$, 0.35% $NaHCO_3$) for 2 minutes to restablish the blue colour of the nuclei. The sections were placed in running tap water for 2 minutes and immersed in undiluted alcoholic eosin Y solution (Surgipath, Cambridgeshire, UK) for 2 minutes. Sections were then dehydrated through a series of alcohols, 70% (2mins) > 90% (2mins) > 100% (2X

5mins) and xylene (10 minutes) before being mounted with coverslips using DPX (Distrene, Plasticiser, Xylene).

2.2.3 Counter staining with haematoxylin

Paraffin embedded sections immunostained using the Iba-1 antibody were counterstained to enable the identification of anatomical landmarks. Following the DAB (3,3′-diaminobenzidine) visualisation stage, sections were rinsed in water for 10 minutes and then placed in haematoxylin for 30 seconds. After a quick wash in water, the sections were placed in acid alcohol for 8 to 10 seconds, then in Scott's tap water for 2 minutes, rinsed in water, dehydrated through a series of alcohols, cleared in xylene and mounted with coverslips using DPX.

2.2.4 Quantification of ischaemic damage following BCCAo in the rat

All histological analyses were conducted blindly over a two days interval. Sections were scored on both days and then the results compared to reduce the variability (see appendix A). Haematoxylin-and-eosin stained sections were used to assess the extent of ischaemic damage. Ischaemic neurons were defined by an intense, darkly stained pyknotic nucleus surrounded by an eosinophilic cytoplasm (fig. 2.2.B) while healthy neurons have large round nuclei and cell bodies with visible cytoplasmic structures (fig.2.2.A). The severity of damage to the perikarya was evaluated bilaterally in the hippocampus and in the caudatoputamen as: 0 = no ischaemic damage, 1 = little presence of ischaemic damage, 2 = moderate ischaemic damage and 3 = extensive ischaemic damage.

Use of hematoxylin and eosin staining

In well-controlled models of focal cerebral ischaemia, hematoxylin and eosin staining demonstrate early ischaemic damage (pyknosis and hyperchromicity) several hours after ischaemic injury (Armiger et al., 1977; Okuno et al., 2001). Meng and collaborators assessed the histopathology in the white and grey matter by two methods: the H&E staining procedure and TUNEL staining technique. They failed to find any differences in terms of positive results, between the two staining methods used (Meng et al., 2005).

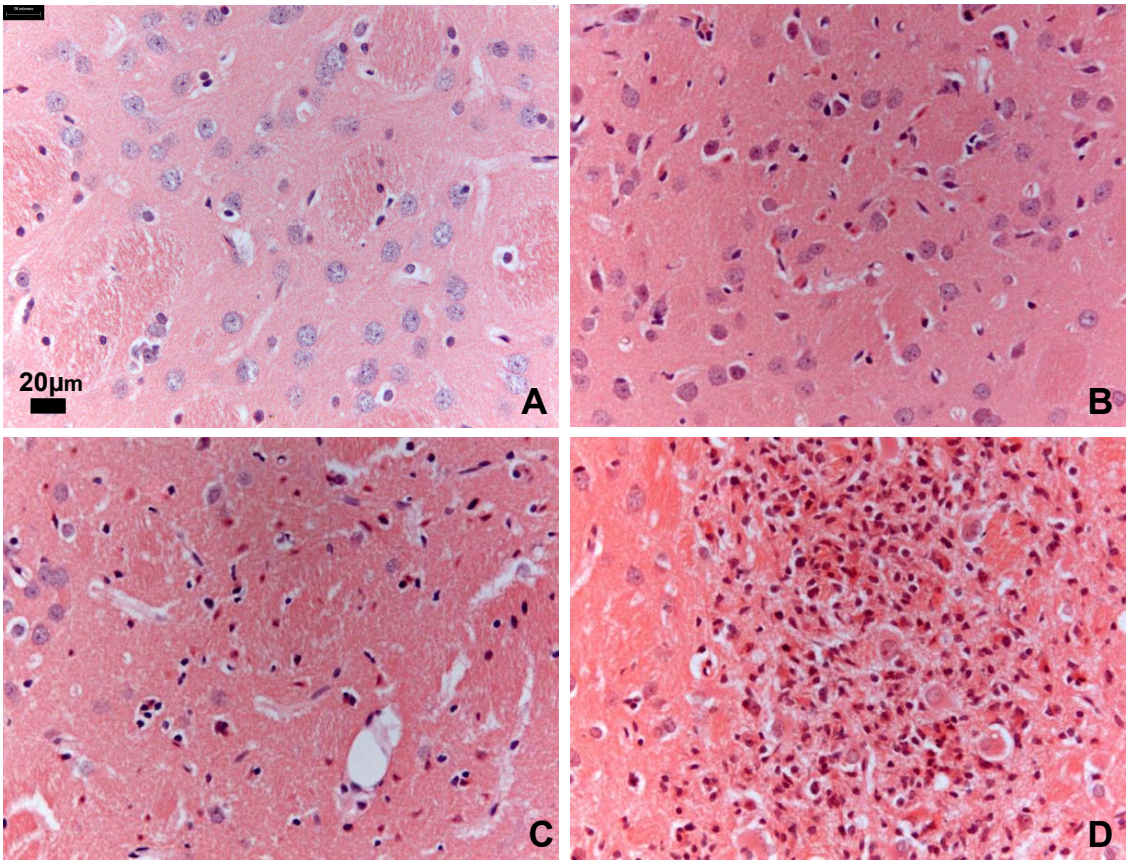

Fig.2.2: Representative images of haematoxylin and eosin staining in the caudatoputamen after BCCAo. Normal neurons appear "round" with a visible cytoplasm and nucleus (A), while ischaemic neurons appear shrinked with a pink cytoplasm (B, C, D).
The presence and extent of damage to perikarya (with pink cytoplasm) was graded as normal (grade 0) in A; scattered presence (B) of ischaemic neurons (grade 1); moderate numbers (C) of ischaemic neurons (grade 2); and near –total (D) ischaemic neurons (grade 3). The scale bar upper left shows 20 µm.

2.3 Immunohistochemistry

All sections used for immunostaining were adjacent to those which had undergone histological analysis and all analyses of immunohistochemistry were conducted blind over two days, sections were scored on both days and results then compared to minimize variability.

2.3.1 General principles

The immunohistochemistry technique is based on an antigen-antibody reaction to localise, within the tissue, the antigen. All immunohistochemistry in this thesis used the avidin-biotin complex (ABC) method to improve the sensitivity and resolution of the technique as well as the reaction between a chromogen (diaminobenzidene: DAB) and peroxidise to produce a brown deposit readily visible under light microscopy. The ABC method (Hsu et al., 1981) is an indirect method for antibody detection which exploits the high binding affinity of avidin, a large glycoprotein from egg whites, to biotin, a low molecular weight protein from egg yolks.

2.3.2 Protocol

Paraffin sections were placed in the oven at 60°C for 30 minutes, then in xylene for 10 minutes to remove the wax, then the sections were rehydrated in absolute alcohol, 100% (2X 5mins) before being immersed in a blocking solution containing 3% dihydrogen hydrogen peroxide (Sigma) in 100% methanol for 30 minutes. The sections were then placed in running tap water for 10 minutes. A limited number of antibodies require one more step of antigen retrieval. Briefly, the sections were submerged in citric acid (10mM,

pH60) and microwaved on full power for 2X 5 minutes until boiling. Following a cooling period of 20 minutes, the sections were rinsed in PBS 2X 5minutes and then ringed with a hydrophobic pen (Vector Labs) before the "block" solution containing 10% normal sera and 0.5% bovine serum albumin (BSA) in PBS for 1 hour at room temperature. This step blocks the non-specific binding sites with the normal sera from the species in which the secondary antibody was raised. Then, the block solution is removed and the primary antibody (raised in an animal against the antigen of interest), diluted at appropriate concentration in PBS was placed at 4°C overnight. Details of the primary antibody concentrations, source, appropriate blocking solution and secondary antibody are described in table 2.3. On the second day, the sections were washed in PBS 2X 10 minutes before receiving the biotinylated secondary antibody (raised against the species of animal that the primary antibody was made) in PBS for 1 hour at room temperature. Thereafter the sections were washed in PBS (2X 10 minutes) and then incubated with a solution of the avidin-biotin-peroxidase complex (Vector Laboratories, UK) made according the manufacturers instructions in PBS at room temperature for 1 hour. Sections were then washed in PBS (2X 10 minutes) and then incubated with DAB solution (Vector Laboratories) in distilled water again according to the manufacturer's instructions for 3 minutes to visualize the antibody binding. Sections were then dehydrated through a series of alcohols, 70% (2 minutes), 90% (2 minutes), 100% (2X 5 minutes) and xylene (10 minutes) before being coverslipped in DPX. Negative controls were performed in all the immunohistochemical protocols by omitting the primary antibody with, as a result, minimal detection.

Primary Antibody	Species, type	Supplier	Dilution	Blocking Sera	Secondary Antibody
APP	Mouse, 22C11	Millipore	1:1000	10% Normal Horse Serum, 0.5% BSA in PBS	Biotinylated anti-mouse
MAG	Goat, Polyclonal	Santa Cruz Biotechnology	1:2000	10% Normal Goat Serum, 0.5% BSA in PBS	Biotinylated anti-goat
Iba-1	Rabbit, Polyclonal	A. Menarini	1:750	10% Normal Goat Serum, 0.5% BSA in PBS	Biotinylated anti-rabbit

Table 2.3: Primary and secondary antibodies used in paraffin embedded immunohistochemical experiments

2.3.3 Quantification of axonal damage following BCCAo in the rat

Amyloid precursor protein (APP) is the step in the metabolism/formation of the amyloid β/A4, which is accumulated in AD brains (Kang et al., 1987). APP is transported by fast anterograde axonal transport (Koo et al., 1990) and its accumulation indicates a disturbance in this transport (Gentleman et al., 1993). In regions where axonal damage occurrs, APP-rich structures are evident as dark, swelling, bulbous and dystrophic axons. The severity of axonal pathology was evaluated bilaterally by a semi-quantitative scale in the corpus callosum, the external capsule, the internal capsule, the optic tract and in the caudatoputamen, the method of quantification was based on those reported by Gentleman et al. (1995), Gleckman et al. (1999) and also Saatman et al. (2003), as: normal (grade 0), slight accumulation of APP (grade 1), moderate accumulation of APP (grade 2), and an extensive accumulation of APP (grade 3), see fig.2.3.

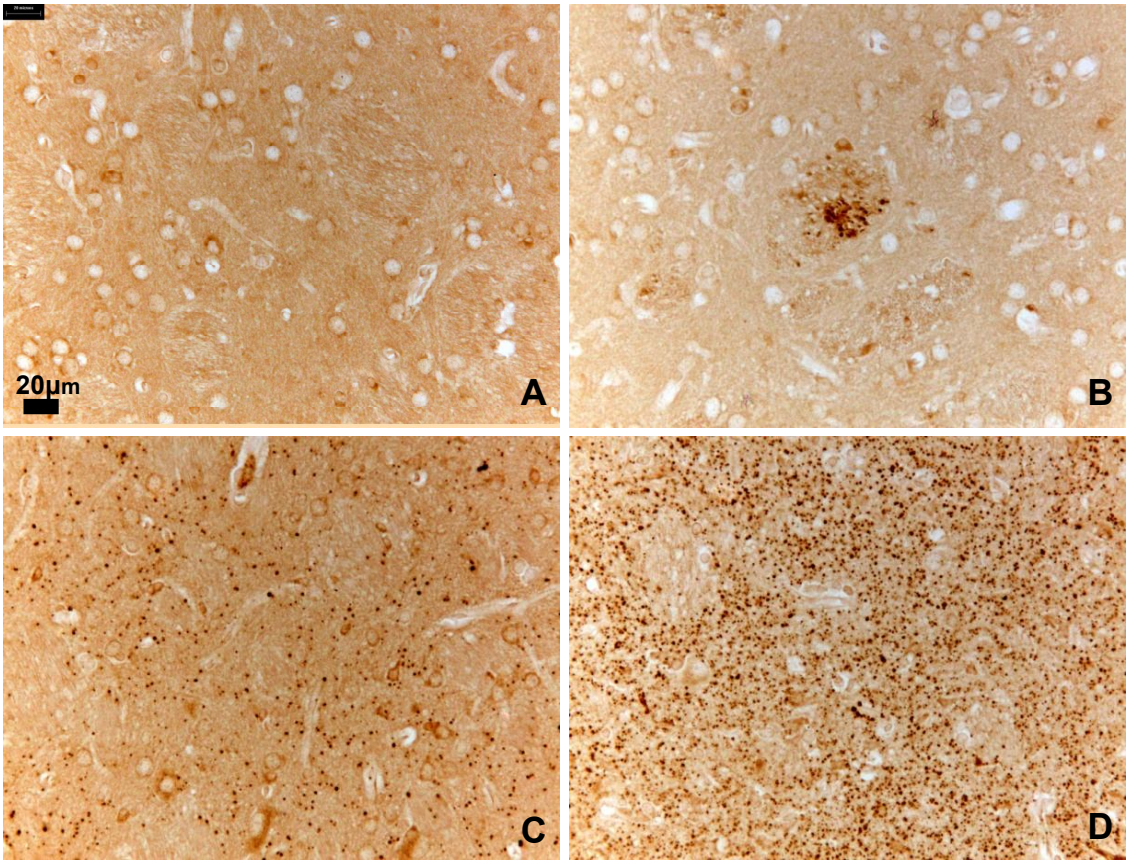

Fig.2.3: Representative images of APP accumulation (black dots) in the caudatoputamen after BCCAo. The presence of axonal damage was graded as absent (grade 0) in A; slight accumulation of APP (grade 1) in B; moderate accumulation of APP (grade 2) in C; and massive accumulation in APP (grade 3) in D. The scale bar upper left shows 20 µm.

2.3.4 Quantification of myelin débris following BCCAo in the rat

MAG is a constituent of myelin sheaths throughout the nervous system and is located in the periaxonal lamellae of myelin sheats. MAG is furthermore involved in cell-surface recognition (Poltorak et al., 1987) and has been identified as one of the first myelin proteins to suffer following ischaemia (Aboul-Enein et al., 2003).

Myelin débris was assessed (fig.2.4) in the corpus callosum, the external capsule, the internal capsule, the optic tract and in the caudatoputamen as: absent, non-existant (grade 0), slight accumulation of myelin débris (grade 1), moderate accumulation of myelin débris (grade 2), and an extent accumulation of myelin débris (grade 3).

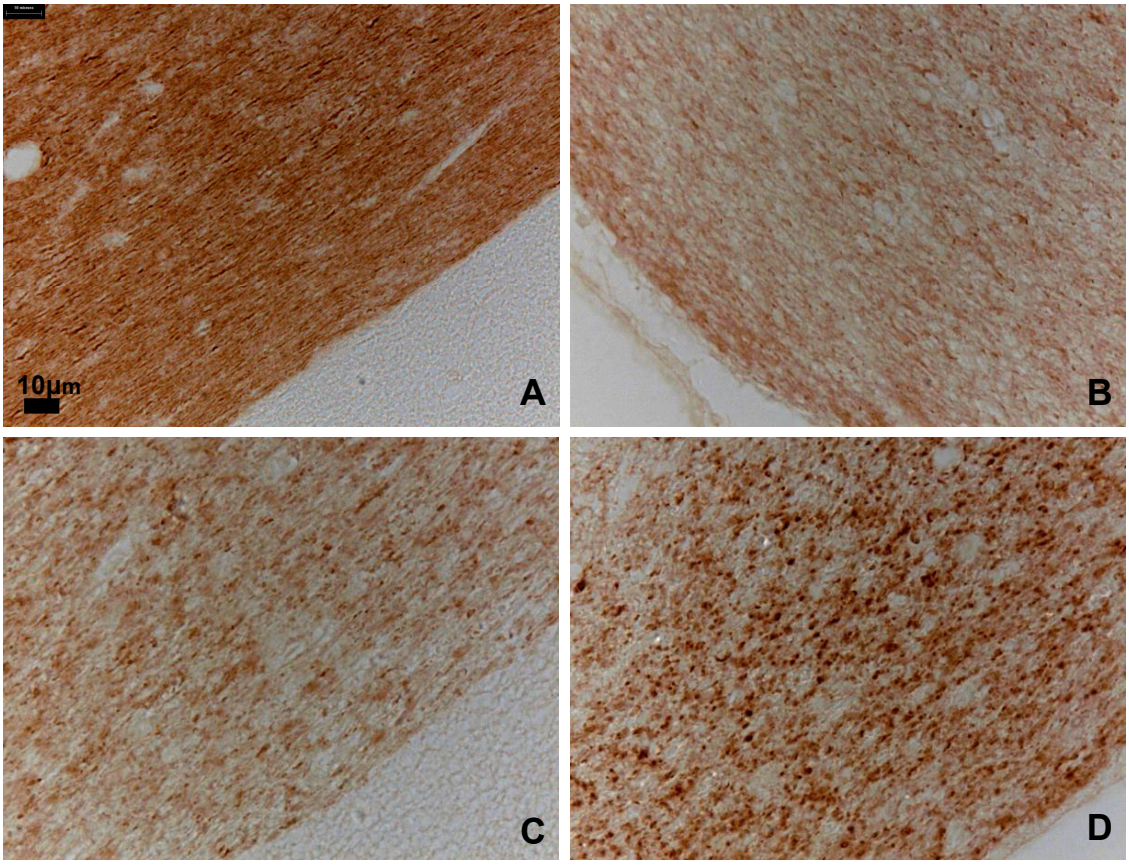

Fig.2.4: Representative images of MAG staining in the optic tract after BCCAo. The degree of presence of myelin débris (black dots) was graded as absent (grade 0) in A; slight accumulation of myelin débris (grade 1) in B; moderate accumulation of myelin débris (grade 2) in C; and severe presence of myelin débris (grade 3) in D. The scale bar upper left shows 10 µm.

2.3.5 Quantification of pathological microglial activation following BCCAo in the rat

The ionized calcium-binding adaptor molecule 1 (Iba-1) is a protein highly and specifically expressed in microglia; Iba-1 plays a role in the regulatory action of activated microglia (Ito et al., 1998).

Because of the difficulty to define with precision individual microglia cells within a tissue that has suffered, a semi-quantitative assessment scale was used. The amount of microglia activated was evaluated (Fig.2.5) as 0 = normal presence of activated microglia, 1 = marked enhancement of microglial activation, 2 = massive enhancement of microglial activation.

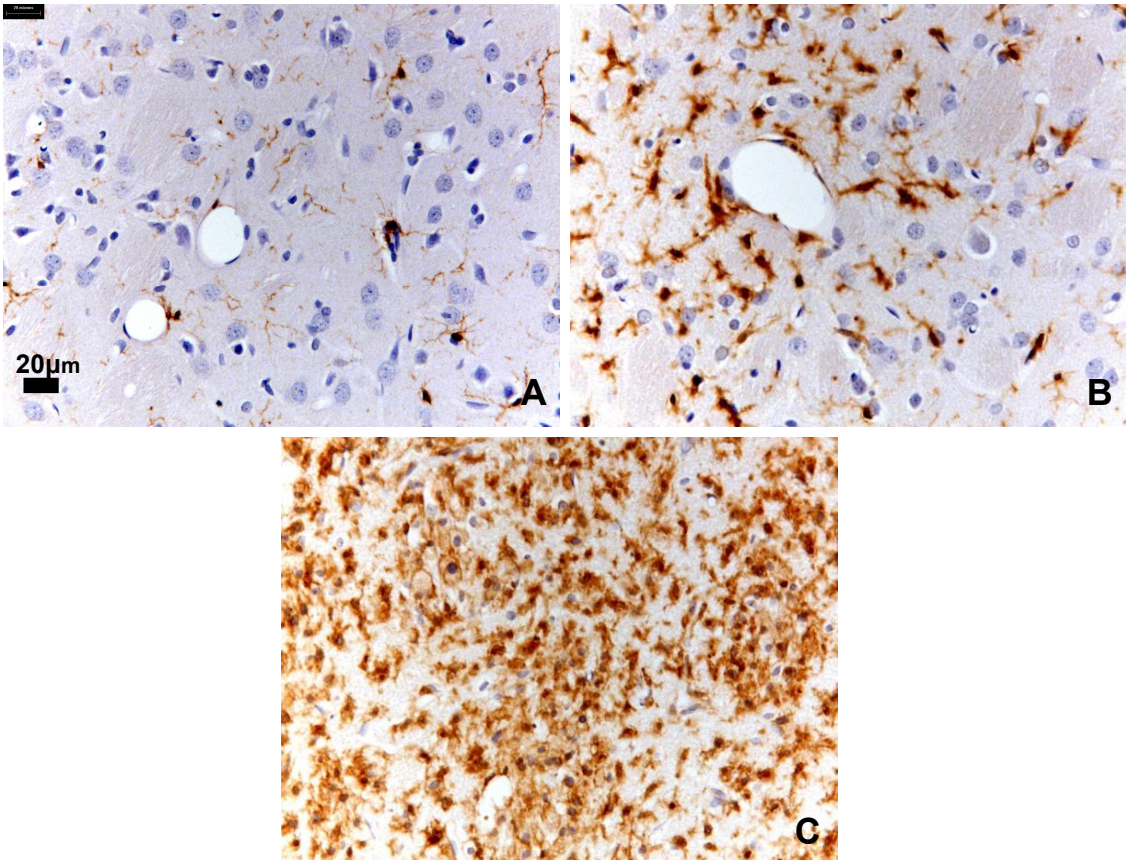

Fig.2.5: Representative images of Iba-1 staining in the caudatoputamen after BCCAo. The presence of activated microglia (in brown) was graded as normal compared to the sham (grade 0) in A; a moderate enhancement of activated of microglia (grade 1) in B; severe enhancement of microglial activation (grade 2) in C. The scale bar upper left shows 20 µm.

2.3.6 Evaluation of axonal damage, myelin débris, damage to the perikarya and microglial activation

As stated earlier, the grey and white matter regions investigated bilaterally in the present study were located at +0.20 and -3.30 mm from the bregma, based on the atlas of Paxinos and Watson (Paxinos and Watson, 1998). The following regions (fig.2.6) were selected: corpus callosum, external capsule, fimbria, internal capsule, optic tract, caudatoputamen and hippocampus. To evaluate the extent and evolution of the pathology induced by carotid ligation, we calculated an individual overall score as: Sum (Σ) of each grade in each region of interest as noted in each hemisphere. A high score indicates widespread pathology; a low score indicates more discrete damage.

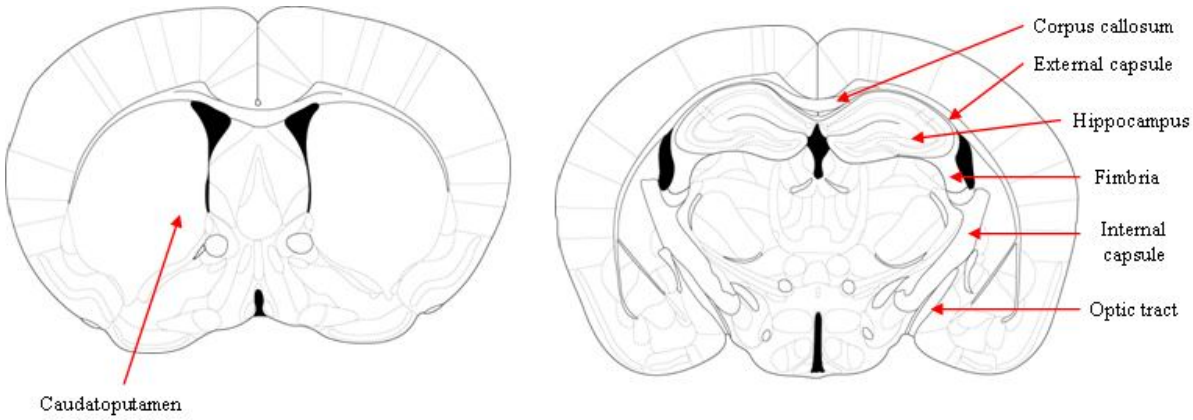

Fig.2.6: Regions of interest of white and grey matter

2.4 In vivo magnetic resonance imaging

2.4.1 Principle

Magnetic resonance imaging (MRI) is a non-invasive method used in radiology that provides detailed three-dimensional images and sectional anatomical precision inside an object. The technology is based on the physical phenomenon of nuclear magnetic resonance, namely to observe the nuclear magnetic resonance of protons in water contained in the body, i.e. the response of nuclei subjected to an external magnetic field and electromagnetic excitation. The intensity collected in a volume element (voxel) depends on the concentration of water at that location and so one obtains a three dimensional image of the distribution of water in the body. According to the method used, the contrast between two voxels can be increased if the relaxation times of nuclear spins (describing the return to equilibrium after excitation of nuclei) differ in both areas. It is therefore possible to observe alterations of tissues (such as tumours) due to differences in density and relaxation of water.

All nuclei have a charge, and this charge turn around a nuclear axis and generates a magnetic dipole which is expressed by a quantity called magnetic moment (μ). In the absence of magnetic fields, the magnetic moments are not oriented. (Fig.2.7).

Fig.2.7: Magnetic moment and its orientation in the absence of magnetic fields

In the presence of a static magnetic field, the magnetic moments take a given orientation which corresponds to a given energy state (Fig.2.8)

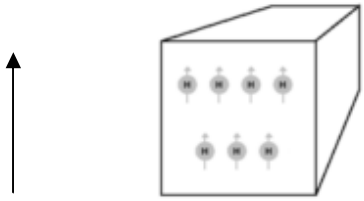

Fig.2.8: Orientation of the magnetic moments in the presence of a magnetic field

To observe the resonance, one must provide energy to allow the nuclei to move from their fundamental state to the excited state. This energy is supplied by a second magnetic field with intensity ($\sim 10^6$) smaller than the previous one.

Relaxation happens after the absorption of electromagnetic energy provided by the second magnetic field; the nuclei tend then to return to their equilibrium position. This relaxation can be decomposed into two phenomena: the longitudinal relaxation (T1) and the transversal relaxation (T2).

The longitudinal relaxation called T1 relaxation corresponds to a return to the equilibrium energy of the system after excitation. The time constant T1 is defined as the time required for the protons to reach the two-thirds of their magnetisation.

The transversal relaxation called T2 is normally defined as the time during which the intensity decreases by two-thirds of its initial value.

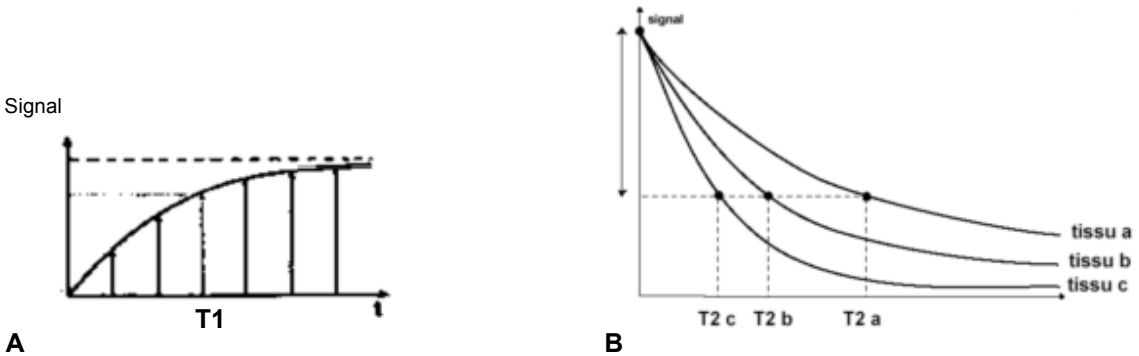

Fig.2.9: Relaxation times of T1 (A) and T2 (B) measurements.

The relaxation times T1 and T2 of tissues depend (fig. 2.9) on the mobility of hydrogen nuclei present in these tissues: the relaxation time increases with the hydration of these tissues and decrease when the hydration decreases. Indeed, an acute lesion, accompanied in most cases with inflammation and oedema, increases the amount of water in these tissues.

MRI is based on the differences in T1 and T2 and the proton density (water content and mobility of water molecules) in tissue and it detects signal from mobile (free) water protons (with long T2). The T2 relaxation time of less mobile water protons (bound) associated with macromolecules and membranes are too short to be detected in MRI (see fig. 2.10).

MTI is based on the magnetization interaction between water protons and macromolecular-bound protons. If an off-resonance radio frequency is applied to the macromolecular protons, the saturation of these protons is transferred to the water protons and leads to a decrease in the signal depending on the magnitude of the magnetization

transfer between tissue macromolecules and water. With MTI, the presence or absence of macromolecules (e.g. in membranes or brain tissue) can be detected.

The magnetization transfer ratio (MTR) is the difference in signal intensity with or without magnetization transfer. A lesser MTR within a region compared to the control indicates a decreased density of macromolecules (tissue or membranes…) to exchange magnetization with the surrounding water molecules. It thus reflects a presence of damage (Iannucci et al., 2001; Wolff and Balaban, 1989).

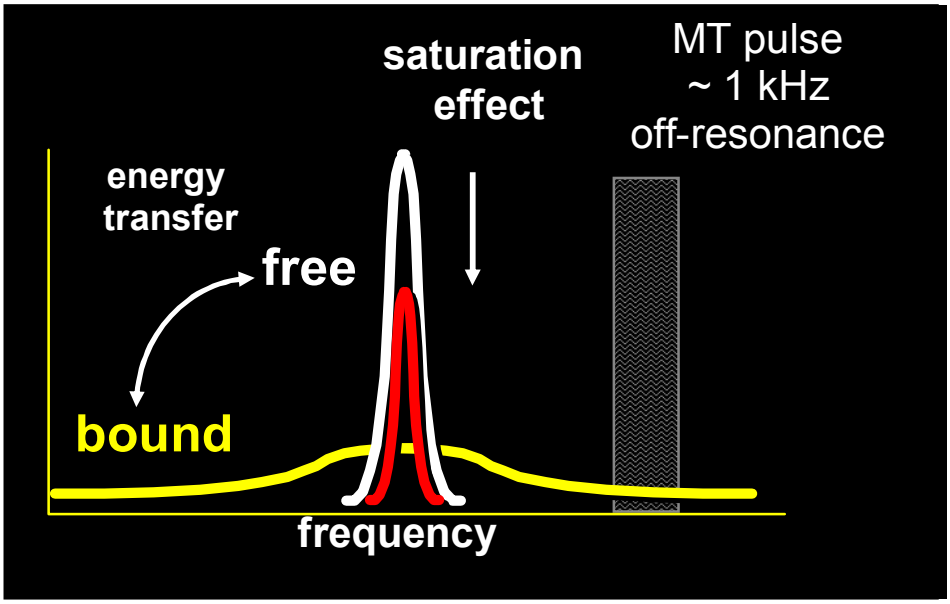

Fig.2.10: The principle of Magnetization Transfer Imaging (MTI)

2.4.2 Experimental design

The experimental design is illustrated in figure 2.11. Rats were divided into two groups either of three hours or of seven days survival time following the BCCAo. After the imposed post-intervention delay, the rats were introduced into the tunnel for the MRI acquisitions. Each animal received an injection of gadolinium (Gd-DOTA; gadoteric acid; DOTAREM; Guerbet) before the MRI acquisition of T1, to measure the integrity of the BBB after the onset of chronic cerebral hypoperfusion.

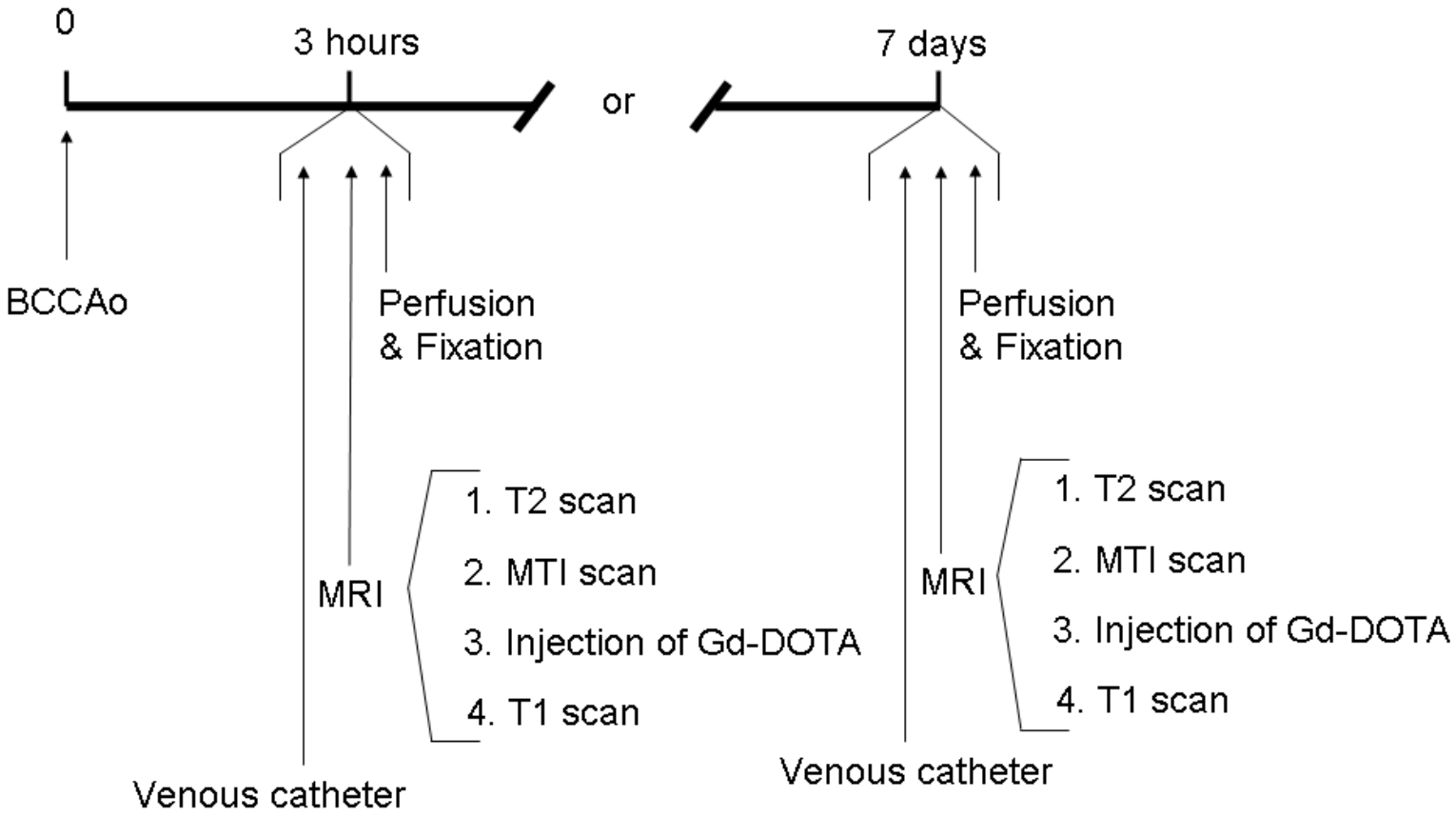

Fig.2.11: Experimental design for MRI acquisition at either three hours or seven days following BCCAo

2.4.3 MRI scans

Following the pose of the femoral venous catheter, the rats were placed in a MRI compatible holder (Rapid Biomedical, Wurzburg, Germany). Rectal temperature and respiration were monitored and controlled throughout the examination (SA Instruments Inc., Stony Brook, NY, US) to ensure normal and stable physiological parameters. MRI data were obtained with a Varian 7T preclinical scanner (Varian Inc., Oxford, UK) fitted with a 72 mm volume coil and a phased array rat brain coil (Rapid Biomedical).

The MRI acquisitions were performed by Dr Maurits Jansen and Mr Gavin Merrifield. Dr Mark Bastin processed the T2 and T1 images and the MTI images were processed into MTR parametric maps. I then analysed blindly the MRI images through the use of ImageJ software (V1.43). Means gray values per sections for each region were measured and compared the two controls and two BCCAo groups.

Each full MRI examination lasted 1 hour and included the undernoted sequences:

- T2 high resolution (structural scan)
- MTI (white matter integrity)
- Baseline for T1
- Injection of Gd
- T1 (BBB integrity)

Nineteen contiguous slices were imaged in T2 for detailed structural resolution with a field-of-view of 26×26 mm, an acquisition matrix of 192X192 and slice thickness of 0.8 mm; the acquisition voxel dimension was 0.2×0.2×0.8 mm. The repetition (TR) and echo (TE) times for each fast spin-echo volume were 3000 and 36 ms.

The T1 acquisition was done to measure BBB integrity with gadolinium as a tracer. Again, nineteen contiguous slices were imaged with a field-of-view of 26×26 mm, an

acquisition matrix of 128X128 and slice thickness of 0.8 mm; the acquisition voxel dimension was 0.2×0.2×0.8 mm. The TR and TE for each fast spin-echo volume were 780 and 9.48 ms.

The MT-MRI protocol employed two spin-echo sequences (TR 2300 and TE 12.52 ms) with identical acquisition parameters as for the T1; one was acquired with a magnetization transfer pulse applied 3 kHz off resonance.

2.4.4 Image analysis

After the acquisitions were processed by Dr Mark Bastin, I selected regions-of-interest (ROI) as detailed by Iannucci and collaborators (2001) and I manually delineated, with ImageJ (version 1.43) software, the corpus callosum (Fig.2.12 A-E-I), the caudatoputamen (Fig.2.12 B-F-J), the external capsule (Fig.2.11 C-G-K) and the internal capsule (Fig.2.12 D-H-L) in both hemispheres on the T2-weighted images (A to D), MTR maps (E to H), and T1-weighted images (I to L). Each area was measured through ImageJ. Mean grey values obtained from ImageJ (see appendices B and D) were compared (MTR) between each BCCAo and appropriate sham group. The signal enhancement (as a percentage) of gadolinium was compared for the T1-weighted images, as explained below (section 2.4.5 and appendices C and D).

To reduce variability, a second analysis was undertaken two days after the initial and the results were correlated on GraphPad Prism (v5.03) (Fig.2.13).

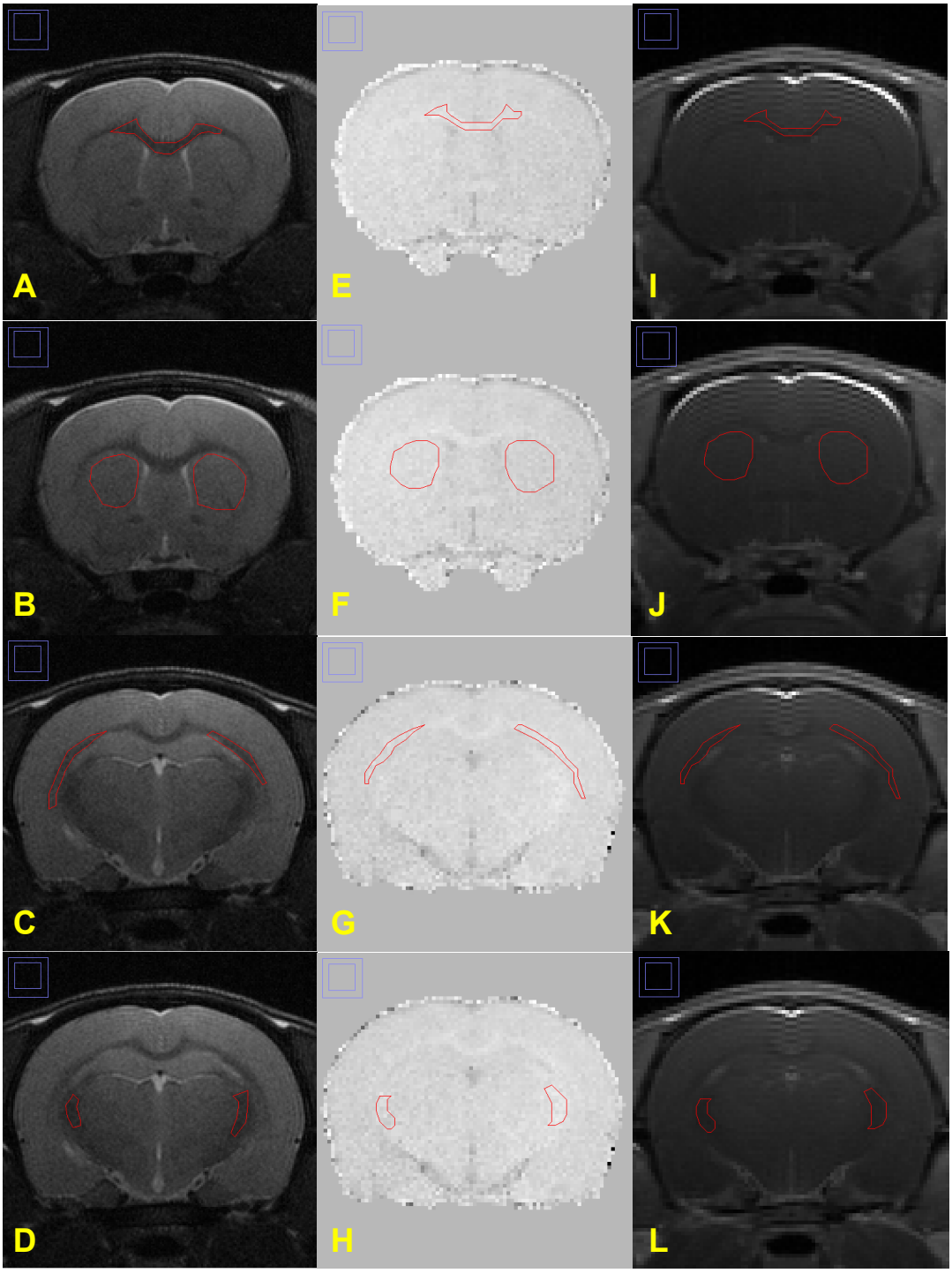

Fig.2.12: Coronal MRI images to show the ROIs selected within the corpus callosum (A, E, I), the caudatoputamen (B, F, J), the external capsule (C, G, K) and the internal capsule (D, H, L), delineated by red boundries, in the T2-weighted images (A-D), MTR parametric maps (E-H) and T1-weighted images after the injection of Gd-DOTA (I-L).

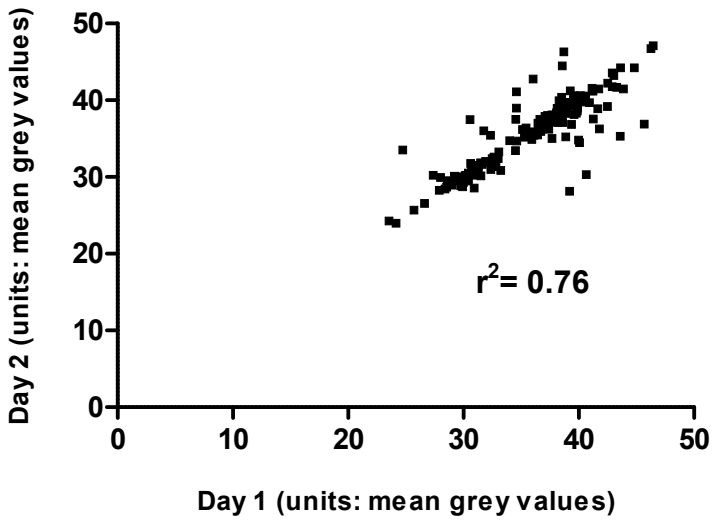

Fig.2.13: First and second assessment of T2, MTR and T1 analyses done on different days and compared by correlation ($p<0.0001$) on GraphPad Prism (v5.03)

2.4.5 Measurement of BBB permeability

A healthy brain capillary with an intact BBB is not permeable to the contrast agent (Gd-DOTA) which remains intravascular, while a capillary in sufferance with a disrupted BBB will become permeable to the agent and leads to an accumulation of the contrast agent in the neuropil. Accordingly, the measurement of the signal enhancement of Gd-DOTA signal may be used as an indicator of BBB dysfunction.

The mean grey values were obtained by ImageJ after selecting the structure as described above. The mean grey value before Gd-DOTA injection represents the baseline. Then the percentage of signal enhancement of Gd-DOTA compared the baseline was calculated as follows for each brain region selected (see appendices C and D):

Signal enhancement of Gd-DOTA (%) = (Mean grey value after Gd-DOTA injection – Mean grey value before Gd-DOTA injection)* 100 / (Mean grey value before injection).

2.5 Western blotting

The western blots and RT-PCR as well as their statistical analyses were performed by Dr Severine Launay and Miss Abigail Herrmann. I performed all the surgerical interventions and to allow the extraction of the brain tissues by Dr Severine Launay.

Western blotting techniques were used to determine the levels of caspase-3, MMP-2 (metalloproteinase-2), VEGF (vascular endothelial growth factor) and HIF-1α (hypoxia inducible factor 1-α) in BCCAo and sham rats at three hours and seven days after the surgery. After each time point, the rats were anaesthetized (5% isoflurane in a 30% oxygen/70% nitrous oxide mixture). When deeply anaesthetized, the rats were decapitated and brains were removed from their skull. Three brain regions were

extracted on dry ice: the cortex, the corpus callosum and the caudatoputamen. The two half-brains were separated to use one for the western blot analysis and the other for the RT-PCR analysis.

All brain structures were homogenised in a buffer consisting 9 M urea, 4% CHAPS (a zwitterionic detergent that protects the native state of proteins - Sigma, C9426) and complete protease inhibitor cocktail (Sigma) and centrifuged at 10,000 rpm for 10 minutes. The supernatants were recovered and stored at -80°C until required. Each sample was assayed for protein concentration by the Bradford method. Samples were denatured at -70°C for 10 minutes before separation on 4-12% Bis-Tris gel (Invitrogen) at 80 V for 150 minutes. Proteins were electro-transferred (30V, 1 hour) on to a nitricellulose membrane (Biorad). After blocking (10 ml Odyssey blocking buffer, 10 ml PBS), membranes were incubated overnight with blocking solution containing either Hif1-α, Caspase-3, VEGF, MMP-2 (see table 2.4). After washing six times for five minutes in PBS/0.1% Tween-20 solution, the membranes were incubated for 1 hour with the appropriate 680 and 800 IR (Infrared) dye secondary antibodies (1:50000, LI-COR Biosciences). The membranes were washed again with PBS/0.1% Tween-20 solution with a final wash carried out in PBS alone. The membranes were imaged through the use of Odyssey infrared imaging system, corrected for background, and analyzed by the Odyssey software (LI-COR Biosciences).

Primary Antibody	Species, type	Supplier	Dilution
Hif1-α	Mouse Monoclonal	Novus Bologicals	1 in 200
Caspase3	Rabbit Polyclonal	Cell Signalling	1 in 500
VEGF	Rabbit Polyclonal	Abcam	1 in 1000
MMP2	Rabbit Polyclonal	Abcam	1 in 1000
GAPDH	Rabbit Polyclonal	Sigma	1 in 50 000
α-Tubulin	Mouse Monoclonal	Abcam	1 in 20 000

Table2.4: Antibodies used for western blots

2.6 Real-Time PCR

Real-time quantitative PCR (RT-PCRq) is derived from classic PCR (Polymerase Chain Reaction). The main difference is that RT-PCR allows the visualization of the quantity of neosynthetized DNA for each PCR cycle and not only the product obtained at the end of the reaction.

RT-PCR allows the detection and precise quantification of a fluorescent emitter, SYBR Green I (Applied Biosystems) which is able to insert itself in double-stranded DNA. This dye emits light only when bound to double-stranded DNA. The increase of fluorescence is directly proportional to the quantity of generated amplicons during the PCR reaction. Therefore, with specific nucleotidic primers, this technique is able to quantify the amplification of target genes.

RT-PCR was used in this study to determine the gene expression of Hif1-α, VEGF and Caspase-3 in three forebrain structures: the cortex (neocortex), the corpus callosum and the caudatoputamen after seven days of BCCAo.

2.6.1 Preparation of PCR primers

Gene specific primers are retrieved from the online PrimerBank database (http://pga.mgh.harvard.edu/primerbank/). These primers are then ordered from the MGH (Massachussets General Hospital) DNA Core Facility. All the primers are desalted and both UV absorbance and capillary electrophoresis are used to assess the quality of primer synthesis.

2.6.2 Reverse Transcription-PCR

RNA from rat half-brain structures were prepared according to the SuperScript First-Strand Synthesis System for RT-PCR as *per* the manufacturer's protocol (Invitorgen). A 10 µl of RNA/primer mixture was prepared for each tube which included 5 µg of total RNA, 3 µl (50 ng/µl) of random hexamers, 1 µl of 10mM dNTP mix and completed to 10 µl with DEPC (Diethylpyrocarbonate) treated water. Thereafter, the samples were incubated at 65°C for five minutes and then put on ice for at least one minute.

A reaction master mixture was then prepared to include 10x RT buffer, 4 µl of 25mM $MgCl_2$, 2 µl of 0.1 M dithiothreitol, 1 µl of RNaseOUT (Recombinant Ribonuclease Inhibitor). The reaction mixture was then added to the RNA/primer mixture, briefly mixed, and then placed at room temperature for two minutes. Then 1 µl of 50 units of SuperScript II RT was added to each tube, mixed and incubated at 25°C for 10 min. The tubes were then incubated at 42°C for 50 minutes, heat inactivated at 70°C for 15 minutes and then chilled on ice. One µl of RNase H was added to remove the RNA template and incubated at 37°C for 20 minutes. The first strand cDNA was then stored at -20°C until use for real-time PCR.

Nucleic acids of interest were amplified by RT-PCR with cDNA as the template.

Real-time PCR were achieved by an ABI Prism 7000 Sequence Detection Systems (Applied Biosystems). Reactions were carried out in microcentrifuge tubes in a thermocycler (Bio-Rad) with a range of cycling conditions. Hot-start PCR was performed with the SYBR Green PCR Master Mix (Buffer, dNTPs, polymerase, MgCl2, SYBR Green I) (Applied Biosystems) In brief, the PCR mixtures [12.5 µl SYBR Green Mix (2x), 0.2 µl liver cDNA, 1 µl primer pair mix (5 pmol/µl each primer), 11.3 µl of water] were pre-heated at 50°C for two minutes and then 95°C for 10 minutes for an initial denaturation and activation of the polymerase, to be followed by 40 cycles of amplification (95°C for 15 seconds; 60°C for 30 seconds; 72°C for 30 seconds). A final extension step was performed at 72°C for 10 minutes. α-Tubuline and glyceraldehyde-3-phosphate dehydrogenase (GAPDH) were used as internal markers. The PCR products were checked by 3% agarose gel with an aliquot of 5 µl from each reaction. The real-time PCR results were then analyzed with the SDS 7000 software to check if there was a bimodal dissociation curve or abnormal amplification plot. Specific gene primers for PCR are shown on Table 2.5.

Gene	Reference sequence accession	Sequence
Hif1-α	NM_024359.1	For TGTTGTAAGTGGTATTATTCAG Rev CTCGTGTCCTCAGATTC
Caspase3	NM_012922.2	For TGGACTGCGGTATTGA Rev GGGTGCGGTAGAGTAA
VEGF	NM_031836.1	For ACCCACGACAGAAGG Rev ACAGGACGGCTTGAA
GAPDH	NM_017008.3	For CAACGGCACAGTCAA Rev CAGCACCAGCATCAC
α-Tubulin	NM_022298.1	For CAAGCGACAAGACCAT Rev TGCGAACTTCATCAATAAC

Table 2.5: Primers used for RT-PCR

2.6.3 Real-Time PCR

Quantitative SYBRgreen RT-PCR was performed on an Opticon Monitor thermocycler machine to validate the results obtained from the Affymetrix® gene array. Three hours or seven days following BCCAo, the structures from the other half-brain (cortex, corpus callosum and caudatoputamen) of BCCAo and sham-operated rats was dissected on ice-cold phosphate buffered saline (pH 7.4 PBS, NaCl 137mM, KCl 2.7mM, NaH_2PO_4 1.4mM, Na_2HPO_4 4.3mM) and immediately frozen on dry ice and stored at -70°C.

mRNA was isolated from those structures and cDNA synthesized as previously described in section 2.6.2.

One µl of cDNA was added to 24 µl of mastermix containing: 0.5µl of each appropriate primer (12.5µM), 10.5µl bidistilled water and 12.5 µl of 2 X SYBRgreen RT-PCR mix (Applied Biosystems). Two serial dilution series of BCCAo or sham cDNA and a blank control that contained no reverse transcriptase cDNA synthesis

products were performed in each experiment. The Opticon Monitor RT-PCR machine was programmed with an initial incubation at 50°C for 2 minutes and then 95°C for 10 minutes for a denaturation and activation of the polymerase followed by 40 cycles of amplification (95°C for 15 seconds; 60°C for 30 seconds; 72°C for 30 seconds). A final extension step was performed at 72°C for 10 minutes.

2.7 Statistical analyses

2.7.1 Histopathology

Comparisons between groups (sham and BCCAo rats) in terms of axonal damage, myelin débris accumulation, neuronal perikaryal damage and microglial activation were assessed by Mann-Whitney's test. The histopathological grade of all the regions of interest were summated to give an overall score per animal and then scores were compared. All calculations were based on GraphPad Prism (version 5.03 for Windows).

2.7.2 MRI analyses

To determine if BCCAo-induced white matter alterations, based on the MTI acquisitions, every selected regions of BCCAo rats were compared to the same region in sham-operated rats by an unpaired t-test.

The comparison in the same rat of % signal enhancement of Gd-DOTA, according to the brain structure, was calculated using an ANOVA-repeated measure followed by a Bonferroni post-test, by comparing the baseline to the time after Gd injection, in both groups (BCCAo and sham). The comparison between the BCCAo and sham group was done using a 1 way-ANOVA.

2.7.3 Western blots and RT-PCR analyses

Western blot data and RT-PCR results were analyzed by unpaired t-tests on GraphPad Prism 5.03.

All data are presented as mean ± standard deviation unless otherwise stated.

CHAPTER 3: Results

3.1 Temporal sequence of pathological events after BCCAo

The rats were divided randomly into groups at three hours, three days, seven days, 14 days and 28 days after BCCAo, as well as a control group (sham) for each time interval. The procedure was performed on a total of 96 rats (54 BCCAo and 42 sham). Among the BCCAo rats, one rat died within 24h; one rat died within three days of ligation and one rat died seven days after BCCAo. The overall mortality rate was approximately 6%. Prior to death, these rats presented with a decreased mobility and a tendency to isolate themselves from the others in the same cage. All BCCAo animals lost 15 to 18% of their original body weight from the second to the fourth day post surgery, and then recovered slowly to regain their original weight by seven to 28 days after the surgical intervention. No morbidity and mortality were noted in the sham rats.

3.1.1 BCCAo-induced axonal damage

The control (sham) rats that underwent the procedure without occlusion of the common carotid arteries showed no axonal pathology in the seven selected regions. Axonal damage after BCCAo was identified by the presence of intense APP immunoreactivity in swollen or bulbous axons (McKenzie et al., 1996). In the occluded groups, APP accumulation was detected as sonn as three hours after the surgery until 28 days post occlusion. At three hours post occlusion, APP accumulation was predominantly detected in the corpus callosum (fig.3.1B and 3.1F) and in the external capsule (Fig.3.1E). Five out of nine BCCAo rats exhibited axonal damage in the corpus callosum and six out of nine BCCAo rats exhibited axonal damage in the

external capsule. The fimbria, the internal capsule and the caudatoputamen also exhibited some APP accumulation. Axonal damage was not detected either in the hippocampus or in the optic tract in any of the three-hour BCCAo group. Table 3.1 presents the number of rats in which APP accumulation was detected in the selected regions as a function of time of the delay following BCCAo. The quantification of axonal damage in all of those (bilateral) seven regions shows that, after three hours of occlusion, BCCAo effected significantly ($p<0.01$) axonal damage, absent in the sham-operated group (Fig.3.6). We need to underline the fact that the pattern of axonal damage after three hours of BCCAo differs in the same group. Some brain structures may exhibit more or less damage according to each animal. The figure 3.1B present APP accumulation in the corpus callosum of one BCCAo animal while in another BCCAo animal the degree of axonal damage in the corpus callosum differs, as it can be seen in the figure 3.1F. This indicates that the BCCAo procedure does not reproduce the same pattern of damage for each animal. After three days post occlusion, axonal damage was detected in the hippocampus, in the corpus callosum, in the external capsule, in the fimbria, in the internal capsule, in the optic tract (fig.3.2 D) and in the caudatoputamen (fig.3.2 B). The regions which most of the animal exhibited axonal damage after three days post BCCAo were the caudatoputamen (five out of nine animals), the internal capsule (four out of nine animals) and the optic tract (six out of nine animals). The sham group did not present any APP accumulation (fig.3.2A and C). The induction of chronic cerebral hypoperfusion for three days leads to significant ($p<0.001$) axonal damage in the BCCAo group compared to the sham group (Fig.3.6). At 7 days post BCCAo, axonal pathology was more important and was detected in the hippocampus, in the corpus callosum, in the external capsule, in the fimbria, in the internal capsule, in the optic tract (Fig.3.3 D) and in the

caudatoputamen (fig.3.3B and E). The optic tract and caudatoputamen being the regions that exhibited the more axonal damage at this time point. Seven days of BCCAo induced more significant ($p<0.001$) axonal damage compared to the control group (Fig.3.6). After 14 days post BCCAo, the hippocampus, the corpus callosum, the external capsule, the internal capsule, the optic tract (Fig. 3.4D) exhibited axonal pathology; the fimbria was the only region that did not present any APP accumulation. The presence of axonal pathology in the BCCAo group was significantly ($p<0.001$) different from the control group (Fig.3.6). The optic tract and the caudatoputamen were the regions that exhibited the more axonal pathology at 14 days post occlusion. However, the damage at 14 days post BCCAo is less important than at seven days post BCCAo. At 28 days post BCCAo, axonal damage was detected in the corpus callosum, in the external capsule, in the hippocampus, in the fimbria, in the internal capsule, in the optic tract (Fig.3.5D) and in the caudatoputamen. The optic tract is the region where axonal damage was the most prominent in terms of time-related injury following BCCAo. Vacuoles present in the corpus callosum and in the optic tract (red arrows in B and D). After 28 days of occlusion, the damage to the axon was significantly different ($p<0.001$) from the sham group (Fig.3.6).

	Three hours post-BCCAo	Three days post-BCCAo	Seven days post BCCAo	14 days post-BCCAo	28 days Post-BCCAo
Hippocampus	**0/9**	**1/9**	**3/12**	**1/10**	**2/11**
Caudatoputamen	**3/9**	**5/9**	**9/12**	**6/10**	**4/11**
Corpus callosum	**5/9**	**2/9**	**5/12**	**2/10**	**6/11**
External capsule	**6/9**	**3/9**	**5/12**	**1/10**	**5/11**
Fimbria	**4/9**	**2/9**	**2/12**	**0/10**	**2/11**
Internal capsule	**4/9**	**4/9**	**11/12**	**3/10**	**9/11**
Optic tract	**0/9**	**6/9**	**11/12**	**10/10**	**10/11**

Table 3.1: Number of rats in which an increase in APP accumulation was detected in the regions selected as a function of time after BCCAo.

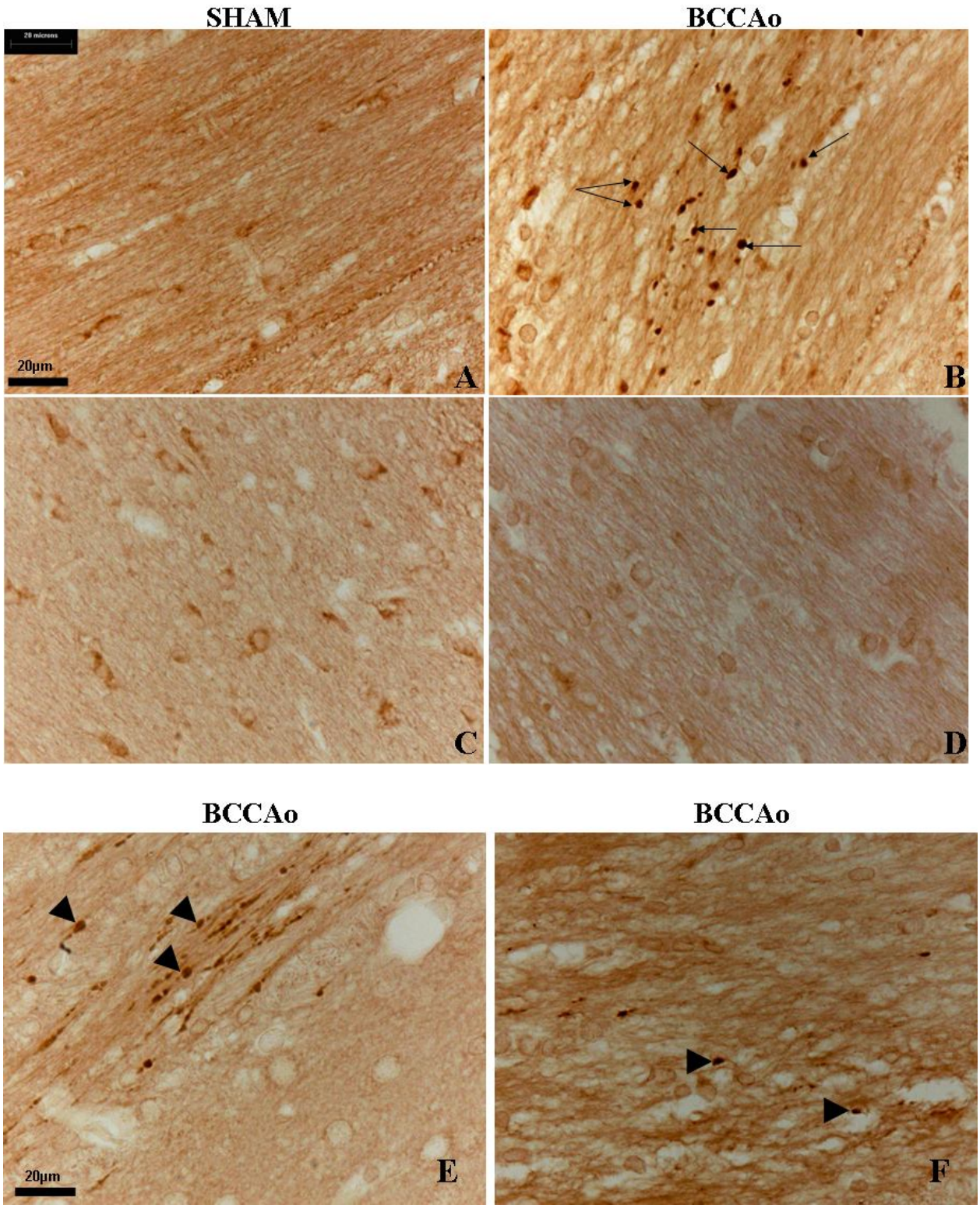

Fig.3.1: APP immunostaining in the corpus callosum (A, B, F), in the optic tract (C and D) and in the external capsule (E) following three hours of BCCAo. APP accumulation appears as dark dot (see arrows in B, E and F). No APP accumulation was detected in the sham-operated rats (A and C) or in the optic tract after three hours of BCCAo.

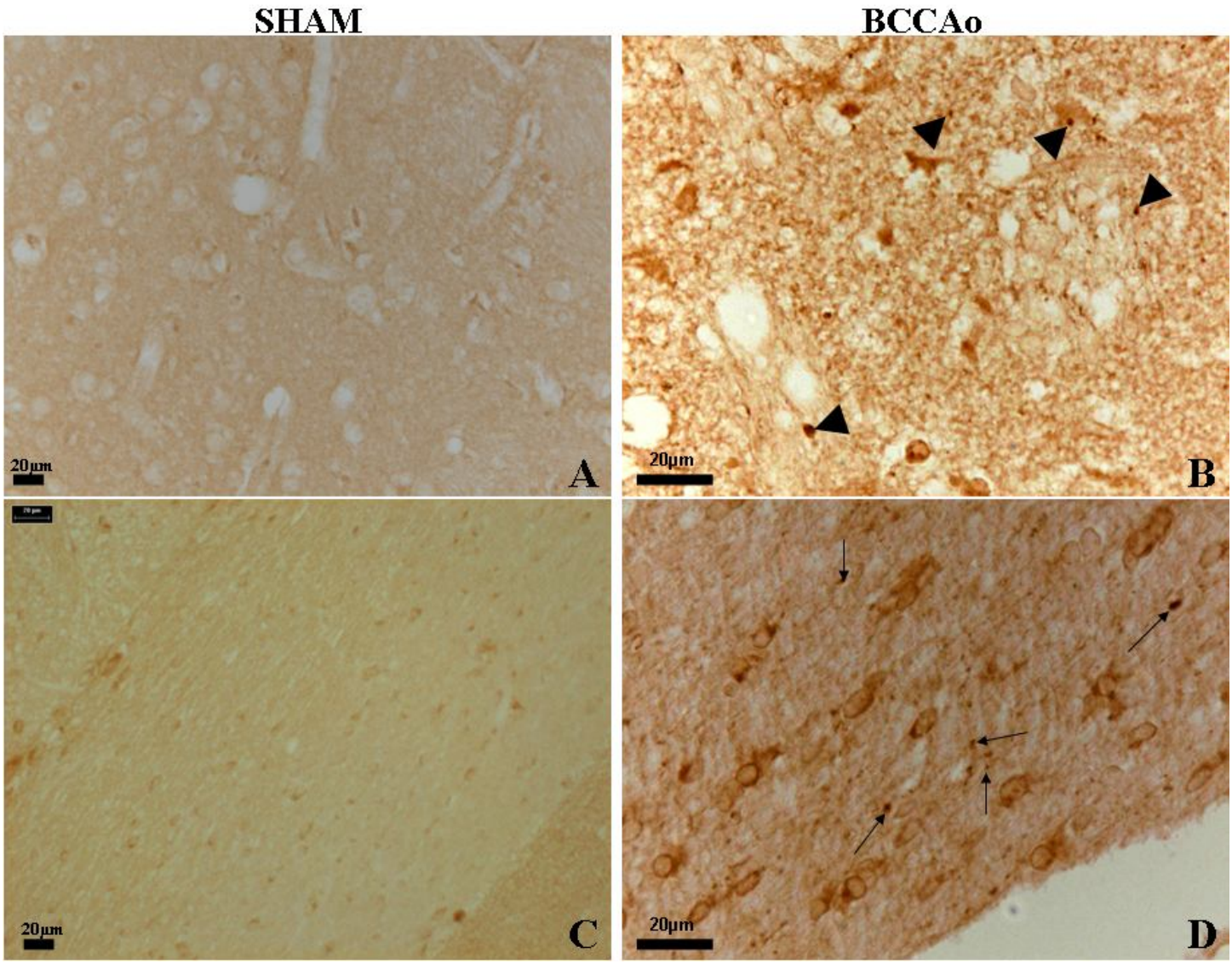

Fig.3.2: APP immunostaining in the caudatoputamen (A and B) and in the optic tract (C and D) following three days of BCCAo. No APP staining was detected in the sham group. Arrows in B and D indicate the presence of APP accumulation. Scale bars in A, B, C, D: 20µm.

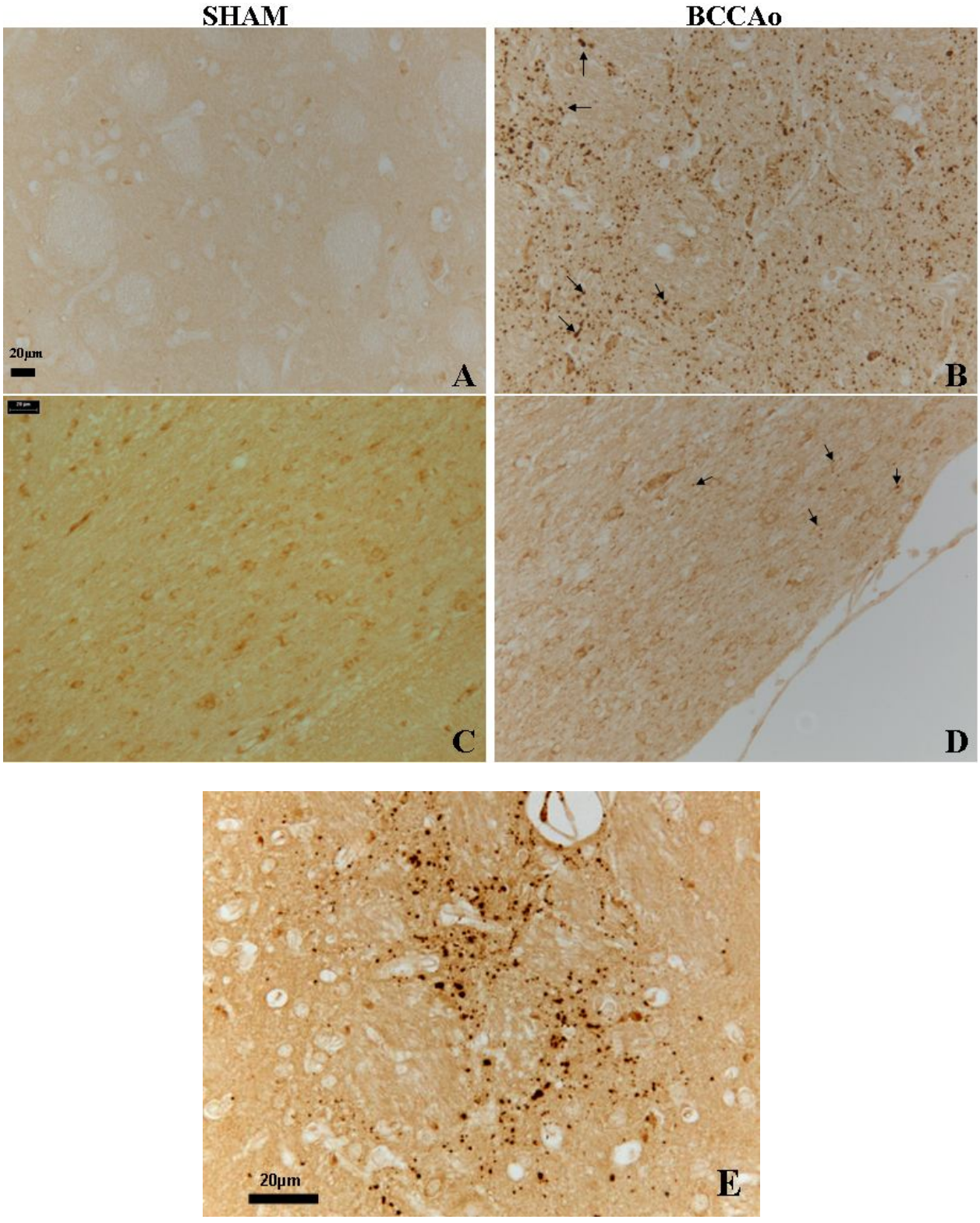

Fig.3.3: APP immunostaining in the caudatoputamen (A, B and E) and in the optic tract (C and D) following seven days of BCCAo. APP accumulation appears as dark dot (see E and arrows in B and D). No APP accumulation was detected in the sham group (A and C) after seven days of BCCAo. Axonal damage appears to be more important with time in the caudatoputamen. Scale bars in A, B, C, D: 20µm.

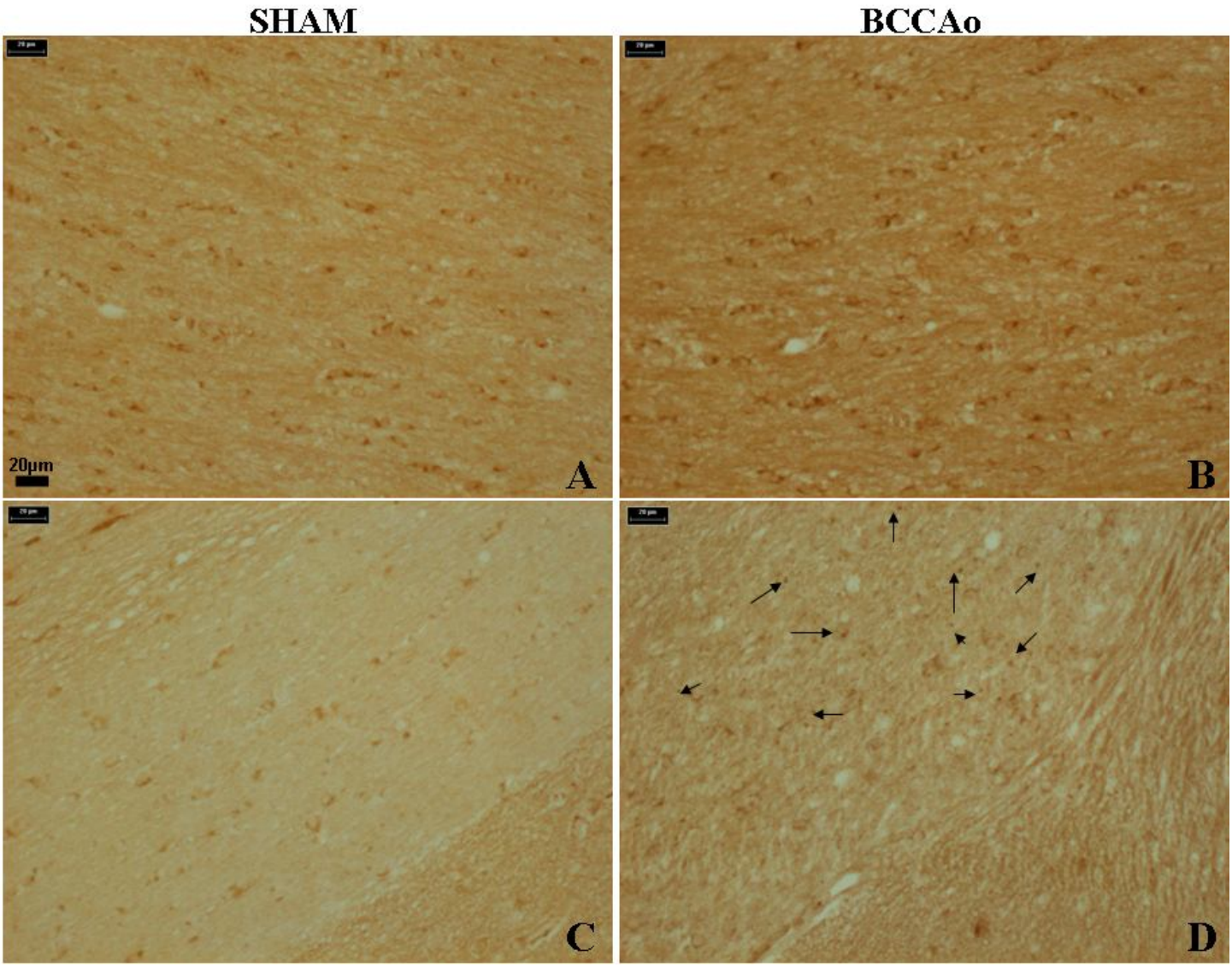

Fig.3.4: APP immunostaining in the corpus callosum (A and B) and in the optic tract (C and D) following 14 days of BCCAo. No APP accumulation was detected in the sham group after 14 days of BCCAo. Arrows in D indicate APP accumulation in the optic tract 14 days post BCCAo. Scale bars in A, B, C, D: 20µm.

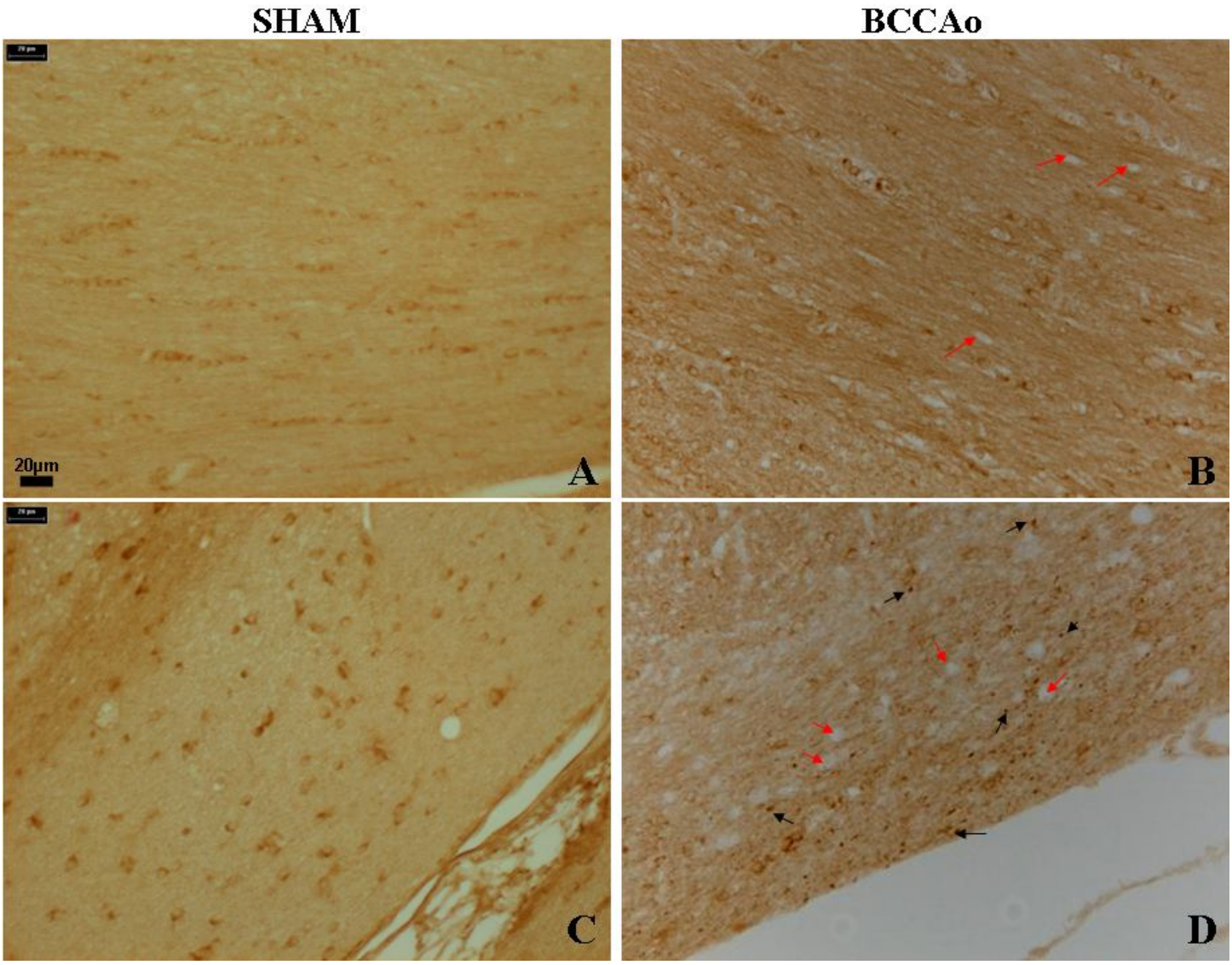

Fig.3.5: APP immunostaining in the corpus callosum (A and B) and in the optic tract (C and D) following 28 days of BCCAo. Red arrows show presence of vacuolizations in the corpus callosum (B) and optic tract (D) 28 days post BCCAo. APP aggregates are indicated on D with black arrows. Scale bars in A, B, C, D: 20µm.

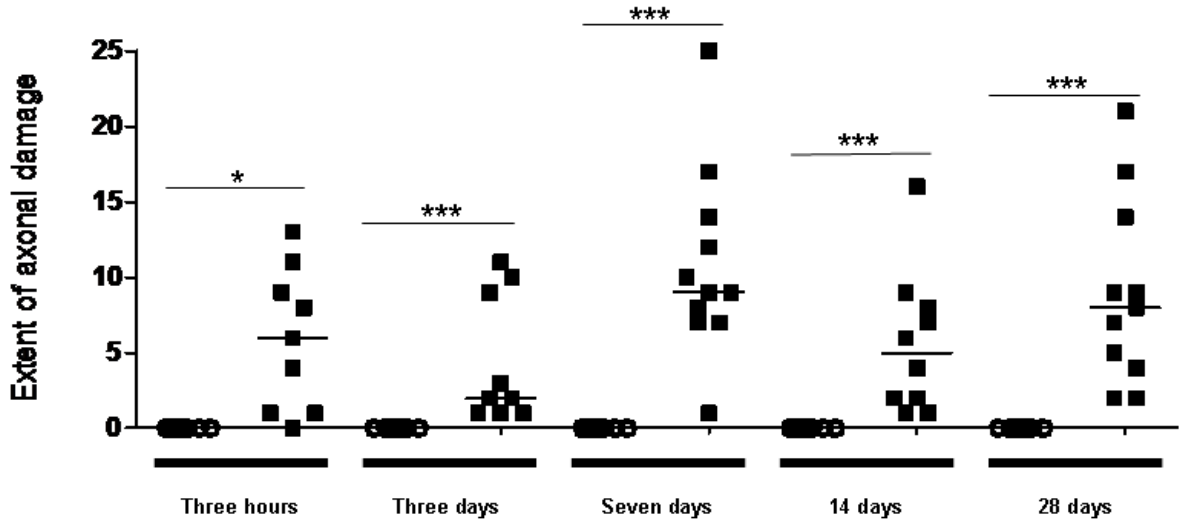

Fig.3.6: Extent of axonal damage with time (∑ grade of bihemisphere regions) following BCCAo.
Quantification of axonal damage in the APP immunostained sections. Data are presented with their median. **P<0.01, ***P<0.001 for comparison with the sham group. (Non parametric Mann-Whitney test). The number of rats in each group was:
Three hours sham, n=8; three hours BCCAo, n=9; three days sham, n=9; three days Bccao, n=9; seven days sham, n=8; seven days BCCAo, n=12; 14 days sham, n= 8; 14 days BCCAo, n=10; 28 days sham, n=9; 28 days BCCAo, n=11.

3.1.2 BCCAo-induced myelin pathology

Stained sections revealed organised networks of myelinated fibres (see black line drawn in fig.3.9A). After chronic cerebral hypoperfusion, myelin débris was detected in areas where myelin sheaths were lost as attested by vacuolisations (red arrow in fig.3.7B and 3.9B). The sham group, that had the surgery without the occlusion of the both common carotid arteries, exhibited also some débris of myelin that may be due to the background of the staining, or to the surgery when separating the vagus nerve from the common carotid artery; Fazan and Lachat (1997) showed that injury to the vagus nerve causes myelin damage in the rat. The table 3.2 presents the number of animals where myelin débris was detected in the selected regions.

After three hours of BCCAo, all white matter regions of interest exhibited myelin débris presented as dark dots (see black arrows) with presence of vacuolisations. Between the sham and the BCCAo group, the difference was significant ($p<0.05$) (Fig.3.12). Three days post occlusion, the damage to the myelin was more intense within each region, especially in the optic tract (Fig.3.8B). The presence of myelin débris in the BCCAo group was significantly ($p<0.001$) different from the sham group (fig.3.12). One more time, we can easily see how the fibers are organised in the optic tract of a sham (fig.3.8A) while in the optic tract of a three days post BCCAo, the organisation of myelin sheats is lost and the presence of myelin débris and vacuolisations increased (fig 3.8B) compared to the sham. Seven days post BCCAo, we noted an increase of myelin débris within the selected regions with more damage in the optic tract. Myelin débris (dark arrows) and vacuolisations (red arrows) were detected (see fig.3.9B). The BCCAo group was significantly different from the sham group ($p<0.001$) after seven days of occlusion (fig. 3.12). After 14 days post BCCAo, myelin débris was detected in all white matter regions (see table 3.2) and the

difference between the control and occluded group was significant ($p<0.01$) (Fig.3.12). 28 days post occlusion the damage remained severe in all white matter regions. The difference between the BCCAo and sham group was significant ($p<0.001$) (Fig.3.12).

Those results show that BCCAo causes significant damage to axon and myelin, both components of the white matter, from three hours to 28 days.

	Three hours post-BCCAo	Three days post-BCCAo	Seven days post BCCAo	14 days post-BCCAo	28 days Post-BCCAo
Caudatoputamen	**1/9**	**7/9**	**11/12**	**9/10**	**11/11**
Corpus callosum	**8/9**	**6/9**	**12/12**	**3/10**	**11/11**
External capsule	**8/9**	**8/9**	**12/12**	**7/10**	**11/11**
Fimbria	**2/9**	**9/9**	**9/12**	**8/10**	**10/11**
Internal capsule	**9/9**	**9/9**	**12/12**	**10/10**	**11/11**
Optic tract	**9/9**	**9/9**	**12/12**	**10/10**	**11/11**

Table 3.2: Number of rats in which an increase in myelin débris was detected in the regions selected as a function of time after BCCAo.

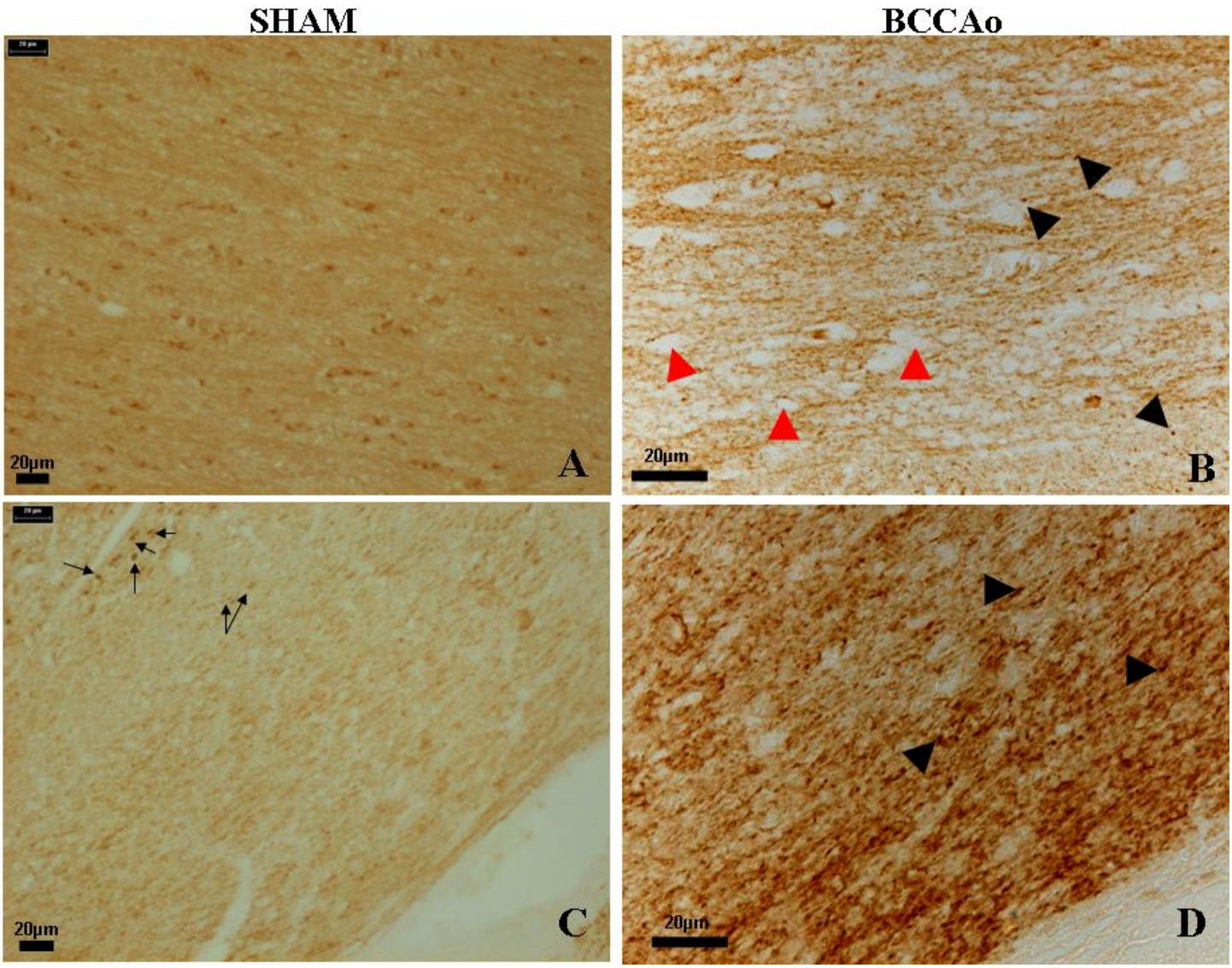

Fig.3.7: MAG immunostaining of the corpus callsoum (A and B) and optic tract (C and D). Myelin débris appear as dark dots (see black arrows). The staining also shows the presence of vacuolizations (red arrows in B) three hours after BCCAo compared to the sham-operated rats. Scale bars in A, B, C, D: 20µm.

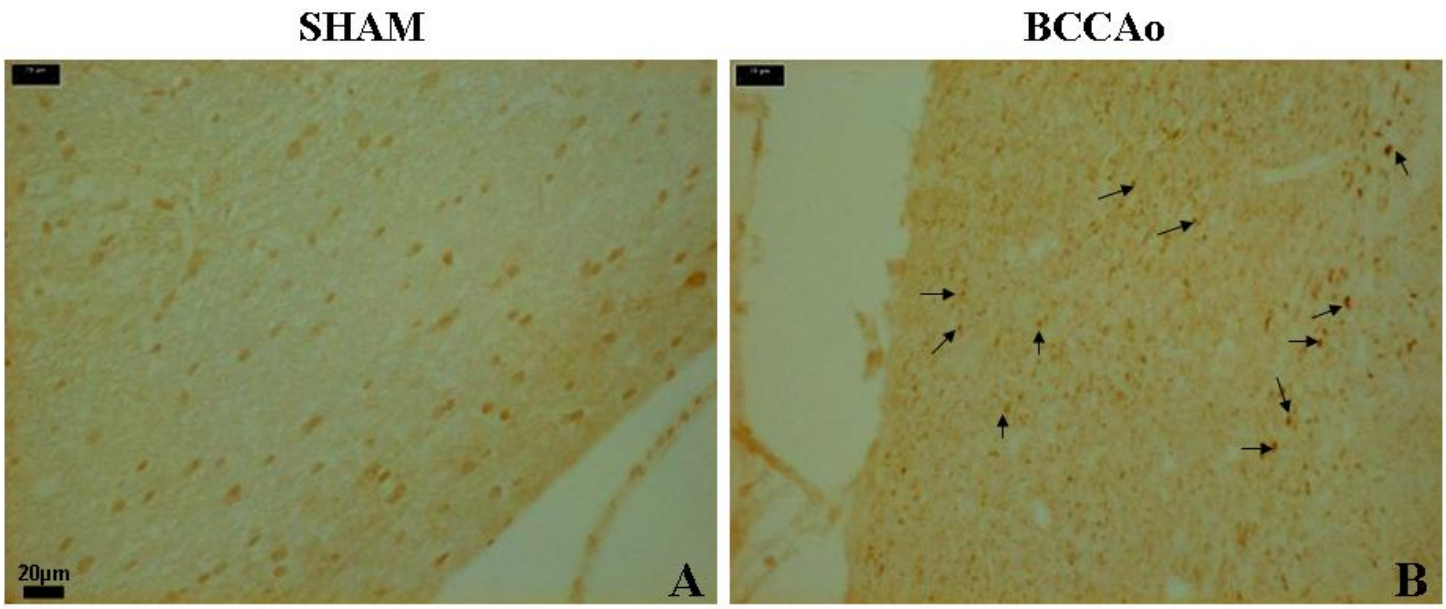

Fig.3.8: MAG immunostaining showing myelin débris which appear as small black dots (B) and presence of vacuolizations and disarrangements of fibres that occur in the optic tract following three days of BCCAo. The fibre organisation in the optic tract of the sham is well organised while in the BCCAo animal the presence of vacuolizations and myelin débris is more important. Scale bars in A, B: 20µm.

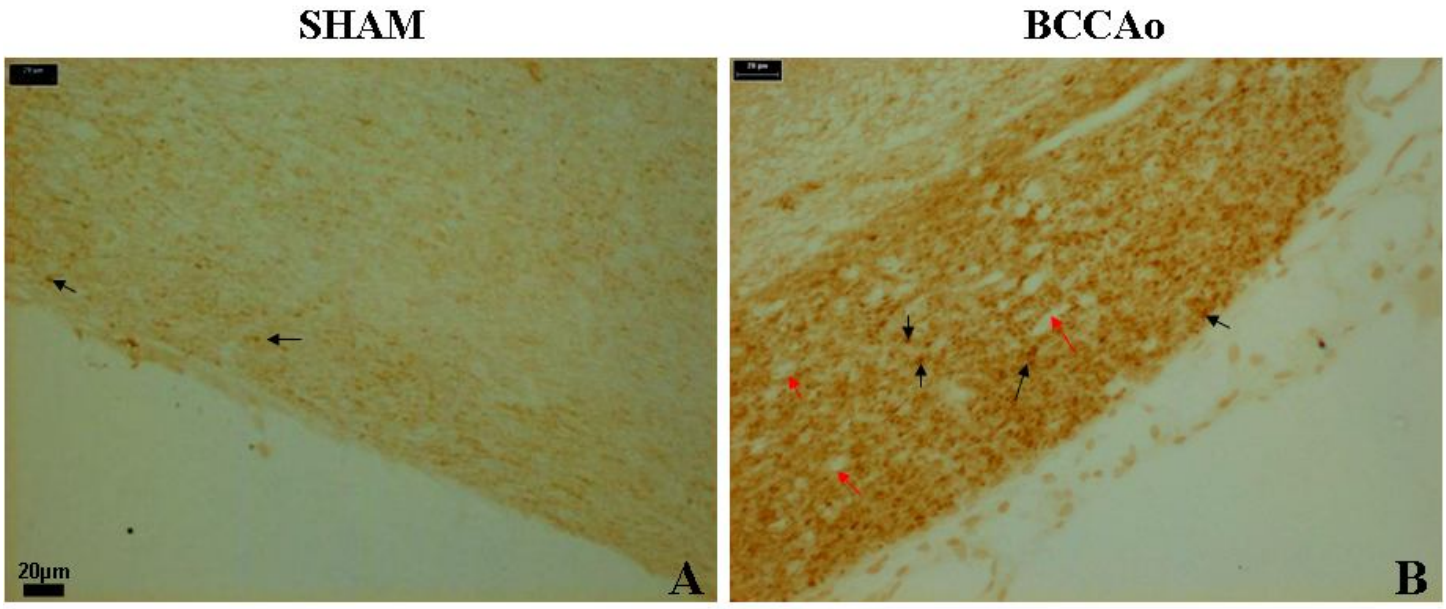

Fig.3.9: MAG immunostaining in the optic tract following seven days of BCCAo. Presence of vacuolizations (see red arrows in B) that occur in the optic tract appear to be more important with time. Scale bars in A, B: 20µm.

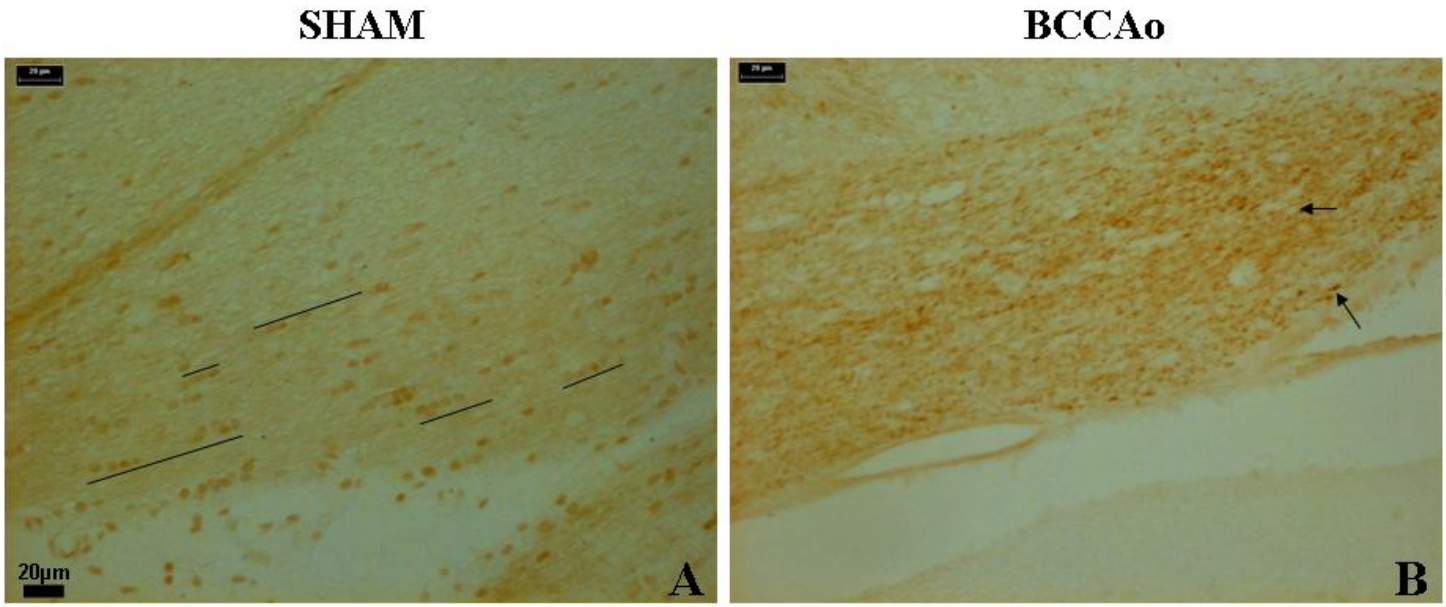

Fig.3.10: MAG immunostaining showing myelin débris which appear as small black dots (B) and presence of vacuolizations and disarrangements of fibres that occur in the optic tract following 14 days of BCCAo. The fiber organisation in the optic tract of the sham is well organised (see black line drawn on fig.3.10A) while in the BCCAo animal, the fiber of the optic tract are less organised due to the presence of vacuolizations and myelin débris (in B see black arrows). Scale bars in A, B: 20µm.

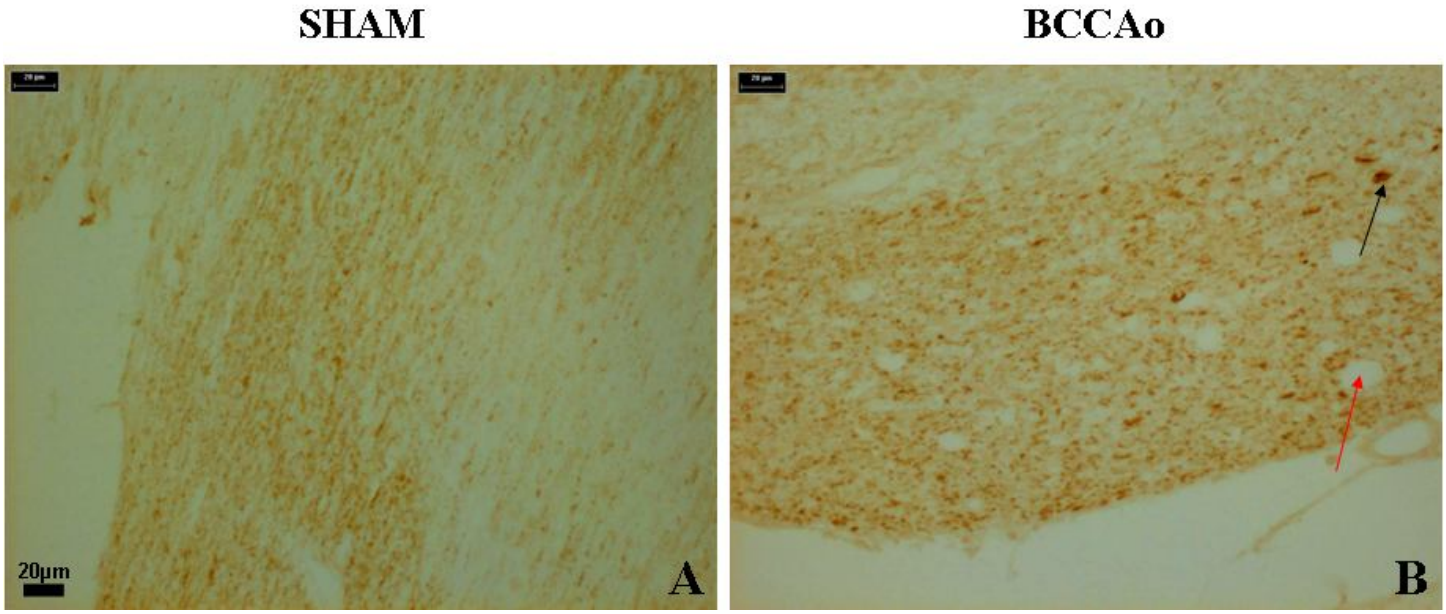

Fig.3.11: MAG immunostaining showing myelin débris (see black arrow in B) vacuolizations (in B see red arrow) and disarrangements of fibres that occur in the optic tract following 28 days of BCCAo. Scale bars in A, B: 20µm.

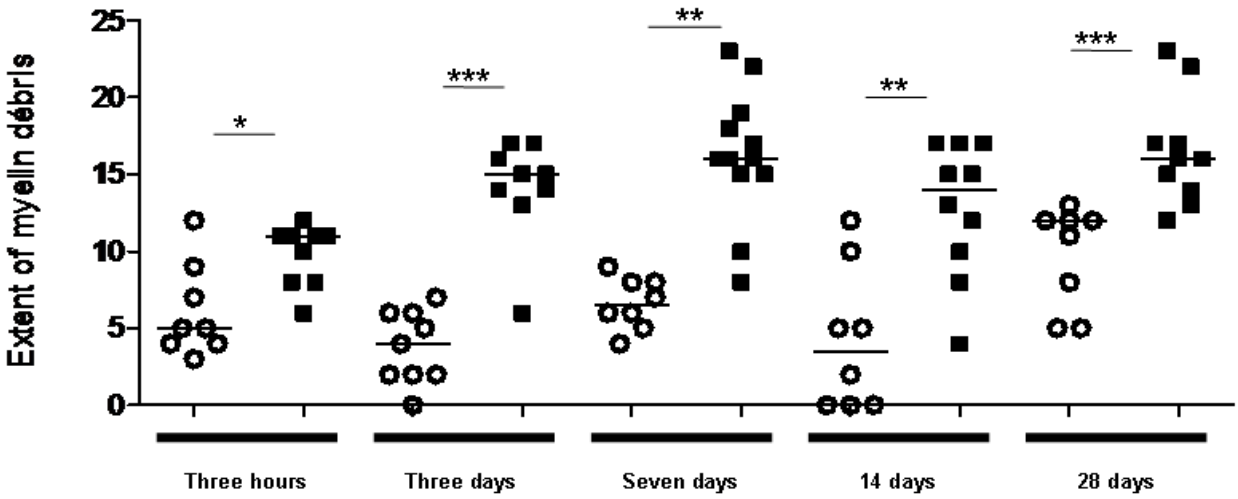

Fig.3.12: Extent of myelin pathology with time (∑ grade of bihemispheric regions) following BCCAo.
Quantification of myelin débris in the MAG immunostained sections. Data are presented with their median. *P<0.05, **P<0.01, ***P<0.001 for comparison with the sham group. (Non parametric Mann-Whitney test).
The number of rats in each group was:
Three hours sham, n=8; three hours BCCAo, n=9; three days sham, n=9; three days Bccao, n=9; seven days sham, n=8; seven days BCCAo, n=12; 14 days sham, n= 8; 14 days BCCAo, n=10; 28 days sham, n=9; 28 days BCCAo, n=11.

3.1.3 BCCAo-induced enhancement of microglial activation

Iba-1 immunostained sections revealed a minimal presence of enhancement of activated microglia in the sham group (Fig.3.13A-C), which can be explained by the surgery and the removal of the common carotid artery from the connective tissue that include the common carotid artery with the vagus nerve.

The quantification of those slides revealed that after three hours of occlusion, there was no enhancement of activated microglia compared to the sham (Fig.3.18) in all the regions of interest. At this stage, ramified microglia do not have the morphology of macrophages. Three days post occlusion, significant ($p<0.001$) enhancement of activated microglia was detected in the Iba-1 immunostained sections of the BCCAo group compared to the sham. The caudatoputamen and the optic tract being the regions that exhibited the more enhancement of activated microglia. After seven days of BCCAo, the enhancement of activated microglia was significantly ($p<0.001$) different from the control group (Fig.3.18). The caudatoputamen and the optic tract being the regions that exhibited the more enhancement of microglial activation detected in most of BCCAo rats (table 3.3). Enhancement of activated microglia appears to be more important in the caudatoputamen (B) and optic tract (D) compared to the sham (A and C). Moreover, the ramifications in microglia present in the caudatoputamen of BCCAo rats (fig.3.15B) seem to be more important than those detected in the sham rats (fig.3.15A). This may indicates a change in the phenotype process of transition of microglia to macrophages with a possible recruitement of leukocytes from the bloodstream (see fig.3.15E).

14 days post BCCAo, the enhancement of activated microglia was substantial in all the regions with a significant difference ($p<0.05$) compared to the sham group (Fig.3.18). The figure 3.16B shows microglia in close contact with endothelial

cerebral vessel which may indicate that the stage of leukocytes recruitement from the bloodstream may continue after 14 days post BCCAo. 28 days post occlusion the level of enhancement of microglial activation was detected, being significantly different ($p<0.01$) to the control group (Fig.3.18). The few level of microglia was observed in the fimbria while the optic tract was the region exhibiting the more enhancement of microglial activation compared to the control, associated with many vacuolisations, indicative of white matter damage (Fig.3.17D). At this stage, microglia phenotype had probably changed. The figure 3.17B may show macrophages. Those results showed that after three hours of BCCAo, no enhancement of activated microglia was observed compared to the sham group. It is from three days post BCCAo that a significant difference in term of enhancement of activated microglia compared to the sham group was detected, until 28 days post BCCAo. Interestingly, the regions, which most animal present enhancement of microglial activation with time post BCCAo, are the caudatoputamen, the internal capsule and the optic tract (see table 3.3).

	Three hours post-BCCAo	Three days post-BCCAo	Seven days post BCCAo	14 days post-BCCAo	28 days Post-BCCAo
Hippocampus	**0/9**	**0/9**	**3/12**	**10/10**	**2/11**
Caudatoputamen	**0/9**	**6/9**	**11/12**	**10/10**	**4/11**
Corpus callosum	**0/9**	**2/9**	**3/12**	**10/10**	**3/11**
External capsule	**0/9**	**2/9**	**3/12**	**10/10**	**3/11**
Fimbria	**0/9**	**0/9**	**3/12**	**10/10**	**1/11**
Internal capsule	**0/9**	**4/9**	**7/12**	**10/10**	**6/11**
Optic tract	**0/9**	**5/9**	**12/12**	**10/10**	**10/11**

Table 3.3: Number of rats in which an increase in enhancement of microglial activation was detected in the regions selected as a function of time after BCCAo.

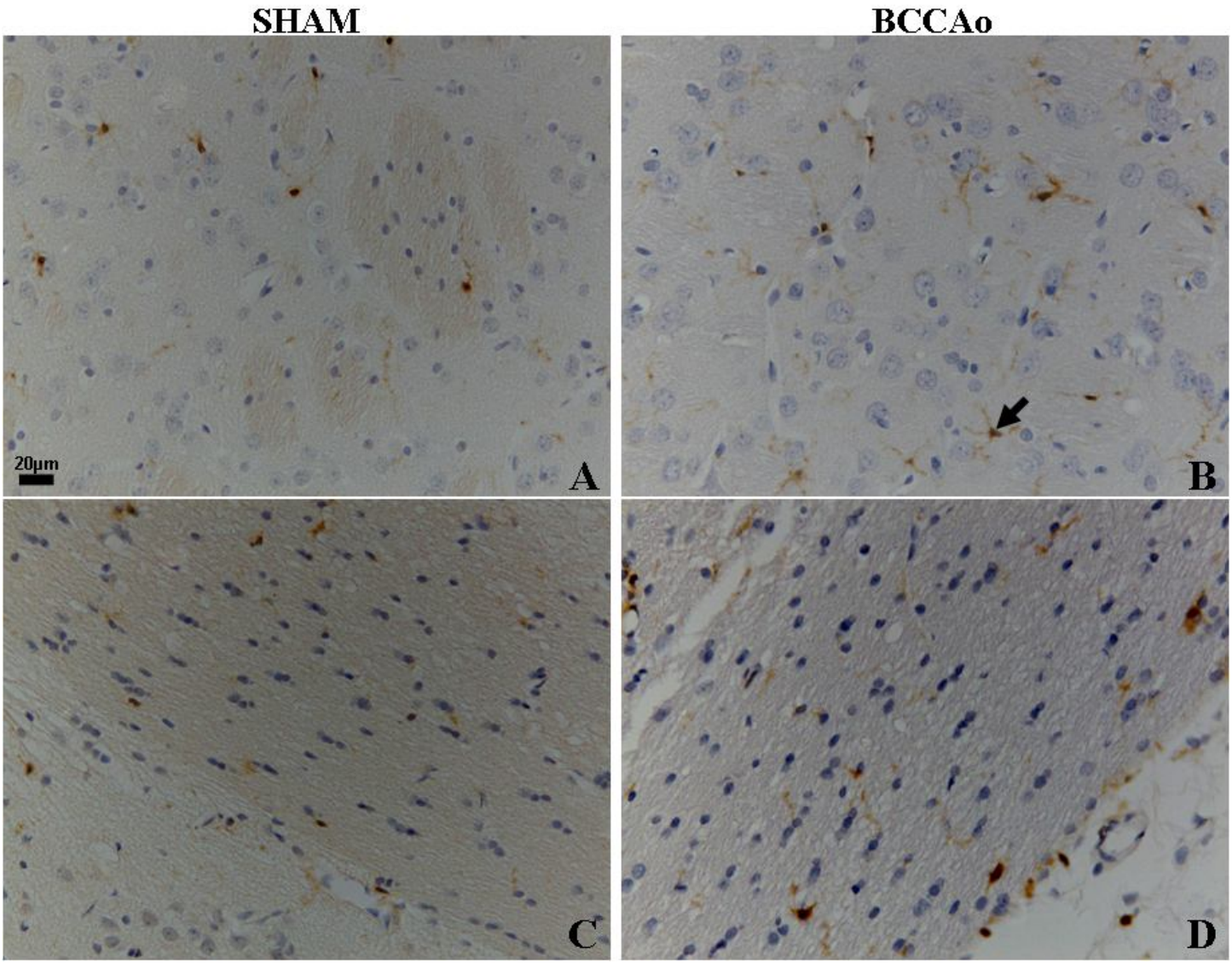

Fig.3.13: Iba-1 immunostaining of microglia (brown) in the caudoputamen (A and B) and in the optic tract (C and D) following three hours of BCCAo. Microglia (see arrow in B) appear as ramified cells structures. Scale bars in A, B: 20µm.

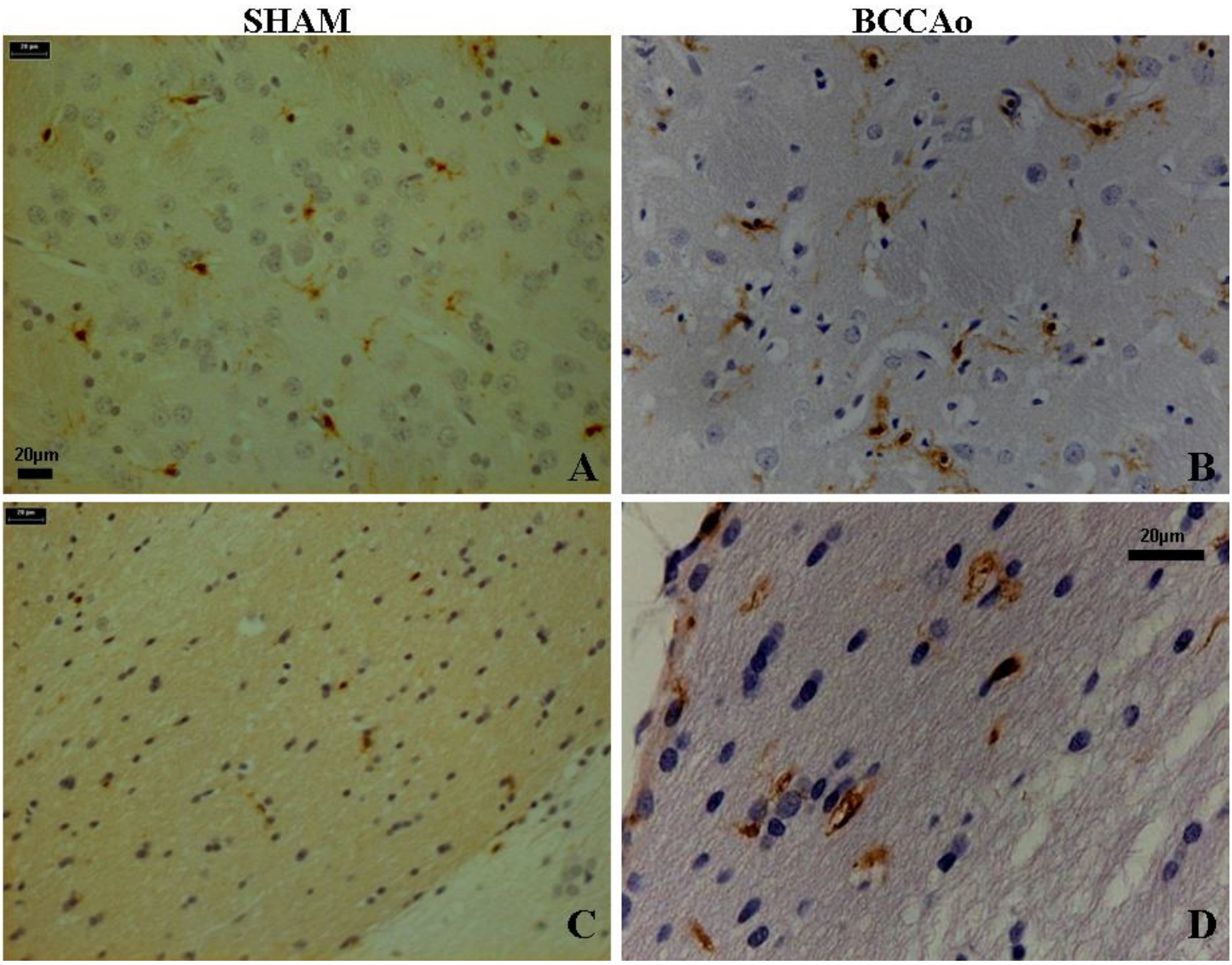

Fig.3.14: Iba-1 immunostaining of microglia (brown) in the caudoputamen (A and B) and in the optic tract (C and D) following three days of BCCAo. At this stage oligodendrocytes appear to be still organised in the optic tract of BCCAo rats (D). Scale bars in A, B, C, D: 20µm.

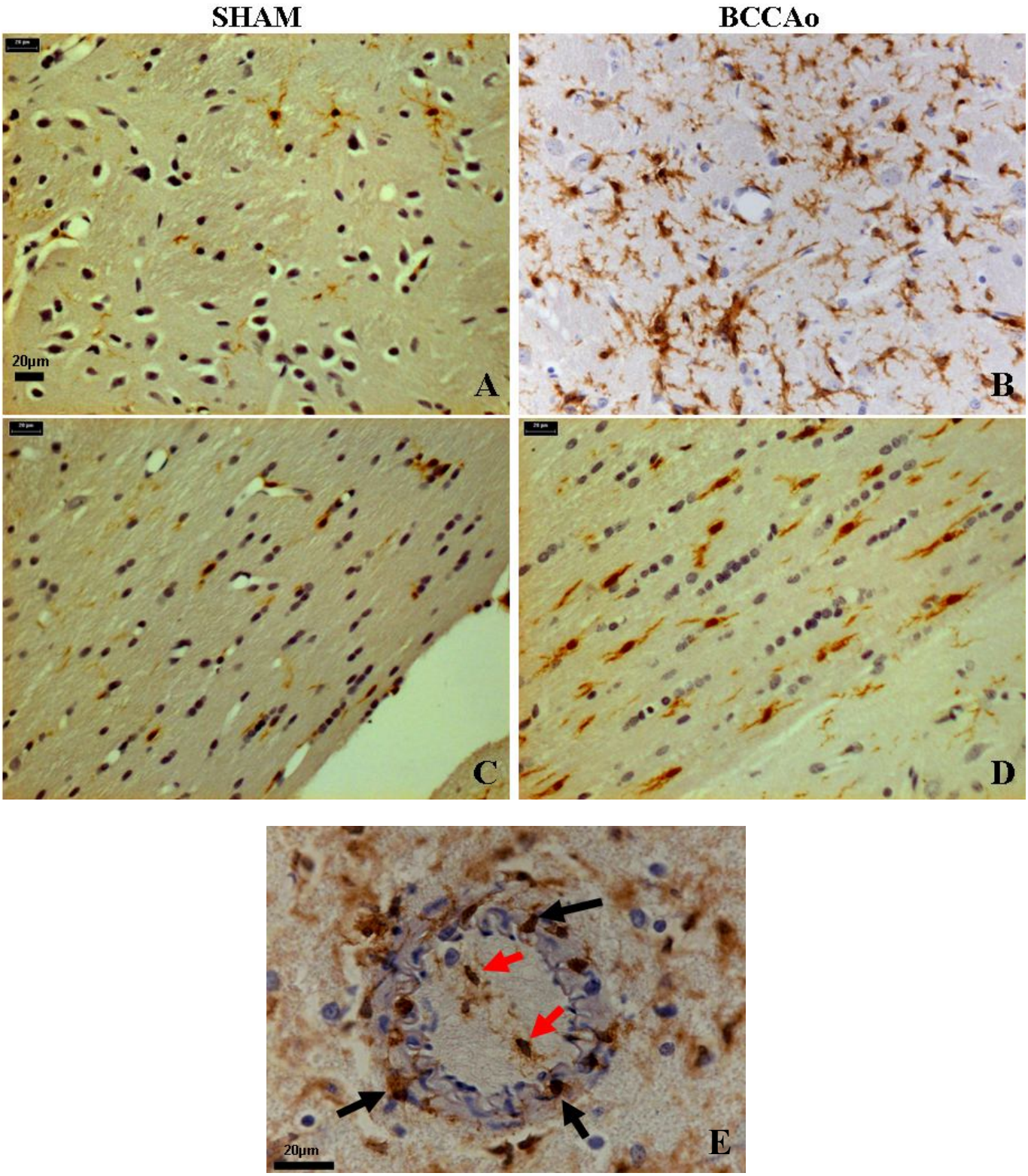

Fig.3.15: Iba-1 immunostaining of microglia (brown) in the caudoputamen (A and B) and in the optic tract (C and D) following seven days of BCCAo. Enhancement of activated microglia appears to be more important in the caudatoputamen (B) and optic tract (D) compared to the sham (A and C). The close contact to the vessel of microglia (black arrow in E) may lead to a recruitement of leukocytes from the bloodstream (red arrow in E). Scale bars in A, B, C, D: 20µm.

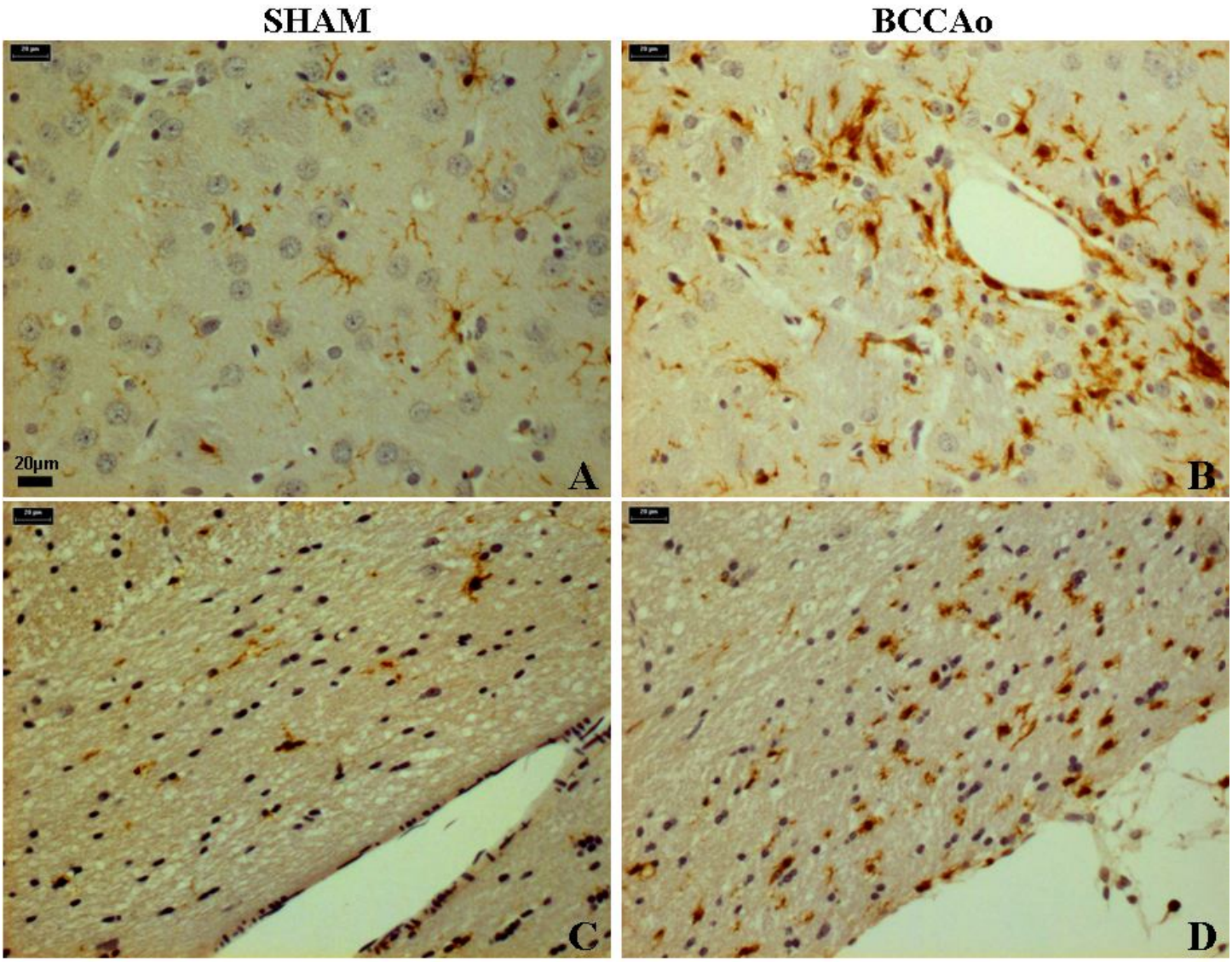

Fig.3.16: Iba-1 immunostaining of microglia (brown) in the caudoputamen (A and B) and in the optic tract (C and D) following 14 days of BCCAo. Picture B shows microglia in close contact with endothelial cells of the vessel which can indicate a possible recruitement of leukocytes. Oligodendrocytes (which appears in blue dark) in the optic tract of sham (C) are aligned while in BCCAo rats (D) oligodendrocytes are not aligned which indicates disarrangements of fibres. Microglial activation appears to be manifest at this stage. Scale bars in A, B, C, D: 20µm.

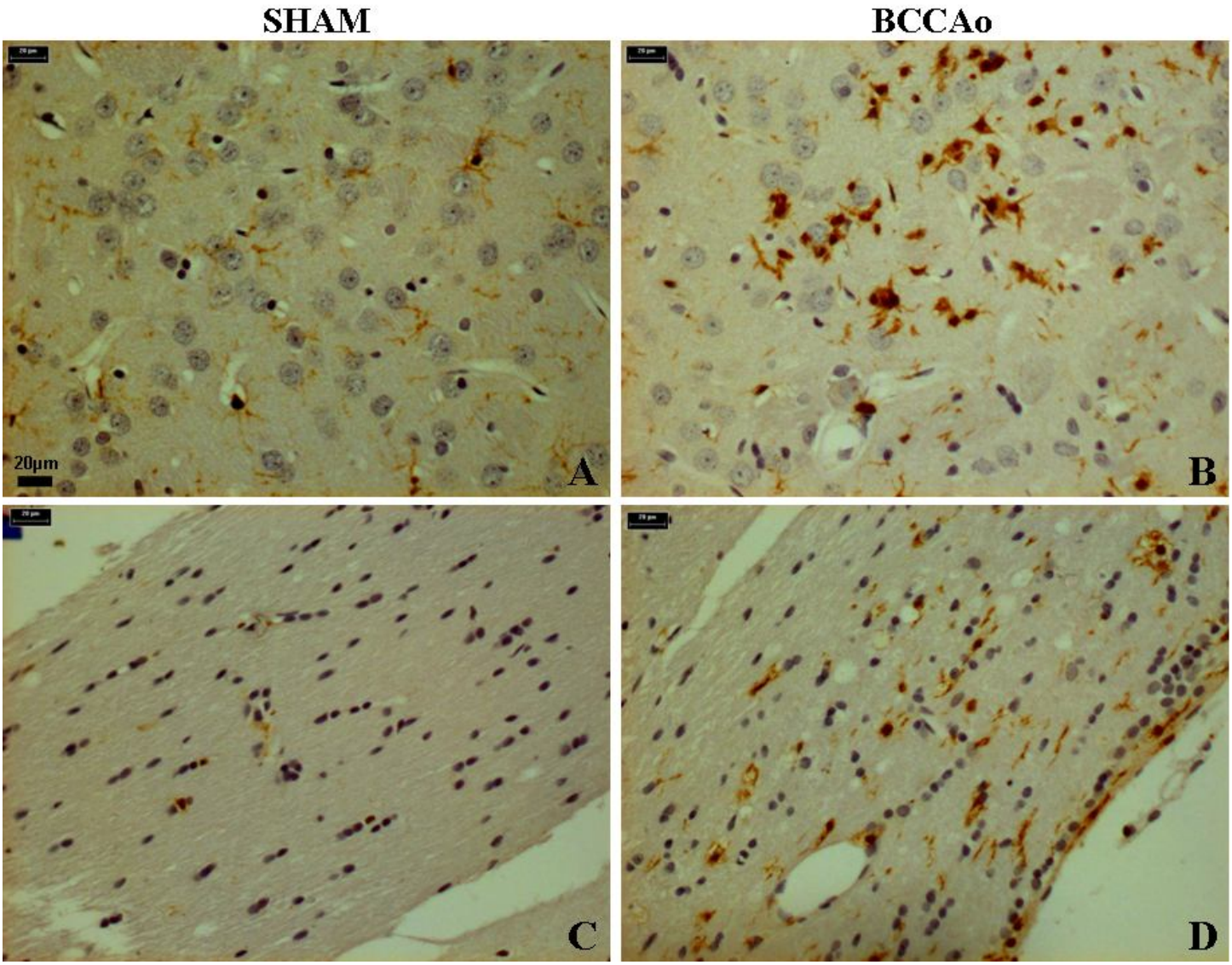

Fig.3.17: Iba-1 immunostaining of microglia (brown) in the caudoputamen (A and B) and in the optic tract (C and D) following 28 days of BCCAo. At this stage the phenotype of microglia in the caudatoputamen of BCCAo rats (B) seems to be different than the one in the sham (A). In B it is probably macrophages. Scale bars in A, B, C, D: 20µm.

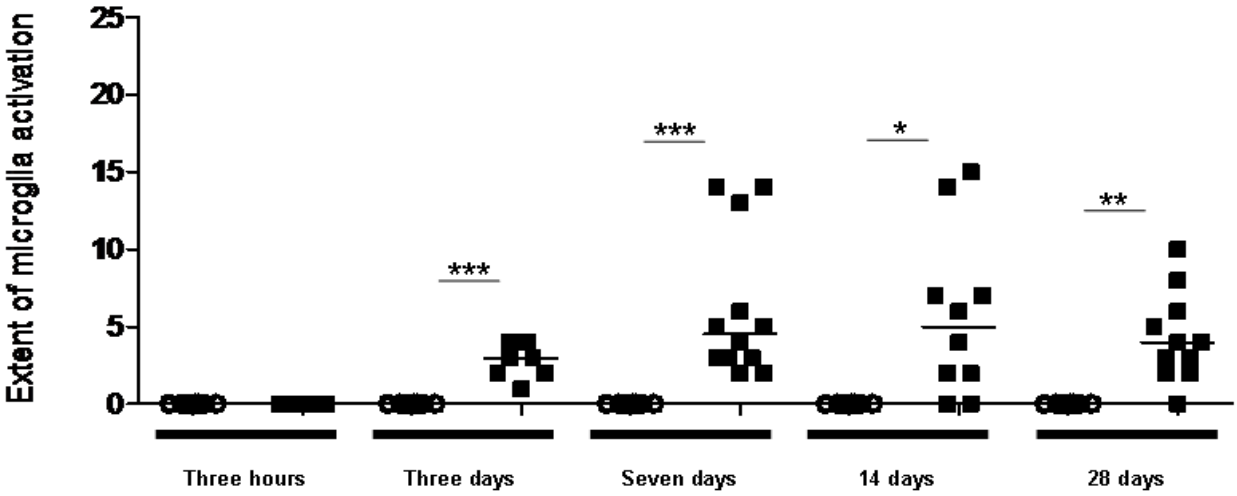

Fig.3.18: Extent of enhancement of microglial activation with time (∑ grade of bihemispheric regions) following BCCAo.
Quantification of microglial activation in the Iba-1 immunostained sections. Data are presented with their median. *P<0.05, **P<0.01, ***P<0.001 for comparison with the sham group. (Non parametric Mann-Whitney test).
The number of rats in each group was:
Three hours sham, n=8; three hours BCCAo, n=9; three days sham, n=9; three days Bccao, n=9; seven days sham, n=8; seven days BCCAo, n=12; 14 days sham, n= 8; 14 days BCCAo, n=10; 28 days sham, n=9; 28 days BCCAo, n=11.

3.1.4 BCCAo-induced damage to neuronal perikarya

H&E stained sections were used to quantify ischaemic neurons (section 2.2.4), in the hippocampus and in the caudatoputamen. Damage to the perikarya of the neurons are defined by an intense darkly stained pyknotic nucleus surrounded by eosinophilic cytoplasm while healthy neurons have large round nuclei and cell bodies visible cytoplasmic structures. After three hours of BCCAo, no ischaemic neurons were detected (see fig.3.19) neither in the hippocampus, nor in the caudatoputamen (table 3.4). Three days post occlusion, some animals exhibited ischaemic neurons in the caudatoputamen and in the hippocampus (fig.3.20B). Only three rats out of nine exhibited damage to the perikarya of neurons in the caudatoputamen, while one rat out of nine presented no ischaemic neuronal parikaryal damage to the hippocampus (table 3.4), hence no significant difference was observed between the control (sham) and BCCAo group (Fig.3.24). After seven days of BCCAo, the damage to the perikarya of neurons was detected in the hippocampus and being more intense in the caudatoputamen (Fig.3.21). Knowing that ten out of twelve rats exhibited neuronal perikaryal damage, the difference between the control and the BCCAo group was significant ($p<0.005$) (Fig.3.24). This result indicates that hippocampus is not the area that is preferably damage after BCCAo. 14 days post occlusion, five out of ten rats presented damage to the perikarya of neurons (Fig.3.24), mainly found in the caudatoputamen (five out of ten rats) while only one out of five who present ischaemic damage has neuronal parikaryal damage to the hippocampus (table 3.4 and fig.3.22), but this was not sufficient to find any statistical differences between the sham and BCCAo group (Fig.3.24). 28 days post occlusion (fig.3.23), the number of rats that exhibited ischaemic damage was less to what we found previously knowing that four out of eleven rats only (see table 3.4) exhibited ischaemic neuronal

perikaryal damage. Thus, no significant difference was observed between the control and BCCAo group (Fig.3.24).

Those data suggest that the chronic cerebral hypoperfusion model lead to a minimal detection of ischaemic neurons at three, 14 and 28 days. However, this experiment revealed two interesting times point: after three hours of permanent BCCAo, no damage to the hippocampus and/or caudatoputamen was detected, while severe neuronal perikaryal damage was observed seven days post BCCAo. Secondly, the hippocampus seems to be better preserved than the caudatoputamen with time post BCCAo. Indeed, only few animals exhibited ischaemic neuronal damage with time. The number of ischaemic neurons appears to be reduced with time post BCCAo, which may be explained either by the fact that microglial cells act as "housekeepers" by cleaning up ischaemic cell death, which may lead to the conclusion that less ischaemic damage was present, just because we cannot detect them. Or this can also be explained by the fact that the BCCAo model change with time and animals.

	Three hours post-BCCAo	Three days post-BCCAo	Seven days post BCCAo	14 days post-BCCAo	28 days Post-BCCAo
Hippocampus	**0/9**	**2/9**	**3/12**	**1/10**	**2/11**
Caudatoputamen	**0/9**	**3/9**	**10/12**	**5/10**	**4/11**

Table 3.4: Number of rats in which an increase in ischaemic neuronal perikaryal damage was detected in the regions selected as a function of time after BCCAo.

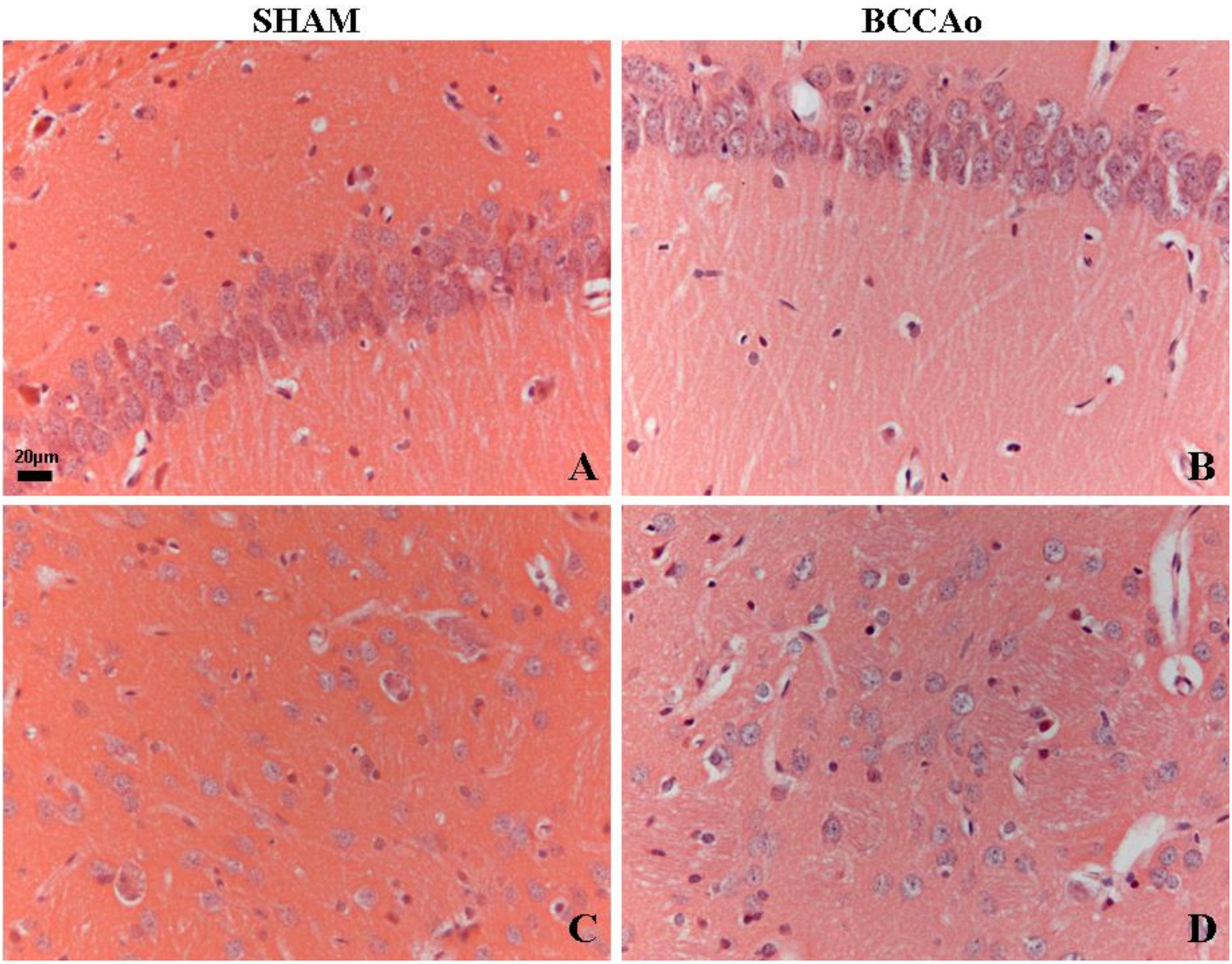

Fig.3.19: H&E staining in the Ca1 area: monolayer of the hippocampus (A-B) and in the caudatoputamen (C-D) following three hours post BCCAo. Scale bars in A, B, C, D: 20µm.

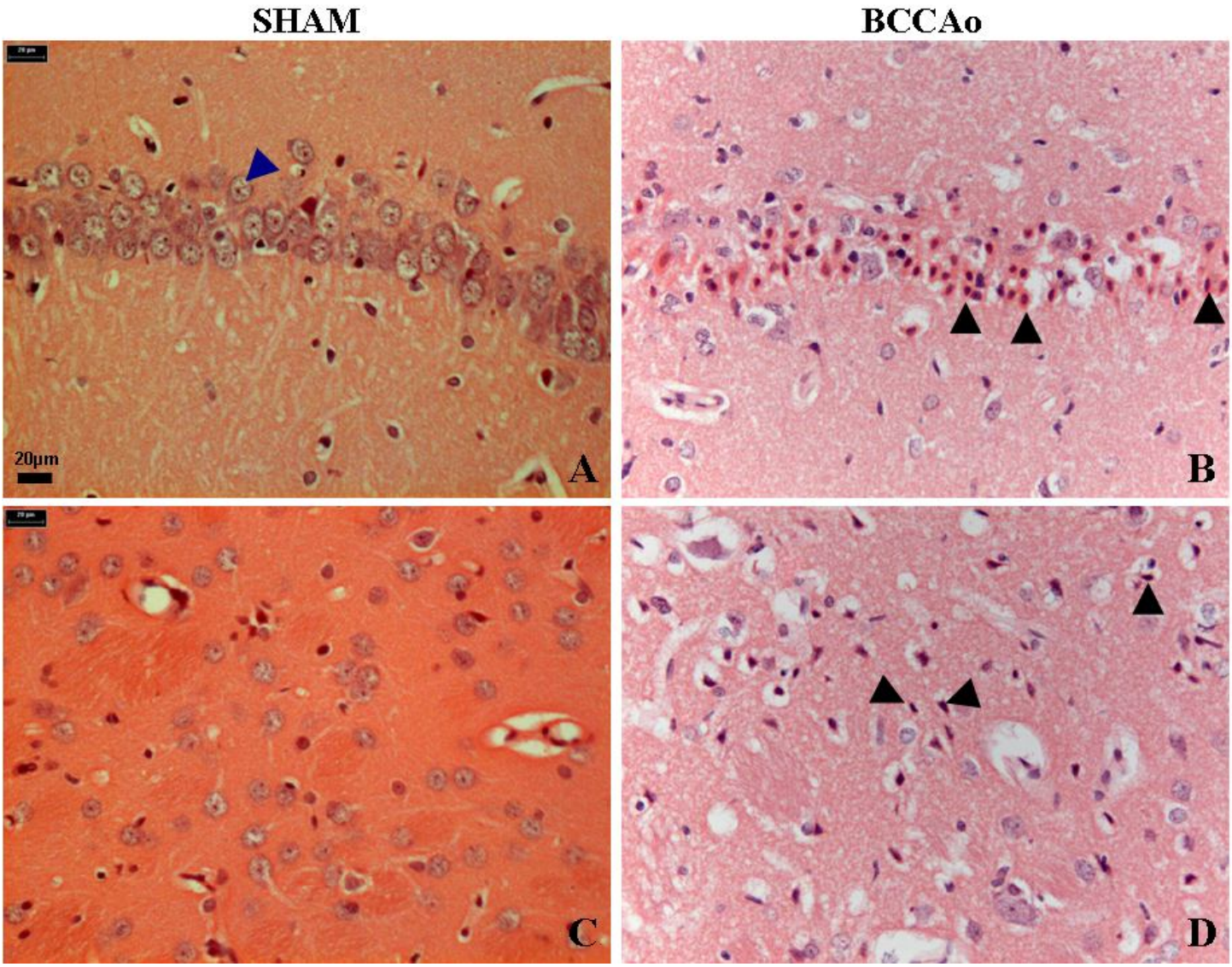

Fig.3.20: H&E staining in the Ca1 area: monolayer of the hippocampus (A-B) and in the caudatoputamen (C-D) following three days post BCCAo. Ischaemic neuronal perikaryal damage can be clearly observed (see black arrows in B). Healthy neurons should appear as round with a clear nucleus and cytoplasm (see blue arrow in A). Ischaemic neurons appear with a shrinked cytoplasm (see arrows in D) and an intense pink coloration (see arrows in B). Scale bars in A, B, C, D: 20µm.

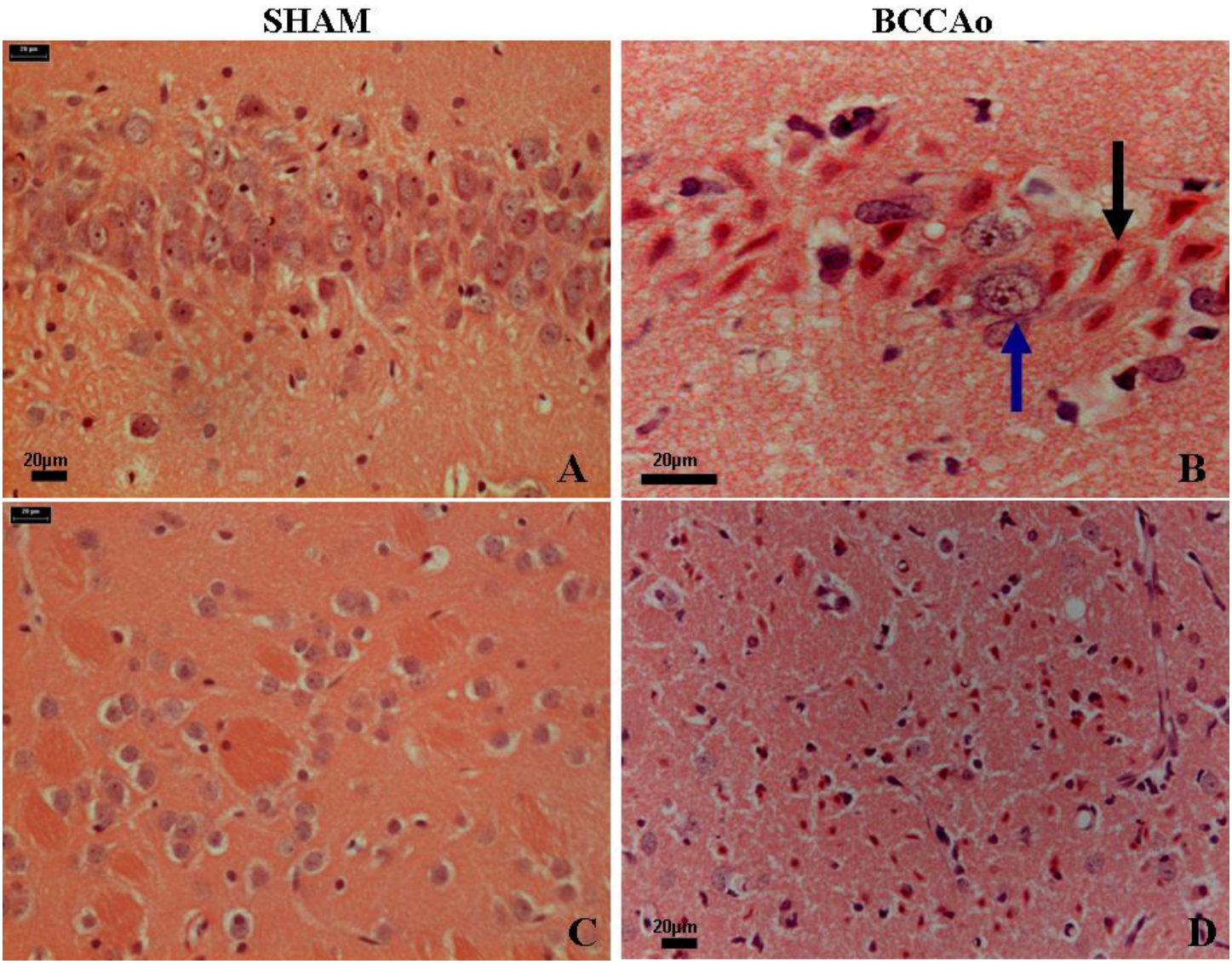

Fig.3.21: H&E staining in the Ca1 layer of the hippocampus (A-B) and in the caudatoputamen (C-D) following seven days post BCCAo. Ischaemic neurons have a shrunken cytoplasm and are intensely hyperchromatic (black arrow in B) compared to adjacent healthy neurons with their round, clear nuclei (blue arrow in B). Scale bars in A, B, C, D: 20µm.

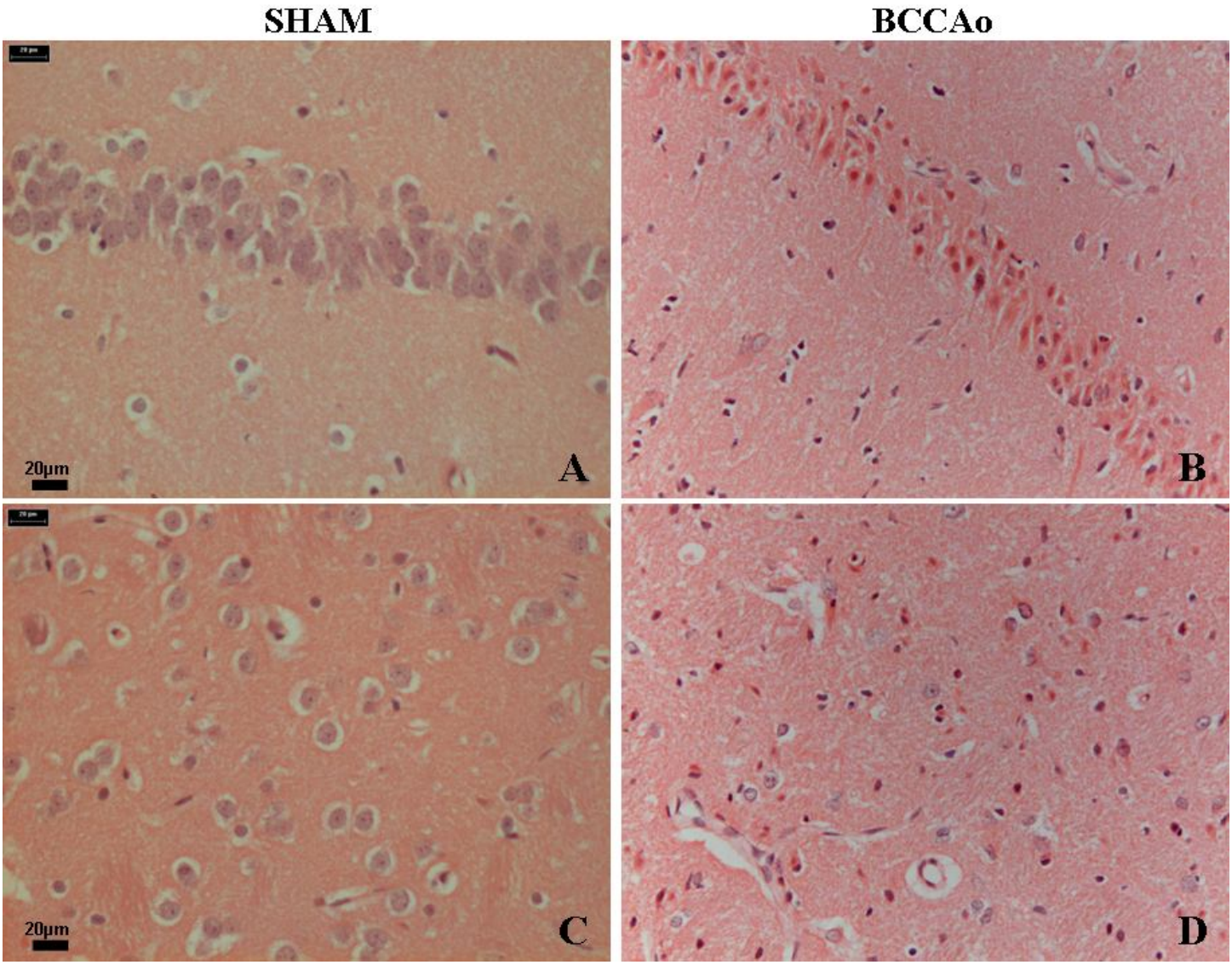

Fig.3.22: H&E staining in the Ca1 area: monolayer of the hippocampus (A-B) and in the caudatoputamen (C-D) following 14 days post BCCAo. (B-D X100). Further details are given in the legends of fig.3.20 and 3.21.

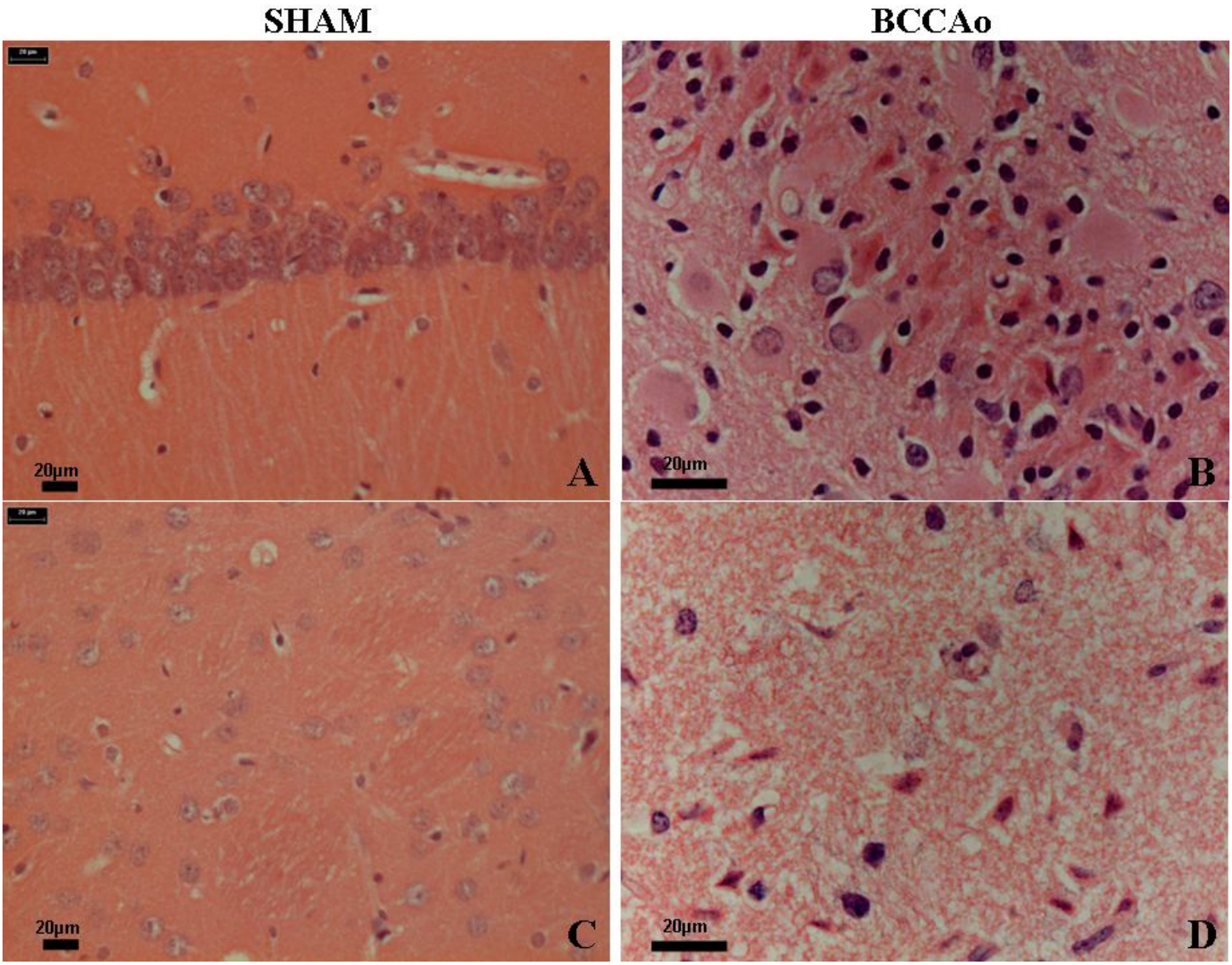

Fig.3.23: H&E staining in the Ca1 area: monolayer of the hippocampus (A-B) and in the caudatoputamen (C-D) following 28 post BCCAo. Further details are given in the legends of fig.3.20 and 3.21. Scale bars in A, B, C, D: 20µm.

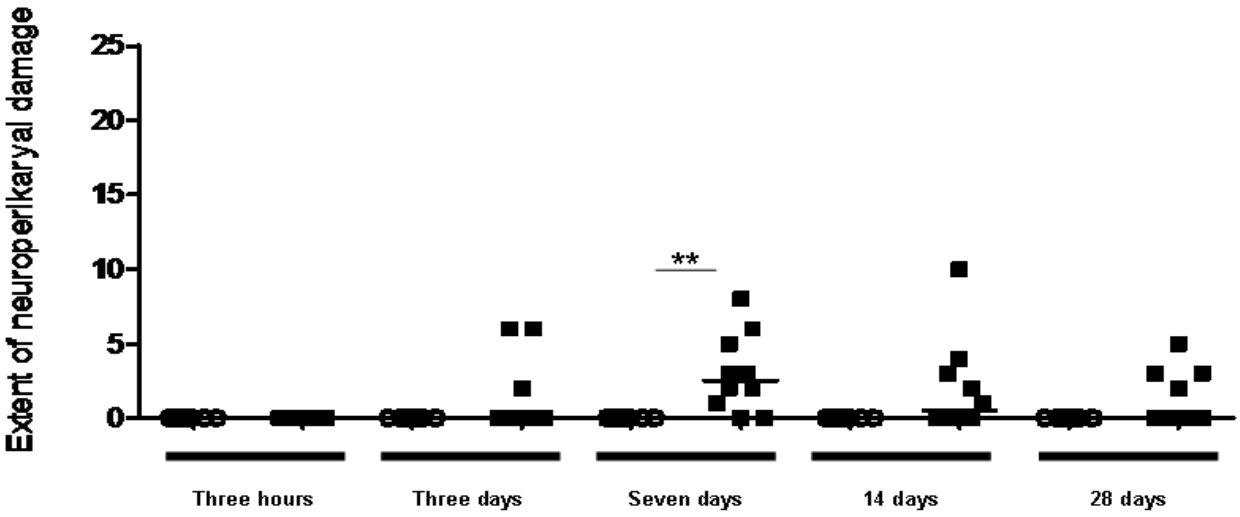

Fig.3.24: Extent of neuronal perikaryal damage with time (∑ grade of bilateral regions) following chronic cerebral hypoperfusion. Quantification of H&E stained sections. Data are presented with their median. **P<0.005 for comparison with the sham group. (Non parametric Mann-Whitney test).
Sham 3 hours, n=8; Bccao 3 hours, n=9; Sham 3 days, n=9; Bccao 3 days, n=9; Sham 7 days, n=8; Bccao 7 days, n=12; Sham 14 days, n= 8; Bccao 14 days, n=10; Sham 28 days, n=9; Bccao 28 days, n=11.

Previous studies on chronic cerebral ischaemia, lacunar infarction or arterial hypertension (Feigin an Popoff, 1963; Tomimoto et al., 1996; Akiguchi et al., 1997) have postulated that white matter damage is related to BBB dysfunction (Wardlaw, 2010). These hypotheses explain why vascular dysfunction is critical in cerebrovascular diseases. BCCAo is a well-characterised model amd especially so at later time point. Nonetheless, the literature is sparce with respect to changes of BBB integrity during chronic cerebral hypoperfusion. Some authors have shown significant changes within the periventricular area of the corpus callosum at three days after BCCAo (Sood et al., 2008; Ueno et al., 2002). Shin and collaborators have demonstrated an increase of claudin-3 immunoreactivity without an explicit discussion as to whether is associated with changes or not in terms of permeability of the BBB. Indeed, it has been demonstrated that increases in claudin-3 expression interfere and, consequently, decrease the permeability of the tight junctions (Coyne et al., 2003; Wolburg et al., 2003). On the other hand, chronic inflammatory stress increased BBB permeability and claudin-3 expression (Brooks et al., 2005). Because SVD are almost synonymous with hypoperfusion of the brain, it remains to be established if BBB permeability is responsible for the damage to the white matter at precocious (three hours post BCCAo) time-points and if BBB integrity may be perturbed seven days after BCCAo, the time at which we observed the most severe pathology in the period of time we observed the evolution of neuropathology following BCCAo.

3.2 BBB integrity after BCCAo in the rat model using MRI

3.2.1 NMDA positive control for BBB permeability

Three anaesthetized adult male Wistar rats (280-320g) were injected NMDA into one hemisphere (ipsilateral) and a PBS injection into the other hemisphere (contralateral). The Hamilton tracks in the brain can be observed in the T2 structural image (fig.3.25 and 3.26 A) by the increase in permeability of the BBB to the gadolinium next to the injection site in both hemispheres (contralateral and ipsilateral). That latter can be detected on the T1 image which shows the signal enhancement of gadolinium (Fig.3.26 B). However, the introduction of the needle containing the solution of NMDA into the ipsilateral cortex leads to a significant enhancement of gadolinium signal ($p<0.001$) compared to the contralateral cortex (fig.3.26 E) in the three animals. The volume of increased gadolinium density was visually greater with the excitotoxic agent (NMDA) than with the physiological vehicle (PBS).

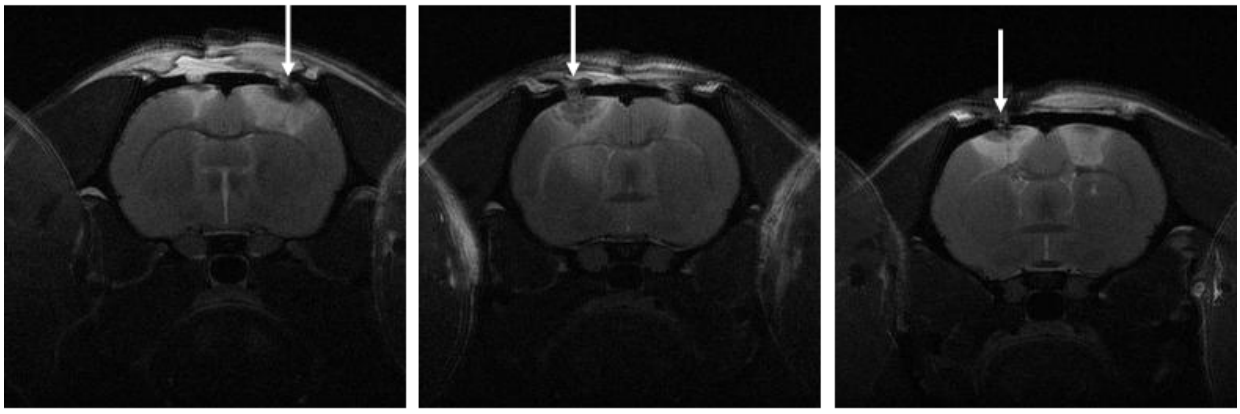

Fig.3.25: T2-weighted structural images to show the injection of NMDA into one hemisphere (ipsilateral) and PBS in the other hemisphere (contralateral) in the three rats. The ipsilateral hemisphere is annoted by a white arrow.

Figure 3.26F represents data from one rat; the two other had an injection limited to the temporal cortex (see fig.3.25, on T2 images acquisitions). The data from one animal (fig.3.26 F) compares the caudatoputamen which received the NMDA injection (ipsilateral) with the caudatoputamen which received the PBS injection (contralateral).

The IgG immunostained sections at the level of the caudatoputamen revealed an uptake of the IgG into the perikarya of the ipsilateral caudatoputamen (Fig.3.26 C), while no such uptake was observed in the contralateral caudatoputamen (fig.3.26 D). The measurement of the gadolinium enhancement showed a significant difference between the ipsilateral and contralateral caudatoputamen, which indicates an increase of the permeability of the BBB (Fig.3.26 F).

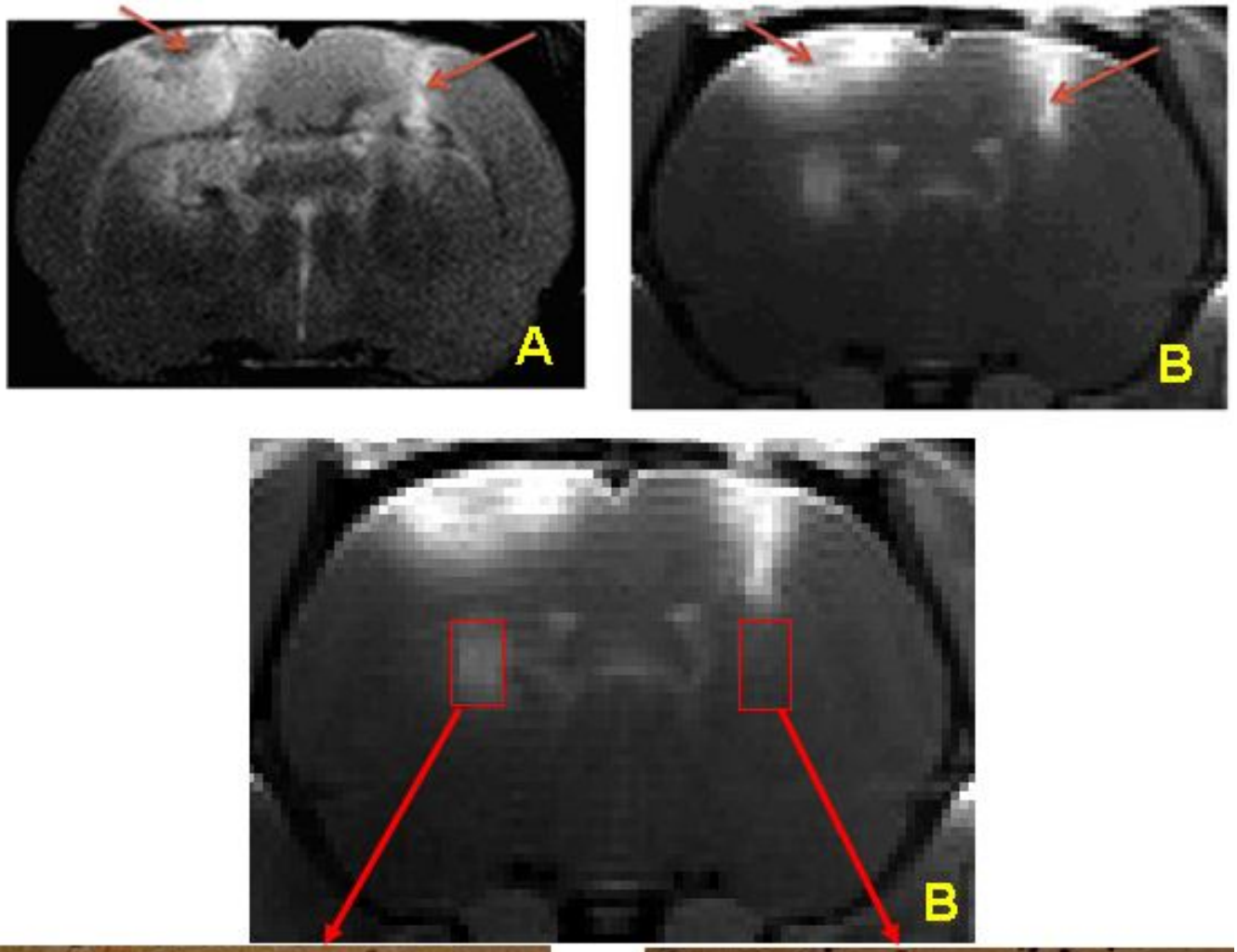

Ipsilateral

Contralateral

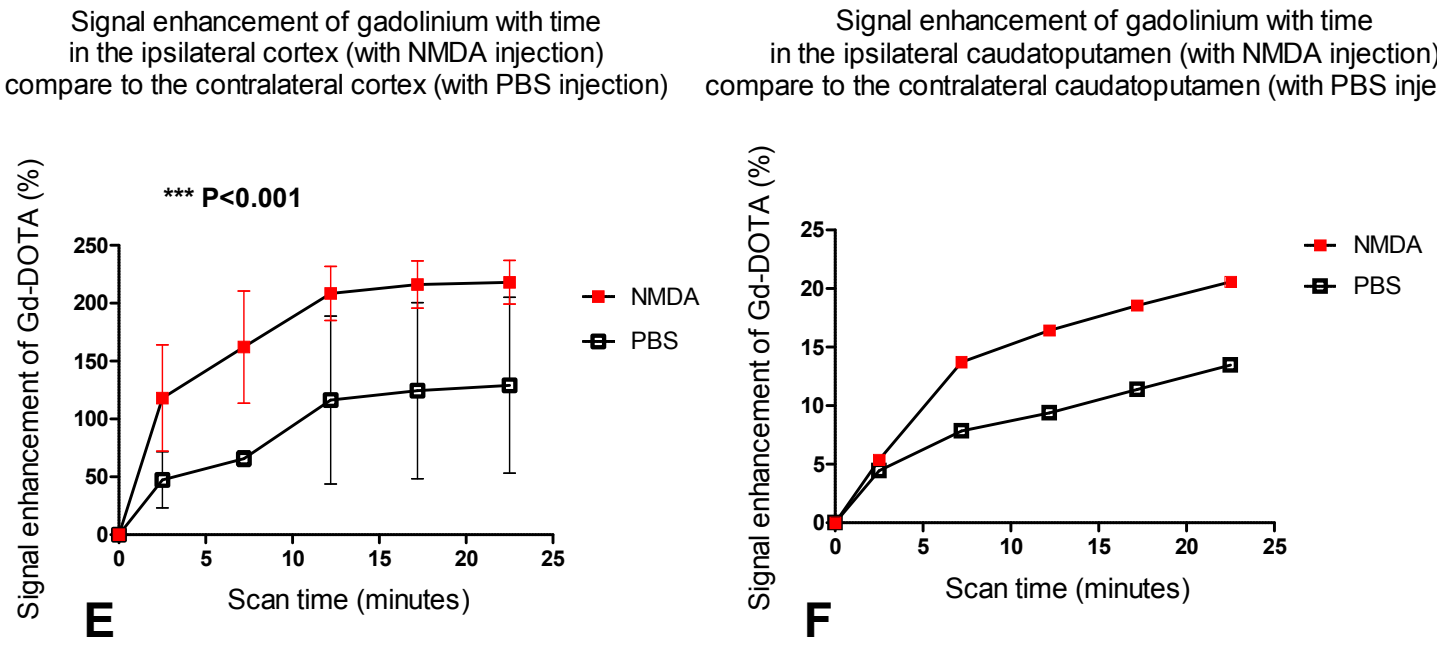

Fig.3.26 (p.114-115): Positive control of BBB permeability 48 hours after NMDA injection in the caudatoputamen. The arrows show the injection site of NDMA in the ipsilateral hemisphere and the injection site of PBS in the controlateral hemisphere. **A:** T2 structural image showing the location of the needle introduction (see arrows). **B:** T1 image showing gadolinium extravasation into the parenchyma (see arrows). **C:** IgG immunostained section in the ipsilateral side of the caudatoputamen (which received NMDA injection) to reveal the neuronal uptake of IgG (black arrows). **D:** IgG immunostained section in the contralateral caudatoputamen (which received the PBS injection) showing no IgG diffusion inside the neurons. **E:** Significant (***P<0.001) Gadolinium signal enhancement with time after NMDA injection in the ipsilateral cortex compared to the injection of PBS in the contralateral cortex. Data are presented with their means (n=3) by a one-way ANOVA with repeated measures. **F:** Gadolinium signal enhancement with time which is more marked after NMDA injection in the ipsilateral caudatoputamen than after the injection of PBS into the controlateral caudatoputamen in one representative rat. Scale bars in C, D: 20µm.

3.2.2 MRI acquisitions after BCCAo in the rat

In the previous study, after three hours of BCCAo only white matter damage was detected by immunohistochemistry, while grey matter and enhancement of activated microglia appeared after three days of BCCAo. The most severe damage in both white and grey matter was found after seven days of BCCAo. This explains why three hours and seven days were chosen to study the integrity of the BBB using MRI. Is an increase of BBB permeability responsible of the damage to the white matter detected at three hours post BCCAo using immunohistochemistry?

Twenty-six male Wistar rats underwent the procedure of chronic cerebral hypoperfusion (section 2.1.1), and were separated into two major groups: three hours post occlusion (seven rats control and seven rats which underwent the BCCAo procedure) and seven days post occlusion (six rats control and six rats which underwent the BCCAo procedure). I have chosen four regions (corpus callosum, caudatoputamen, external capsule and internal capsule) to undergo the analyses (as described in section 2.4.5) on T1-weighted images (see Appendices C, D) and on MTR maps, processed by Dr Mark Bastin.

3.2.2.1 MTR measurements

3.2.2.1.1 Regional MTR variations after three hours of BCCAo

The MTR of the BCCAo and sham group at three hours post surgeries showed significant regional differences between brain regions (Fig.3.27 e). MTR was highest in the corpus callosum, external capsule and internal capsule, and it was lowest in the caudatoputamen. The MTR of grey matter structure was significantly lower ($p<0.0001$) than that of white matter (fig.3.27 e). However, no significant differences in MTR was found between the two groups, showing that after three hours, BCCAo did not show any differences in white matter physiology compared to the control group using MTI acquisitions.

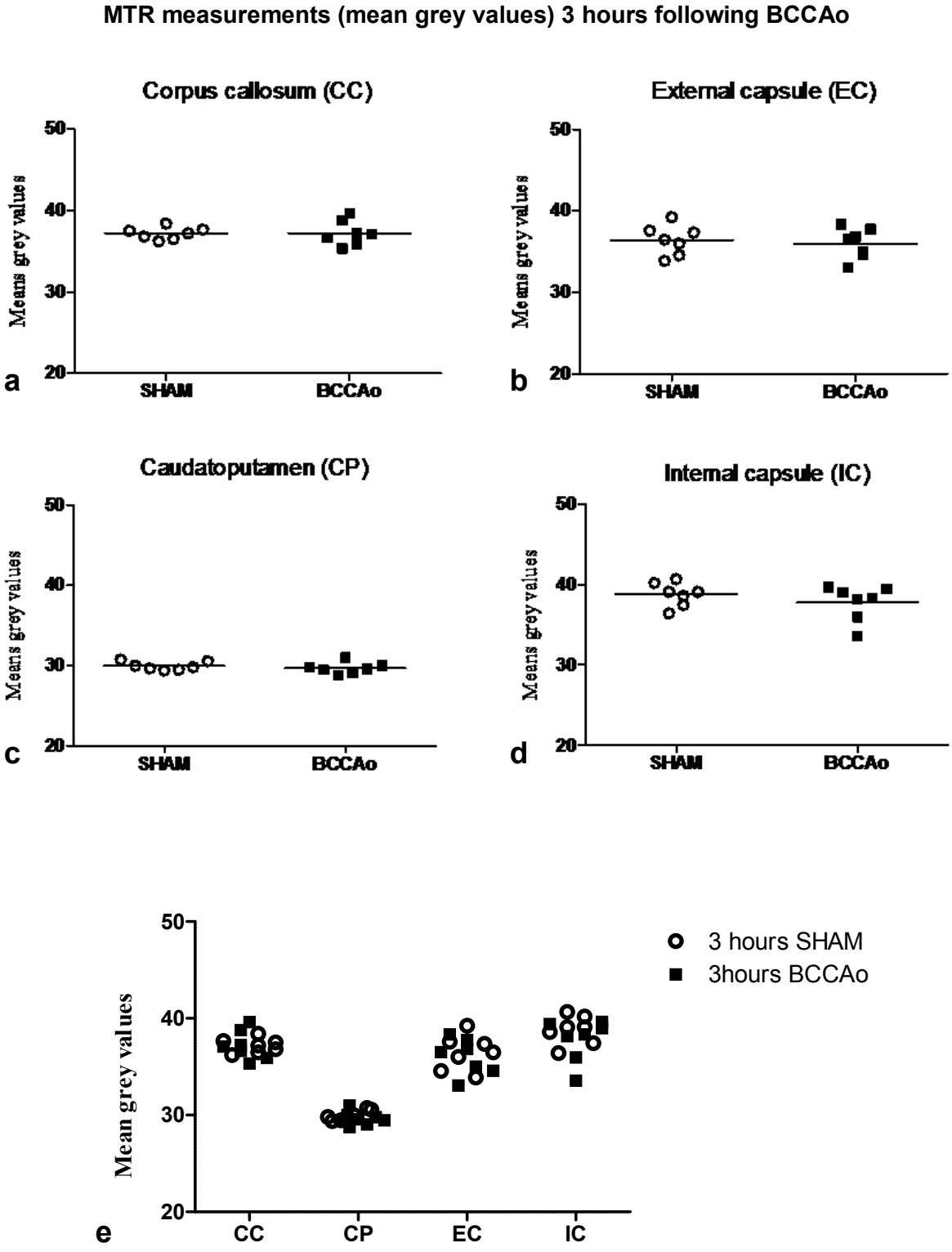

Fig.3.27: MTR values BCCAo compared to sham rats following three hours intervention (**a**, **b**, **c**, **d**). Data are presented with their means (Unpaired t-test). Sham 3 hours, n=7; BCCAo 3 hours, n=7. No significant difference was found between sham and BCCAo groups.
(**e**): Regional MTR variations: corpus callosum (CC), caudatoputamen (CP), external capsule (EC) and internal capsule (IC).

3.2.2.1.2 Regional MTR variations after seven days of BCCAo

The MTR of the two groups at seven days post surgery showed significant regional differences between brain regions (Fig.3.28). MTR was highest in regions in which white matter predominates such as the corpus callosum, the external capsule and the internal capsule. MTR was lowest in the caudatoputamen which is a mixed white/grey matter region. Indeed, the MTR of the caudatoputamen was significantly lower ($p<0.0001$) than that of white matter (fig. 3.28e). However, no significant differences in MTR was found between the two groups (sham and BCCAo) which would indicate that, at seven days post BCCAo, MTI acquisitions failed to reveal any differences in white matter physiology after BCCAo compared to the sham-operated group.

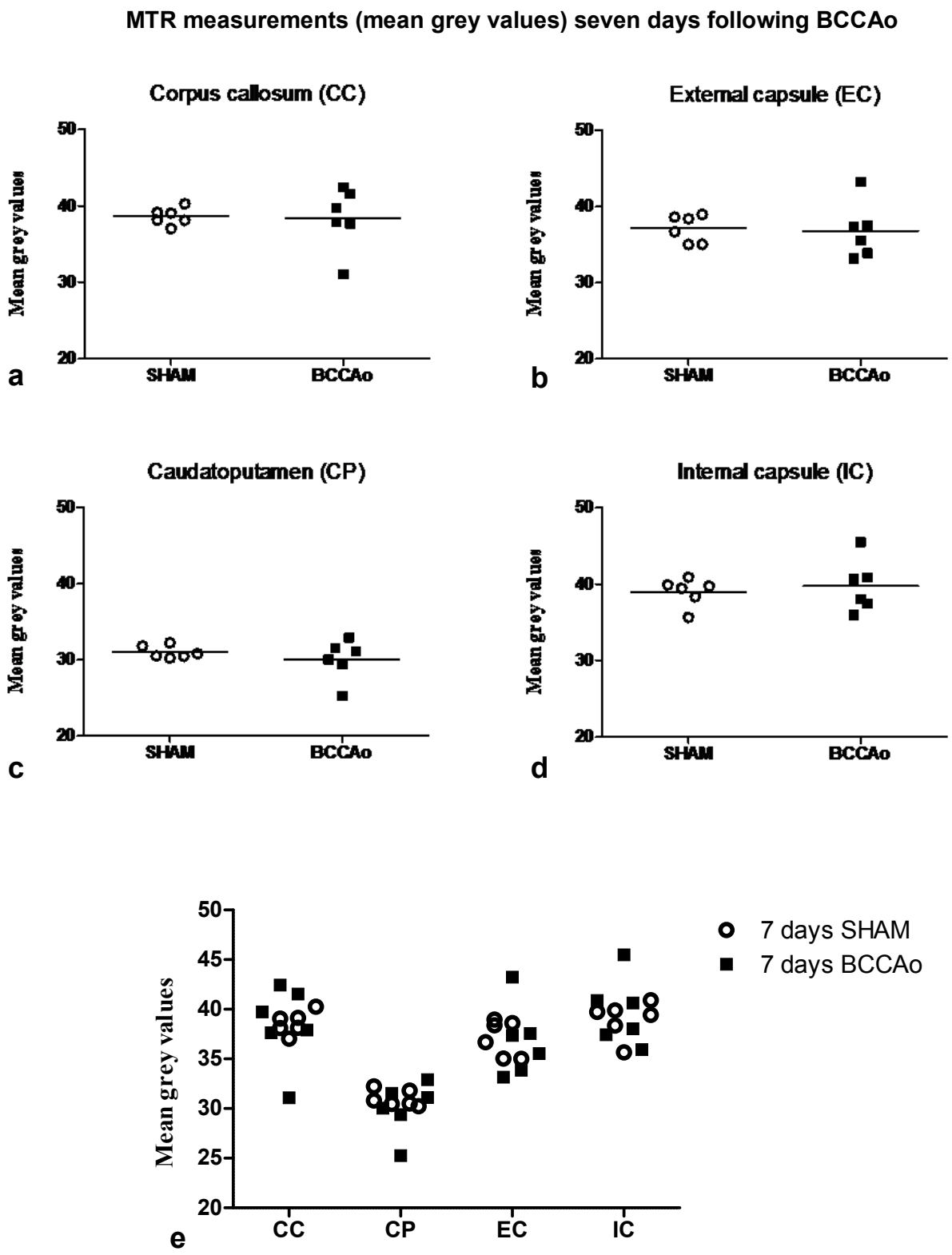

Fig.3.28: MTR values BCCAo compared to sham rats following three hours intervention (**a**, **b**, **c**, **d**). Data are presented with their means (Unpaired t-test). Sham 7 days, n=6; BCCAo 7 days, n=6. No significant difference was found between sham and BCCAo groups.
(**e**): Regional MTR variations: corpus callosum (CC), caudatoputamen (CP), external capsule (EC) and internal capsule (IC).

3.2.2.2 MRI-T1 acquisitions related to the integrity of the BBB

3.2.2.2.1 MRI-T1 acquisition at three hours post BCCAo

After three hours of BCCAo (or their appropriate sham-operated rats), the gadolinium-induced enhancement of the MRI-acquired signal was calculated, from the T1 images, in selected regions-of-interest as described in section 2.4.5 of the methods chapter. The data are presented in figure 3.29. No significant differences were found compared to the sham-operated group, in any of the four selected regions.

3.2.2.2.2 MRI-T1 acquisition at seven days post BCCAo

The procedure described above (3.2.2.2.1) was repeated in two groups of rats studied seven days after sham or BCCAo interventions. In BCCAo rats, an enhancement of the gadolinium signal was detected in all the four chosen regions. In all, the gadolinium signal was found to be greater than in the sham group and significant deifferences between the BCCAo and the sham group were observed in the caudatoputamen ($p<0.05$) and in the external capsule ($p<0.01$) at seven days post BCCAo (Fig.3.30).

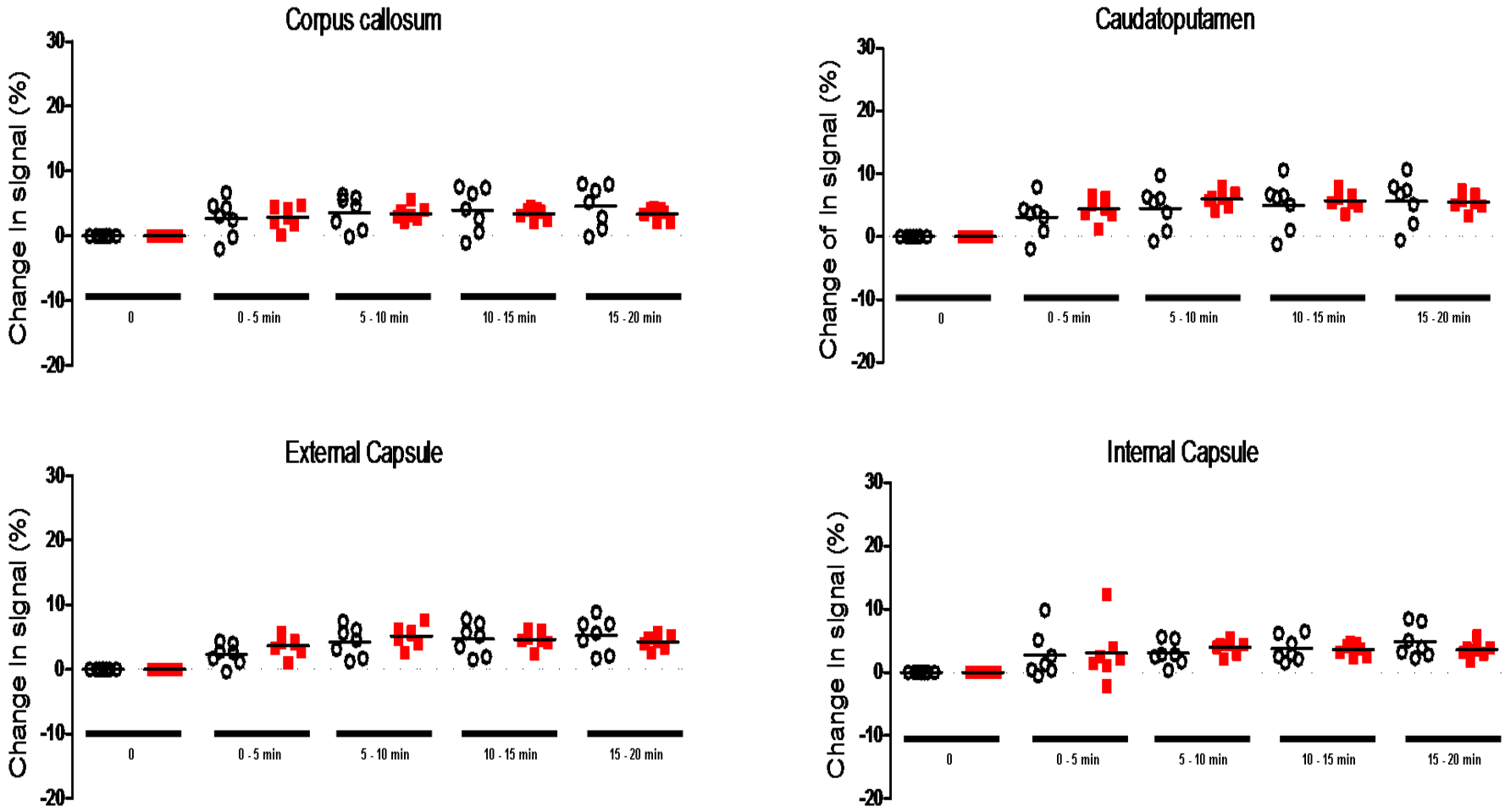

Fig.3.29: Evolution of the gadolinium-induced increase in signal as a function of time (min) following administration of the paramagnetic tracer. Three hours after intervention both sham (open circles, black, n=7) and BCCAo (filled squares, red, n=7) rats were studied. The horizontal bars represent the meam group values. There were no differences between groups either as a function of time or region (tests explained in section 2.7.2).

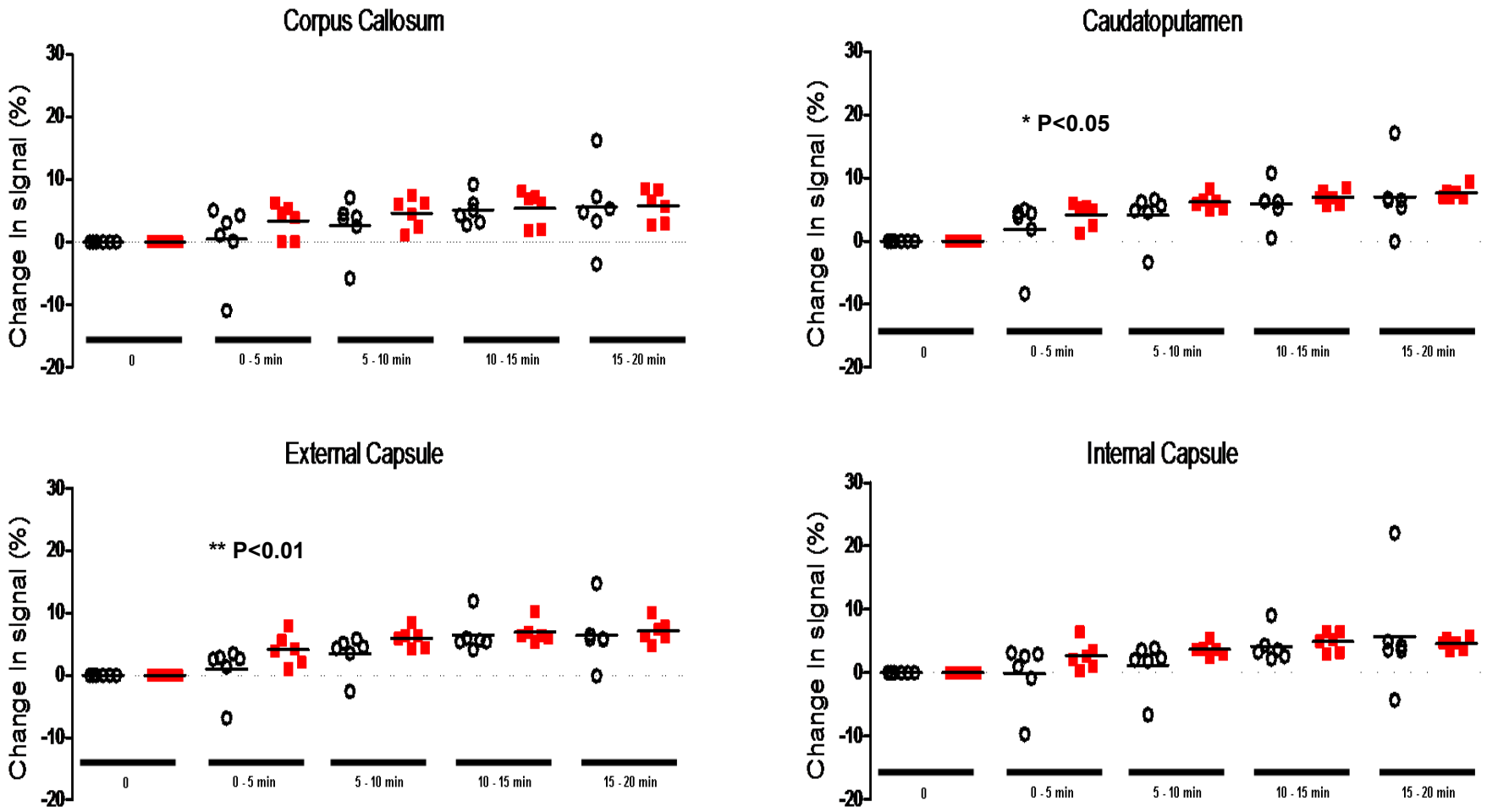

Fig.3.30: Evolution of the gadolinium-induced increase in signal as a function of time (min) following administration of the paramagnetic tracer. Seven days after intervention both sham (open circles, black, n=6) and BCCAo (filled squares, red, n=6) rats were studied. The horizontal bars represent the meam group values. Significant differences between groups were found as a function of regions: in the caudatoputamen ($p<0.05$) and in the external capsule ($p<0.01$). (Tests explained in section 2.7.2).

3.2.3 Histology and Immunohistochemistry assessment

3.2.3.1 Axonal pathology after four hours post surgery

Following three hours of occlusion, the rats underwent the MRI scans with duration of 45 to 60 minutes per animal. So the perfusion which occurred one hour later the MRI scan led us to analyse a pathology of four hours post BCCAo, and not three hours.

After the onset of BCCAo, the APP immunostained sections revealed that 3/6 animals presented APP accumulation (see table 3.5). No significant differences (fig.3.31) were observed between the two groups (sham and BCCAo).

Four hours post surgery	SHAM (APP accumulation)	BCCAo (APP accumulation)
Hippocampus	0/6	0/6
Caudatoputamen	1/6	3/6
Corpus callosum	1/6	1/6
External capsule	2/6	3/6
Internal capsule	0/6	0/6
Optic tract	0/6	1/6

Table 3.5: Number of rats in which an increase in APP accumulation was detected in the regions selected following four hours of BCCAo.

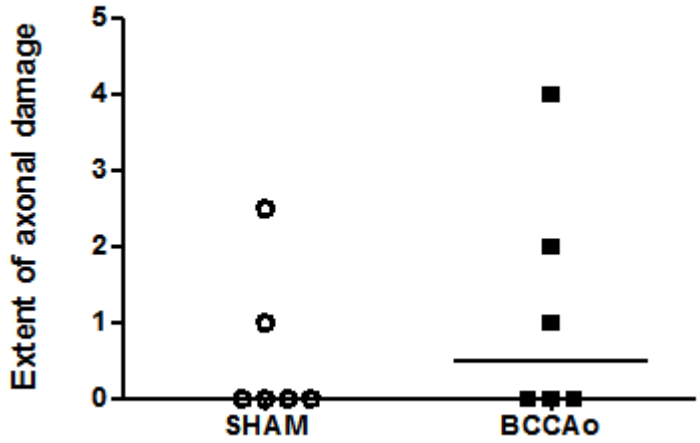

Fig.3.31: Extent of axonal damage with time (∑ grade of bilateral regions) following four hours of BCCAo. Quantification of APP accumulation. Data are presented with their median for comparison with the sham group. (Non parametric test with Mann-Whitney test). Sham 4 hours, n=6; Bccao 4 hours, n=6.

3.2.3.2 Axonal pathology after seven days post surgery

Seven days following surgery, the APP immunostained sections revealed that 3/6 animals which underwent the permanent BCCAo present APP accumulation. No animals of the control group presented any APP accumulation. The table below exposes the regions where APP accumulation (Fig.3.32a D) was detected (table 3.6). No significant differences were found between the two groups (Fig.3.32b).

Seven days post surgery	SHAM (APP accumulation)	BCCAo (APP accumulation)
Hippocampus	0/6	0/6
Caudatoputamen	0/6	2/6
Corpus callosum	0/6	1/6
External capsule	0/6	0/6
Internal capsule	0/6	0/6
Optic tract	0/6	1/6

Table 3.6: Number of rats in which an increase in APP accumulation was detected in the regions selected following seven days of BCCAo.

.

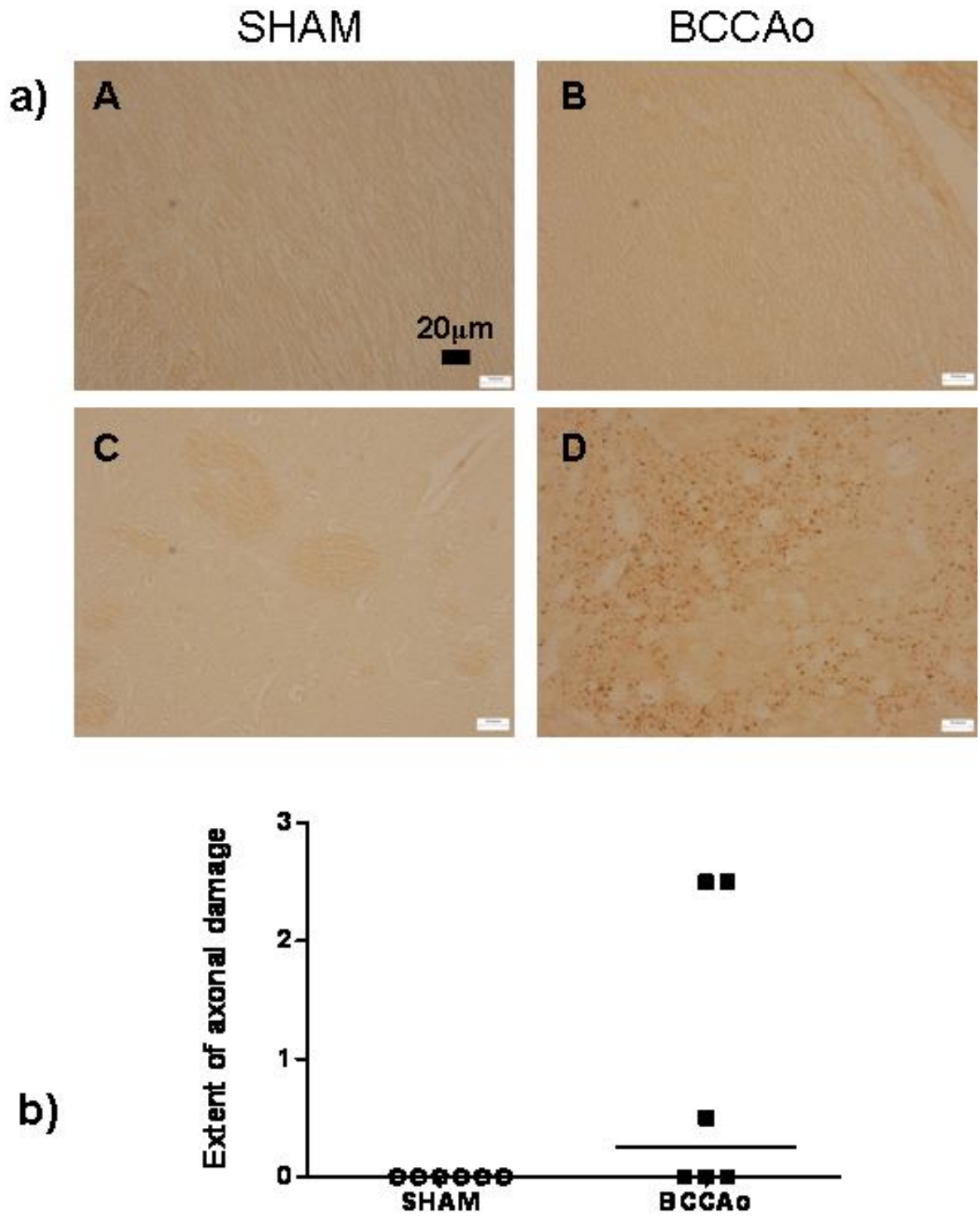

Fig.3.32: a) APP immunostaining (X200) in the corpus callosum (A and B) and in the caudatoputamen (C and D) following seven days of BCCAo (B and D) or Sham (A and C). **b)** Extent of APP accumulation with time (∑ grade of bilateral regions) following seven days of BCCAo. Quantification of APP accumulation. Data are presented with their median for comparison with the sham group. (Non parametric Mann-Whitney test). Sham 3 hours, n=6; Bccao 3 hours, n=6. Scale bars in A, B, C, D: 20µm.

3.2.3.3 Enhancement of microglial activation after four hours post surgery

Iba-1 immunostained sections revealed an enhancement of activated microglia in the sham group (Fig.3.33). The quantification of those slides (section 2.3.6) revealed that after 4 hours of occlusion, there were no differences compared to the sham (Fig.3.33).

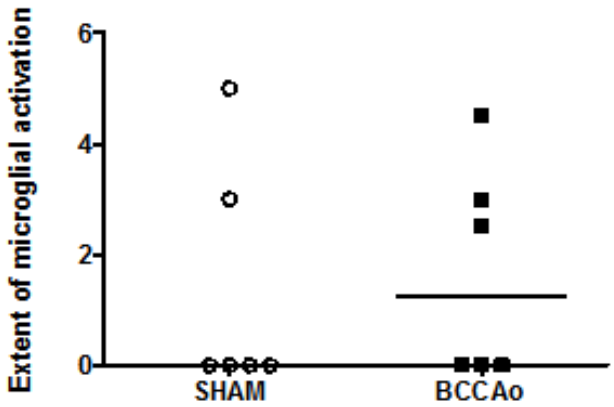

Fig.3.33: Extent of enhancement of microglial activation with time (∑ grade of bilateral regions) following four hours of BCCAo. Quantification of presence of Iba-1. Data are presented with their median for comparison with the sham group. (Non parametric Mann-Whitney test). Sham 4 hours, n=6; Bccao 4 hours, n=6.

3.2.3.4 Enhancement of microglial activation following seven days post surgery

Seven days following the procedure of permanent BCCAo, the Iba-1 immunostained sections (Fig.3.34a) revealed some enhancement of activated microglia in the sham group, which can be due by the number of procedure that a rat underwent (surgery for the separation of the common carotid arteries from the vagus nerve, then the introduction of the catheter in the femoral vein seven days later which was followed by the MRI scans of an hour). The Mann-Whitney test showed a significant difference ($p<0.01$) between the sham and BCCAo group (Fig.3.34b).

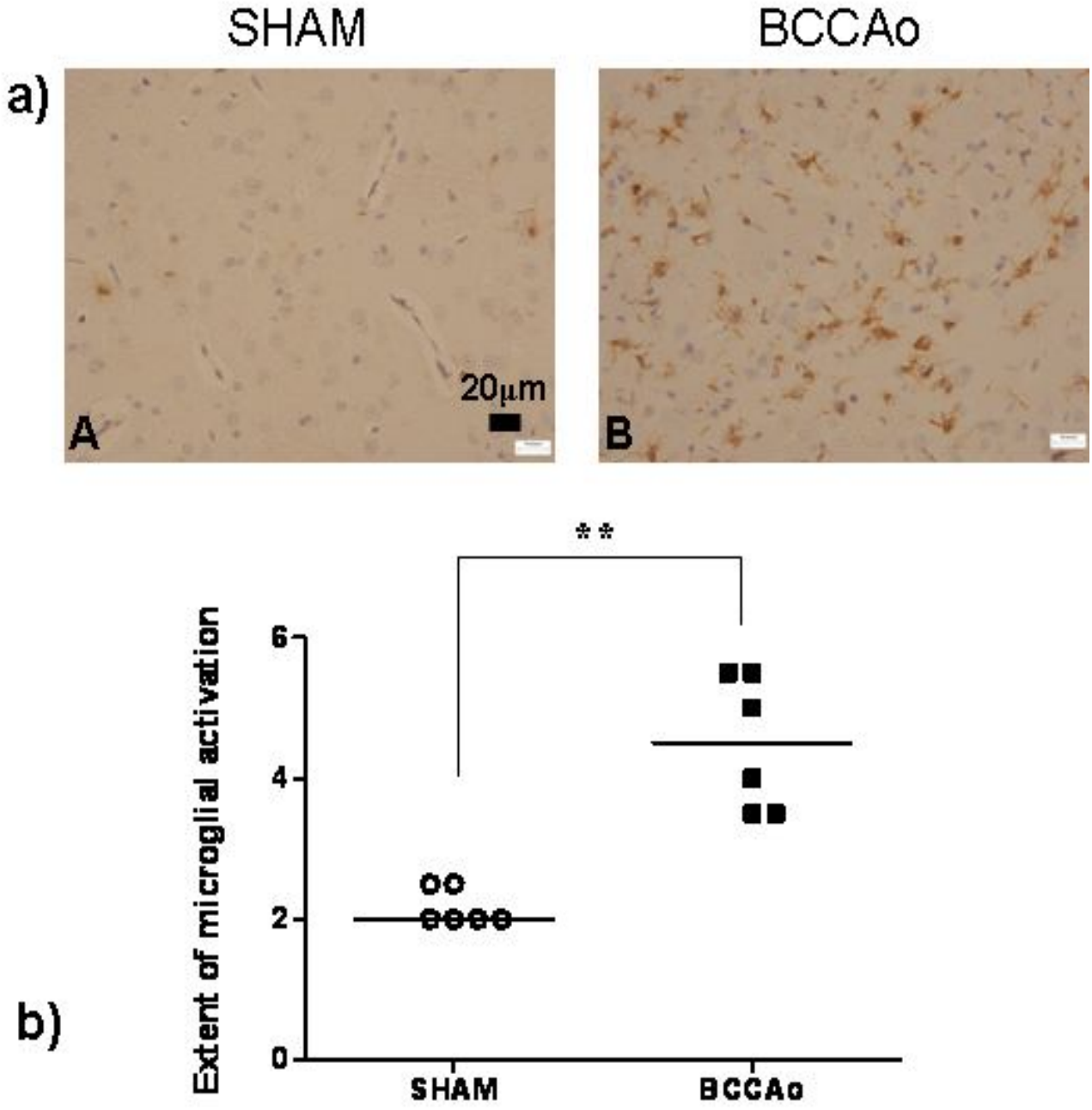

Fig.3.34: **a)** Iba-1 immunostaining in the caudatoputamen following seven days of BCCAo (B) or Sham (A). **b)** Extent of enhancement of microglial activation with time (∑ grade of bilateral regions) following seven days of BCCAo. Quantification of presence of Iba-1. Data are presented with their median **P<0.01 for comparison with the sham group. (Non parametric Mann-Whitney test). Sham 7 days, n=6; Bccao 7 days, n=6. Scale bars in A, B: 20µm.

3.2.3.5 Neuronal perikaryal damage after four hours post surgery

H&E stained sections were used to quantify ischaemic neurons (section 2.2.3), in the hippocampus and in the caudatoputamen. Damage to the perikarya of neurons are defined by an intense darkly stained pyknotic nucleus surrounded by eosinophilic cytoplasm while healthy neurons have large round nuclei and cell bodies visible cytoplasmic structures.

After four hours of BCCAo, no ischaemic neurons were detected neither in the hippocampus, nor in the caudatoputamen. Therefore no differences with the control (sham) group were observed (Fig.3.35).

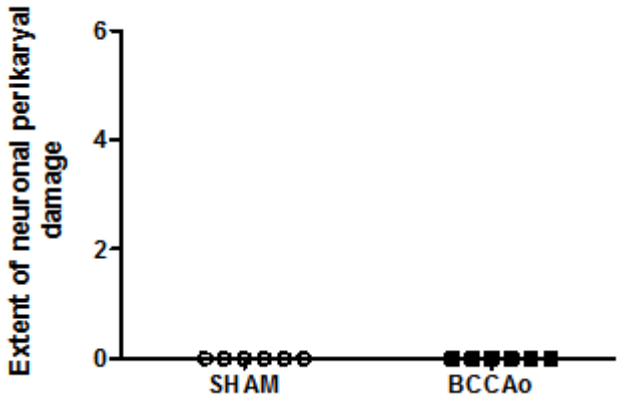

Fig.3.35: Extent of neuronal perikaryal damage (∑ grade of bilateral regions) following four hours of BCCAo. Quantification of presence of ischaemic neurons. Data are presented with their median for comparison with the sham group. (Non parametric Mann-Whitney test). Sham 4 hours, n=6; Bccao 4 hours, n=6.

3.2.3.6 Neuronal perikaryal damage after seven days post surgery

After seven days of BCCAo, damage to the perikarya of neurons was not detected in the hippocampus but only in the caudatoputamen, where 3/6 BCCAo rats exhibited ischaemic neurons (Fig.3.36a B). The difference between the sham and the BCCAo group was not significant (Fig.3.36b).

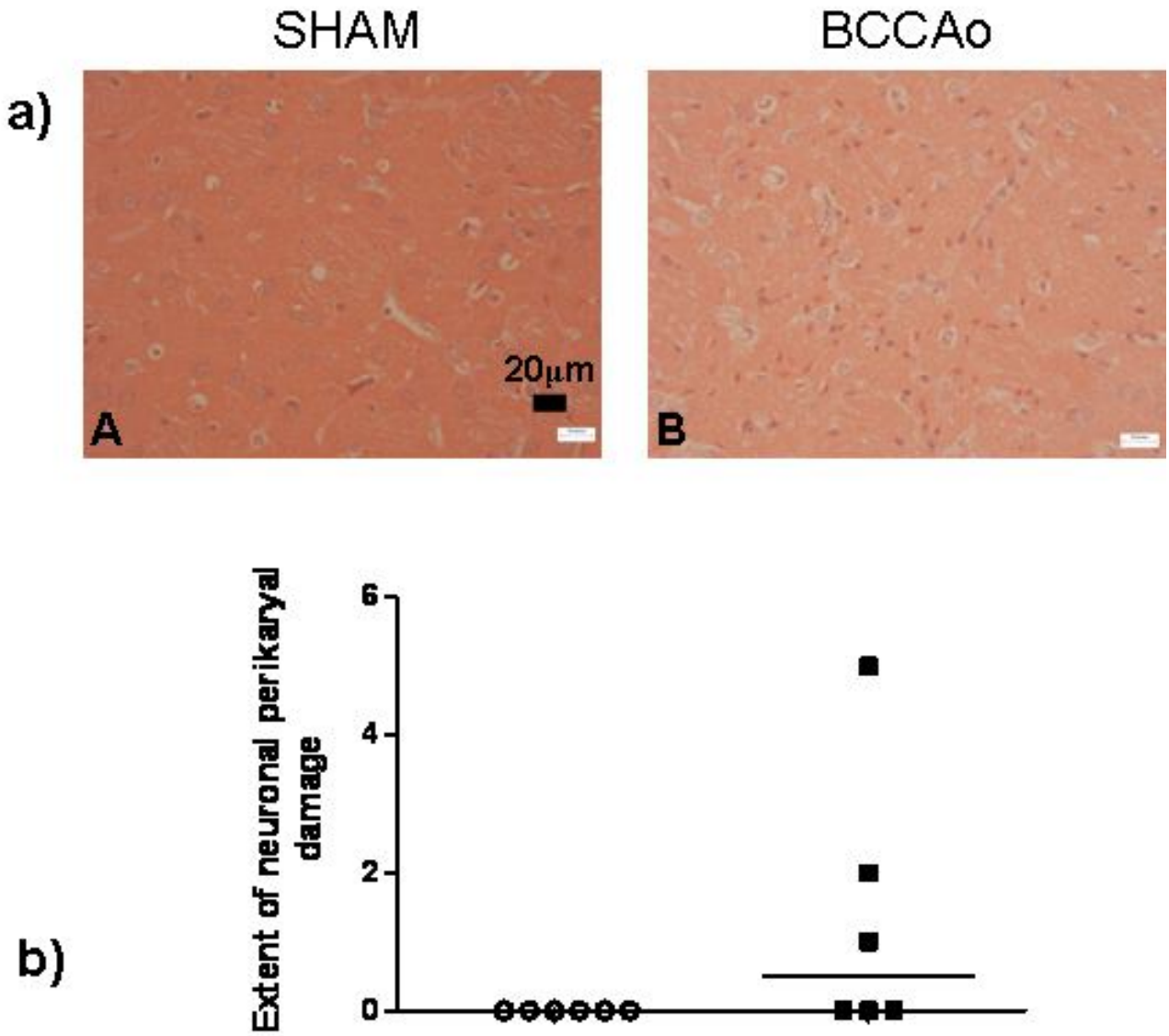

Fig.3.36: a) H&E staining in the caudatoputamen following seven days of BCCAo (B) or Sham (A). **b)** Extent of neuronal perikaryal damage (∑ grade of bilateral regions) following seven days of BCCAo. Quantification of presence of ischaemic neurons. Data are presented with their median for comparison with the sham group. (Non parametric test with Mann-Whitney test). Sham 7 days, n=6; Bccao 7 days, n=6. Scale bars in A, B: 20μm.

This is the first study to assess the integrity of the BBB at earlier time point using MRI. Moreover, it is the first study that showed an increase of Gadolinium signal enhancement in the caudatoputamen and in the external capsule, in the rat model of permanent BCCAo. The results suggest that permanent BCCAo does not in itself induce an increase of BBB permeability, but the presence of damage and activated microglia may play a role in the modulation of the properties of the BBB. . I then hypothesize that the damage to the white matter may be due by some factors expressed in an environment of decrease of blood supply related to a decrease of oxygen and glucose leading to a hypoxic statement. It is well known that under hypoxic conditions, hypoxic inducible factor-1α (HIF-1α) is expressed and its overexpression causes apoptosis (Krick et al., 2005) by activating different factors including p53, p21, (Greijer and Van der Wall, 2004; Carmeliet et al., 1998), caspase-3, vascular endothelial growth factor (VEGF) and matrix metalloproteinases (MMPs) (Narumiya et al., 2001). Increased VEGF has been detected at 24 hours and seven days of chronic cerebral hypoperfusion and its expression is mainly associated with endothelial cells in Sprague-Dawley rats (Hai et al., 2003). Also, the protein tumor necrosis factor (TNF)-α is increased at six and 24 hours after cerebral ischaemia (Haddad et al., 2006). Neurons and microglias are major sources of TNF-α which leads to oedema formation and demyelination under ischaemic conditions (Selmaj and al., 1988; Taupin et al., 1997).

If we add to our results those informations, it may give a better understanding of possible mechanisms in white and grey matter pathology and their inter-relationships. Certainly, the damage in the white matter is not induced by the activation of the microglia *per se*, but the injury to the perikarya can be due, in part, to activated microglia which produce TNF-α and can differentiate into cytotoxic cells (Banati et

al., 1993); this sequence then leads to perikarya damage. Moreover, it has been demonstrated that matrix metalloproteinase-2 (MMP-2) plays a major role in chronic cerebral hypoperfusion (Nakaji et al., 2006) and that after 3 days of hypoperfusion, the expression of MMP-2 induces microglial activation (Ihara et al., 2001; Wakita et al., 2002). Also, MMP-2 increases the permeability of the BBB by disrupting the tight junctions (Yang et al., 2007).

It is then from our interest to check the expression of those factors after BCCAo in the male wistar rat to have a better understanding of the damage that occurs in the white matter specifically, and in the grey matter.

3.3 Proteins implicated in the pathology of white matter in the rat model of chronic cerebral hypoperfusion

Rats were divided randomly into two groups at three hours and seven days after BCCAo, as well as a control group (sham) for each time (section 2.1.1). The procedure was performed on a total of 29 rats (15 BCCAo and 14 sham). One rat among the BCCAo group died within 24h. (See Appendix E for full runs of western blots).

3.3.1 Western blot analysis of protein levels following hypoperfusion

3.3.1.1 HIF-1α Western blotting

Western blot analysis of HIF-1α levels in the cortex, corpus callosum and in the caudatoputamen in a hemi-brain detected no change in response to hypoperfusion between sham and BCCAo after seven days (fig.3.37). However, a variation of HIF-1α levels between cortex, corpus callosum and caudatoputamen can be noted following three hours of BCCAo.

3.3.1.2 VEGF Western blotting

Western blot analysis of VEGF levels in the cortex and in the corpus callosum in a hemi-brain detected no change in response to cerebral hypoperfusion between sham and BCCAo animals after three hours or seven days post surgery (fig. 3.38 and 3.39). Between three hours and seven days, VEGF levels are doubled in the cortex and increased in the corpus callosum in both sham and BCCAo groups.

3.3.1.3 Caspase-3 Western blotting

Western blot analysis of caspase-3 levels in the in the cortex, corpus callosum and in the caudatoputamen in a hemi-brain detected no change in response to hypoperfusion between sham and BCCAo, in any of the regions examined (fig.3.40 and 3.41). In the corpus callosum, caspase-3 levels are half-reduced between three hours and seven days following surgery, in botth sham and BCCAo groups.

3.3.1.4 MMP-2 Western blotting

Western blot analysis of MMP-2 levels in the in the cortex and corpus callosum (fig.3.42) as well as in the caudatoputamen (fig.3.43). The tissues from the cortex and corpus callosum were studied at three hours, the cortex and caudatoputamen at seven days following either sham or BCCAo intervents. No occlusion-related changes in MMP-2 levels were significantly different.

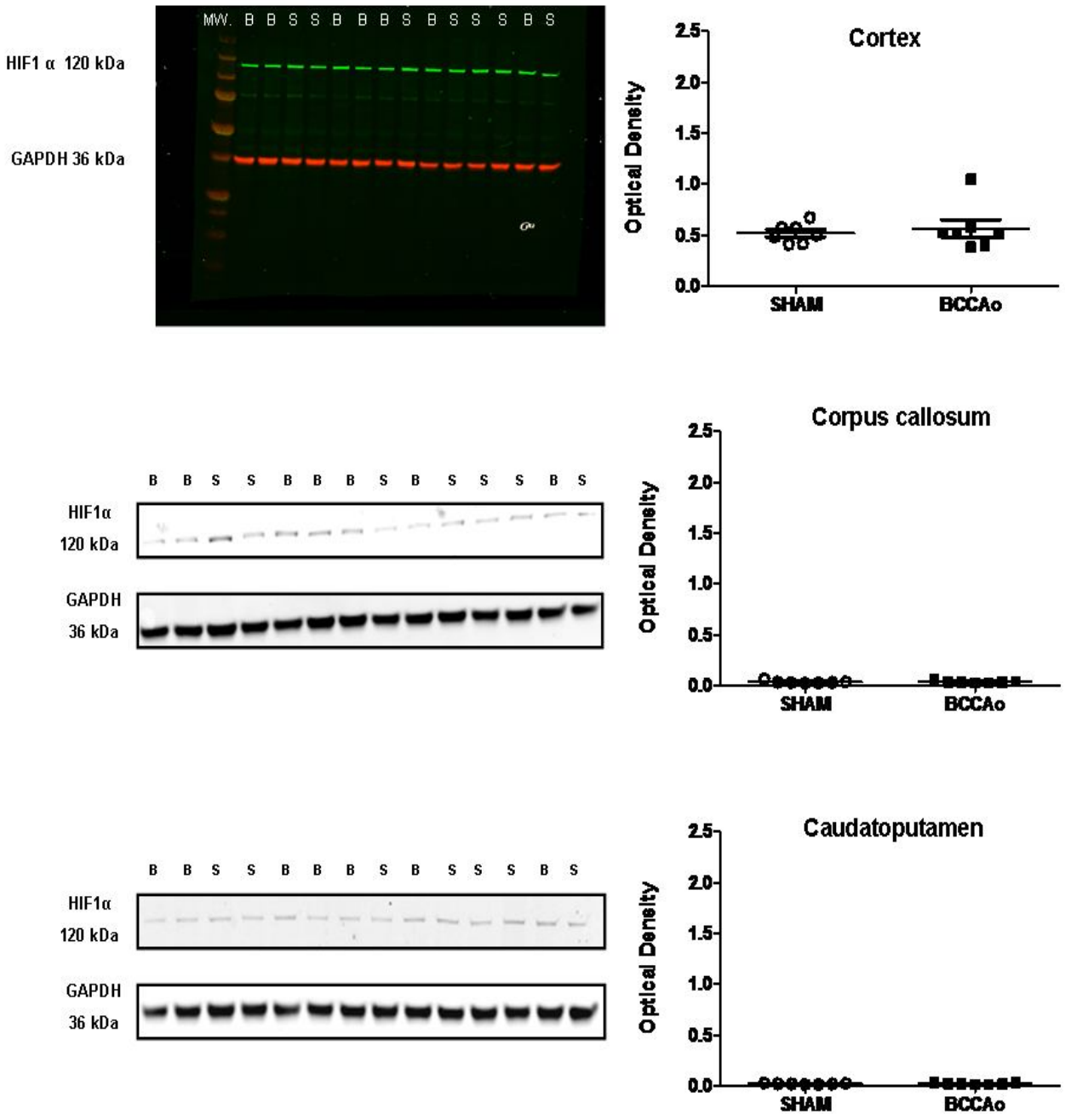

Fig.3.37: HIF-1α Western blot analysis in the cortex, the corpus callosum and caudatoputamen of a half-brain, seven days following intervention (sham or BCCAo). The horizontal lines in the graphics represent the mean values ± SEM.

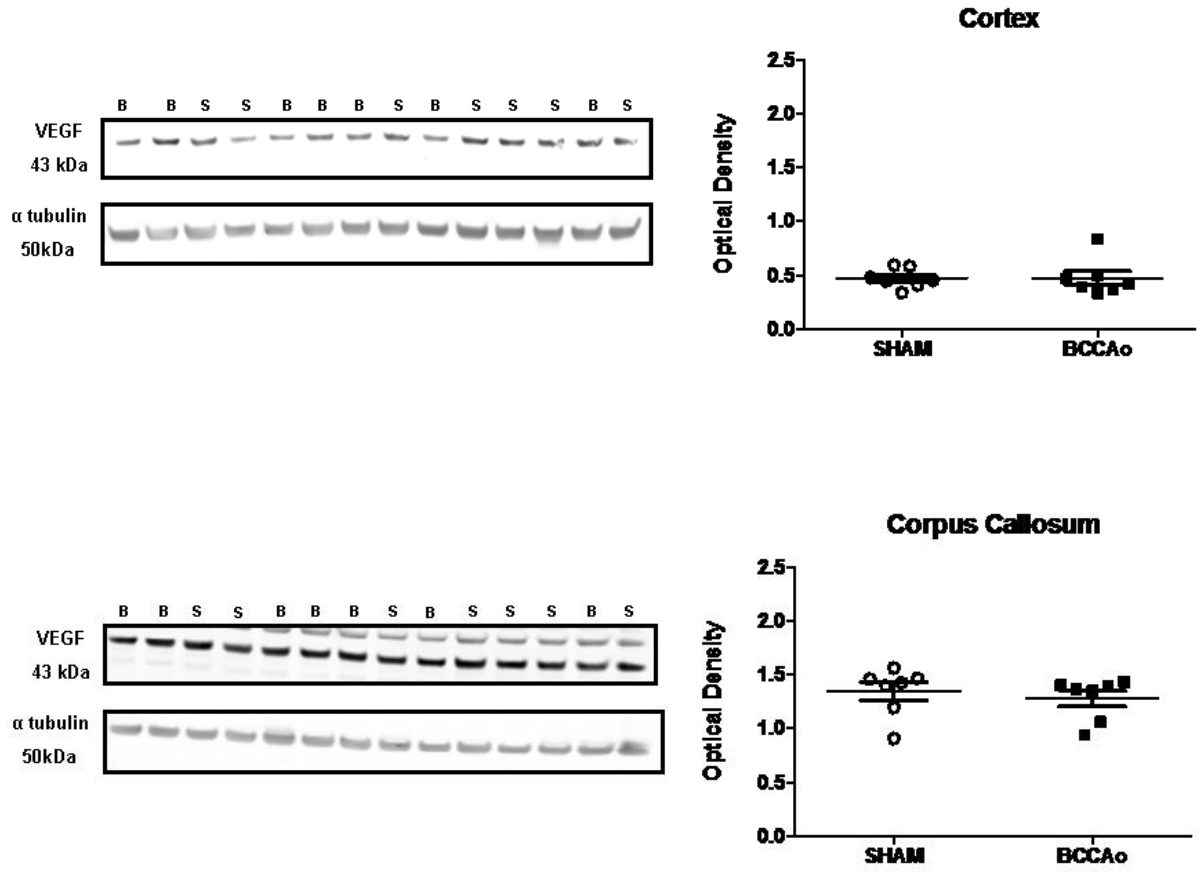

Fig.3.38: VEGF Western blot analysis in the cortex and the corpus callosum of a half-brain, three hours following intervention (sham or BCCAo). The horizontal lines in the graphics represent the mean values ± SEM.

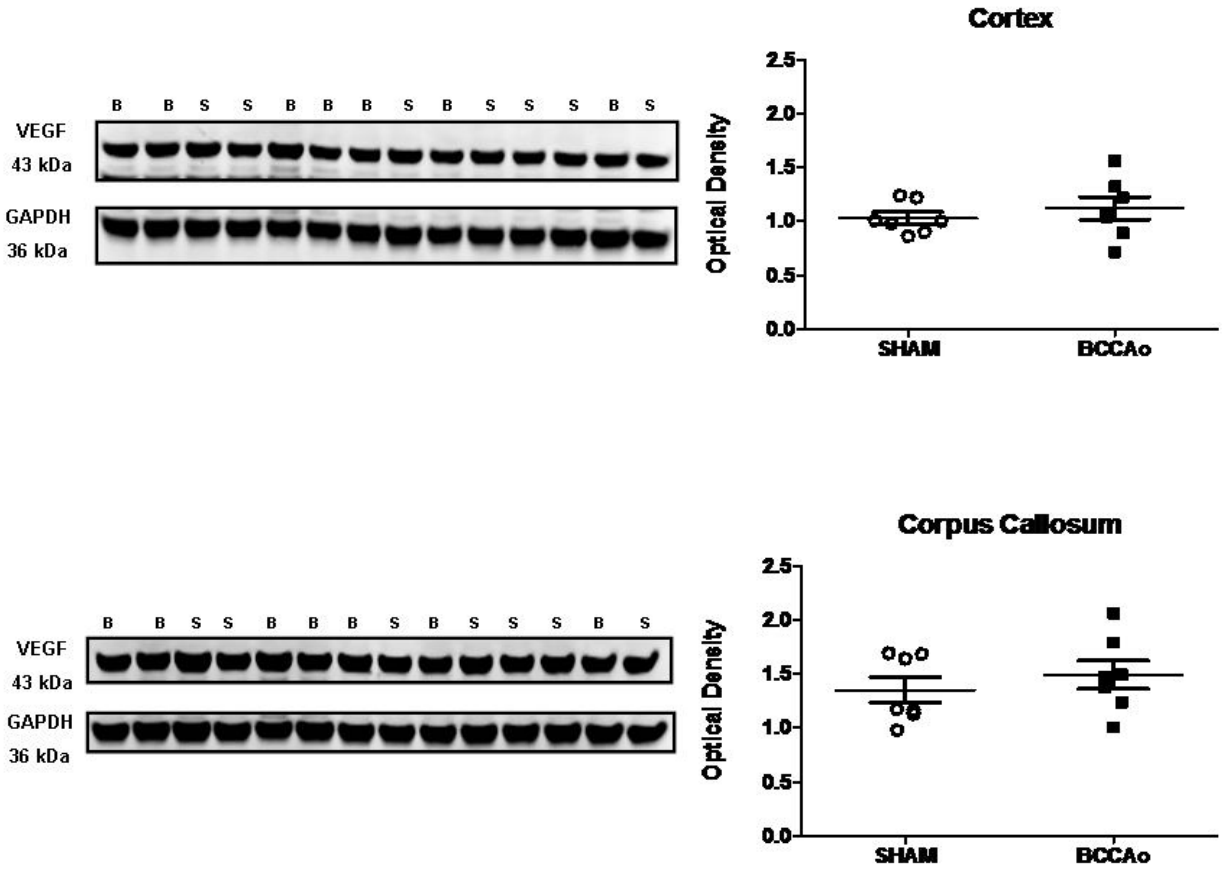

Fig.3.39: VEGF Western blot analysis in the cortex and the corpus callosum of a half-brain, seven days following intervention (sham or BCCAo). The horizontal lines in the graphics represent the mean values ± SEM.

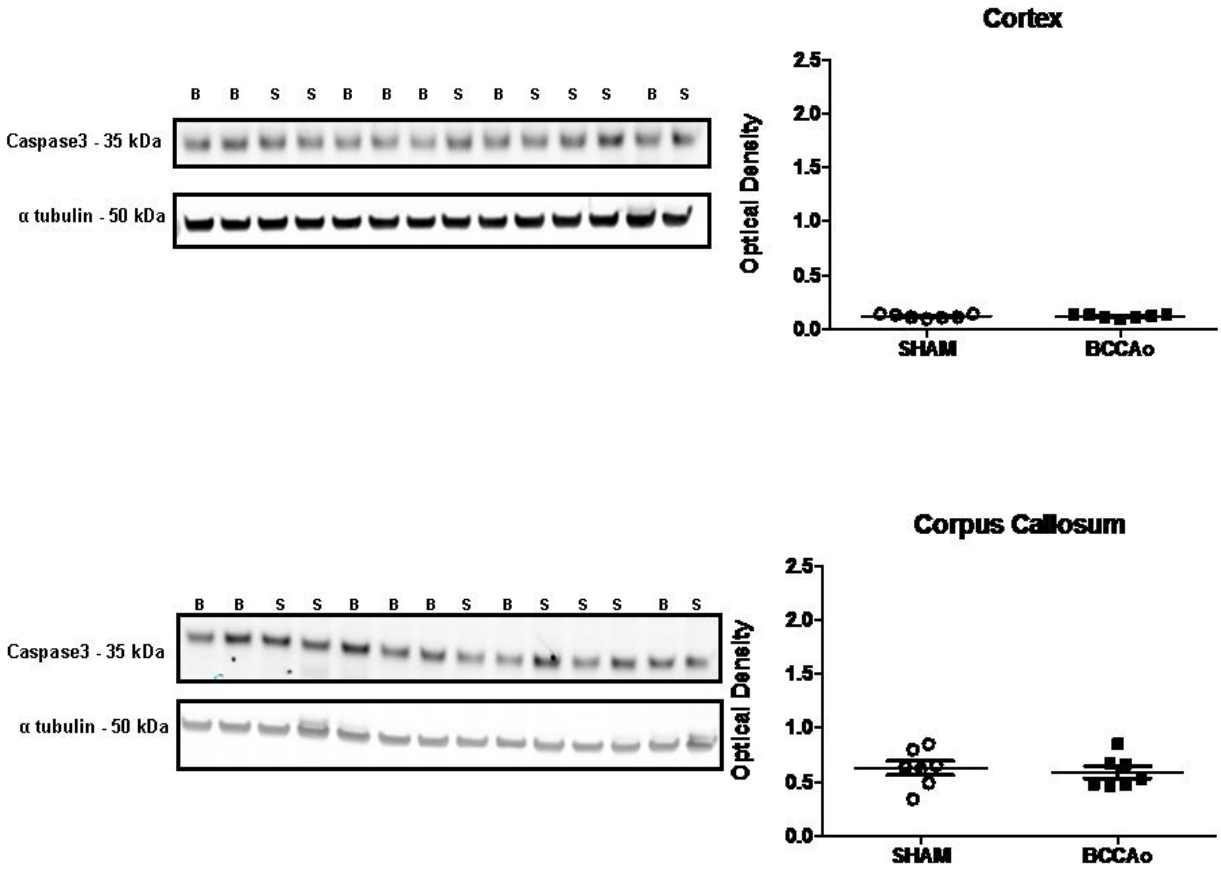

Fig.3.40: Caspase-3 Western blot analysis in the cortex and the corpus callosum of a half-brain, three hours following intervention (sham or BCCAo). The horizontal lines in the graphics represent the mean values ± SEM.

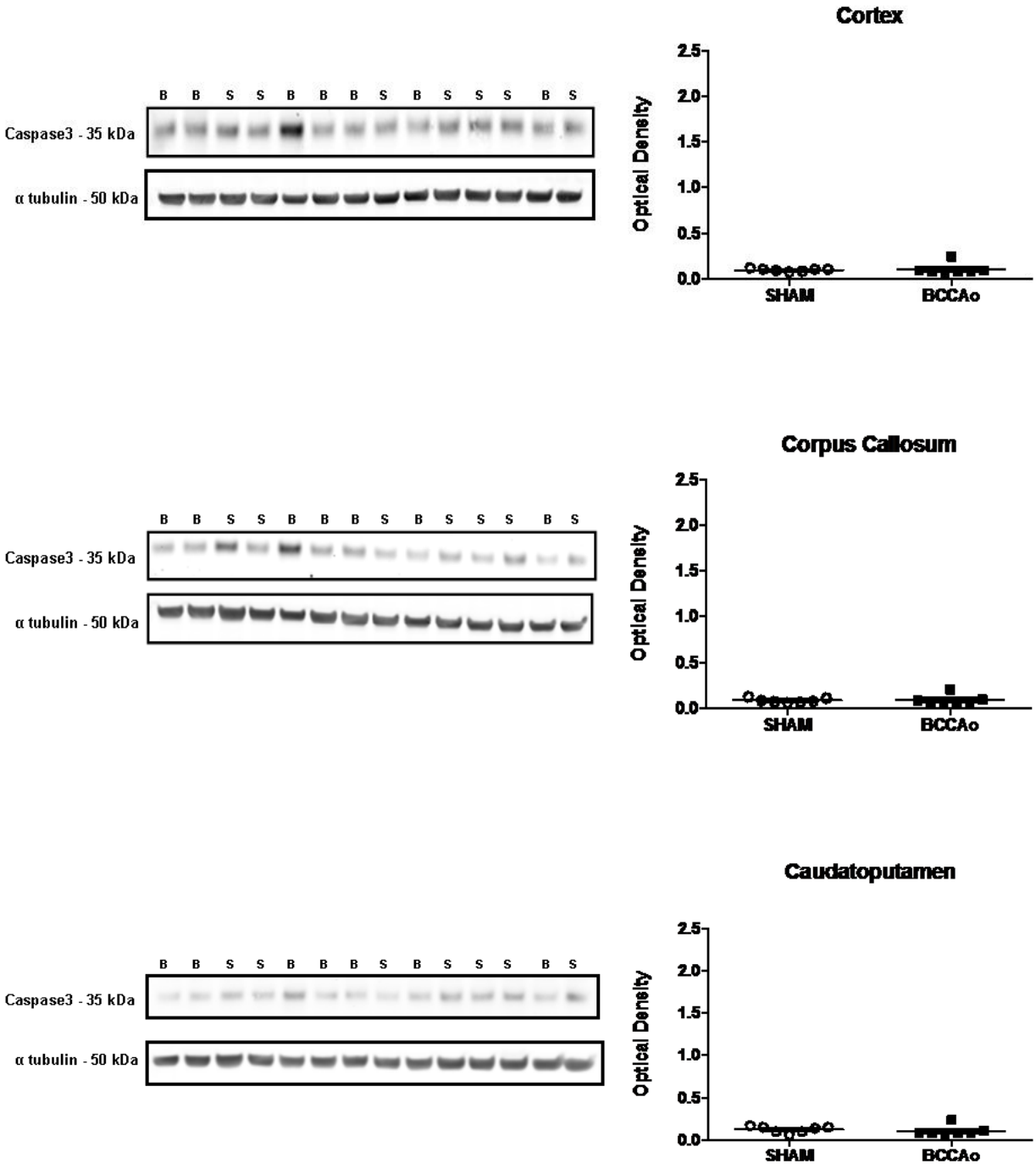

Fig.3.41: Caspase-3 Western blot analysis in the cortex, the corpus callosum and in the caudatoputamen of a half-brain, seven days following intervention (sham or BCCAo). The horizontal lines in the graphics represent the mean values ± SEM.

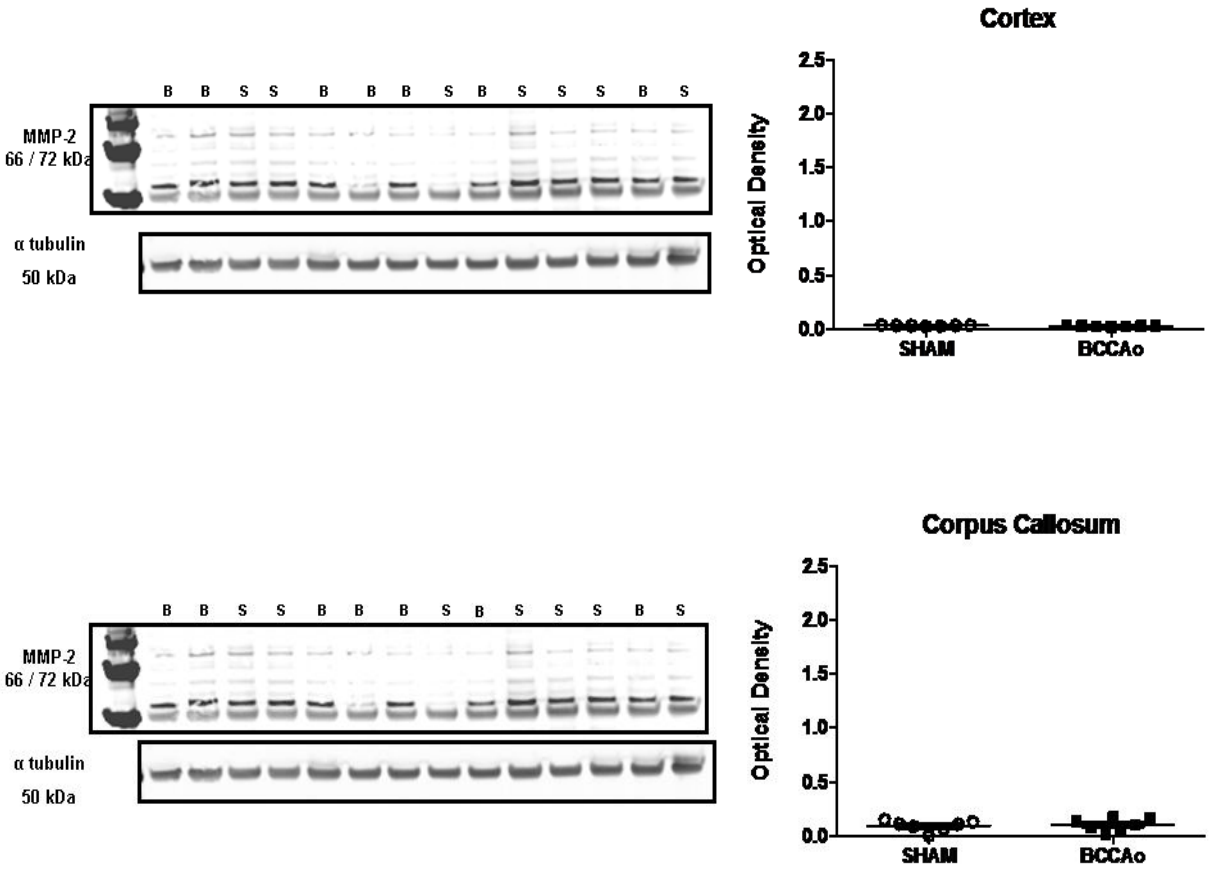

Fig.3.42: MMP-2 Western blot analysis in the cortex and the corpus callosum and caudatoputamen of a half-brain, three hours following intervention (sham or BCCAo). The horizontal lines in the graphics represent the mean values ± SEM.

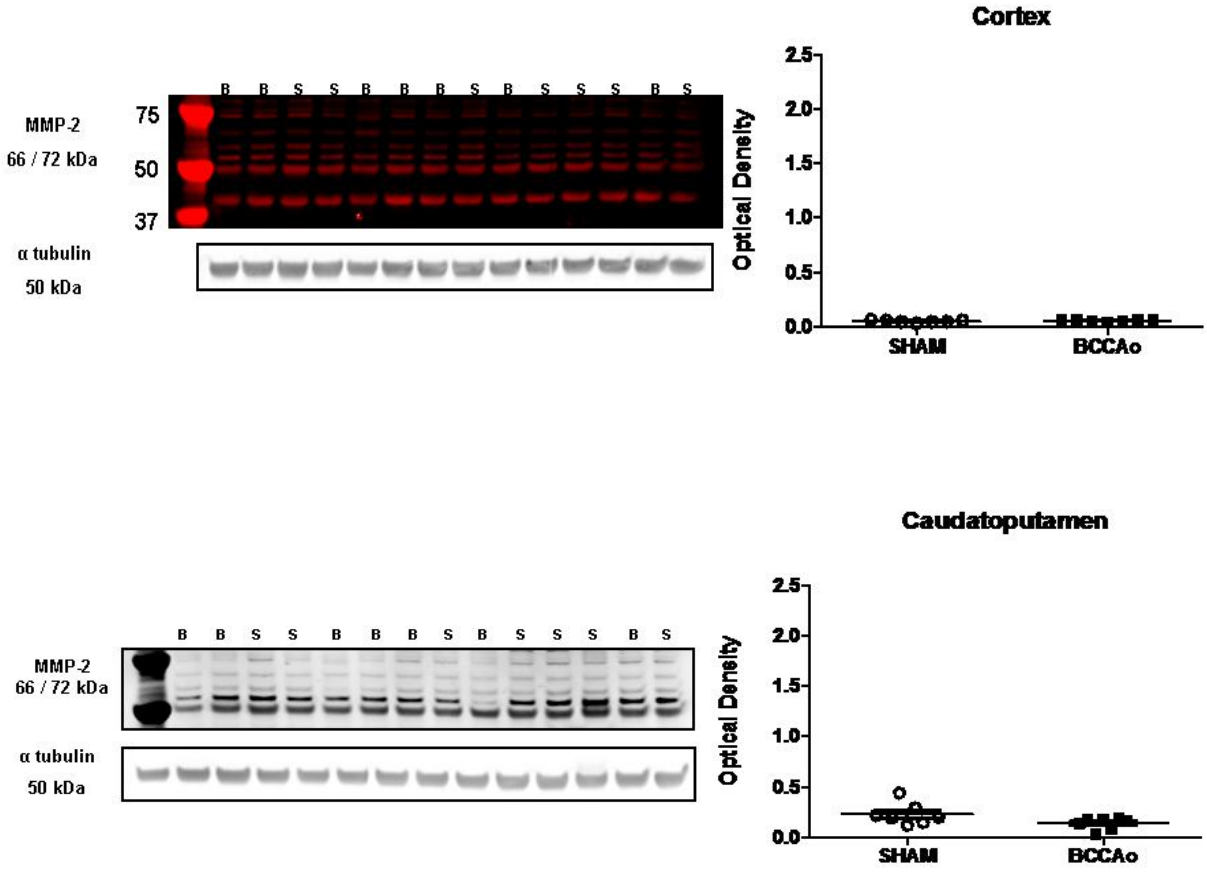

Fig.3.43: MMP-2 Western blot analysis in the cortex and the corpus callosum and caudatoputamen of a half-brain, seven days following intervention (sham or BCCAo). The horizontal lines in the graphics represent the mean values ± SEM.

3.3.2 Gene expression of proteins which may be implicated in white and grey matter injury following hypoperfusion

3.3.2.1 Expression of HIF-1α mRNA

RT-PCR analysis of HIF-1α expression in the cortex, corpus callosum and in the caudatoputamen in a hemi-brain detected no change in response to hypoperfusion between sham and BCCAo, in any of the regions examined (fig.3.44 A).

3.3.2.2 Expression of Caspase-3 mRNA

RT-PCR analysis of caspase-3 expression in the cortex, corpus callosum and in the caudatoputamen in a hemi-brain detected no change in response to hypoperfusion between sham and BCCAo, in any of the regions examined (fig.3.44 B).

3.3.2.3 Expression of VEGF mRNA

RT-PCR analysis of VEGF expression in the cortex, corpus callosum and in the caudatoputamen in a hemi-brain detected significant change in response to hypoperfusion between sham and BCCAo, in all of the regions examined (fig.3.44 C).

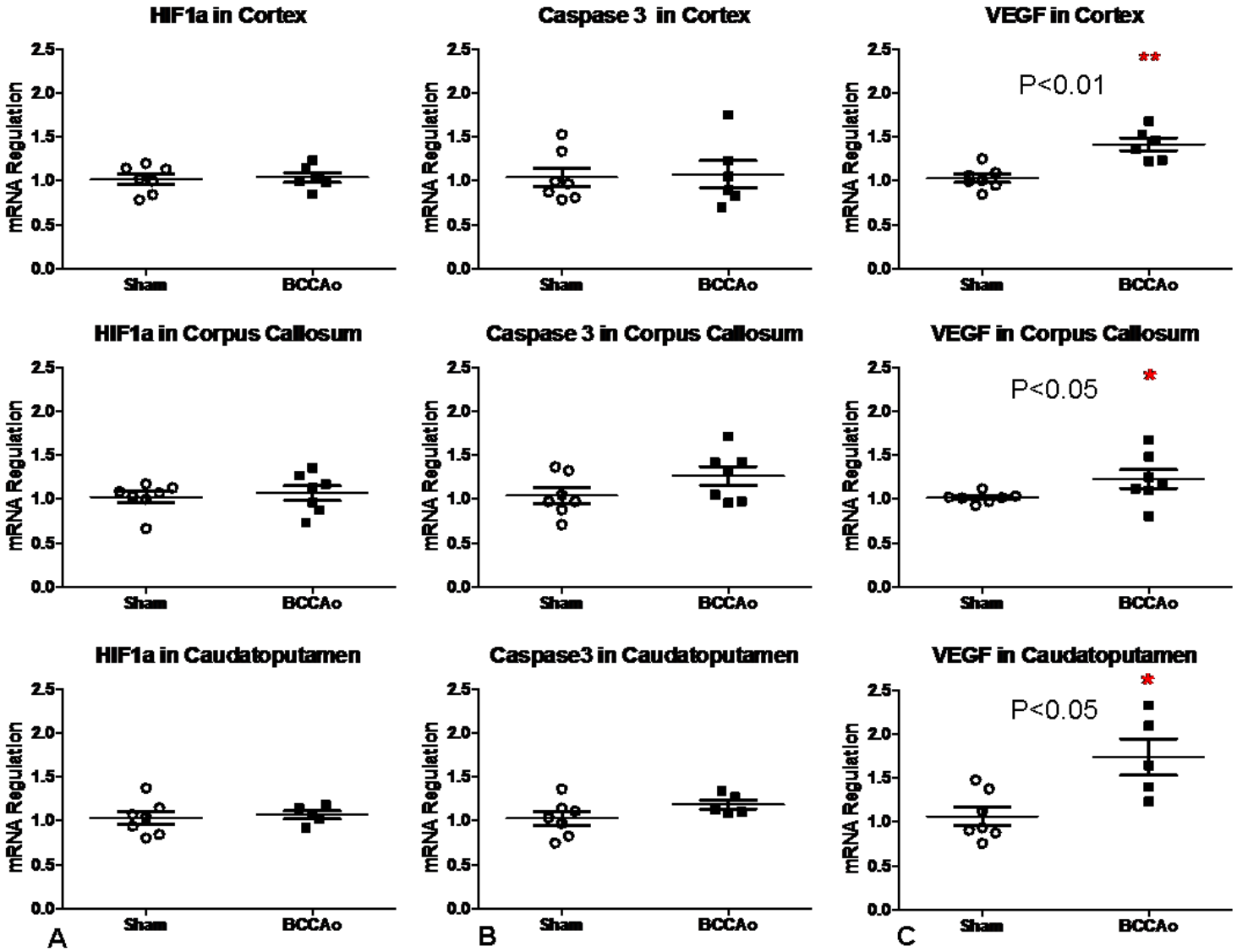

Fig.3.44: RT-PCR analysis of HIF-1α mRNA (A), Caspase3 mRNA (B) and VEGF mRNA (C) in the cortex, corpus callosum and in the caudatoputamen seven days post surgery. The samples were taken from one hemisphere.

CHAPTER 4: Discussion

BCCAo is a model – or paradigm – of neurodegenration within the brain (and retina – *vide infra*) that has been widely studied over several decades. There are, as of now, approximately 1000 articles referenced in the literature. A pertinent and recent review covered the 107 publications that focused on the BCCAo-induced vascular cognitive impairement to further our understanding of vascular dementia in man. The 107 studies were divided into 16 distinct animal models (Jiwa et al., 2010).

Their review opens avenues for future investigations. For example, the neuropsychological impairement listed were primarily deficits in working and reference memory. Vascular cognitive impairement encompasses a variety of cerebrovascular diseases such as small vessel disease, multi-infarct dementia, focal stroke, arteriopathy and many other disease states. However, the most-used model was that of BCCAo to provoke chronic cerebral hypoperfusion and its related but poorly defined white matter injury. It is on the basis of this abundant literature that our thesis has attempted to unravel the temporal modifications in the different cell types in the CNS following BCCAo.

General considerations

Different studies have compared the histological changes produced by BCCAo in white and/or grey matter, but none has compared the progression of damage between them. The studies performed in this thesis have indicated the vulnerability of white and grey matter to permanent ligation of both common carotid arteries with time, as a model of SVD. Initially, axonal and myelin pathology preceding microglial activation and perikaryal damage were characterised in the present model. An increase of permeability of the BBB in the BCCAo model was not detected at earlier time point

through the use of MRI, but at only after seven days of BCCAo which leads to the conclusion that the damage observed in white matter at earlier time points is not due to an increase of BBB permeability. Finally, the apoptotic pathway does not seem to be a cause of white matter damage at three hours or seven days post BCCAo, but a significant expression of VEGF was detected at seven days post BCCAo, which can be associated with the increase of BBB permeability that we detected in MRI at seven days post BCCAo.

Differing temporal patterns of neuropathological changes in the adult male Wistar rat were noted after the experimental induction of BCCAo. Marked dissimilarities exist in the evolution of histological damage within and between the white and grey matter structure selected for the study. Random patterns between animals and within the same group were also observed. This dispersion can be explained by variations of the blood supply as well as the different anastomoses that exist in some rat brains but not in others (Otori et al., 2003). Indeed, the "normal" circle of Willis in the rat is found in a minority of anatomical specimens; same is the case in man (Alpers et al., 1959). The decrease in weight during the first two days after the induction of BCCAo can be also explained by the blood supply via the external carotid artery which supplies the neck, the face, the tongue, and the lips. A decrease in external carotid blood flow could impair the apparatus of mastication and hence lead to a disturbance in food uptake.

BCCAo causes white matter damage

Several studies have already shown, in the permanent BCCAo model, that chronic cerebral hypoperfusion induces white matter damage in the adult rat (Wakita et al., 2002; Wakita et al., 2003). Only two papers (Wakita el al., 2002 and Wakita et al.,

2003) have focused on axonal damage induced by BCCAo. Theu have shown that axonal damage was apparent at one day in the corpus callosum, in the internal capsule and in the caudatoputamen and that only traces of axonal damage were observed in the optic tract after one hour of BCCAo (Wakita et al., 2002). These data support our findings, in that, even after three hours of occlusion, no axonal damage was detected in the optic tract, whereas, at the same time, the corpus callosum, the external capsule, the fimbria, the internal capsule and the caudatoputamen exhibited clear axonal damage. The fact should be underlined that, after three hours of BCCAo, myelin débris was detected in the optic tract. It has been shown that the first anoxia-induced pathological change in the white matter was periaxonal damage in the myelin sheaths (Waxman et al., 1992). The antibody that we used, raised against the myelin associated glycoprotein (MAG), was chosen to detect this protein localised in the periaxonal region of the myelin sheath. A primarly loss of MAG has been found in multiple sclerosis, in virus encephalitis and in acute stroke-induced lesions, whereas the other proteins of myelin were well preserved (Aboul-Enein et al., 2003). Those data can explain the dichotomy between the detection of myelin damage but not axonal damage in the optic tract after three hours of BCCAo.

The damage in white matter regions appeared to be more pronounced from three days to 28 days after BCCAo. White matter regions exhibited a varying degree of vulnerability to BCCAo, with the optic tract being the most severely and time-related rarefied region. This predisposition of this structure can also be explained by its blood supply from the ophthalmic artery and the anterior cerebral artery which are branches of the internal carotid artery.

Based on these results, the hypothesis arose that myelin damage occurs prior axonal damage after three hours of BCCAo in the optic tract; the myelin seems to be more

sensitive than the axons themselves after an abrupt and sustained decrease in carotid blood flow.

BCCAo causes neuronal perikaryal damage

The present data suggest that the perikarya (cell bodies of neurons) were spared in the first three hours following BCCAo but, at later time intervals of three, seven, 14 and 28 days, displayed those hyperchromatic and pyknotic changes that are characteristic of ischaemia-induced insults, presenting a severe pattern of damage after seven days of BCCAo.

The number of animals at three hours and three days is the same and, despite no significant difference between the sham and BCCAo group of three days, neuronal perikaryal damage was detected from this time point, not before.

Both axonal and myelin damage was observed in several white matter structures: corpus callosum, external and internal capsules, the fimbria and the optic tract. The absence at three hours of histological damage in the perikarya of neurons and the presence of white matter injury, at this time point, allows the conclusion that white matter pathology precedes grey matter damage in the BCCAo model. The analysis of the blood flow data in the literature (see fig.2.1) suggests that flow is reduced by approximately 50% on the minutes following occlusion. Even if (and this is debatable) the flow was measured in the seconds following the simultaneous clamping of both common carotid arteries, then the theoretical reduction would be approximately 70% (i.e. the "intercept") of the regression analysis. What to make of these facts? The flow decreases are severe and greater than these achieved in psychological situations such as voluntary hyperventilation to induce severe arterial hypocapnia. However decreases in flow of the order -50 to -70% are not severe and

severe enough to provoke early ischaemic changes in cortical neurons (i.e. perikaryal damage) (Kuroiwa et al., 1985; Somjen et al., 1988).

Other arguments may be adduced. In neonatal rats, a model of hypoxia-ischaemia (i.e. a massive ischaemic insult), it has been shown that white matter injury precedes grey matter damage at one hour after hypoxia-ischaemia and that damage was apparent in both grey and white matter 24 hours later (Meng et al., 2005). Interestingly, Meng and collaborators assessed the histopathology in the white and grey matter by two methods: the H&E staining procedure and TUNEL staining technique. They failed to find any differences in terms of positive reesults, between the two staining methods used (Meng et al., 2005).

BCCAo enhances the activation of microglia

Previous studies have demonstrated that microglial activation is increased from seven to 30 days post BCCAo (Wakita et al., 1994) and after three months of BCCAo; this augmentation was related to white matter injury (Farkas et al., 2004). However, there are no publications in which the state of microglial activation has been addressed at earlier time points and none has compared the progression with time of the damage in relation to the pattern of white and grey matter pathology. It is of note that activated microglia were enhanced (*i.e.* modified phenotype) from three days to 28 days after BCCAo when compared to time-matched shams. A change in microglial morphology was not observed after three hours of BCCAo compared to the sham group. At seven days post BCCAo, all the animals of the BCCAo group showed an important enhancement of microglial activation and also marked damage within the white and grey matters.

Those results indicate that the presence of white matter damage does not seem to be initially due to an enhancement of microglial activation. Certainly, the damage in the white matter is not induced by an enhancement of microglial activation *per se*, but the damage to the perikarya can be due, in part, to a magnification of activated microglia that can differentiate into cytotoxic cells (Banati et al., 1993); this possible sequence then may lead to perikaryal damage. As was observed, white matter pathology is more important at later time points, a sequence which may be explained by the production of TNF-α from both microglia and dying neurons which then exacerbates the damage to the white matter (Banati et al., 1993). The protein, tumor necrosis factor (TNF-α) is increased at six and 24 hours after cerebral ischaemia (Haddad et al., 2006). The ischaemic damage in the perikarya of neurons and the enhancement of microglial activation, both expressing TNF-α, may exacerbate the pathology to white and grey matter (Selmaj et al., 1988; Taupin et al., 1997). Neurons and microglia are major sources of TNF-α which leads to oedema formation and demyelination under ischaemic conditions (Selmaj et al., 1988; Taupin et al., 1997).

Moreover, it has been demonstrated that matrix metalloproteinase-2 (MMP-2) plays a major role in chronic cerebral hypoperfusion (Nakaji et al., 2006) and that, after three days of hypoperfusion, the expression of MMP-2 induces microglial activation (Ihara et al., 2001; Wakita et al., 1994). MMP-2 increases the permeability of the BBB by disrupting the tight junctions (Yang et al., 2007). Increased VEGF has been detected at 24 hours and seven days of chronic ischaemia and its expression is principally associated with endothelial cells in Sprague-Dawley rats (Hai et al., 2003). Both the expression of MMP-2 and VEGF lead to an increase in the permeability of the BBB. In the present investigation it is not improbable that the white matter injury seen three

hours after BCCAo was secondary to, or associated with, an increased permeability of the BBB.

BBB permeability to gadolinium as assessed by MRI

Studies done on patients with Binswanger's disease (characterized by cerebrovascular white matter lesions (Caplan, 1995)) and in patients with periventricular hyperintensities but no dementia, Hanyu and colleagues (2002) demonstrated, with MRI, a significant difference in the enhancement of gadolinium signal compared to patients with normal white matter. These observations indicate that white matter lesions seem to be related to a disruption of the BBB. However, it should be emphasized that this study was performed on patients ranging in age from 69 to 83 years old. BBB disruption has also been observed in the MCAo model, by MRI, after three hours of reperfusion (Sood et al., 2007).

These data do not support the hypothesis that BBB disruption is the primary cause of brain damage. No published data based on the MRI methodology have examined the BBB permeability at earlier time points in the BCCAo model. To investigate which pathways may be implicated in white matter lesions (seen here after three hours of BCCAo) MRI studies should be extended to optimize our understanding of the relationships between BBB dysfunction and chronic cerebral hypoperfusion.

Three hours after arterial occlusion, an enhancement of the signal of gadolinium was detected in both control and BCCAo groups and there were no differences between the four regions selected in each of the two groups of rats. Seven days following BCCAo; an enhancement of the gadolinium signal was also detected in both groups (sham and BCCAo) but greater in the BCCAo group than in the sham group.

Moreover, a significant difference of gadolinium signal enhancement between the two groups was detected in the external capsule and in the caudatoputamen (cf fig. 3.30).

Histopathology of the enhanced microglial activation in white matter after BCCAo

Both white and grey matter exhibited abnormal histology, revealed to be significant in terms of microglial activation, after seven days of BCCAo.

Four hours post BCCAo, axonal damage and microglial activation were detected, while no damage to the perikarya of neurons was apparent. Seven days post BCCAo, perikaryal damage was detected in the BCCAo group, with axonal damage and microglial activation. However, despite the fact that axonal damage and ischaemic neuronal damage was detected in some rats, no significant differences were observed between the sham and BCCAo group. These data differ from the first study in that there were no significant differences between the sham and BCCAo groups. A possible explanation for this dichotomy could be the limited number of animals that was subjected to the MRI study (*i.e.* under-powered) whereas in the histopathological study a more important number of rats were analysed.

White matter injury was noted after four hours of BCCAo in the histopathological study in the absence of any apparent damage to the perikarya. These observations broadly replicate those found in the initial investigation (three hours post-BCCAo) in which structural modifications in the white matter were manifest. The cell bodies of neurons in the grey matter were microscopically normal. It should be underlined that the time point in this second study was four and not three hours post BCCAo, because of practical difficulties as explained below. Microglial activation was detected in the MRI study (four hours post BCCAo), which was not the case after three hours following BCCAo in the earlier investigation.

Combining the results found with MRI to detect any modification in BBB permeability, it is reasonable to conclude that BCCAo induces in the initial phase, white matter injury in the absence of any alteration in BBB permeability. To summarize the results so far obtained: rapidly following BCCAo there is an acute decrease in CBF which initial causes detectable white matter lesions and this in the context of normal BBB permeability.

Seven days post BCCAo, the MRI investigations revealed a significant enhancement of gadolinium in the white and grey matter, a finding which is translated as an increase of BBB permeability. This "leakiness" of the BBB coincides with the time at which there was a significant increase of activated microglia compared to the sham group found at seven days post BCCAo. Yenari and collaborators (2006) have shown that microglial activation radically impairs the integrity of the BBB in an *in vivo* model of experimental stroke. The mechanisms of this deleterious effect have been established. Microglial activation induces neuronal cell death by secreting nitric oxide (NO) (Chao et al., 1992). NO itself, which is a vasodilatatory agent, has been found to induce an increase of BBB permeability (Shukla et al., 1996). The hypothesis outlined above is in accordance supported by the work of Pantoni and collaborators (1996) who demonstrated that white matter is highly vulnerable to focal ischaemia and that a lethal swelling of glial cells preceded by several hours the appearance of necrotic neurons. This damage to the white matter leads to an activation of microglia with time, which could be responsible of the neuronal damage, in parallel, by the secretion of NO, an increase of the permeability of the BBB.

In another rat model of chronic cerebral hypoperfusion, the expression of adhesion molecules of the cerebrovascular endothelial cells was induced (at one and three days) and lead to the infiltration of activated leukocytes into the brain parenchyma which

could potentially induce white matter lesions (Huang et al., 2010). However, the infiltration of activated leukocytes is not a pathological event but physiological, namely diapedesis. This enhanced microglial activation might lead with time to an assault to the integrity of the BBB. The article of Huang and collaborators (2010) tails to answer the question: "Is endothelial dysfunction of cerebral small vessel responsible for white matter lesions after chronic cerebral hypoperfusion in rats?". These authors observed an increase in the expression of adherens molecules of the endothelial cells. Is this sufficient to claim a dysfunction of the endothelial cells while diapedesis is a physiological system of defence**,** and while they did not measure in this study the permeability of the BBB?

Others studies demonstrated an increase of BBB permeability after chronic cerebral hypoperfusion in rats. Ueno and collaborators (2002) stated that it is chronic cerebral hypoperfusion which induces BBB permeability at one, three and seven days following BCCAo. They noted that they detected to a "small degree" the reaction product of Horseradish peroxidase using electronic microscopy after three hours of BCCAo. Moreover, Sood and collaborators (2008) detected an increase in BBB permeability after three days of BCCAo in the rat.

The MRI in-vivo study that we implemented to detect BBB permeability appears to be an interesting tool for further exploration of the integrity of the BBB.

In conclusion, this is the first study in the model of BCCAo to assess the integrity of the BBB at earlier time point using MRI. Moreover, it is the first study in the rat model of permanent BCCAo that showed an increase of Gadolinium signal enhancement in the caudatoputamen and in the external capsule. The results suggest that permanent BCCAo does not induce in itself an increase of BBB permeability, but

the presence of damage and activated microglia may play a role in the modulation of the properties of the BBB.

Which pathways could lead to white and grey matter pathology related to BBB permeability?

The last study aimed to investigate how cerebral hypoperfusion may affect levels and expression of proteins involved in the apoptotic and non-apoptotic pathways, to understand which pathways may lead to white and grey matter injury.

Non-apoptotic pathway after three hours or seven days post BCCAo

Western blot analysis of brain structures from the hemi-brain revealed no changes in HIF-1α, caspase-3, VEGF, MMP-2 levels compared to the sham group. On the other hand, RT-PCR analysis of the cortex, the corpus callosum and the caudatoputamen from the other hemi-brain indicated a significant expression of VEGF mRNA in the hypoperfused animals in those three regions compared to the sham, seven days post BCCAo. However, there was no difference in caspase-3 mRNA and HIF-1α mRNA following seven days post BCCAo compared to the sham. In a diferrent model of chronic cerebral hypoperfusion, by a formation of a fistula between the right external jugular vein and the ipsilateral common carotid artery, followed by ligation of the left vein of the sinus transverse and the bilateral common carotid arteries, Hai and collaborators (2003) demonstrated a peak of VEGF mRNA expression at seven days, which is consistent with our results, and also consistent with the finding of Pichiule and collaborators (1999) in the model of transient global ischaemia induced by cardiac arrest and resuscitation. In contrast to the present study, Tomimoto and collaborators (2003), using the same model of BCCAo we used, detected that the

caspase-3 mRNA was upregulated compared to the sham at one, three, seven and 30 days post BCCAo. We have to underline that only three rats were used in Tomimoto's experiment to compare the caspase-3 mRNA between the BCCAo and the sham animals. I have already underlined that this model of chronic cerebral hypoperfusion is variable between animals within the same group. To reduce this variability, it is important to increase the number of animals to use, to not find a result that describes the characteristics of one animal and not of the entire group. In our study we used eight animals for the BCCAo procedure compared to eight in sham, this may explains why we did not find a significant difference between the control and the BCCAo group in caspase-3 mRNA.

MMP-2 mRNA did not appear to be changed after seven days post BCCAo in the study of Ihara and collaborators (2001), which supports also our finding. In contrast, in a severe model of focal cerebral ischaemia, in the MCAo model, Heo and collaborators (1999) found that MMP-2 was significantly up-regulated after one hour post MCAo. This can be explained by the decrease of the cerebral blood supply being considerable, and impairs delivery of all blood constituents such as glucose and O_2, establishing then a hypoxic environment, and activating HIF 1-α which promotes the expression of MMP-2.

When examining the results of the last study, an interesting point has to be highlighted.

The apoptotic pathway does not seem to be the cause of damage to the white matter. Indeed, I previously described that injury occur first to the white matter, then into the perikarya of neurons. Moreover, the activation of the microglia is subsequent to the damage to the white matter tract. Then the results in this study indicate that the

decrease of the CBF due to BCCAo is not sufficiently low to overexpress HIF-1α. But the injury to the white matter can be explained by the fact that it appears to be highly sensitive to any disturbances of the CBF in contrary to the grey matter that seems to be more resistant to small changes of the blood supply (Pantoni et al., 1996).

Krick et al. (2005) showed that overexpression of HIF-1α resulted in increased apoptosis; which should have resulted, in our model, to a significant increase of Caspase-3 compare to the control group (sham). It was reported that in glioma tumor cells, the levels of HIF-1α increase in proportion with the level of the tumor and contributes to tumor proliferation through angiogenesis (Zagzag et al., 2000). HIF-1α gene is transcribed in the nucleus, then translated in the cytoplasm, and during hypoxia, it can re-enter the nucleus to form a complex with HIF-1β regulating the VEGF gene (Ziello et al., 2007). However, the lack of significant difference in our last study of HIF-1α mRNA expression between the BCCAo and the sham group, at seven days post surgery, remains unclear. Nevertheless, later time points in this BCCAo model may exhibit a significant HIF-1α mRNA expression.

How can we understand an upregulation of HIF1-α in cerebral white matter found in Leukoaraiosis, being attributed to white matter hypoperfusion (Fernando et al., 2006)?

The work done by Fernando and collaborators in 2006 showing an upregulation of HIF1-α after white matter hypoperfusion cannot be compared with the rat model of cerebral hypoperfusion, knowing that their investigation was based on a post-mortem cohort of ageing human brains. Indeed the rat hypoperfusion model is not a model of the senescent rat; rather, BCCAo mimics the condition of hypoperfused brain seen in SVD but without any comorbities. Hypoperfused patients are in a longer state of

hypoperfusion than in the rat model. The data (Fernando et al., 2006) have shown that the cerebral white matter is in a hypoxic environment with a persistent expression of HIF1-α, which can explain the consequences of chronic and long-lasting hypoperfusion in ageing subjects. It is premature to say that the cause of the damage to the white matter is due to HIF 1-α, in that no study on the hypoperfused rat model has shown any time-dependent upregulation of this factor. As a hypothesis, the upregulation of HIF-1α observed in the hypoperfused ageing brain is the consequence of a chronic cerebral hypoperfusion, leading to a more severe hypoxic state.

VEGF mRNA expression at seven days post BCCAo

A novel finding of the present study is that the VEGF mRNA was significantly increased compared to the sham group after seven days of BCCAo. This result has not been previously reported in comparable models. This significant expression of VEGF mRNA at seven days post BCCAo could be one of the factors that lead to an increase of BBB permeability as found with MRI. Previous work has shown that VEGF negatively modifies BBB permeability in a model of focal cerebral ischaemia (Valable et al., 2005). In many neuropathological situations, the instability of the endothelial-glial interactions induces capillaries to release the VEGF which will then increase the permeability of the BBB (Abbott et al., 2006). In our western blot result for VEGF, no differences were detected between the BCCAo and sham group. The western blot represents the level of proteins present in the tissue, while the RT-PCR gives information on the expression of proteins in the tissue. These elements would explain that later time points should show a clearer difference between BCCAo and

sham group in terms of VEGF protein level as assessed by the western blot methodology.

The findings detailed in this thesis supported by the scientific publications in this field, lead us to state that chronic cerebral hypoperfusion is a major risk for cerebral white and grey matter injury. To further determine the mechanisms of white and grey matter pathology with time in this model of SVD, an extension of studies in the BCCAo model is necessary. Figure 4.1 proposes a working hypothesis for the development of cerebral hypoperfusion leading to white matter injury a paradigm which could be the basis for future research projects:

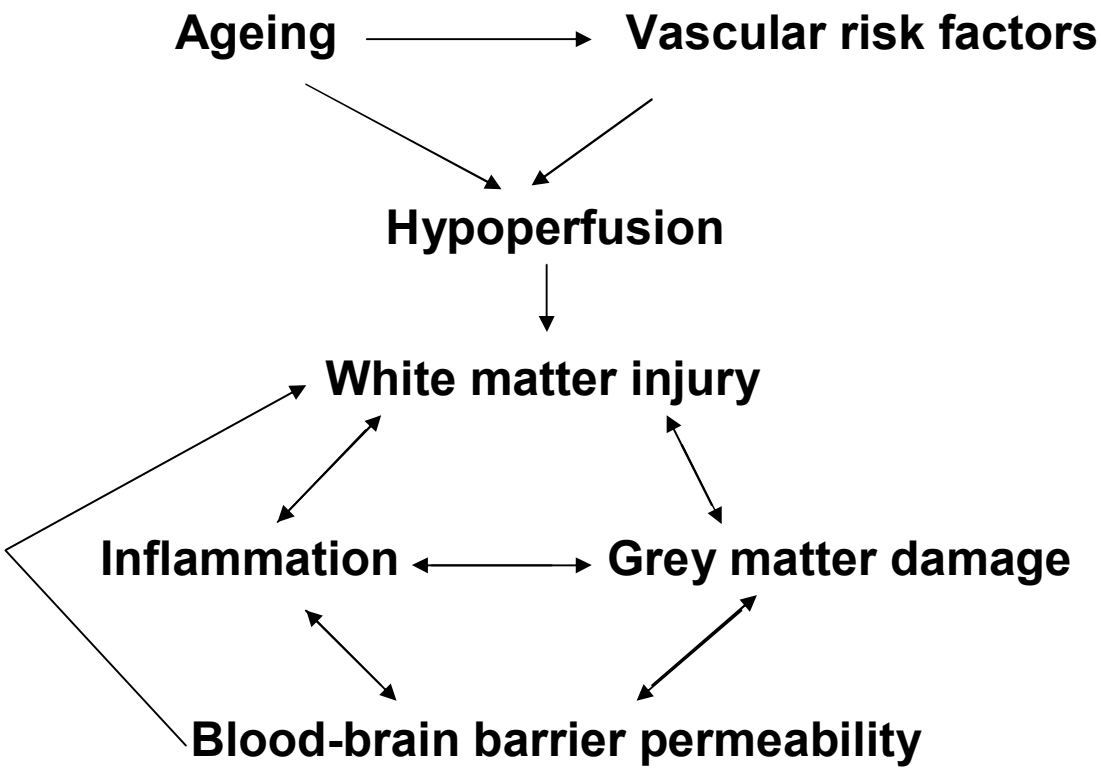

Fig.4.1: Proposed pathway for the development of white matter pathology. Ageing associated with vascular risk factors are the main causes of the development of white matter damage. BBB permeability may occur at a later stage which would further exacerbate the injury to white matter.

4.1 Critics and limits of the studies

Lack of information on BBB-related proteins

One of the main hypotheses of this body of work was to understand if an increase of BBB permeability was the possible cause of white matter damage after BCCAo. However, we were unable to determine the level of proteins of the BBB such as tight junctions and adherens junctions. To complement the MRI study, it would have been of interest to measure the proteins levels of the tight junction (between endothelial brain cells) as a function of time in our model of BCCAo.

No measurement of CBF

Major pathological differences occurred between animals within the same group. It would have been interested to measure the CBF before and after the surgery, though the method that would ideally measure CBF is unclear. Given the dispersion of the lesions in neuroanatomical space and time, the solution would be to adopt multi-modal, three-dimensional imaging to compare state-of-the-art MRI and micro-PET. Abnormalities detected early after BCCAo could be followed to better understand the evolution of white matter lesions. As stated before, there is an abundant literature on CBF following BCCAo in rats (see fig.2.1). Thus, global CBF measurements are of little interest as it varies from -50% (three days) to -25% (28 days).

Limits tothe MRI study

Due to practical difficulties, MRI acquisitions utilized in this study were limited and failed to detect any white matter changes because of the small number of animal used and the optimal resolution. The dispersion of the lesions has already been underlined with the differences between animals and group. To decrease the variability between

animals within a group is to increase the number of animals. Davies et al. (2005) noted that the rate of MTR decreases significantly in the grey matter compared to the white matter which corresponds to the results found in this thesis. However, no significant differences in MTR between the BCCAo and sham group were evidenced. In retrospect it is unfortunate that we did include a positive control to assure the certainty of identifying white matter lesions in the rat.

Holland and collaborators (2010) showed that, with MRI, small changes of white matter physiology were detectable in hypoperfused mice. The effectives were important (Holland et al., 2010). Diffusion tensor MRI (DT-MRI) has been used to identify microstructural alterations in aged, compared to young brains (Pfefferbaum et al., 2000). Indeed, fractional anisotropy (FA), a MRI paradigm, which indicates the fraction of the magnitude of the diffusion tensor which can be assigned to anisotropic water in each voxel, was shown to be decreased even in the absence of any structural changes in the white matter (Harsan et al., 2008). The combination of MTR and FA in a large group of animals in our study would have been indicated for the detection of white matter changes. This was not possible in our study. The DT MRI acquisition lasts for two hours and the T1 acquisition to check BBB permeability to gadolinium lasts for one hour. The rat is fragile after three hours of maintence anaesthesia. This combination of factors explains why the number and nature of the MRI sequences was suboptimal.

Early pathology, practical difficulties

The T1 acquisition last for one hour, the animals of the “three hours group” were the perfused so that the pathology was analysed at 4 hours post BCCAo instead of three hours post BCCAo. The T1 acquisition was done at three hours post BCCAo. These technical obstacles explain, the practical difficulties incombining the two techniques (MRI+histology) at the earliest time points.

The fact that no significant difference in APP immunostaining were observed at four hours post BCCAo, compared to the sham group, does not contradict the results of theinitial experiments. A significant difference was detected between the BCCAo and sham group from three hours to 28 days. The fact should be emphasized that the number of animal in the first study was greater than that in the second.

The BCCAo rat model is not reproducible and seems to change with time and other factors. This variability renders reproducibility and statistical analyses difficult but nonetheless represents the reality of the situation in man. Patients with small vessel diseases do have neither the same structural damage nor the same pattern of brain damage presumably because of the cerebrovasculature that differs with individuals and a function of age.

4.2 Future studies

The findings described herein could be extended by future investigation of the mechanisms involved in the pathological alterations detailed in the thesis. Figure 4.2 demonstrates the intimity between activated microglia with endothelial cells after BCCAo. Phenotypic modifications, gene expression and antigen/antibody production are all areas in which a research effort would be largely justified to understand the glial/endothelial interactions.

Electron microscopic studies have revealed that, during experimental autoimmune encephalomyelitis, leukocytes cross the cerebral microvessels by a transendothelial process, without "opening" the endothelial tight junctions (Wolburg et al., 2005). In vivo two-photon microscopy (Okada, 2010) in the BCCAo model could be applied to the observations of the effects of chronic cerebral hypoperfusion on leukocytic migration through the cerebral microvessels: specifically to know the temporal progression of the migratory process wether this process occurs via the tight junctions or the endothelial cells themselves.

As stated above, the identification of the level and expression of proteins in the tight and adherens junctions, at earlier and later time points, would allow a better understanding of the integrity of the BBB, a key component in cerebrovascular diseases.

An activation of NMDA receptors in models of cerebral ischaemia leads to a state of ischaemic tolerance and thus confers neuroprotection (Saleh et al., 2009). The question arises if glutaminergic mechanisms precondition the exchange vessels of the brain, a question which supposes variable permeability of the BBB as a function of the nature and duration of the insult. Such avenues would require in vivo

investigations which could compare and contrast permeability in white and grey matter. Again, and as stated earlier, the most powerful tools available (high field MRI combined with micro-PET) for in vivo studies are clearly excellent to shed light on the temporal evolution of BCCAo-induced pathology.

The ophthalmic and, hence its major branch, the central retinal, artery is the first and major intracranial branch of the internal carotid artery. Accordingly, bilateral common carotid artery occlusion has long been studied as a model of retinal ischaemia (Karpiak et al., 1989; Bacigaluppi et al., 2010 – part one; Bacigaluppi et al., 2010 – part two). BCCAo induces a moderate decrease in ocular blood flow which provokes, in sequence: the death of retinal ganglion cells (~ 1 week); neurons in the inner nuclear layer (~ 2 months); and, finally, the photoreceptors (~ 4 months) (Yamamoto et al., 2006). The early non-neuronal cell death and later loss of retinal neurons recapitulates some of the observations in the present thesis.

With hindsight, it could be of considerable scientific interest to compare and contrast the evolution of retinal and cerebral tissues following BCCAo in the same Wistar rat. The same panel of antibodies would be employed to characterise the various reactive and degenerative changes in those two embryologically similar organs. A direct comparison of retinal and cerebral pathologies provoked by BCCAo could well be the subject of future research projects. An additional interest would be that, as with a blood-brain barrier, a blood-retinal barrier exists but this latter can be circumvented by the intra-ocular administration of pharmacological agents, antibodies or other barrier-limited compounds.

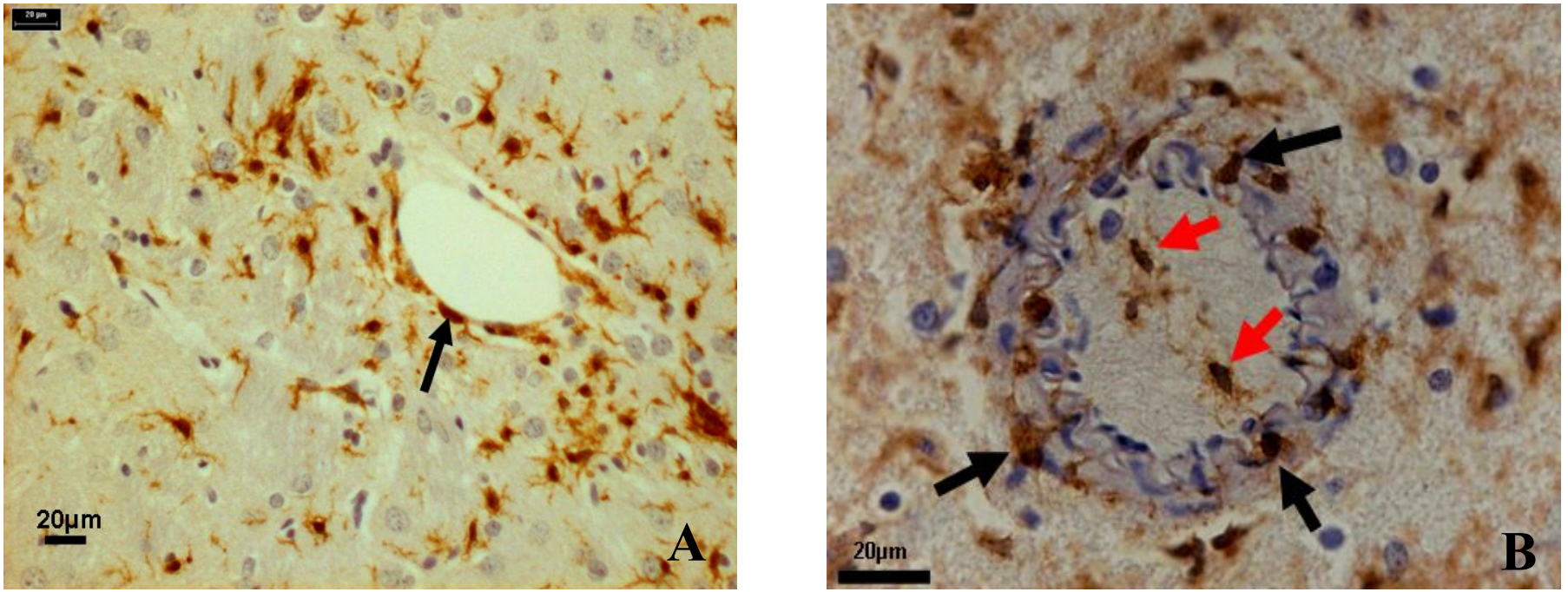

Fig.4.2: Iba-1 immunostaining counterstained with haematoxylin to indicate activated microglia (in brown) in the caudatoputamen of a rat brain after 14 days of BCCAo (A) and seven days post BCCAo (B). The black arrows show activated perivascular microglia while the red arrows show activated cells in the lumen (B). In B, activated microglia seem to be indissociable from the endothelial cells which may indicate migration of macrophages accross the BBB.

4.3 Conclusion

The results from this thesis - when taken in the context of other studies in the literature - demonstrate that chronic cerebral hypoperfusion initiates, even at early times following the acute decrease in brain blood flow, a specific pathology of white matter which is nonetheless variable in time and space (*i.e.* neuroanatomical location). These features are reminiscent of "small vessel disease" – one of the hallmarks of cerebrovascular and neurodegenerative (*eg* dementia) disorders.

If one accepts the postulate that, in the face of a mild but long-lasting perfusion, white matter pathology is the most precocious precursor of later widespread, irreversible neuronal loss, then the possibility for future preventative and therapeutic approaches is opened. At this moment in time such approaches (modulation of the functionality of cerebral endothelial cells, stem cell gratts in critical white matter tracts) remain both hypothetical and conjectural.

CHAPTER 5: References

Aaslid R, Lindegaard KF, Sorteberg W, Nornes H. (1989) Cerebral autoregulation dynamics in humans. *Stroke* 20:45-52

Abbott NJ, Patabendige AAK, Dolman DEM, Yusof SR, Begley DJ. (2010) Structure and function of the blood-brain barrier. *Neurobiol Dis* 37:13-25

Abbott NJ, Ronnback L, Hansson E. (2006) Astrocyte-endothelial interactions at the blood-brain barrier. *Nat Rev Neurosci* 7:41-53

Aboul-Enein F, Rauschka H, Kornek B, Stadelmann C, Stefferl A, Brück W, Lucchinetti C, Schmidbauer M, Jellinger K, Lassmann H. (2003) Preferential loss of myelin-associated glycoprotein reflects hypoxia-like white matter damage in stroke and inflammatory brain diseases. *J Neuropathol Exp Neurol* 62:25-33

Adams RA, Bauer J, Flick MJ, Sikorski SL, Nuriel T, Lassmann H, Degen JL, Akassoglou K. (2007) The fibrin-derived γ377-395 peptide inhibits microglia activation and suppresses relapsing paralysis in central nervous system autoimmune disease. *J Exp Med* 204:571-582

Akiguchi I, Tomimoto H, Suenaga T, Wakita H, Budka H. (1997) Blood-brain barrier dysfunction in Binswanger's disease; an immunohistochemical study. *Acta Neuropathol* 95:78-84

Allen NJ, Barres BA. (2009) Glia - more than just brain glue. *Nature* 457:675-677

Alpers BJ, Berry RG, RM P. (1959) Anatomical studies of the circle of Willis in normal brain. *Arch Neurol Psychiatr* 81:409-418

Araujo DM, Cotman CW. (1992) ß-Amyloid stimulates glial cells in vitro to produce growth factors that accumulate in senile plaques in Alzheimer's disease. *Brain Res* 569:141-145

Armiger LC, Wheeler EE, Geraghty DE, Herdson PB. (1977) An experimental evaluation of staining techniques for the detection of early ischaemic injury to the myocardium. *Pathology* 9:161-171

Astrup J, Siesjö BK, Symon L. (1981) Thresholds in cerebral ischemia - the ischemic penumbra. *Stroke* 12:723-725

Bacigaluppi M, Comi G, Hermann D. (2010) Animal models of ischemic stroke. Part One: modeling risk factors. *Open Neurol J* 4:26-33

Bacigaluppi M, Comi G, Hermann D. (2010) Animal models of ischemic stroke. Part Two: modeling cerebral ischemia. *Open Neurol J* 4:34-38

Balin BJ, Broadwell RD, Salcman M. (1987) Tubular profiles do not form transendothelial channels through the blood-brain barrier. *J Neurocytol* 16:721-735

Ballabh P, Braun A, Nedergaard M. (2004) The blood-brain barrier: an overview: Structure, regulation, and clinical implications. *Neurobiol Dis* 16:1-13

Baltan S, Besancon EF, Mbow B, Ye Z, Hamner MA, Ransom BR. (2008) White Matter Vulnerability to Ischemic Injury Increases with Age Because of Enhanced Excitotoxicity. *J Neurosci* 28:1479-1489

Banati RB, Gehrmann J, Schubert P, Kreutzberg GW. (1993) Cytotoxicity of microglia. *Glia* 7:111-118

Baron JC, Bousser MG, Rey A, Guillard A, Comar D, Castaigne P. (1981) Reversal of focal "misery-perfusion syndrome" by extra-intracranial arterial bypass in hemodynamic cerebral ischemia. A case study with 15O positron emission tomography. *Stroke* 12:454-459

Bartzokis G, Cummings JL, Sultzer D, Henderson VW, Nuechterlein KH, Mintz J. (2003) White Matter Structural Integrity in Healthy Aging Adults and Patients With Alzheimer Disease: A Magnetic Resonance Imaging Study. *Arch Neurol* 60:393-398

Batchelor PE, Liberatore GT, Wong JYF, Porritt MJ, Frerichs F, Donnan GA, Howells DW. (1999) Activated Macrophages and Microglia Induce Dopaminergic Sprouting in the Injured Striatum and Express Brain-Derived Neurotrophic Factor and Glial Cell Line-Derived Neurotrophic Factor. *J Neurosci* 19:1708-1716

Baumann N, Pham-Dinh D. (2001) Biology of oligodendrocyte and myelin in the mammalian central nervous system. *Physiol Rev* 81:871-927

Begley DJ, Brightman MW. (2003) Structural and functional aspects of the blood-brain barrier. *Prog Drug Res* 61:39-78

Bell RD, Winkler EA, Sagare AP, Singh I, LaRue B, Deane R, Zlokovic BV. (2010) Pericytes control key neurovascular functions and neuronal phenotype in the adult brain and during brain aging. *Neuron* 68:409-427

Bennett SA, Tenniswood M, Chen J-H, Davidson CM, Keyes MT, Fortin T, Pappas BA. (1998) Chronic cerebral hypoperfusion elicits neuronal apoptosis and behavioral impairment. *NeuroReport* 9:161-166

Berne RM, Winn HR, R R. (1981) The local regulation of cerebral blood flow. *Prog Cardiovasc Dis* 24:243-260

Bield A, Kraus R. (1898) Über eine bisher unbekannte toxische Wirkung der Gallensauren auf das Zentralnervensystem. *Zhl Inn Med* 19:1185–1200

Brīede J, Duburs G. (2007) Protective effect of cerebrocrast on rat brain ischaemia induced by occlusion of both common carotid arteries. *Cell Biochem Func* 25:203-210

Brooks TA, Hawkins BT, Huber JD, Egleton RD, Davis TP. (2005) Chronic inflammatory pain leads to increased blood-brain barrier permeability and tight junction protein alterations. *Am J Physiol* 289:H738-H743

Brun A, Englund E. (1986) A white matter disorder in dementia of the Alzheimer type: a pathoanatomical study. *Ann Neurol* 19:253-262

Brundin P. (2002) GDNF treatment in Parkinson's disease: time for controlled clinical trials? *Brain* 125:2149-2151

Buée LUC, Hof PR, Delacourte A. (1997) Brain microvascular changes in Alzheimer's disease and other dementia. *Ann NY Acad Sci* 826:7-24

Burns EM, Dobben GD, Kruckeberg TW, Gaetano PK. (1981) Blood-brain barrier: morphology, physiology, and effects of contrast media. *Adv Neurol* 30:159-165

Busch H-J, Buschmann IR, Mies G, Bode C, Hossmann K-A. (2003) Arteriogenesis in hypoperfused rat brain. *JCBFM* 23:621-628

Bushong EA, Martone ME, Jones YZ, Ellisman MH. (2002) Protoplasmic astrocytes in CA1 stratum radiatum occupy separate anatomical domains. *J Neurosci* 22:183-192

Buss A, Schwab ME. (2003) Sequential loss of myelin proteins during Wallerian degeneration in the rat spinal cord. *Glia* 42:424-432

Butovsky O, Talpalar AE, Ben-Yaakov K, Schwartz M. (2005) Activation of microglia by aggregated β-amyloid or lipopolysaccharide impairs MHC-II expression and renders them cytotoxic whereas IFN-γ and IL-4 render them protective. *Mol Cell Neurosci* 29:381-393

Caplan LR. (1995) Binswanger's disease--revisited. *Neurology* 45:626-633

Cardoso FL, Brites D, Brito MA. (2010) Looking at the blood-brain barrier: Molecular anatomy and possible investigation approaches. *Brain Res Rev* 64:328-363

Carlson SL, Parrish ME, Springer JE, Doty K, Dossett L. (1998) Acute inflammatory response in spinal cord following impact injury. *Exp Neurol* 151:77-88

Carmeliet P, Dor Y, Herbert JM, Fukumura D, Brusselmans K, Dewerchin M, Neeman M, Bono F, Abramovitch R, Maxwell P, Koch CJ, Ratcliffe P, Moons L, Jain RK, Collen D, Keshert E. (1998) Role of HIF-1α in hypoxia-mediated apoptosis, cell proliferation and tumour angiogenesis. *Nature* 394:485-490

Carvey PM, Hendey B, Monahan AJ. (2009) The blood–brain barrier in neurodegenerative disease: a rhetorical perspective. *J Neurochem* 111:291-314

Chao CC, Hu S, Molitor TW, Shaskan EG, Peterson PK. (1992) Activated microglia mediate neuronal cell injury via a nitric oxide mechanism. *J Immunol* 149:2736-2741

Cho K-O, La HO, Cho Y-J, Sung K-W, Kim SY. (2006) Minocycline attenuates white matter damage in a rat model of chronic cerebral hypoperfusion. *J Neurosci Res* 83:285-291

Choi JY, Morris JC, Hsu CY. (1998) Aging and cerebrovascular disease. *Neurol Clin* 16:687-711

Choy M, Ganesan V, Thomas DL, Thornton JS, Proctor E, King MD, van der Weerd L, Gadian DG, Lythgoe MF. (2006) The chronic vascular and haemodynamic response after permanent bilateral common carotid occlusion in newborn and adult rats. *JCBFM* 26:1066-1075

Coull JAM, Beggs S, Boudreau D, Boivin D, Tsuda M, Inoue K, Gravel C, Salter MW, De Koninck Y. (2005) BDNF from microglia causes the shift in neuronal anion gradient underlying neuropathic pain. *Nature* 438:1017-1021

Coyne CB, Gambling TM, Boucher RC, Carson JL, Johnson LG. (2003) Role of claudin interactions in airway tight junctional permeability. *Am J Physiol* 285:L1166-L1178

Cserr HF, Bundgaard M. (1984) Blood-brain interfaces in vertebrates: a comparative approach. *Am J Physiol* 246:R277-R288

Davalos D, Grutzendler J, Yang G, Kim JV, Zuo Y, Jung S, Littman DR, Dustin ML, Gan W-B. (2005) ATP mediates rapid microglial response to local brain injury in vivo. *Nat Neurosci* 8:752-758

Davidson CM, Pappas BA, Stevens WD, Fortin T, Bennett SAL. (2000) Chronic cerebral hypoperfusion: loss of pupillary reflex, visual impairment and retinal neurodegeneration. *Brain Res* 859:96-103

Davies G, Altmann D, Hadjiprocopis A, Rashid W, Chard D, Griffin C, Tofts P, Barker G, Kapoor R, Thompson A, Miller D. (2005) Increasing normal-appearing grey and white matter magnetisation transfer ratio abnormality in early relapsing-remitting multiple sclerosis. *J Neurol* 252:1037-1044

De Jong GI, Farkas E, Stienstra CM, Plass JRM, Keijser JN, de la Torre JC, Luiten PGM. (1999) Cerebral hypoperfusion yields capillary damage in the hippocampal CA1 area that correlates with spatial memory impairment. *Neuroscience* 91:203-210

De Keyser J, Steen C, Mostert JP, Koch MW. (2008) Hypoperfusion of the cerebral white matter in multiple sclerosis: possible mechanisms and pathophysiological significance. *JCBFM* 28:1645-1651

de la Monte SM. (1989) Quantitation of cerebral atrophy in preclinical and end-stage Alzheimer's disease. *Ann Neurol* 25:450-459

de La Torre JC. (2000) Impaired cerebromicrovascular perfusion: summary of evidence in support of its causality in Alzheimer's disease. *Ann NY Acad Sci* 924:136-152

de la Torre JC. (2010) The vascular hypothesis of Alzheimer's disease: bench to bedside and beyond. *Neurodegener Dis* 7:116-121

de la Torre JC. (2010) Vascular risk factor detection and control may prevent Alzheimer's disease. *Ageing Res Rev* 9:218-225

de la Torre JC, Čada A, Nelson N, Davis G, Sutherland RJ, Gonzalez-Lima F. (1997) Reduced cytochrome oxidase and memory dysfunction after chronic brain ischemia in aged rats. *Neurosci Lett* 223:165-168

de la Torre JC, Fortin T. (1994) A chronic physiological rat model of dementia. *Behav Brain Res* 63:35-40

de Wilde MC, Farkas E, Gerrits M, Kiliaan AJ, Luiten PGM. (2002) The effect of n-3 polyunsaturated fatty acid-rich diets on cognitive and cerebrovascular parameters in chronic cerebral hypoperfusion. *Brain Res* 947:166-173

Del Maschio A, De Luigi A, Martin-Padura I, Brockhaus M, Bartfai T, Fruscella P, Adorini L, Martino G, Furlan R, De Simoni MG, Dejana E. (1999) Leukocyte recruitment in the cerebrospinal fluid of mice with experimental meningitis is inhibited by an antibody to junctional adhesion molecule (JAM). *J Exp Med* 190:1351-1356

Deli MA. (2009) Potential use of tight junction modulators to reversibly open membranous barriers and improve drug delivery. *BBA* 1788:892-910

Dietrich WD, Busto R, Yoshida S, Ginsberg MD. (1987) Histopathological and hemodynamic consequences of complete versus incomplete ischemia in the rat. *JCBFM* 7:300-308

Edaravone Acute Infarction Study Group. (2003) Effect of a novel free radical scavenger, edaravone (MCI-186), on acute brain infarction. *Cerebrovasc Dis* 15:222-229

Ehrlich P. (1885) Das Sauerstoff-Bedürfniss des organismus : eine farbenanalytische Studie. *Hirschwald, Berlin*.

El Khoury J, Hickman SE, Thomas CA, Loike JD, Silverstein SC. (1998) Microglia, scavenger receptors, and the pathogenesis of alzheimer's disease. *Neurobiol Aging* 19:S81-S84

El Khoury J, Toft M, Hickman SE, Means TK, Terada K, Geula C, Luster AD. (2007) Ccr2 deficiency impairs microglial accumulation and accelerates progression of Alzheimer-like disease. *Nat Med* 13:432-438

Elkabes S, DiCicco-Bloom EM, Black IB. (1996) Brain microglia/macrophages express neurotrophins that selectively regulate microglial proliferation and function. *J Neurosci* 16:2508-2521

Falcao ALE, Reutens DC, Markus R, Koga M, Read SJ, Tochon-Danguy H, Sachinidis J, Howells DW, Donnan GA. (2004) The resistance to ischemia of white and gray matter after stroke. *Ann Neurol* 56:695-701

Farkas E, Annaházi A, Institóris Á, Mihály A, Luiten PGM, Bari F. (2005) Diazoxide and dimethyl sulphoxide alleviate experimental cerebral hypoperfusion-induced white matter injury in the rat brain. *Neurosci Lett* 373:195-199

Farkas E, Donka G, de Vos RA, Mihaly A, Bari F, Luiten PG. (2004) Experimental cerebral hypoperfusion induces white matter injury and microglial activation in the rat brain. *Acta Neuropathol* 108:57-64

Farkas E, Institóris Á, Domoki F, Mihály A, Luiten PGM, Bari F. (2004) Diazoxide and dimethyl sulphoxide prevent cerebral hypoperfusion-related learning dysfunction and brain damage after carotid artery occlusion.*Brain Res* 1008:252-260

Farkas E, Luiten PGM. (2001) Cerebral microvascular pathology in aging and Alzheimer's disease. *Progress in Neurobiology* 64:575-611

Farkas E, Luiten PGM, Bari F. (2007) Permanent, bilateral common carotid artery occlusion in the rat: A model for chronic cerebral hypoperfusion-related neurodegenerative diseases. *Brain Res Rev* 54:162-180

Farrall AJ, Wardlaw JM. (2009) Blood–brain barrier: Ageing and microvascular disease – systematic review and meta-analysis. *Neurobiol Aging* 30:337-352

Fédérici C, Camoin L, Créminon C, Chaverot N, Strosberg AD, Couraud PO. (1995) Cultured astrocytes release a factor that decreases endothelin-1 secretion by brain microvessel endothelial cells. *J Neurochem* 64:1008-1015

Feigin I, Popoff N. (1963) Neuropathological changes late in cerebral edema: the relationship to trauma, hypertensive disease and binswanger's encephalopathy. *J Neuropathol Exp Neurol* 22:500-511

Fernando MS, Simpson JE, Matthews F, Brayne C, Lewis CE, Barber R, Kalaria RN, Forster G, Esteves F, Wharton SB, Shaw PJ, O'Brien JT, Ince PG. (2006) White Matter Lesions in an Unselected Cohort of the Elderly. *Stroke* 37:1391-1398

Ferrer I, Kaste M, Kalil J. (2008) Vascular diseases. In Love S, Louis D, Ellison D, (eds.). *Greenfield's Neuropthology*. *London: Arnold*: 121-220

Fisher C. (1972) Cerebral miliary aneurysms in hypertension. *Am J Pathol* 66:313-330

Frade JMa, Barde Y-A. (1998) Microglia-derived nerve growth factor causes cell death in the developing retina. *Neuron* 20:35-41

Fujii M, Hara H, Meng W, Vonsattel JP, Huang Z, Moskowitz MA. (1997) Strain-related differences in susceptibility to transient forebrain ischemia in SV-129 and C57Black/6 mice. *Stroke* 28:1805-1811

Gentleman S, Roberts G, Gennarelli T, Maxwell W, Adams J, Kerr S, Graham D. (1995) Axonal injury: a universal consequence of fatal closed head injury? *Acta Neuropathol* 89:537-543

Gentleman SM, Nash MJ, Sweeting CJ, Graham DI, Roberts GW. (1993) [beta]-Amyloid precursor protein ([beta]APP) as a marker for axonal injury after head injury. *Neurosci Lett* 160:139-144

Ginsberg MD, Busto R. (1989) Rodent models of cerebral ischemia. *Stroke* 20:1627-1642

Gleckman AM, Bell MD, Evans RJ, Smith TW. (1999) Diffuse axonal injury in infants with nonaccidental craniocerebral trauma. *Arch Pathol Lab Med* 123:146-151

Godeau G, Robert AM. (1979) Mechanism of action of collagenase on the blood-brain barrier permeability. Increase of endothelial cell pinocytotic activity as shown with horse-radish peroxidase as a tracer. *Cell Biol Int Rep* 3:747-751

Goldmann E. (1909) Die aussere und innere sekretion des gesunden und kranken Organismus im Licht der vitalen Farburg. *Beitr Klin Chir* 64:192–265

González-Mariscal L, Tapia R, Chamorro D. (2008) Crosstalk of tight junction components with signaling pathways. *BBA* 1778:729-756

Gordon S. (2003) Alternative activation of macrophages. *Nat Rev Immunol* 3:23-35

Gordon S, Taylor PR. (2005) Monocyte and macrophage heterogeneity. *Nat Rev Immunol* 5:953-964

Graeber MB, López-Redondo F, Ikoma E, Ishikawa M, Imai Y, Nakajima K, Kreutzberg GW, Kohsaka S. (1998) The microglia/macrophage response in the neonatal rat facial nucleus following axotomy. *Brain Res* 813:241-253

Greijer AE, van der Wall E. (2004) The role of hypoxia inducible factor 1 (HIF-1) in hypoxia induced apoptosis. *J Clin Pathol* 57:1009-1014

Guang H-M, Du G-H. (2006) Protections of pinocembrin on brain mitochondria contribute to cognitive improvement in chronic cerebral hypoperfused rats. *Europ J Pharmacol* 542:77-83

Haddad M, Rhinn H, Bloquel C, Coqueran B, Szabo C, Plotkine M, Scherman D, Margaill I. (2006) Anti-inflammatory effects of PJ34, a poly(ADP-ribose) polymerase inhibitor, in transient focal cerebral ischemia in mice. *Brit J Pharmacol* 149:23-30

Hagberg H, Ichord R, Palmer C, Yager JY, Vannucci SJ. (2002) Animal models of developmental brain injury: relevance to human disease. *Devel Neurosci* 24:364-366

Hai J, Li ST, Lin Q, Pan QG, Gao F, Ding MX. (2003) Vascular endothelial growth factor expression and angiogenesis induced by chronic cerebral hypoperfusion in rat brain. *Neurosurgery* 53:963-970; discussion 970-962

Hanyu H, Asano T, Tanaka Y, Iwamoto T, Takasaki M, Abe K. (2002) Increased blood-brain barrier permeability in white matter lesions of Binswanger's disease evaluated by contrast-enhanced MRI. *Dement Geriatr Cognit Disord* 14:1-6

Harper AM. (1966) Autoregulation of cerebral blood flow: influence of the arterial blood pressure on the blood flow through the cerebral cortex. *J Neurol Neurosurg Psychiatry* 29:398–403

Harsan L-A, Steibel J, Zaremba A, Agin A, Sapin R, Poulet P, Guignard B, Parizel N, Grucker D, Boehm N, Miller RH, Ghandour MS. (2008) Recovery from chronic demyelination by thyroid hormone therapy: myelinogenesis induction and assessment by diffusion tensor magnetic resonance imaging. *J Neurosci* 28:14189-14201

Hattori H, Takeda M, Kudo T, Nishimura T, Hashimoto S. (1992) Cumulative white matter changes in the gerbil brain under chronic cerebral hypoperfusion. *Acta Neuropathol* 84:437-442

Hawkins BT, Davis TP. (2005) The blood-brain barrier/neurovascular unit in health and disease. *Pharmacol Rev* 57:173-185

Haydon PG, Carmignoto G. (2006) Astrocyte control of synaptic transmission and neurovascular coupling. *Physiolog Rev* 86:1009-1031

Heese K, Fiebich BL, Bauer J, Otten U. (1997) Nerve growth factor (NGF) expression in rat microglia is induced by adenosine A2α-receptors. *Neurosci Lett* 231:83-86

Heo JH, Lucero J, Abumiya T, Koziol JA, Copeland BR, del Zoppo GJ. (1999) Matrix metalloproteinases increase very early during experimental focal cerebral ischemia. *JCBFM* 19:624-633

Hirase T, Staddon JM, Saitou M, Ando-Akatsuka Y, Itoh M, Furuse M, Fujimoto K, Tsukita S, Rubin LL. (1997) Occludin as a possible determinant of tight junction permeability in endothelial cells. *J Cell Sci* 110 (Pt 14):1603-1613

Holland PR, Bastin ME, Jansen MA, Merrifield GD, Coltman RB, Scott F, Nowers H, Khallout K, Marshall I, Wardlaw JM, Deary IJ, McCulloch J, Horsburgh K. (2010) MRI is a sensitive marker of subtle white matter pathology in hypoperfused mice. *Neurobiol Aging* 32:2325.e2321-2325.e2326

Hsu SM, Raine L, Fanger H. (1981) Use of avidin-biotin-peroxidase complex (ABC) in immunoperoxidase techniques: a comparison between ABC and unlabeled antibody (PAP) procedures. *J Histochem Cytochem* 29:577-580

Huang Y, Zhang W, Lin L, Feng J, Chen F, Wei W, Zhao X, Guo W, Li J, Yin W, Li L. (2010) Is endothelial dysfunction of cerebral small vessel responsible for white matter lesions after chronic cerebral hypoperfusion in rats? *J Neurological Sci* 299: 72-80

Iannucci G, Dichgans M, Rovaris M, Bruning R, Gasser T, Giacomotti L, Yousry TA, Filippi M. (2001) Correlations between clinical findings and magnetization transfer imaging metrics of tissue damage in individuals with cerebral autosomal dominant arteriopathy with subcortical infarcts and leukoencephalopathy. *Stroke* 32:643-648

Ihara M, Tomimoto H, Kinoshita M, Oh J, Noda M, Wakita H, Akiguchi I, Shibasaki H. (2001) Chronic cerebral hypoperfusion induces MMP-2 but not MMP-9 expression in the microglia and vascular endothelium of white matter. *JCBFM* 21:828-834

Ito D, Imai Y, Ohsawa K, Nakajima K, Fukuuchi Y, Kohsaka S. (1998) Microglia-specific localisation of a novel calcium binding protein, Iba1. *Brain Res* 57:1-9

Janzer RC, Raff MC. (1987) Astrocytes induce blood-brain barrier properties in endothelial cells. *Nature* 325:253-257

Johnson PW, Abramow-Newerly W, Seilheimer B, Sadoul R, Tropak MB, Arquint M, Dunn RJ, Schachner M, Roder JC. (1989) Recombinant myelin-associated glycoprotein confers neural adhesion and neurite outgrowth function. *Neuron* 3:377-385

Joo F. (1971) Increased production of coated vesicles in the brain capillaries during enhanced permeability of the blood-brain barrier. *Br J Exp Pathol* 52:646-649

Kalaria RN. (1999) The Blood-brain barrier and cerebrovascular pathology in Alzheimer's disease. *Annals of the New York Academy of Sciences* 893:113-125

Kang J, Lemaire HG, Unterbeck A, Salbaum JM, Masters CL, Grzeschik KH, Multhaup G, Beyreuther K, Muller-Hill B. (1987) The precursor of Alzheimer's disease amyloid A4 protein resembles a cell-surface receptor. *Nature* 325:733-736

Karpiak SE, Tagliavia A, Wakade CG. (1989) Animal models for the study of drugs in ischemic stroke. *Annu Rev Pharmacol Toxicol* 29:403-414

Kasparova S, Brezová V, Valko M, Horecký J, Mlynárik V, Liptaj T, Vancová Og, Ulicná Og, Dobrota D. (2005) Study of the oxidative stress in a rat model of chronic brain hypoperfusion. *Neurochem Int* 46:601-611

Kawai K, Takahashi H, Ikuta F. (1989) Ultracytochemical study of capillary Ca^{2+}-ATPase activity in brain edema. *Acta Neuropathol* 77:449-454

Kiefer R, Gold R, Gehrmann J, Lindholm D, Wekerle H, Kreutzberg GW. (1993) Transforming growth factor beta expression in reactive spinal cord microglia and meningeal inflammatory cells during experimental allergic neuritis. *J Neurosci Res* 36:391-398

Kim J-S, Yun I, Choi YB, Lee K-S, Kim Y-I. (2008) Ramipril protects from free radical induced white matter damage in chronic hypoperfusion in the rat. *J Clin Neurosci* 15:174-178

Kim S-K, Cho K-O, Kim SY. (2009) The plasticity of posterior communicating artery influences on the outcome of white matter injury induced by chronic cerebral hypoperfusion in rats. *Neurolog Res* 31:245-250

Kitamura A, Fujita Y, Oishi N, Kalaria RN, Washida K, Maki T, Okamoto Y, Hase Y, Yamada M, Takahashi J, Ito H, Tomimoto H, Fukuyama H, Takahashi R, Ihara M. Selective white matter abnormalities in a novel rat model of vascular dementia. *Neurobiol Aging* 33:1012.e1025-1012.e1035

Kleine TO, Hackler R, Zöfel P. (1993) Age-related alterations of the blood-brain-barrier (bbb) permeability to protein molecules of different size. *Zeitschrift für Gerontologie* 26:256-259

Kobayashi K, Hayashi M, Nakano H, Fukutani Y, Sasaki K, Shimazaki M, Koshino Y. (2002) Apoptosis of astrocytes with enhanced lysosomal activity and oligodendrocytes in white matter lesions in Alzheimer's disease. *Neuropathol Appl Neurobiol* 28:238-251

Koo EH, Sisodia SS, Archer DR, Martin LJ, Weidemann A, Beyreuther K, Fischer P, Masters CL, Price DL. (1990) Precursor of amyloid protein in Alzheimer disease undergoes fast anterograde axonal transport. *Proc Natl Acad Sci U S A* 87:1561-1565

Kreutzberg GW. (1996) Microglia: a sensor for pathological events in the CNS. *Trends in Neurosciences* 19:312-318

Krick S, Eul BG, Hanze J, Savai R, Grimminger F, Seeger W, Rose F. (2005) Role of hypoxia-inducible factor-1{alpha} in hypoxia-induced apoptosis of primary alveolar epithelial type II cells. *Am J Respir Cell Mol Biol* 32:395-403

Kudo T, Tada K, Takeda M, Nishimura T. (1990) Learning impairment and microtubule-associated protein 2 decrease in gerbils under chronic cerebral hypoperfusion. *Stroke* 21:1205-1209

Kuroiwa T, Ting P, Martinez H, Klatzo I. (1985) The biphasic opening of the blood-brain barrier to proteins following temporary middle cerebral artery occlusion. *Acta Neuropathologica* 68:122-129

Lalancette-Hébert M, Gowing G, Simard A, Weng YC, Kriz J. (2007) Selective ablation of proliferating microglial cells exacerbates ischemic injury in the brain. *J Neurosci* 27:2596-2605

Lammie G. (2000) Pathology of small vessel stroke. *British Medical Bulletin* 56:296-306

Lee C, Landreth G. (2010) The role of microglia in amyloid clearance from the AD brain. *J Neural Transm* 117:949-960

Lee JH, Park SY, Shin YW, Hong KW, Kim CD, Sung S-M, Kim KY, Lee WS. (2006) Neuroprotection by cilostazol, a phosphodiesterase type 3 inhibitor, against apoptotic white matter changes in rat after chronic cerebral hypoperfusion. *Brain Res* 1082:182-191

Lehrmann E, Kiefer R, Christensen T, Toyka KV, Zimmer J, Diemer NH, Hartung H-P, Finsen B. (1998) Microglia and macrophages are major sources of locally produced transforming growth factor-β1 after transient middle cerebral artery occlusion in rats. *Glia* 24:437-448

Levy BI. (2001) Artery changes with aging: degeneration or adaptation? *Dialogues in Cardiovascular Medicine* 6:104 - 111

Lewandowsky M. (1900) Zur lehre der zerebrospinalflussigkeit. *Ztschr F Klin Méd* 40:480–484

Liu H-x, Zhang J-j, Zheng P, Zhang Y. (2005) Altered expression of MAP-2, GAP-43, and synaptophysin in the hippocampus of rats with chronic cerebral hypoperfusion correlates with cognitive impairment. *Mol Brain Res* 139:169-177

Liu J, Jin D-Z, Xiao L, Zhu X-Z. (2006) Paeoniflorin attenuates chronic cerebral hypoperfusion-induced learning dysfunction and brain damage in rats. *Brain Res* 1089:162-170

Longa EZ, Weinstein PR, Carlson S, Cummins R. (1989) Reversible middle cerebral artery occlusion without craniectomy in rats. *Stroke* 20:84-91

Luo X-G, Chen S-D. (2012) The changing phenotype of microglia from homeostasis to disease. *Translational Neurodegeneration* 1:9

Macrae IM. Preclinical stroke research – advantages and disadvantages of the most common rodent models of focal ischaemia. *Brit J Pharmacol* 164:1062-1078

Mallat M, Houlgatte R, Brachet P, Prochiantz A. (1989) Lipopolysaccharide-stimulated rat brain macrophages release NGF in vitro. *Dev Biol* 133:309-311

Marstrand JR, Garde E, Rostrup E, Ring P, Rosenbaum S, Mortensen EL, Larsson HBW. (2002) Cerebral perfusion and cerebrovascular reactivity are reduced in white matter hyperintensities. *Stroke* 33:972-976

Maxwell WL, Irvine A, Adams JH, Graham DI, Gennarelli TA. (1988) Response of cerebral microvasculature to brain injury. *J Pathol* 155:327-335

McKenzie KJ, McLellan DR, Gentleman SM, Maxwell WL, Gennarelli TA, Graham DI. (1996) Is β-APP a marker of axonal damage in short-surviving head injury? *Acta Neuropathol* 92:608-613

Meng S, Qiao M, Foniok T, Tuor U. (2005) White matter damage precedes that in gray matter despite similar magnetic resonance imaging changes following cerebral hypoxia-ischemia in neonatal rats. *Exp Brain Res* 166:56-60

Miyamoto E, Tomimoto H, Nakao S-i, Wakita H, Akiguchi I, Miyamoto K, Shingu K. (2001) Caudoputamen is damaged by hypocapnia during mechanical ventilation in a rat model of chronic cerebral hypoperfusion. *Stroke* 32:2920-2925

Miyamoto N, Tanaka R, Shimura H, Watanabe T, Mori H, Onodera M, Mochizuki H, Hattori N, Urabe T. (2009) Phosphodiesterase III inhibition promotes differentiation and survival of oligodendrocyte progenitors and enhances regeneration of ischemic white matter lesions in the adult mammalian brain. *JCBFM* 30:299-310

Mooradian AD. (1988) Effect of aging on the blood-brain barrier. *Neurobiol Aging* 9:31-39

Mukhopadhyay G, Doherty P, Walsh FS, Crocker PR, Filbin MT. (1994) A novel role for myelin-associated glycoprotein as an inhibitor of axonal regeneration. *Neuron* 13:757-767

Nag S. (2003) The Blood-Brain Barrier: Biology and Research Protocols. *Nag S (Ed) Humana Press* 89

Nagahori T, Nishijima M, Endo S, Takaku A, Iwasaki Y. (1994) Ischemic brain damage induced by repeated brief occlusions of bilateral common carotid artery in rats. *Tohoku J Exp Med* 172:253-262

Nakaji K, Ihara M, Takahashi C, Itohara S, Noda M, Takahashi R, Tomimoto H. (2006) Matrix metalloproteinase-2 plays a critical role in the pathogenesis of white matter lesions after chronic cerebral hypoperfusion in rodents. *Stroke* 37:2816-2823

Nakajima K, Tohyama Y, Kohsaka S, Kurihara T. (2002) Ceramide activates microglia to enhance the production/secretion of brain-derived neurotrophic factor (BDNF) without induction of deleterious factors in vitro. *J Neurochem* 80:697-705

Narumiya H, Zhang Y, Fernandez-Patron C, Guilbert LJ, Davidge ST. (2001) Matrix metalloproteinase-2 is elevated in the plasma of women with preeclampsia. *Hypertension in pregnancy* 20:185-194

Nave K-A. (2010) Myelination and support of axonal integrity by glia. *Nature* 468:244-252

Ni J-w, Ohta H, Matsumoto K, Watanabe H. (1994) Progressive cognitive impairment following chronic cerebral hypoperfusion induced by permanent occlusion of bilateral carotid arteries in rats. *Brain Res* 653:231-236

O'Brien JT, Erkinjuntti T, Reisberg B, Roman G, Sawada T, Pantoni L, Bowler JV, Ballard C, DeCarli C, Gorelick PB, Rockwood K, Burns A, Gauthier S, DeKosky ST. (2003) Vascular cognitive impairment. *Lancet Neurol* 2:89-98

Ohta H, Nishikawa H, Kimura H, Anayama H, Miyamoto M. (1997) Chronic cerebral hypoperfusion by permanent internal carotid ligation produces learning impairment without brain damage in rats. *Neuroscience* 79:1039-1050

Okada T. (2010) Two-photon microscopy analysis of leukocyte trafficking and motility. *Semin Immunopathol* 32:215-225

Okuno S, Nakase H, Sakaki T. (2001) Comparative study of 2,3,5-triphenyltetrazolium chloride (TTC) and hematoxylin & eosin staining for quantification of early brain ischemic injury in cats. *Neurol Res* 23:657-661

Otori T, Katsumata T, Muramatsu H, Kashiwagi F, Katayama Y, Terashi A. (2003) Long-term measurement of cerebral blood flow and metabolism in a rat chronic hypoperfusion model. *Clin Exp Pharmacol Physiol* 30:266-272

Pantoni L. (2002) Pathophysiology of age-related cerebral white matter changes. *Cerebrovasc Dis* 13:7-10

Pantoni L, Garcia JH. (1997) Pathogenesis of leukoaraiosis: a review. *Stroke* 28:652-659

Pantoni L, Garcia JH, Gutierrez JA (1996) Cerebral white matter is highly vulnerable to ischemia. *Stroke* 27:1641-1647

Pappas BA, de la Torre JC, Davidson CM, Keyes MT, Fortin T. (1996) Chronic reduction of cerebral blood flow in the adult rat: late-emerging CA1 cell loss and memory dysfunction. *Brain Res* 708:50-58

Pardridge WM. (2003) Blood-brain barrier drug targeting: the future of brain drug development. *Mol Interv* 3:90-105

Paxinos G, Watson C. (1998) The Rat Brain in Stereotaxic Coordinates, 4th edn. *Academic Press Ltd London*

Peppiatt CM, Howarth C, Mobbs P, Attwell D. (2006) Bidirectional control of CNS capillary diameter by pericytes. *Nature* 443:700-704

Persidsky Y, Ramirez S, Haorah J, Kanmogne G. (2006) Blood–brain barrier: structural components and function under physiologic and pathologic conditions. *J Neuroimm Pharmacol* 1:223-236

Petersen MA, Dailey ME. (2004) Diverse microglial motility behaviors during clearance of dead cells in hippocampal slices. *Glia* 46:195-206

Pfefferbaum A, Sullivan EV, Hedehus M, Lim KO, Adalsteinsson E, Moseley M. (2000) Age-related decline in brain white matter anisotropy measured with spatially corrected echo-planar diffusion tensor imaging. *Magn Reson Med* 44:259-268

Pichiule P, Chávez JC, Xu K, LaManna JC. (1999) Vascular endothelial growth factor upregulation in transient global ischemia induced by cardiac arrest and resuscitation in rat brain. *Mol Brain Res* 74:83-90

Plaschke K. (2005) Aspects of ageing in chronic cerebral oligaemia. Mechanisms of degeneration and compensation in rat models. *J Neur Transm* 112:393-413

Poltorak M, Sadoul R, Keilhauer G, Landa C, Fahrig T, Schachner M. (1987) Myelin-associated glycoprotein, a member of the L2/HNK-1 family of neural cell adhesion molecules, is involved in neuron-oligodendrocyte and oligodendrocyte-oligodendrocyte interaction. *J Cell Biol* 105:1893-1899

Povlishock JT, Kontos HA. (1982) The pathophysiology of pial and intraparenchymal vasculature dysfunction. *In: Grossman G, Gildenberg PL eds. Head injury: basic and clinical aspects. New York: Raven Press*: 15-29

Quarles RH, Barbarash GR, Figlewicz DA, McIntyre LJ. (1983) Purification and partial characterization of the myelin-associated glycoprotein from adult rat brain. *BBA* 757:140-143

Ramon Y Cajal S. (1913) Contribucion al conocimiento de la neuroglia del cerebro humano. *Trab Lab Invest Biol* 11:255–315

Ransohoff RM, Perry VH. (2009) Microglial physiology: unique stimuli, specialized responses. *Annu Rev Immunol* 27:119-145

Raz N. (2001) Ageing and the brain. In: *eLS*

Readnower RD, Chavko M, Adeeb S, Conroy MD, Pauly JR, McCarron RM, Sullivan PG. (2010) Increase in blood–brain barrier permeability, oxidative stress, and activated microglia in a rat model of blast-induced traumatic brain injury. *J Neurosci Res* 88:3530-3539

Rio Hortega D. (1921) Histogenesis y evolucion normal; exodo y distribucion regional de la microglia. *Memor Real Soc Esp Hist Nat* 11:213–268

Ritchie LJ, De Butte M, Pappas BA. (2004) Chronic mild stress exacerbates the effects of permanent bilateral common carotid artery occlusion on CA1 neurons. *Brain Res* 1014:228-235

Saatman KE, Abai B, Grosvenor A, Vorwerk CK, Smith DH, Meaney DF. (2003) Traumatic axonal injury results in biphasic calpain activation and retrograde transport impairment in mice. *JCBFM* 23:34-42

Sadoshima S, Fujishima M, Ogata J, Ibayashi S, Shiokawa O, Omae T. (1983) Disruption of blood-brain barrier following bilateral carotid artery occlusion in spontaneously hypertensive rats. A quantitative study. *Stroke* 14:876-882

Saleh MC, Connell BJ, Saleh TM. (2009) Ischemic tolerance following low dose NMDA involves modulation of cellular stress proteins. *Brain Res* 1247:212-220

Scheltens P, Barkhof F, Leys D, Wolters EC, Ravid R, Kamphorst W. (1995) Histopathologic correlates of white matter changes on MRI in Alzheimer's disease and normal aging. *Neurology* 45:883-888

Schmidt-Kastner R, Truettner J, Lin B, Zhao W, Saul I, Busto R, Ginsberg MD. (2001) Transient changes of brain-derived neurotrophic factor (BDNF) mRNA expression in hippocampus during moderate ischemia induced by chronic bilateral common carotid artery occlusions in the rat. *Mol Brain Res* 92:157-166

Schwartz M, Butovsky O, Brück W, Hanisch U-K. (2006) Microglial phenotype: is the commitment reversible? *Trends Neurosci* 29:68-74

Sekhon LHS, Morgan MK, Spence I, Weber NC. (1997) Chronic cerebral hypoperfusion: pathological and behavioral consequences. *Neurosurgery* 40:548-556

Selmaj KW, Raine CS. (1988) Tumor necrosis factor mediates myelin and oligodendrocyte damage in vitro. *Ann Neurol* 23:339-346

Shang Y, Cheng J, Qi J, Miao H. (2005) Scutellaria flavonoid reduced memory dysfunction and neuronal injury caused by permanent global ischemia in rats. *Pharmacol Biochem Behav* 82:67-73

Shibata M, Ohtani R, Ihara M, Tomimoto H. (2004) White Matter Lesions and Glial Activation in a novel mouse model of chronic cerebral hypoperfusion. *Stroke* 35:2598-2603

Shin JS, Hyun SY, Kim DH, Lee S, Jung JW, Choi JW, Ko KH, Kim JM, Ryu JH. (2008) Chronic hypoperfusion increases claudin-3 immunoreactivity in rat brain. *Neurosci Lett* 445:144-148

Shukla A, Dikshit M, Srimal RC. (1996) Nitric oxide-dependent blood-brain barrier permeability alteration in the rat brain. *Cell Mol Life Sci* 52:136-140

Somjen G, Kirino T, Tamura A, Sano K. (1988) Early and late neuronal damage following cerebral ischemia. *Springer US*, pp 23-34

Sood R, Yang Y, Taheri S, Candelario-Jalil E, Estrada EY, Walker EJ, Thompson J, Rosenberg GA. (2008) Increased apparent diffusion coefficients on MRI linked with matrix metalloproteinases and edema in white matter after bilateral carotid artery occlusion in rats. *JCBFM* 29:308-316

Sood RR, Taheri S, Candelario-Jalil E, Estrada EY, Rosenberg GA. (2007) Early beneficial effect of matrix metalloproteinase inhibition on blood-brain barrier permeability as measured by magnetic resonance imaging countered by impaired long-term recovery after stroke in rat brain. *JCBFM* 28:431-438

Sopala M, Danysz W. (2001) Chronic cerebral hypoperfusion in the rat enhances age-related deficits in spatial memory. *J Neural Transm* 108:1445-1456

Spangler KM, Challa VR, Moody DM, Bell MA. (1994) Arteriolar tortuosity of the white matter in aging and hypertension. A microradiographic study. *J Neuropathol Exp Neurol* 53:22-26

Strbian D, Durukan A, Pitkonen M, Marinkovic I, Tatlisumak E, Pedrono E, Abo-Ramadan U, Tatlisumak T. (2008) The blood-brain barrier is continuously open for several weeks following transient focal cerebral ischemia. *Neuroscience* 153:175-181

Streit WJ, Xue Q. Alzheimer's disease, neuroprotection, and CNS immunosenescence. *Front Pharmacol* 3

Suzuki H, Imai F, Kanno T, Sawada M. (2001) Preservation of neurotrophin expression in microglia that migrate into the gerbil's brain across the blood-brain barrier. *Neurosci Lett* 312:95-98

Takano T, Tian G-F, Peng W, Lou N, Libionka W, Han X, Nedergaard M. (2006) Astrocyte-mediated control of cerebral blood flow. *Nat Neurosci* 9:260-267

Takebayashi S, Kaneko M. (1983) Electron microscopic studies of ruptured arteries in hypertensive intracerebral hemorrhage. *Stroke* 14:28-36

Takizawa S, Fukuyama N, Hirabayashi H, Kohara S, Kazahari S, Shinohara Y, Nakazawa H. (2003) Quercetin, a natural flavonoid, attenuates vacuolar formation in the optic tract in rat chronic cerebral hypoperfusion model. *Brain Res* 980:156-160

Tamura A, Graham DI, McCulloch J, Teasdale GM. (1981) Focal cerebral ischaemia in the rat: 1. description of technique and early neuropathological consequences following middle cerebral artery occlusion. *JCBFM* 1:53-60

Tanaka K, Ogawa N, Asanuma M, Kondo Y, Nomura M. (1996) Relationship between cholinergic dysfunction and discrimination learning disabilities in Wistar rats following chronic cerebral hypoperfusion. *Brain Res* 729:55-65

Tanaka K, Wada N, Hori K, Asanuma M, Nomura M, Ogawa N. (1998) Chronic cerebral hypoperfusion disrupts discriminative behavior in acquired-learning rats. *J Neurosci Meth* 84:63-68

Tang J-P, Melethil S. (1995) Effect of aging on the kinetics of blood-brain barrier uptake of tryptophan in rats. *Pharm Res* 12:1085-1091

Taupin V, Renno T, Bourbonniere L, Peterson AC, Rodriguez M, Owens T. (1997) Increased severity of experimental autoimmune encephalomyelitis, chronic macrophage/microglial reactivity, and demyelination in transgenic mice producing tumor necrosis factor-α in the central nervous system. *Eur J Immunol* 27:905-913

Terry R, Gonatas NK, M. W. (1964) Ultrastructural studies in Alzheimer's preneuritic dementia. *Am J Pathol* 44 269–297

The national institute of neurological disorders and stroke rt-PA stroke study group. (1995) Tissue plasminogen activator for acute ischemic stroke. *New England J Med* 333:1581-1588

Tomimoto H, Akiguchi I, Suenaga T, Nishimura M, Wakita H, Nakamura S, Kimura J. (1996) Alterations of the blood-brain barrier and glial cells in white-matter lesions in cerebrovascular and Alzheimer's disease patients. *Stroke* 27:2069-2074

Tomimoto H, Akiguchi I, Wakita H, Suenaga T, Nakamura S, Kimura J. (1997) Regressive changes of astroglia in white matter lesions in cerebrovascular disease and Alzheimer's disease patients. *Acta Neuropathol* 94:146-152

Tomimoto H, Ihara M, Wakita H, Ohtani R, Lin JX, Akiguchi I, Kinoshita M, Shibasaki H. (2003) Chronic cerebral hypoperfusion induces white matter lesions and loss of oligodendroglia with DNA fragmentation in the rat. *Acta Neuropathol* 106:527-534

Traystman RJ. (2003) Animal models of focal and global cerebral ischemia. *ILAR Journal* 44:85-95

Tsuchiya M, Sako K, Yura S, Yonemasu Y. (1992) Cerebral blood flow and histopathological changes following permanent bilateral carotid artery ligation in Wistar rats. *Exp Brain Res* 89:87-92

Turc JD, Chollet F, Berry I, Sabatini U, Démonet JF, Celsis P, Marc-Vergnes JP, Rascol A. (1994) Cerebral blood flow, cerebral blood flow reactivity to acetazolamide, and cerebral blood volume in patients with leukoaraiosis. *Cerebrovasc Dis* 4:287-293

Ueno M, Tomimoto H, Akiguchi I, Wakita H, Sakamoto H. (2002) Blood-brain barrier disruption in white matter lesions in a rat model of chronic cerebral hypoperfusion. *JCBFM* 22:97-104

Ueno Y, Zhang N, Miyamoto N, Tanaka R, Hattori N, Urabe T. (2009) Edaravone attenuates white matter lesions through endothelial protection in a rat chronic hypoperfusion model. *Neuroscience* 162:317-327

Ulrich PT, Kroppenstedt S, Heimann A, Kempski O. (1998) Laser-Doppler Scanning of Local Cerebral Blood Flow and Reserve Capacity and Testing of Motor and Memory Functions in a Chronic 2-Vessel Occlusion Model in Rats. *Stroke* 29:2412-2420

Valable S, Montaner J, Bellail A, Berezowski V, Brillault J, Cecchelli R, Divoux D, MacKenzie ET, Bernaudin M, Roussel S, Petit E. (2005) VEGF-induced BBB permeability is associated with an MMP-9 activity increase in cerebral ischemia: both effects decreased by Ang-1. *JCBFM* 25:1491-1504

Van Itallie CM, Anderson JM. (2004) The molecular physiology of tight junction pores. *Physiology* 19:331-338

van Rossum D, Hanisch U-K. (2004) Microglia. *Metabol Brain Dis* 19:393-411

Verkhratsky A, Steinhäuser C. (2000) Ion channels in glial cells. *Brain Res Rev* 32:380-412

Virchow R. (1846) Ueber das granulirte aussehen der wandungen der gehirnventrikel. *Allg Z Psychiatr* 3:242–250

Vorbrodt AW, Dobrogowska DH. (2003) Molecular anatomy of intercellular junctions in brain endothelial and epithelial barriers: electron microscopist's view. *Brain Res Rev* 42:221-242

Wakita H, Tomimoto H, Akiguchi I, Kimura J. (1994) Glial activation and white matter changes in the rat brain induced by chronic cerebral hypoperfusion: an immunohistochemical study. *Acta Neuropathol* 87:484-492

Wakita H, Tomimoto H, Akiguchi I, Matsuo A, Lin J-X, Ihara M, McGeer P-L. (2002) Axonal damage and demyelination in the white matter after chronic cerebral hypoperfusion in the rat. *Brain Res* 924:63-70

Wakita H, Tomimoto H, Akiguchi I, Lin J-X, Ihara M, Ohtani R, Shibata M. (2003) Ibudilast, a phosphodiesterase inhibitor, protects against white matter damage under chronic cerebral hypoperfusion in the rat. *Brain Res* 992:53-59

Wardlaw JM. (2010) Blood-brain barrier and cerebral small vessel disease. *J Neurolog Sci* 299:66-71

Wardlaw JM, Farrall A, Armitage PA, Carpenter T, Chappell F, Doubal F, Chowdhury D, Cvoro V, Dennis MS. (2008) Changes in background blood-brain barrier integrity between lacunar and cortical ischemic stroke subtypes. *Stroke* 39:1327-1332

Watanabe T, Zhang N, Liu M, Tanaka R, Mizuno Y, Urabe T. (2006) Cilostazol protects against brain white matter damage and cognitive impairment in a rat model of chronic cerebral hypoperfusion. *Stroke* 37:1539-1545

Waxman SG, Black JA, Stys PK, Ransom BR. (1992) Ultrastructural concomitants of anoxic injury and early post-anoxic recovery in rat optic nerve. *Brain Res* 574:105-119

Wegiel J, Imaki H, Wang K-C, Wegiel J, Rubenstein R. (2004) Cells of monocyte/microglial lineage are involved in both microvessel amyloidosis and fibrillar plaque formation in APPsw tg mice. *Brain Res* 1022:19-29

Wegiel J, Imaki H, Wang K-C, Wegiel J, Wronska A, Osuchowski M, Rubenstein R. (2003) Origin and turnover of microglial cells in fibrillar plaques of APPsw transgenic mice. *Acta Neuropathol* 105:393-402

Wegiel J, Wang K-C, Imaki H, Rubenstein R, Wronska A, Osuchowski M, Lipinski WJ, Walker LC, LeVine H. (2001) The role of microglial cells and astrocytes in fibrillar plaque evolution in transgenic APPSW mice. *Neurobiol Aging* 22:49-61

Westergaard E, Go G, Klatzo I, Spatz M. (1976) Increased permeability of cerebral vessels to horseradish peroxidase induced by ischemia in Mongolian Gerbils. *Acta Neuropathol* 35:307-325

Wolburg H. (1994) Modulation of tight junction structure in blood-brain barrier endothelial cells: Effects of tissue culture, second messager and cocultured astrocytes. *J Cell Sci* 107:1347-1357

Wolburg H. (2003) Localization of claudin-3 in tight junctions of the blood-brain barrier is selectively lost during experimental autoimmune encephalomyelitis and human glioblastoma multiforme. *Acta Neuropathol* 105:586-592

Wolburg H, Lippoldt A. (2002) Tight junctions of the blood-brain barrier: development, composition and regulation. *Vasc Pharmacol* 38:323-337

Wolburg H, Wolburg-Buchholz K, Engelhardt B. (2005) Diapedesis of mononuclear cells across cerebral venules during experimental autoimmune encephalomyelitis leaves tight junctions intact. *Acta Neuropathol* 109:181-190

Wolff SD, Balaban RS. (1989) Magnetization transfer contrast (MTC) and tissue water proton relaxation in vivo. *Magn Res Med* 10:135-144

Yamamoto H, Schmidt-Kastner R, Hamasaki DI, Yamamoto H, Parel J-M. (2006) Complex neurodegeneration in retina following moderate ischemia induced by bilateral common carotid artery occlusion in Wistar rats. *Exp Eye Res* 82:767-779

Yang GY, Betz AL. (1994) Reperfusion-induced injury to the blood-brain barrier after middle cerebral artery occlusion in rats. *Stroke* 25:1658-1664

Yang Y, Estrada EY, Thompson JF, Liu W, Rosenberg GA. (2007) Matrix metalloproteinase-mediated disruption of tight junction proteins in cerebral vessels is reversed by synthetic matrix metalloproteinase inhibitor in focal ischemia in rat. *JCBFM* 27:697-709

Yenari MA, Xu L, Tang XN, Qiao Y, Giffard RG. (2006) Microglia potentiate damage to blood-brain barrier constituents. *Stroke* 37:1087-1093

Yrjänheikki J, Tikka T, Keinänen R, Goldsteins G, Chan PH, Koistinaho J. (1999) A tetracycline derivative, minocycline, reduces inflammation and protects against focal cerebral ischemia with a wide therapeutic window. *PNAS* 96:13496-13500

Zagzag D, Zhong H, Scalzitti JM, Laughner E, Simons JW, Semenza GL. (2000) Expression of hypoxia-inducible factor 1α in brain tumors. *Cancer* 88:2606-2618

Zhan X, Kuczynski B, Sharp FR. (2011) Post stroke intervention: is the window widening? *Neuropharmacology* 60:1000-1002

Ziello JE, Jovin IS, Huang Y. (2007) Hypoxia-Inducible Factor (HIF)-1 regulatory pathway and its potential for therapeutic intervention in malignancy and ischemia. *Yale J Biol Med* 80:51–60

Appendix A: Quantification of damage following BCCAo

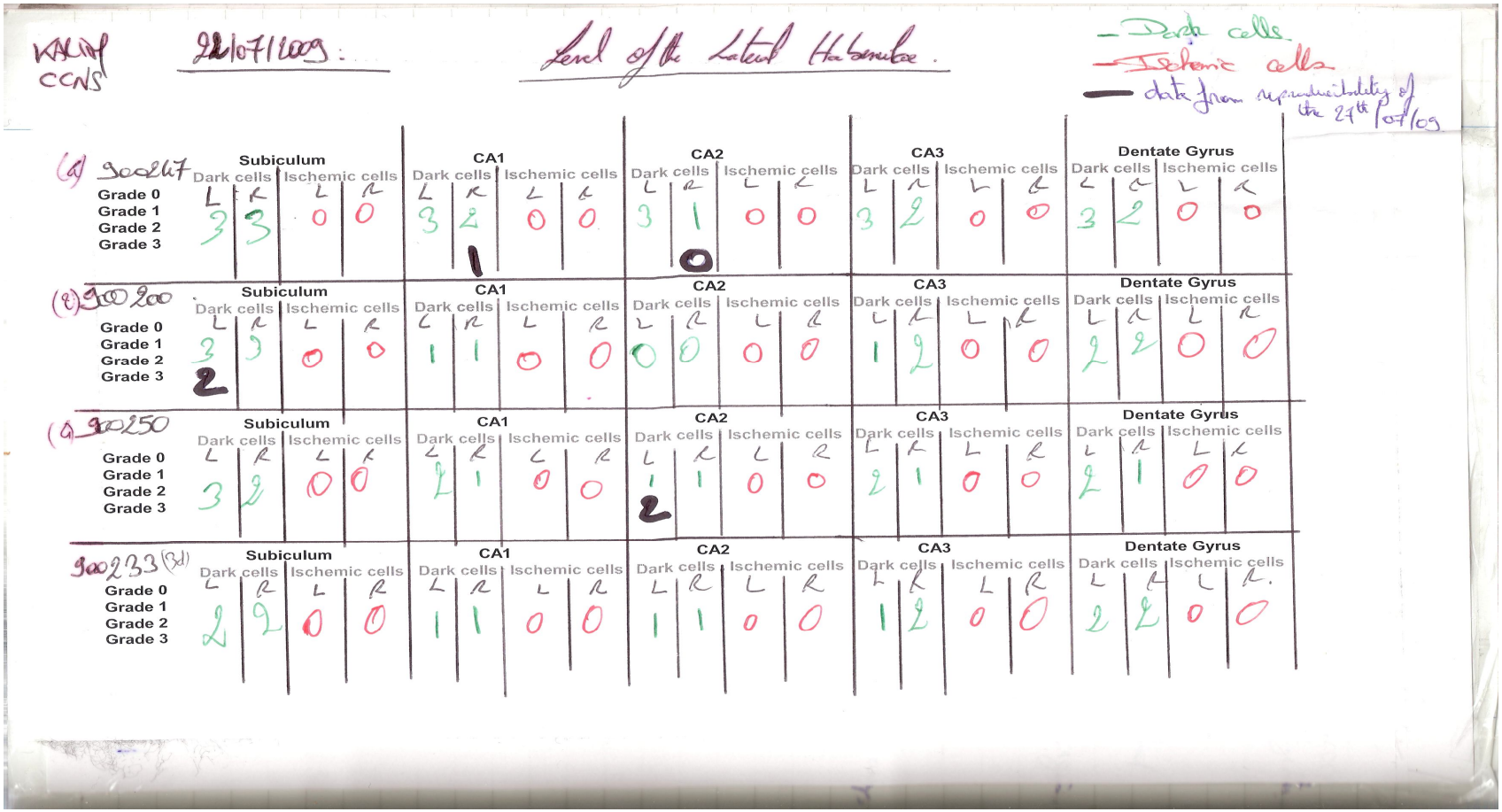

Quantification of ischaemic damage and presence of dark cells following chronic cerebral hypoperfusion in the rat

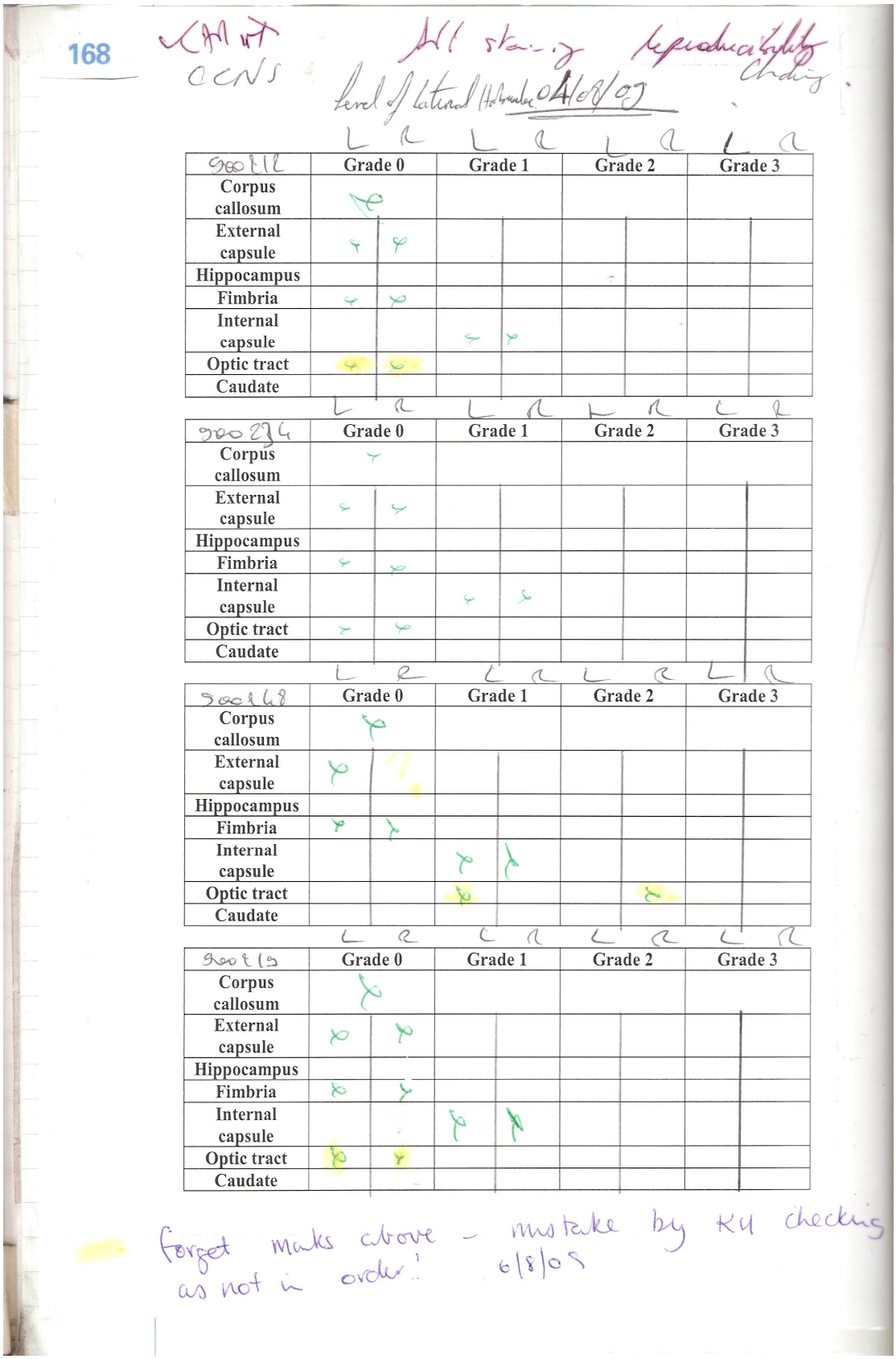

168

All WT
OCNS

All staining hyperchromatolysis checking

level of lateral Habenula 04/08/09

900812	Grade 0		Grade 1		Grade 2		Grade 3	
	L	R	L	R	L	R	L	R
Corpus callosum	✓							
External capsule	✓	✓						
Hippocampus								
Fimbria	✓	✓						
Internal capsule			✓	✓				
Optic tract	✓	✓						
Caudate								

900824	Grade 0		Grade 1		Grade 2		Grade 3	
	L	R	L	R	L	R	L	R
Corpus callosum	✓							
External capsule	✓	✓						
Hippocampus								
Fimbria	✓	✓						
Internal capsule			✓	✓				
Optic tract	✓	✓						
Caudate								

900848	Grade 0		Grade 1		Grade 2		Grade 3	
	L	R	L	R	L	R	L	R
Corpus callosum	✓							
External capsule	✓	✓						
Hippocampus								
Fimbria	✓	✓						
Internal capsule			✓	✓				
Optic tract			✓			✓		
Caudate								

900819	Grade 0		Grade 1		Grade 2		Grade 3	
	L	R	L	R	L	R	L	R
Corpus callosum	✓							
External capsule	✓	✓						
Hippocampus								
Fimbria	✓	✓						
Internal capsule			✓	✓				
Optic tract	✓	✓						
Caudate								

Forget marks above - mistake by KH checking as not in order! 6/8/09

Quantification of axonal damage following chronic cerebral hypoperfusion in the rat (approved by KH: Karen Horsburgh)

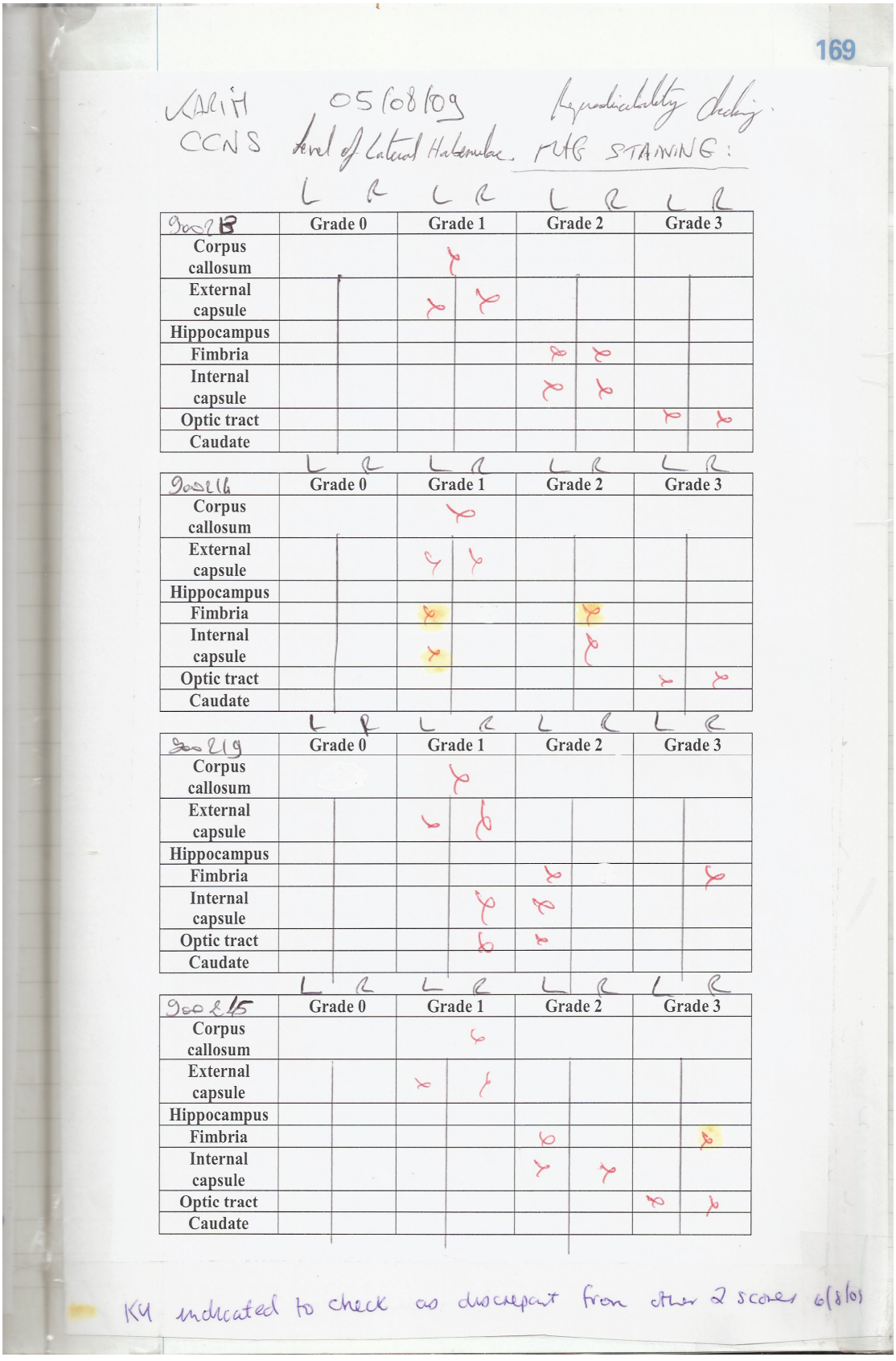

169

KARIH 05/08/09 Reproducibility checking.
CCNS level of Lateral Habenulae. MBP STAINING:

900218	Grade 0		Grade 1		Grade 2		Grade 3	
	L	R	L	R	L	R	L	R
Corpus callosum			2					
External capsule			2	2				
Hippocampus								
Fimbria					2	2		
Internal capsule					2	2		
Optic tract							2	2
Caudate								

900216	Grade 0		Grade 1		Grade 2		Grade 3	
	L	R	L	R	L	R	L	R
Corpus callosum			2					
External capsule			2	2				
Hippocampus								
Fimbria			2			2		
Internal capsule			2			2		
Optic tract							2	2
Caudate								

900219	Grade 0		Grade 1		Grade 2		Grade 3	
	L	R	L	R	L	R	L	R
Corpus callosum			2					
External capsule			2	2				
Hippocampus								
Fimbria					2			2
Internal capsule				2	2			
Optic tract				2	2			
Caudate								

900215	Grade 0		Grade 1		Grade 2		Grade 3	
	L	R	L	R	L	R	L	R
Corpus callosum			2					
External capsule			2	2				
Hippocampus								
Fimbria					2			2
Internal capsule					2	2		
Optic tract							2	2
Caudate								

KH indicated to check as discrepant from other 2 scores 6/8/09

Quantification of myelin débris following chronic cerebral hypoperfusion in the rat (approved by KH: Karen Horsburgh)

Appendix B: Mean grey values obtained form ImageJ after MRI acquisitions

GROUP 3 HOURS										
	Corpus callosum	Caudate Nucleus A	Caudate Nucleus B	Mean	External capsule A	External capsule B	Mean	Internal capsule A	Internal capsule B	Mean
1000171	37.184	30.21	29.772	29.991	36.916	36.039	36.4775	38.99	39.185	39.0875
1000172	36.808	28.742	30.539	29.6405	37.242	41.241	39.2415	36.858	44.485	40.6715
1000173	37.24	29.508	30.063	29.7855	38.101	34.906	36.5035	35.936	40.395	38.1655
1000174	39.61	31.518	30.449	30.9835	38.361	38.297	38.329	38.883	40.402	39.6425
1000175	36.225	29.478	30.133	29.8055	35.756	36.275	36.0155	38.982	39.194	39.088
1000177	36.631	28.843	28.682	28.7625	34.466	34.714	34.59	37.38	40.609	38.9945
1000178	38.78	28.456	30.038	29.247	37.536	38.004	37.77	39.756	39.083	39.4195
1000348	38.416	32.396	25.672	29.034	36.723	32.386	34.5545	33.422	41.473	37.4475
1000350	37.099	29.54	31.955	30.7475	37.305	36.373	36.839	39.68	37.009	38.3445
1000351	37.505	29.926	30.091	30.0085	34.815	39.925	37.37	35.467	41.692	38.5795
1000352	37.674	30.89	30.242	30.566	36.852	38.311	37.5815	41.46	38.919	40.1895
1000365	35.342	28.263	30.509	29.386	35.204	30.933	33.0685	35.766	31.337	33.5515
1000366	35.908	28.925	30.202	29.5635	29.434	40.603	35.0185	30.834	41.094	35.964
1000367	36.499	24.264	34.669	29.4665	37.467	30.316	33.8915	43.569	29.251	36.41

GROUP 7 days										
	Corpus callosum	Caudate Nucleus A	Caudate Nucleus B	Mean	External capsule A	External capsule B	Mean	Internal capsule A	Internal capsule B	Mean
1000353	37.038	29.801	31.847	30.824	28.143	42.751	35.447	31.753	47.106	39.4295
1000354	41.546	31.042	32.011	31.5265	37.616	37.087	37.3515	36.538	39.514	38.026
1000355	38.124	29.661	30.821	30.241	37.074	39.705	38.3895	41.195	38.302	39.7485
1000356	37.9	28.545	30.209	29.377	36.723	38.401	37.562	39.544	41.755	40.6495
1000357	37.633	31.088	29.008	30.048	37.582	33.506	35.544	36.407	35.445	35.926
1000358	39.13	31.982	31.664	31.823	31.499	38.585	35.042	36.18	40.543	38.3615
1000359	40.27	33.29	31.174	32.232	38.596	39.319	38.9575	38.606	43.22	40.913
1000360	38.142	30.033	30.988	30.5105	35.224	38.127	36.6755	36.286	35.041	35.6635
1000361	39.747	32.597	29.648	31.1225	30.998	35.323	33.1605	35.45	46.313	40.8815
1000362	42.43	34.625	31.183	32.904	42.27	25.432	33.851	44.1	30.767	37.4335
1000363	39.054	30.12	30.802	30.461	39.03	38.187	38.6085	42.964	36.797	39.8805
1000364	31.093	23.974	26.572	25.273	44.214	42.243	43.2285	46.724	44.243	45.4835

MTR mean grey values obtained from ImageJ after MTI acquisitions

GROUP 3 HOURS											
	Corpus callosum	Caudate Nucleus A	Caudate Nucleus B	Mean	External capsule A	External capsule B	Mean	Internal capsule A	Internal capsule B	Mean
1000171	4179.687	4050.289	3559.641	3804.965	4318.551	3335.724	3827.1375	3369.748	2860.212	3114.98
1000172	4060.075	3704.189	3662.385	3683.287	4046.05	3667.369	3856.7095	3089.799	2906.064	2997.9315
1000173	4083.063	3739.6	3515.525	3627.5625	3706.371	3365.361	3535.866	3017.515	2824.175	2920.845
1000174	4589.413	4029.957	4034.424	4032.1905	3642.802	3797.86	3720.331	3216.377	3036.373	3126.375
1000175	4274.771	4068.862	3766.418	3917.64	4113.242	3584.646	3848.944	3394.657	2991.416	3193.0365
1000177	3916.947	3663.792	3564.602	3614.197	3629.693	3512.834	3571.2635	3091.958	3008.943	3050.4505
1000178	4044.721	3857.323	3610.805	3734.064	3776.145	3457.323	3616.734	3149.347	2930.261	3039.804
1000348	3588.097	3302.269	3153.86	3228.0645	3464.174	2934.62	3199.397	2969.053	2609.82	2789.4365
1000350	3674.246	3308.545	3151.802	3230.1735	3589.279	3194.771	3392.025	3126.156	2807.04	2966.598
1000351	3793.144	3627.554	3342.099	3484.8265	3738.035	3426.032	3582.0335	3111.674	2815.116	2963.395
1000352	3855.093	3631.06	3362.387	3496.7235	3522.974	3111.79	3317.382	3068.333	2782.876	2925.6045
1000365	3863.307	3742.323	3475.95	3609.1365	3742.514	3209.608	3476.061	3165.053	2825.402	2995.2275
1000366	3656.084	3591.998	3306.733	3449.3655	3776.944	3119.43	3448.187	3166.096	2710.477	2938.2865
1000367	3158.62	2980.016	2809.676	2894.846	3258.946	2855.819	3057.3825	2662.119	2283.064	2472.5915

Baseline mean grey values obtained from T1 weighted images in ImageJ for the selected regions

Corpus callosum					
GROUP 3 HOURS	T1pre	T1post0	T1post5	T1post10	T1post15
1000173	4083.06	4264.409	4239.726	4250.529	4261.31
1000174	4589.41	4685.39	4771.202	4776.353	4783.094
1000177	3916.95	4078.134	4020.998	4040.769	4048.714
1000178	4044.72	4157.491	4169.689	4129.286	4127.048
1000350	3674.25	3738.377	3753.244	3764.488	3749.152
1000365	3863.31	3868.224	3977.671	4008.051	4004.669
1000366	3656.08	3827.617	3859.636	3820.6	3807.475
1000171	4179.69	4095.751	4173.658	4135.155	4175.163
1000172	4060.08	4330.44	4096.693	4084.8	4104.899
1000175	4274.77	4266.878	4368.976	4390.545	4396.63
1000348	3588.1	3744.891	3800.812	3855.292	3874.402
1000351	3793.14	3888.201	3968.239	3951.733	3991.744
1000352	3855.09	3972.339	4068.113	4148.435	4164.527
1000367	3158.62	3305.628	3358.622	3365.008	3378.84

Caudatoputamen					
GROUP 3 HOURS	T1pre	T1post0	T1post5	T1post10	T1post15
1000173	3627.56	3854.289	3878.146	3864.482	3872.103
1000174	4032.19	4238.788	4354.583	4354.466	4329.927
1000177	3614.2	3851.247	3834.888	3811.055	3796.732
1000178	3734.06	3870.565	3908.506	3866.381	3854.076
1000350	3230.17	3373.089	3417.431	3386.01	3388.919
1000365	3609.14	3650.855	3756.199	3827.74	3818.982
1000366	3449.37	3568.123	3666.717	3635.626	3635.359
1000171	3804.97	3729.801	3837.677	3843.687	3882.124
1000172	3683.29	3795.943	3655.836	3637.565	3662.034
1000175	3917.64	3951.035	4068.605	4115.719	4117.864
1000348	3228.06	3482.245	3542.534	3568.911	3572.122
1000351	3484.83	3623.344	3705.479	3717.91	3760.196
1000352	3496.72	3624.575	3687.736	3713.011	3755.001
1000367	2894.85	3021.681	3070.103	3084.151	3090.323

Mean grey values obtained from T1 weighted images in ImageJ for the selected regions in sham and BCCAo after 3 hours of the surgery, at 0 (T1post0), 5 (T1post5), 10 (T1post10) and 15 (T1post15) minutes after gadolinium injection. "T1pre" represents the baseline.

External capsule					
GROUP 3 HOURS	T1pre	T1post0	T1post5	T1post10	T1post15
1000173	3535.87	3677.387	3700.299	3693.727	3675.836
1000174	3720.33	3884.318	3950.336	3952.193	3935.511
1000177	3571.26	3775.74	3765.385	3742.864	3727.44
1000178	3616.73	3718.871	3708.572	3705.097	3710.301
1000350	3392.03	3530.197	3649.015	3599.816	3564.433
1000365	3476.06	3511.793	3615.099	3618.21	3646.052
1000366	3448.19	3562.969	3648.935	3605.879	3563.661
1000171	3827.14	3813.032	3893.028	3886.714	3905.554
1000172	3856.71	3922.248	3905.337	3931.323	3922.129
1000175	3848.94	3892.872	3969.669	3983.847	4022.695
1000348	3199.4	3339.622	3437.663	3428.691	3483.227
1000351	3582.03	3677.974	3743.762	3787.016	3834.041
1000352	3317.38	3408.482	3521.161	3575.937	3549.87
1000367	3057.38	3179.771	3229.205	3216.373	3229.548
Internal capsule					
GROUP 3 HOURS	T1pre	T1post0	T1post5	T1post10	T1post15
1000173	2920.85	2992.962	3050.583	3030.663	3012.656
1000174	3126.38	3513.081	3296.895	3274.954	3304.734
1000177	3050.45	3169.108	3182.813	3176.409	3165.674
1000178	3039.8	3101.763	3128.198	3114.002	3127.565
1000350	2966.6	3006.789	3096.014	3103.892	3081.622
1000365	2995.23	2929.491	3059.958	3088.871	3100.567
1000366	2938.29	2970.452	3054.314	3003.752	2991.328
1000171	3114.98	3098.085	3125.567	3162.004	3184.469
1000172	2997.93	3292.425	3071.677	3072.186	3081.463
1000175	3193.04	3206.509	3283.063	3339.405	3353.824
1000348	2789.44	2931.972	2938.735	2969.041	3025.606
1000351	2963.4	2972.629	3046.986	3045.093	3079.794
1000352	2925.6	3001.293	3089.798	3106.161	3162.509
1000367	2472.59	2502.42	2514.383	2523.784	2551.184

Mean grey values obtained from T1 weighted images in ImageJ for the selected regions in sham and BCCAo after 3 hours of the surgery, at 0 (T1post0), 5 (T1post5), 10 (T1post10) and 15 (T1post15) minutes after gadolinium injection. "T1pre" represents the baseline.

GROUP 7 days										
				Mean			Mean			Mean
	Corpus callosum	Caudate Nucleus A	Caudate Nucleus B		External capsule A	External capsule B		Internal capsule A	Internal capsule B	
1000353	3849.924	3409.845	3393.685	3401.765	3465.966	3287.786	3376.876	2797.274	2964.262	2880.768
1000354	3973.184	3714.652	3857.154	3785.903	3716.776	3669.244	3693.01	3201.588	3023.749	3112.6685
1000355	3879.383	3709.172	3399.197	3554.1845	3545.337	3187.795	3366.566	2993.566	2555.093	2774.3295
1000356	3502.135	3431.723	3242.12	3336.9215	3553.165	3277.468	3415.3165	2979.351	2717.899	2848.625
1000357	3683.963	3609.489	3284.725	3447.107	3769.648	3190.668	3480.158	2966.824	2593.087	2779.9555
1000358	3963.359	3766.852	3682.308	3724.58	3803.094	3641.468	3722.281	2953.749	2993.563	2973.656
1000359	4130.606	3971.303	3858.992	3915.1475	3833.276	3885.964	3859.62	3224.753	3002.977	3113.865
1000360	3651.21	3608.56	3187.599	3398.0795	3719.868	3201.124	3460.496	3018.19	2520.591	2769.3905
1000361	3626.579	3425.54	3277.988	3351.764	3623.185	3212.615	3417.9	2781.669	2662.379	2722.024
1000362	3269.721	3232.618	2927.703	3080.1605	3273.713	3139.64	3206.6765	2590.489	2624.288	2607.3885
1000363	3913.644	3662.012	3346.62	3504.316	3610.334	3374.333	3492.3335	2917.809	2607.597	2762.703
1000364	3534.452	3461.201	3203.984	3332.5925	3518.396	3104.916	3311.656	2691.893	2459.088	2575.4905

Baseline mean grey values obtained from T1 weighted images in ImageJ for the selected regions

Corpus callosum						
GROUP 7 days	T1pre	T1post0	T1post5	T1post10	T1post15	
1000354	3973.18	3972.62	4014.806	4043.465	4090.749	
1000356	3502.14	3504.393	3587.019	3571.558	3597.275	
1000357	3683.96	3915.387	3956.373	3938.091	3894.537	
1000361	3626.58	3790.926	3843.509	3885.973	3929.636	
1000362	3269.72	3446.22	3472.587	3533.193	3546.188	
1000364	3534.45	3671.983	3688.456	3751.842	3768.185	
1000353	3849.92	3430.162	3626.942	4203.71	3715.072	
1000355	3879.38	3998.219	4035.076	4043.721	4062.773	
1000358	3963.36	4131.69	4139.219	4164.381	4173.828	
1000359	4130.61	4136.523	4234.559	4243.611	4799.905	
1000360	3651.21	3691.895	3781.901	3767.088	3772.8	
1000363	3913.64	4112.425	4188.492	4151.886	4196.365	

Caudatoputamen						
GROUP 7 days	T1pre	T1post0	T1post5	T1post10	T1post15	
1000354	3785.9	3878.584	3976.861	4047.312	4086.921	
1000356	3336.92	3378.933	3500.527	3528.374	3564.83	
1000357	3447.11	3652.709	3730.073	3719.482	3684.208	
1000361	3351.76	3513.902	3571.921	3581.622	3611.869	
1000362	3080.16	3246.809	3275.995	3342.315	3369.261	
1000364	3332.59	3506.953	3528.143	3520.724	3564.206	
1000353	3401.77	3118.585	3768.297	4047.312	3400.906	
1000355	3554.18	3730.593	3781.456	3528.374	3784.63	
1000358	3724.58	3893.171	3959.346	3719.482	3961.16	
1000359	3915.15	3988.52	4116.049	3581.622	4584.966	
1000360	3398.08	3547.848	3612.06	3342.315	3627.426	
1000363	3504.32	3636.57	3665.062	3520.724	3691.944	

Mean grey values obtained from T1 weighted images in ImageJ for the selected regions in sham and BCCAo after 7 days of the surgery, at 0 (T1post0), 5 (T1post5), 10 (T1post10) and 15 (T1post15) minutes after gadolinium injection. "T1pre" represents the baseline.

External capsule						
GROUP 7 days	T1pre	T1post0	T1post5	T1post10	T1post15	
1000354	3693.01	3770.467	3856.024	3891.894	3928.439	
1000356	3415.32	3448.132	3558.634	3621.702	3666.748	
1000357	3480.16	3758.1	3703.323	3701.484	3647.569	
1000361	3417.9	3550.812	3620.241	3653.047	3687.633	
1000362	3206.68	3386.51	3476.914	3535.914	3530.504	
1000364	3311.66	3453.429	3521.587	3524.341	3514.397	
1000353	3376.88	3144.636	3290.436	3779.497	3373.575	
1000355	3366.57	3453.716	3521.035	3549.141	3584.885	
1000358	3722.28	3830.208	3883.549	3922.801	3937.942	
1000359	3859.62	3910.924	3996.593	4017.012	4428.71	
1000360	3460.5	3552.696	3662.664	3655.573	3664.371	
1000363	3492.33	3614.026	3672.33	3700.875	3690.098	

Internal capsule						
GROUP 7 days	T1pre	T1post0	T1post5	T1post10	T1post15	
1000354	3112.67	3113.584	3221.208	3230.002	3276.248	
1000356	2848.63	2857.616	2934.948	2933.889	2984.992	
1000357	2779.96	2958.343	2931.979	2959.556	2912.155	
1000361	2722.02	2791.666	2787.232	2857.917	2821.263	
1000362	2607.39	2662.224	2701.788	2776.816	2754.868	
1000364	2575.49	2600.88	2670.43	2657.613	2667.08	
1000353	2880.77	2601.754	2690.423	3141.872	2757.476	
1000355	2774.33	2861.838	2874.142	2893.857	2910.87	
1000358	2973.66	3002.101	3028.304	3080.61	3098.706	
1000359	3113.87	3087.084	3186.781	3182.115	3800.582	
1000360	2769.39	2841.168	2825.94	2859.259	2865.821	
1000363	2762.7	2844.317	2870.198	2835.165	2861.669	

Mean grey values obtained from T1 weighted images in ImageJ for the selected regions in sham and BCCAo after 7 days of the surgery, at 0 (T1post0), 5 (T1post5), 10 (T1post10) and 15 (T1post15) minutes after gadolinium injection. "T1pre" represents the baseline.

Appendix C: Tables of values of % signal enhancement of Gd-DOTA in BCCAo and sham animal according to the regions

Corpus callosum

GROUP 3 HOURS	T1pre	T1post0	T1post0-T1pre	T1-0 change	T1post5	T1post5-T1pre	T1-5 change	T1post10	T1post10-T1pre	T1-10 change	T1post15	T1post15-T1pre	T1-15 change
1000171	4179.687	4095.751	-83.936	-2.00819	4173.658	-6.029	-0.14425	4135.155	-44.532	-1.06544	4175.163	-4.524	-0.10823777
1000172	4060.075	4330.44	270.365	6.659113	4096.693	36.618	0.901905	4084.8	24.725	0.608979	4104.899	44.824	1.10401901
1000175	4274.771	4266.878	-7.893	-0.18464	4368.976	94.205	2.203744	4390.545	115.774	2.708309	4396.63	121.859	2.85065563
1000348	3588.097	3744.891	156.794	4.369837	3800.812	212.715	5.928351	3855.292	267.195	7.446705	3874.402	286.305	7.97929933
1000351	3793.144	3888.201	95.057	2.506021	3968.239	175.095	4.616092	3951.733	158.589	4.180938	3991.744	198.6	5.23576221
1000352	3855.093	3972.339	117.246	3.041327	4068.113	213.02	5.525677	4148.435	293.342	7.609207	4164.527	309.434	8.02662867
1000367	3158.62	3305.628	147.008	4.654184	3358.622	200.002	6.331942	3365.008	206.388	6.534119	3378.84	220.22	6.97203209

Caudatoputamen

GROUP 3 HOURS	T1pre	T1post0	T1post0-T1pre	T1-0 change	T1post5	T1post5-T1pre	T1-5 change	T1post10	T1post10-T1pre	T1-10 change	T1post15	T1post15-T1pre	T1-15 change
1000171	3804.965	3729.8005	-75.1645	-1.97543	3837.677	32.7115	0.859706	3843.687	38.722	1.01767	3882.124	77.159	2.02785045
1000172	3683.287	3795.9425	112.6555	3.058559	3655.836	-27.4515	-0.7453	3637.565	-45.7225	-1.24135	3662.034	-21.2535	-0.57702536
1000175	3917.64	3951.0345	33.3945	0.852414	4068.605	150.965	3.853468	4115.719	198.0785	5.056067	4117.864	200.2235	5.11081927
1000348	3228.065	3482.245	254.1805	7.874084	3542.534	314.4695	9.741735	3568.911	340.846	10.55883	3572.122	344.057	10.6583062
1000351	3484.827	3623.344	138.5175	3.974875	3705.479	220.6525	6.331807	3717.91	233.083	6.688511	3760.196	275.369	7.90194289
1000352	3496.724	3624.575	127.8515	3.656323	3687.736	191.012	5.462599	3713.011	216.287	6.185419	3755.001	258.2775	7.38627175
1000367	2894.846	3021.6805	126.8345	4.38139	3070.103	175.2565	6.054087	3084.151	189.3045	6.539363	3090.323	195.4765	6.75256991

External capsule

GROUP 3 HOURS	T1pre	T1post0	T1post0-T1pre	T1-0 change	T1post5	T1post5-T1pre	T1-5 change	T1post10	T1post10-T1pre	T1-10 change	T1post15	T1post15-T1pre	T1-15 change
1000171	3827.138	3813.032	-14.1055	-0.36857	3893.028	65.89	1.721652	3886.714	59.5765	1.556686	3905.554	78.4165	2.04895957
1000172	3856.71	3922.2475	65.538	1.699324	3905.337	48.6275	1.260855	3931.323	74.6135	1.934641	3922.129	65.419	1.69623872
1000175	3848.944	3892.8715	43.9275	1.141287	3989.669	120.725	3.136575	3983.847	134.9025	3.504922	4022.695	173.751	4.51425118
1000348	3199.397	3339.622	140.225	4.382857	3437.663	238.266	7.447216	3428.691	229.294	7.166788	3483.227	283.83	8.8713592
1000351	3582.034	3677.9735	95.94	2.678367	3743.762	161.7285	4.514991	3787.016	204.9825	5.722518	3834.041	252.007	7.0353055
1000352	3317.382	3408.482	91.1	2.746141	3521.161	203.7785	6.142751	3575.937	258.5545	7.793932	3549.87	232.488	7.00817693
1000367	3057.383	3179.771	122.3885	4.003048	3229.205	171.822	5.619905	3216.373	158.9905	5.200216	3229.548	172.1655	5.63114036

Internal capsule

GROUP 3 HOURS	T1pre	T1post0	T1post0-T1pre	T1-0 change	T1post5	T1post5-T1pre	T1-5 change	T1post10	T1post10-T1pre	T1-10 change	T1post15	T1post15-T1pre	T1-15 change
1000171	3114.98	3098.085	-16.895	-0.54238	3125.567	10.5865	0.339858	3162.004	47.0235	1.509592	3184.469	69.489	2.23080084
1000172	2997.932	3292.4245	294.493	9.823206	3071.677	73.745	2.459863	3072.186	74.254	2.476841	3081.463	83.5315	2.78630449
1000175	3193.037	3206.5085	13.472	0.421918	3283.063	90.0265	2.819464	3339.405	146.3685	4.583991	3353.824	160.787	5.03555158
1000348	2789.437	2931.9715	142.535	5.109813	2938.735	149.2985	5.352282	2969.041	179.604	6.43872	3025.606	236.169	8.46654871
1000351	2963.395	2972.629	9.234	0.311602	3046.986	83.5905	2.820768	3045.093	81.698	2.756906	3079.794	116.399	3.92789351
1000352	2925.605	3001.293	75.6885	2.587106	3089.798	164.1935	5.612293	3106.161	180.5565	6.171596	3162.509	236.904	8.09760855
1000367	2472.592	2502.42	29.8285	1.206366	2514.383	41.7915	1.69019	2523.784	51.192	2.070378	2551.184	78.5925	3.17854769

T1 changes of sham animals after 3 hours of surgery representing the *% signal enhancement of Gd-DOTA = (Mean grey value after Gd-DOTA injection (T1post) – Mean grey value before Gd-DOTA injection (T1pre))* 100 / (Mean grey value before injection (T1pre))*.

Corpus callosum														
GROUP 3 HOURS	T1pre	T1post0			T1post5			T1post10			T1post15			
			T1post0-T1pre	T1-0 change		T1post5-T1pre	T1-5 change		T1post10-T1pre	T1-10 change		T1post15-T1pre	T1-15 change
1000173	4083.063	4264.409	181.346	4.441421	4239.726	156.663	3.836899	4250.529	167.466	4.10148	4261.31	178.247	4.36552167
1000174	4589.413	4685.39	95.977	2.09127	4771.202	181.789	3.961051	4776.353	186.94	4.073288	4783.094	193.681	4.22016933
1000177	3916.947	4078.134	161.187	4.115118	4020.998	104.051	2.656431	4040.769	123.822	3.161187	4048.714	131.767	3.36402305
1000178	4044.721	4157.491	112.77	2.788079	4169.689	124.968	3.089657	4129.286	84.565	2.09075	4127.048	82.327	2.03541851
1000350	3674.246	3738.377	64.131	1.745419	3753.244	78.998	2.150047	3764.488	90.242	2.456069	3749.152	74.906	2.03867678
1000365	3863.307	3868.224	4.917	0.127274	3977.671	114.364	2.960262	4008.051	144.744	3.746635	4004.669	141.362	3.6590931
1000366	3656.084	3827.617	171.533	4.691714	3859.636	203.552	5.567487	3820.6	164.516	4.499787	3807.475	151.391	4.14079655

Caudatoputamen														
GROUP 3 HOURS	T1pre	T1post0			T1post5			T1post10			T1post15			
			T1post0-T1pre	T1-0 change		T1post5-T1pre	T1-5 change		T1post10-T1pre	T1-10 change		T1post15-T1pre	T1-15 change
1000173	3627.563	3854.2885	226.726	6.250092	3878.146	250.5835	6.907765	3864.482	236.9195	6.531094	3872.103	244.5405	6.74117951
1000174	4032.191	4238.788	206.5975	5.123704	4354.583	322.392	7.995456	4354.466	322.275	7.992554	4329.927	297.736	7.38397653
1000177	3614.197	3851.2465	237.0495	6.558843	3834.888	220.691	6.106225	3811.055	196.858	5.446798	3796.732	182.535	5.05049946
1000178	3734.064	3870.5645	136.5005	3.655548	3908.506	174.442	4.671639	3866.381	132.317	3.543512	3854.076	120.012	3.21397812
1000350	3230.174	3373.089	142.9155	4.424391	3417.431	187.257	5.797119	3386.01	155.836	4.824385	3388.919	158.745	4.9144419
1000365	3609.137	3650.8545	41.718	1.1559	3756.199	147.062	4.074714	3827.74	218.6035	6.056947	3818.982	209.8455	5.81428549
1000366	3449.366	3568.1225	118.757	3.442865	3666.717	217.3515	6.301202	3635.626	186.26	5.399834	3635.359	185.993	5.39209313

External capsule														
GROUP 3 HOURS	T1pre	T1post0			T1post5			T1post10			T1post15			
			T1post0-T1pre	T1-0 change		T1post5-T1pre	T1-5 change		T1post10-T1pre	T1-10 change		T1post15-T1pre	T1-15 change
1000173	3535.866	3677.387	141.521	4.002442	3700.299	164.4325	4.650417	3693.727	157.861	4.464564	3675.836	139.97	3.95857762
1000174	3720.331	3884.3175	163.9865	4.407847	3950.336	230.0045	6.182367	3952.193	231.862	6.232295	3935.511	215.1795	5.78388052
1000177	3571.264	3775.74	204.4765	5.725607	3765.385	194.1215	5.435653	3742.864	171.6005	4.805036	3727.44	156.178	4.37313013
1000178	3616.734	3718.8705	102.1365	2.823998	3708.572	91.838	2.539252	3705.097	88.3625	2.443157	3710.301	93.5665	2.587044
1000350	3392.025	3530.197	138.172	4.073437	3649.015	256.99	7.5763	3599.816	207.791	6.125869	3584.433	172.4075	5.08273082
1000365	3476.061	3511.793	35.732	1.027945	3615.099	139.0375	3.999858	3618.21	142.149	4.08937	3646.052	169.991	4.8903342
1000366	3448.187	3562.969	114.782	3.328764	3648.935	200.7475	5.821828	3605.879	157.6915	4.573171	3563.681	115.4735	3.3488178

Internal capsule														
GROUP 3 HOURS	T1pre	T1post0			T1post5			T1post10			T1post15			
			T1post0-T1pre	T1-0 change		T1post5-T1pre	T1-5 change		T1post10-T1pre	T1-10 change		T1post15-T1pre	T1-15 change
1000173	2920.845	2992.9615	72.1165	2.469029	3050.583	129.738	4.441797	3030.663	109.818	3.759802	3012.656	91.811	3.14330271
1000174	3126.375	3513.0805	386.7055	12.36913	3296.895	170.52	5.45424	3274.954	148.579	4.752437	3304.734	178.3585	5.70496182
1000177	3050.451	3169.1075	118.657	3.889819	3182.813	132.3625	4.339113	3176.409	125.9585	4.129177	3165.674	115.2235	3.77726175
1000178	3039.804	3101.7625	61.9585	2.03824	3128.198	88.394	2.907885	3114.002	74.1975	2.440865	3127.585	87.7605	2.88704469
1000350	2966.598	3006.789	40.191	1.354784	3096.014	129.416	4.362438	3103.892	137.2935	4.627978	3081.622	115.024	3.87730323
1000365	2995.228	2929.491	-65.7365	-2.19471	3059.958	64.73	2.161105	3088.871	93.6435	3.126424	3100.567	105.339	3.51689479
1000366	2938.287	2970.4515	32.165	1.094686	3054.314	116.0275	3.948815	3003.752	65.465	2.227999	2991.328	53.0415	1.80518476

T1 changes of BCCAo animals after 3 hours of surgery representing the *% signal enhancement of Gd-DOTA = (Mean grey value after Gd-DOTA injection (T1post) – Mean grey value before Gd-DOTA injection (T1pre))* 100 / (Mean grey value before injection (T1pre))*.

Corpus callosum														
GROUP 7 days	T1pre	T1post0	T1post0-T1pre	T1-0 change	T1post5	T1post5-T1pre	T1-5 change	T1post10	T1post10-T1pre	T1-10 change	T1post15	T1post15-T1pre	T1-15 change
1000353	3849.924	3430.162	-419.762	-10.9031	3626.942	-222.982	-5.79185	4203.71	353.786	9.189428	3715.072	-134.852	-3.5027185
1000355	3879.383	3998.219	118.836	3.063271	4035.076	155.693	4.013344	4043.721	164.338	4.236189	4062.773	183.39	4.72729813
1000358	3963.359	4131.69	168.331	4.24718	4139.219	175.86	4.437145	4164.381	201.022	5.072011	4173.828	210.469	5.31036931
1000359	4130.606	4136.523	5.917	0.143248	4234.559	103.953	2.516653	4243.611	113.005	2.735797	4799.905	669.299	16.2034094
1000360	3651.21	3691.895	40.685	1.114288	3781.901	130.691	3.579389	3767.088	115.878	3.173688	3772.8	121.59	3.33012892
1000363	3913.644	4112.425	198.781	5.079179	4188.492	274.848	7.022816	4151.886	238.242	6.087472	4196.365	282.721	7.22398358

Caudatoputamen													
GROUP 7 days	T1pre	T1post0	T1post0-T1pre	T1-0 change	T1post5	T1post5-T1pre	T1-5 change	T1post10	T1post10-T1pre	T1-10 change	T1post15	T1post15-T1pre	T1-15 change
1000353	3401.765	3118.5845	-283.181	-8.32452	3768.297	366.532	10.77476	4047.312	645.5465	18.97681	3400.908	-0.8595	-0.0252663
1000355	3554.185	3730.593	176.4085	4.963403	3781.456	227.2715	6.394477	3528.374	-25.8105	-0.7262	3784.63	230.4455	6.48377989
1000358	3724.58	3893.171	168.591	4.526443	3959.346	234.766	6.303154	3719.482	-5.098	-0.13687	3961.16	236.58	6.35185712
1000359	3915.148	3988.52	73.3725	1.874067	4116.049	200.9015	5.13139	3581.622	-333.526	-8.51886	4584.966	669.818	17.108372
1000360	3398.08	3547.8475	149.768	4.407431	3612.06	213.9805	6.297101	3342.315	-55.7645	-1.64106	3627.426	229.3465	6.74929765
1000363	3504.316	3636.57	132.254	3.774032	3865.062	160.7455	4.587072	3520.724	16.408	0.468223	3691.944	187.6275	5.35418324

External capsule													
GROUP 7 days	T1pre	T1post0	T1post0-T1pre	T1-0 change	T1post5	T1post5-T1pre	T1-5 change	T1post10	T1post10-T1pre	T1-10 change	T1post15	T1post15-T1pre	T1-15 change
1000353	3376.876	3144.636	-232.24	-6.87736	3290.436	-86.4405	-2.55978	3779.497	402.6205	11.92287	3373.575	-3.3015	-0.0977679
1000355	3366.566	3453.716	87.15	2.588691	3521.035	154.469	4.588325	3549.141	182.5745	5.423167	3584.885	218.319	6.48491668
1000358	3722.281	3830.2075	107.9265	2.899472	3883.549	161.2675	4.332491	3922.801	200.52	5.387019	3937.942	215.661	5.79378612
1000359	3859.62	3910.9235	51.3035	1.329237	3996.593	136.973	3.548873	4017.012	157.3915	4.077901	4428.71	569.09	14.7447158
1000360	3460.496	3552.6955	92.1995	2.664343	3662.664	202.168	5.842168	3655.573	195.0765	5.637241	3664.371	203.8745	5.89148203
1000363	3492.334	3614.026	121.6925	3.484561	3672.33	179.996	5.154032	3700.875	208.5415	5.971409	3690.098	197.764	5.66280397

Internal capsule													
GROUP 7 days	T1pre	T1post0	T1post0-T1pre	T1-0 change	T1post5	T1post5-T1pre	T1-5 change	T1post10	T1post10-T1pre	T1-10 change	T1post15	T1post15-T1pre	T1-15 change
1000353	2880.768	2601.754	-279.014	-9.6854	2690.423	-190.346	-6.60746	3141.872	261.104	9.063694	2757.476	-123.292	-4.2798309
1000355	2774.33	2861.838	87.5085	3.154222	2874.142	99.8125	3.597716	2893.857	119.5275	4.308338	2910.87	136.5405	4.92156754
1000358	2973.656	3002.1005	28.4445	0.95655	3028.304	54.648	1.837738	3080.61	106.9535	3.5967	3098.706	125.0495	4.20524432
1000359	3113.865	3087.0835	-26.7815	-0.86007	3186.781	72.916	2.341656	3182.115	68.25	2.19181	3800.582	686.7165	22.0535091
1000360	2769.391	2841.1675	71.777	2.591798	2825.94	56.5495	2.041947	2859.259	89.8685	3.245064	2865.821	96.4305	3.48201166
1000363	2762.703	2844.3165	81.6135	2.954118	2870.198	107.4945	3.890918	2835.165	72.462	2.622866	2861.669	98.9655	3.5821983

T1 changes of sham animals after 7 days of surgery representing the *% signal enhancement of Gd-DOTA = (Mean grey value after Gd-DOTA injection (T1post) – Mean grey value before Gd-DOTA injection (T1pre))* 100 / (Mean grey value before injection (T1pre))*.

Corpus callosum															
GROUP 7 days	T1pre	T1post0			T1post5			T1post10			T1post15				
			T1post0-T1pre	T1-0 change		T1post5-T1pre	T1-5 change		T1post10-T1pre	T1-10 change		T1post15-T1pre	T1-15 change
1000354	3973.184	3972.62	-0.564	-0.0142	4014.806	41.622	1.047573	4043.465	70.281	1.768884	4090.749	117.565	2.95896188
1000356	3502.135	3504.393	2.258	0.064475	3587.019	84.884	2.423779	3571.558	69.423	1.982305	3597.275	95.14	2.716628571
1000357	3683.963	3915.387	231.424	6.281931	3956.373	272.41	7.394483	3938.091	254.128	6.898223	3894.537	210.574	5.715964031
1000361	3626.579	3790.926	164.347	4.531736	3843.509	216.93	5.98167	3885.973	259.394	7.152581	3929.636	303.057	8.356553104
1000362	3269.721	3446.22	176.499	5.397983	3472.587	202.866	6.204383	3533.193	263.472	8.057935	3546.188	276.467	8.455369739
1000364	3534.452	3671.983	137.531	3.891155	3688.456	154.004	4.357224	3751.842	217.39	6.1506	3768.185	233.733	6.612991208

Caudatoputamen													
GROUP 7 days	T1pre	T1post0			T1post5			T1post10			T1post15		
			T1post0-T1pre	T1-0 change		T1post5-T1pre	T1-5 change		T1post10-T1pre	T1-10 change		T1post15-T1pre	T1-15 change
1000354	3785.903	3878.5835	92.6805	2.448042	3978.861	190.9575	5.043909	4047.312	261.4085	6.904786	4086.921	301.018	7.951022517
1000356	3336.922	3378.9325	42.011	1.258975	3500.527	163.605	4.902872	3528.374	191.4525	5.737399	3564.83	227.9085	6.829902951
1000357	3447.107	3652.709	205.602	5.96448	3730.073	282.9655	8.208782	3719.482	272.375	7.901553	3684.208	237.1005	6.878246019
1000361	3351.764	3513.9015	162.1375	4.837378	3571.921	220.157	6.568392	3581.622	229.8575	6.857807	3611.869	260.1045	7.760227152
1000362	3080.161	3246.809	166.6485	5.410384	3275.995	195.8345	6.357932	3342.315	262.1545	8.511066	3369.261	289.1005	9.385890768
1000364	3332.593	3506.9525	174.36	5.231963	3528.143	195.55	5.867804	3520.724	188.1315	5.6452	3564.206	231.6135	6.949949626

External capsule													
GROUP 7 days	T1pre	T1post0			T1post5			T1post10			T1post15		
			T1post0-T1pre	T1-0 change		T1post5-T1pre	T1-5 change		T1post10-T1pre	T1-10 change		T1post15-T1pre	T1-15 change
1000354	3693.01	3770.4665	77.4565	2.097381	3856.024	163.014	4.414123	3891.894	198.8835	5.385404	3928.439	235.4285	6.374975968
1000356	3415.317	3448.1315	32.815	0.960819	3558.634	143.317	4.196302	3621.702	206.3855	6.042939	3666.748	251.431	7.361865291
1000357	3480.158	3758.1	277.942	7.986476	3703.323	223.165	6.412496	3701.484	221.3255	6.359639	3647.569	167.411	4.810442514
1000361	3417.9	3550.8115	132.9115	3.888689	3620.241	202.341	5.920039	3653.047	235.1465	6.879853	3687.633	269.7325	7.891761023
1000362	3206.677	3386.5095	179.833	5.608081	3476.914	270.237	8.427323	3535.914	329.2375	10.26725	3530.504	323.827	10.09852413
1000364	3311.656	3453.429	141.773	4.28103	3521.587	209.931	6.339155	3524.341	212.6845	6.422301	3514.397	202.7405	6.122027771

Internal capsule													
GROUP 7 days	T1pre	T1post0			T1post5			T1post10			T1post15		
			T1post0-T1pre	T1-0 change		T1post5-T1pre	T1-5 change		T1post10-T1pre	T1-10 change		T1post15-T1pre	T1-15 change
1000354	3112.669	3113.5835	0.915	0.029396	3221.208	108.539	3.487008	3230.002	117.333	3.769531	3276.248	163.579	5.255265699
1000356	2848.625	2857.616	8.991	0.315626	2934.948	86.323	3.030339	2933.889	85.264	2.993163	2984.992	136.3665	4.787099039
1000357	2779.956	2958.343	178.3875	6.416919	2931.979	152.023	5.468541	2959.556	179.6	6.460535	2912.155	132.1995	4.755453819
1000361	2722.024	2791.6655	69.6415	2.558445	2787.232	65.208	2.39557	2857.917	135.893	4.992351	2821.263	99.239	3.645779758
1000362	2607.389	2662.2235	54.835	2.103062	2701.788	94.3995	3.620462	2776.816	169.4275	6.497977	2754.868	147.479	5.656195845
1000364	2575.491	2600.88	25.3895	0.985812	2670.43	94.9395	3.686269	2657.613	82.1225	3.188616	2667.08	91.5895	3.556196383

T1 changes of BCCAo animals after 7 days of surgery representing the *% signal enhancement of Gd-DOTA = (Mean grey value after Gd-DOTA injection (T1post) – Mean grey value before Gd-DOTA injection (T1pre))* 100 / (Mean grey value before injection (T1pre))*.

Appendix D: T2 and T1 images acquisitions with time

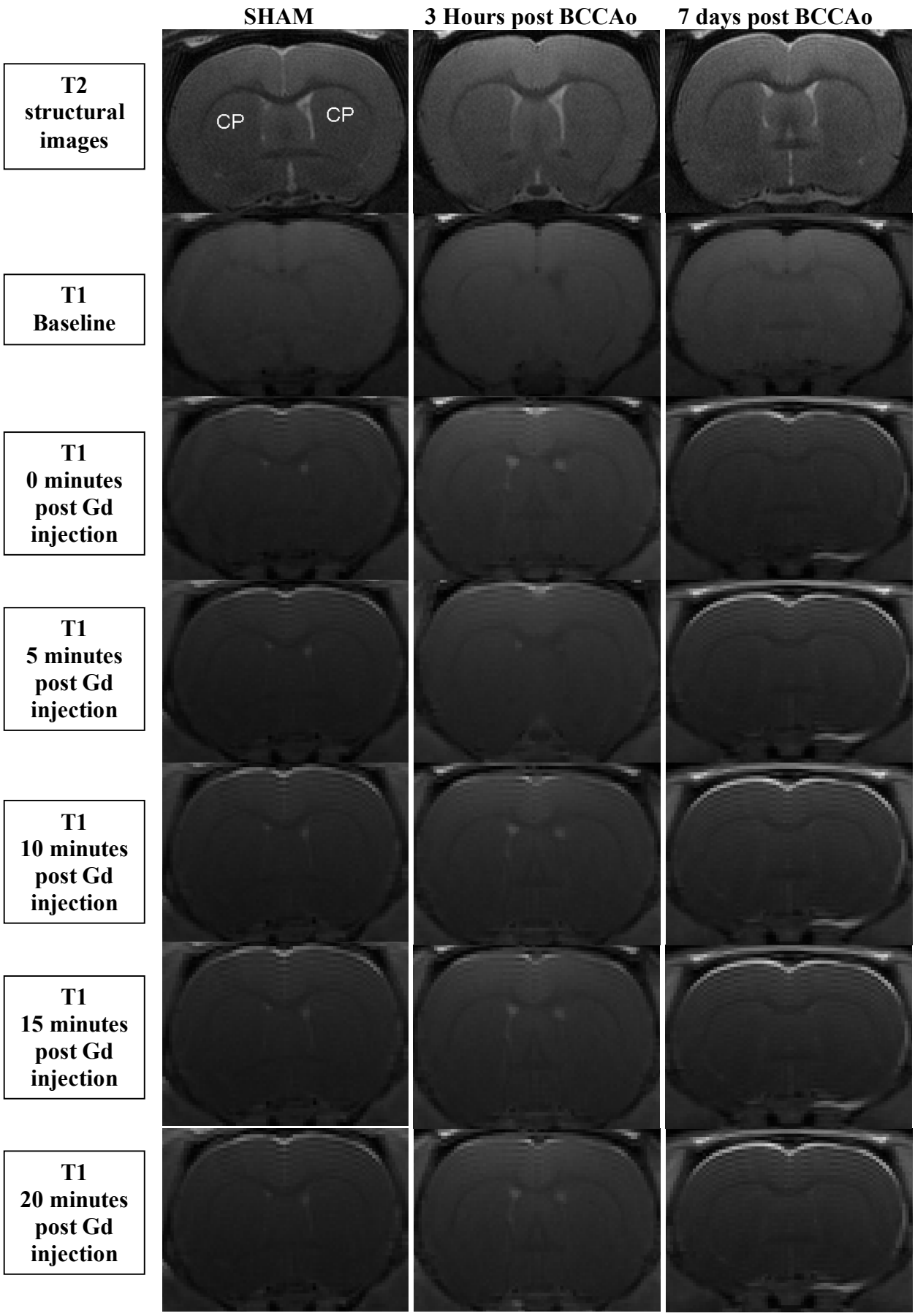

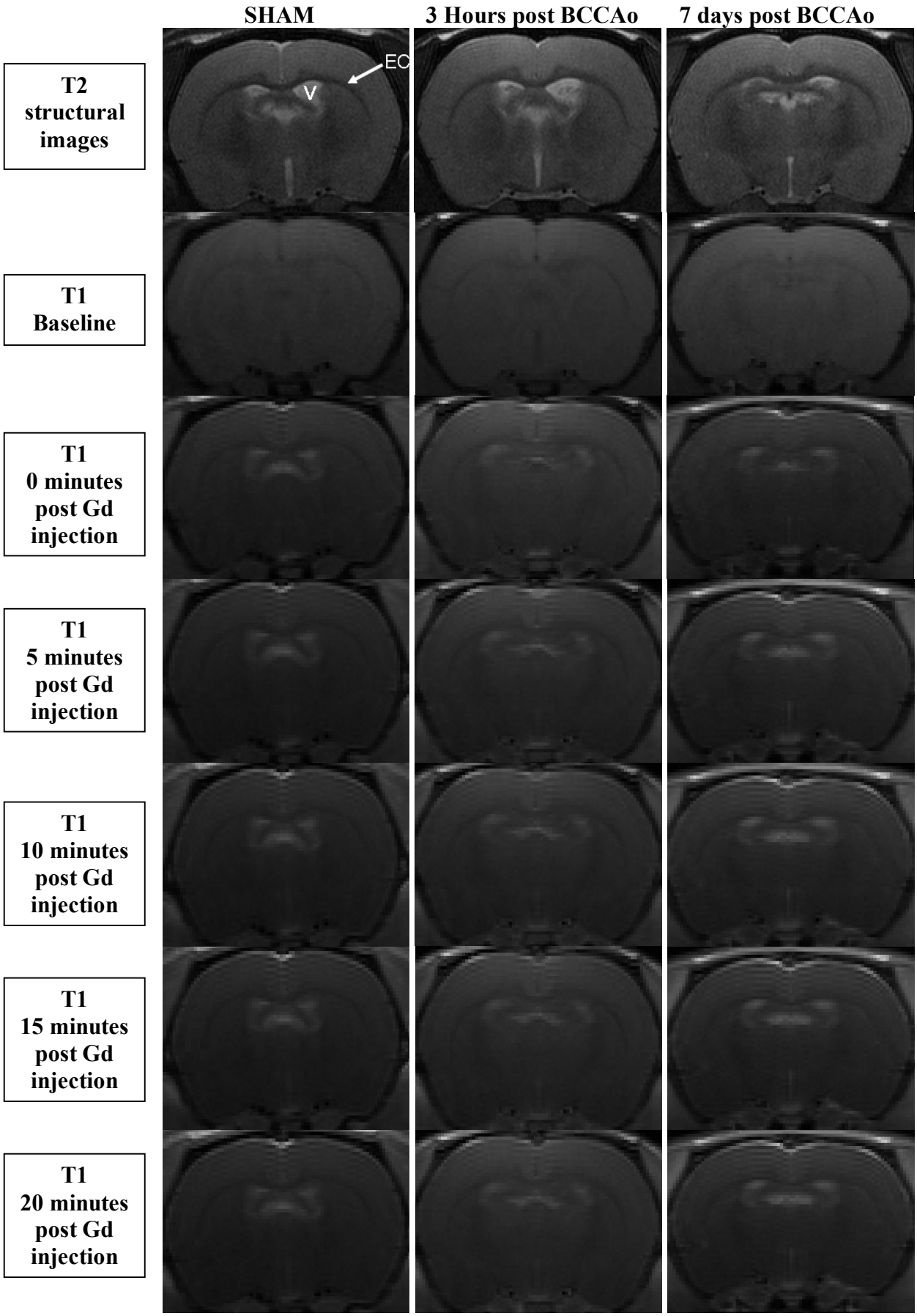

CP: Caudatoputamen; EC: External Capsule; V: Ventricules

Appendix E: Full runs of Western Blots

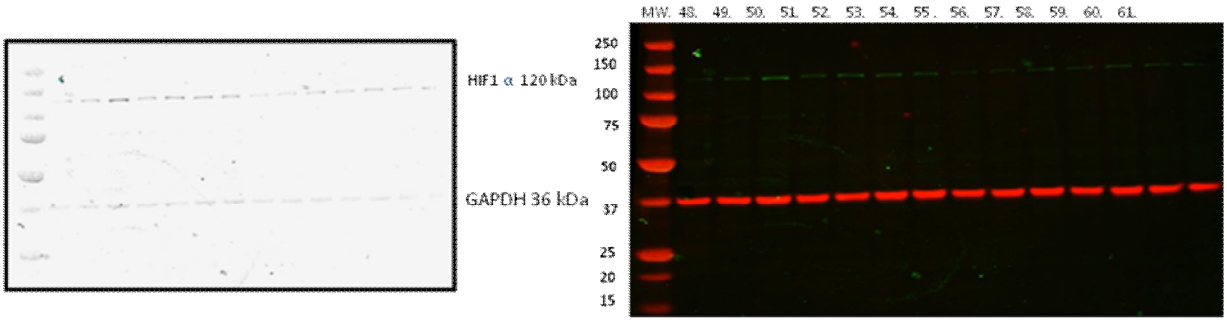

Levels of HIF-1α in the Corpus Callosum (full run) 7 days post BCCAo

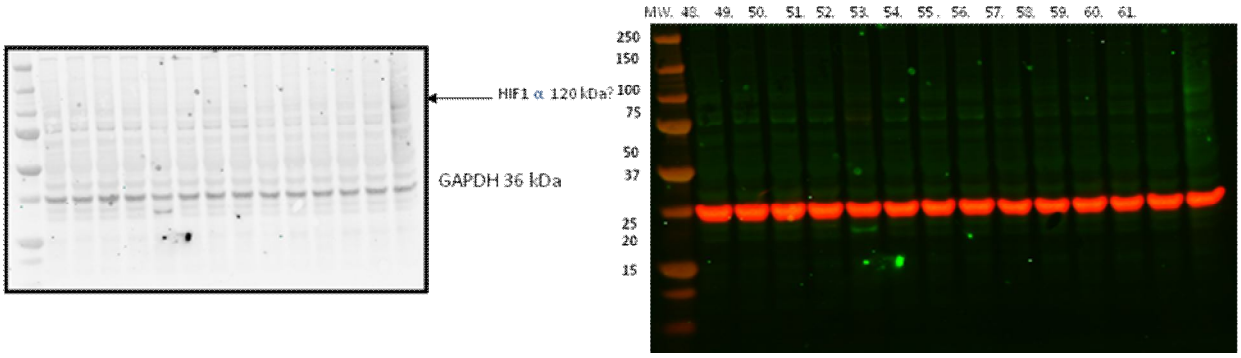

Levels of HIF-1α in the Cortex (full run) 7 days post BCCAo

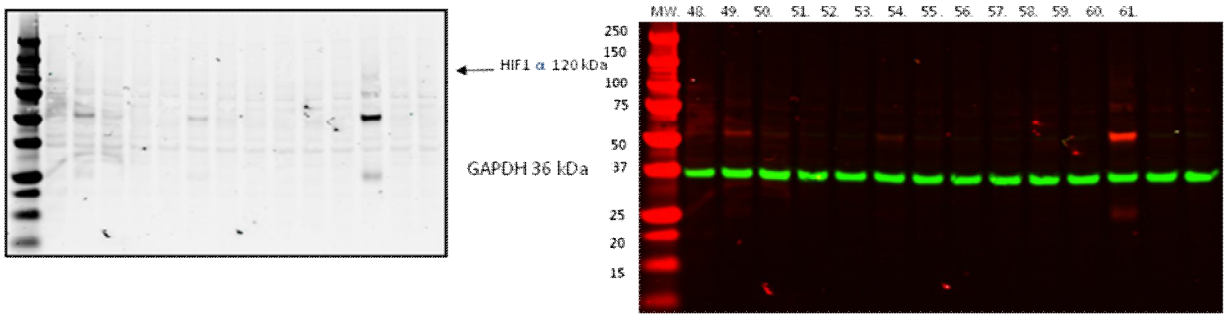

Levels of HIF-1α in the Caudatoputamen (full run) 7 days post BCCAo

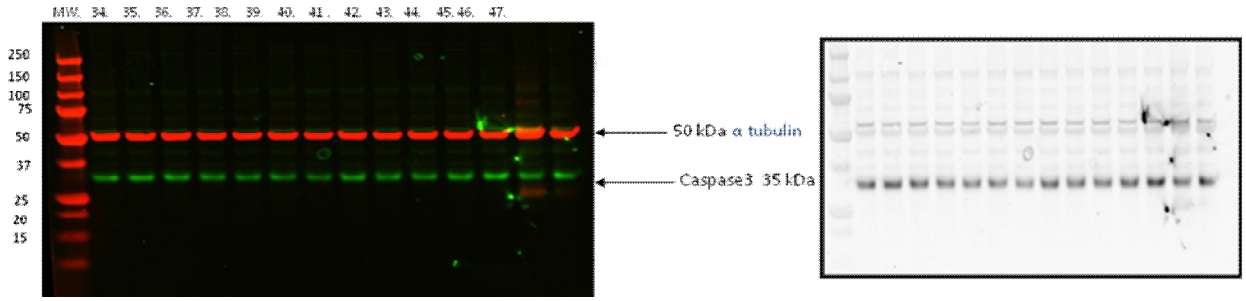

Levels of Caspase-3 in the Cortex (full run) 3 hours post BCCAo

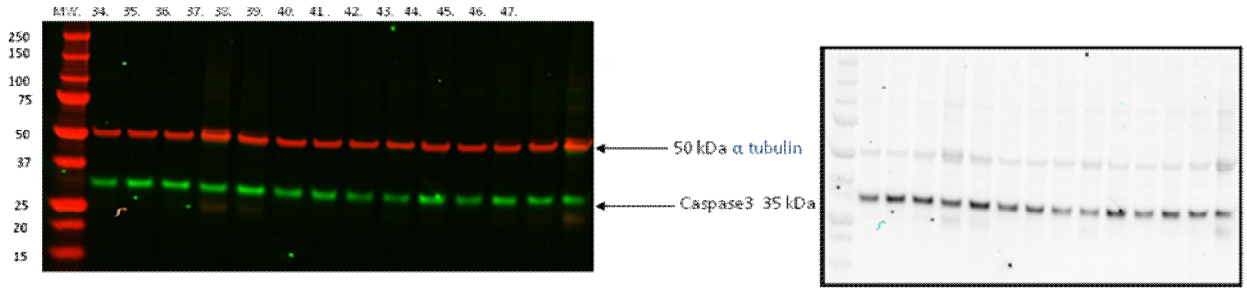

Levels of Caspase-3 in the Corpus Callosum (full run) 3 hours post BCCAo

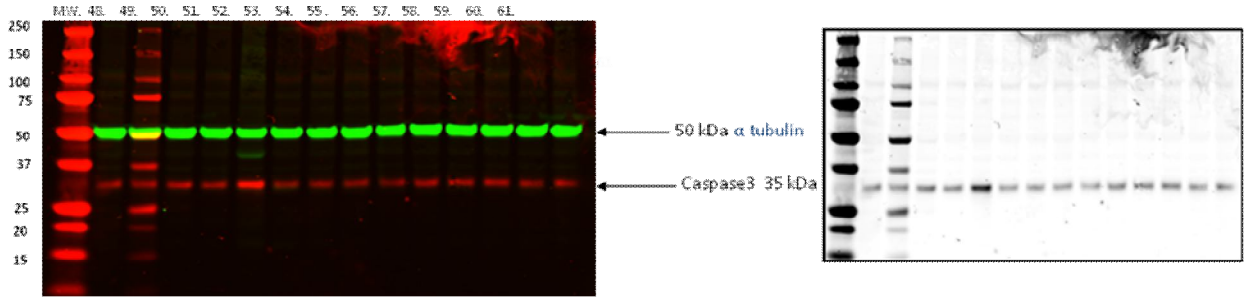

Levels of Caspase-3 in the Cortex (full run) 7 days post BCCAo

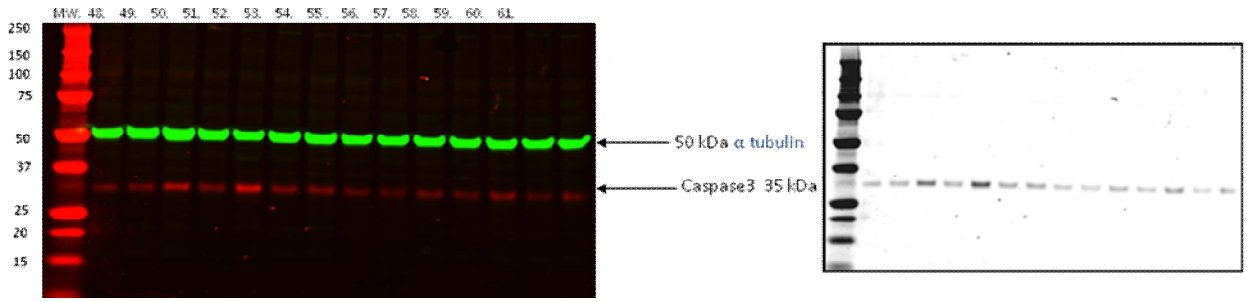

Levels of Caspase-3 in the Corpus Callosum (full run) 7 days post BCCAo

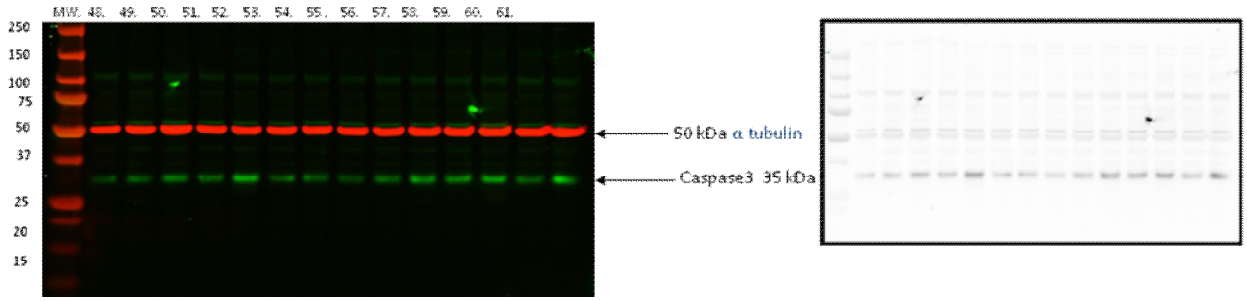

Levels of Caspase-3 in the Caudatoputamen (full run) 7 days post BCCAo

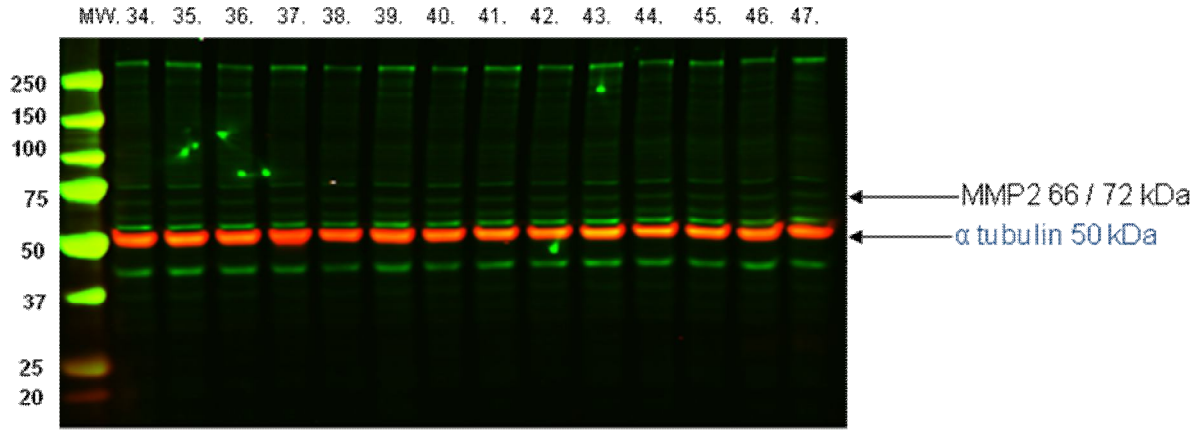

Levels of MMP-2 in the Cortex (full run) 3 hours post BCCAo

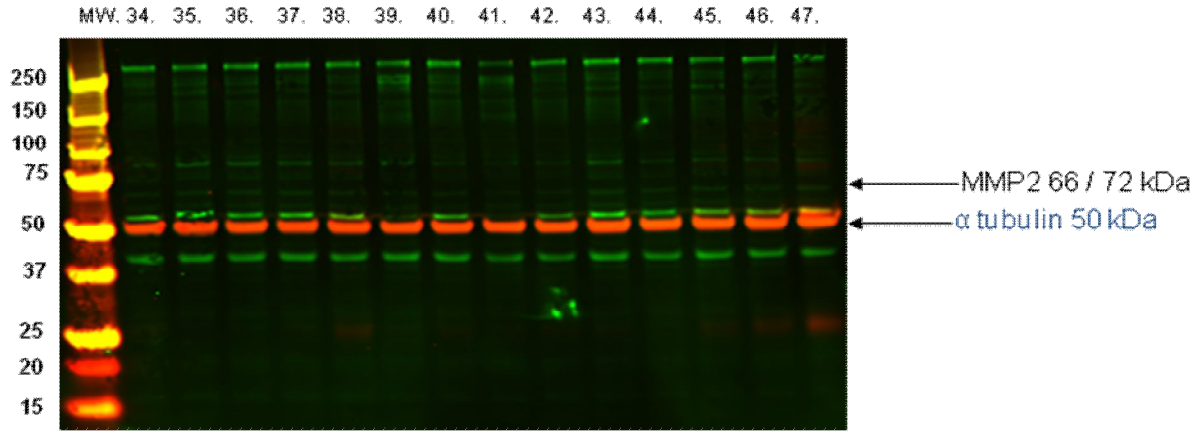

Levels of MMP-2 in the Corpus Callosum (full run) 3 hours post BCCAo

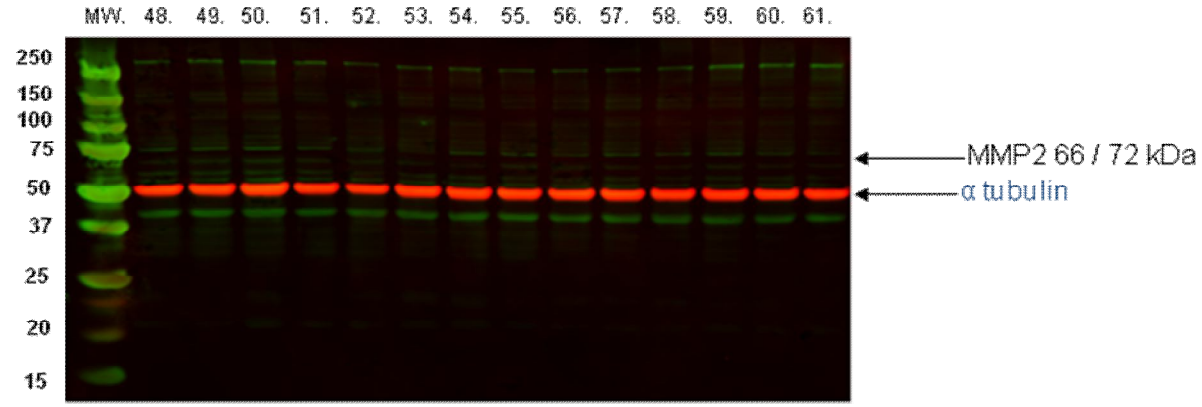

Levels of MMP-2 in the Cortex (full run) 7 days post BCCAo

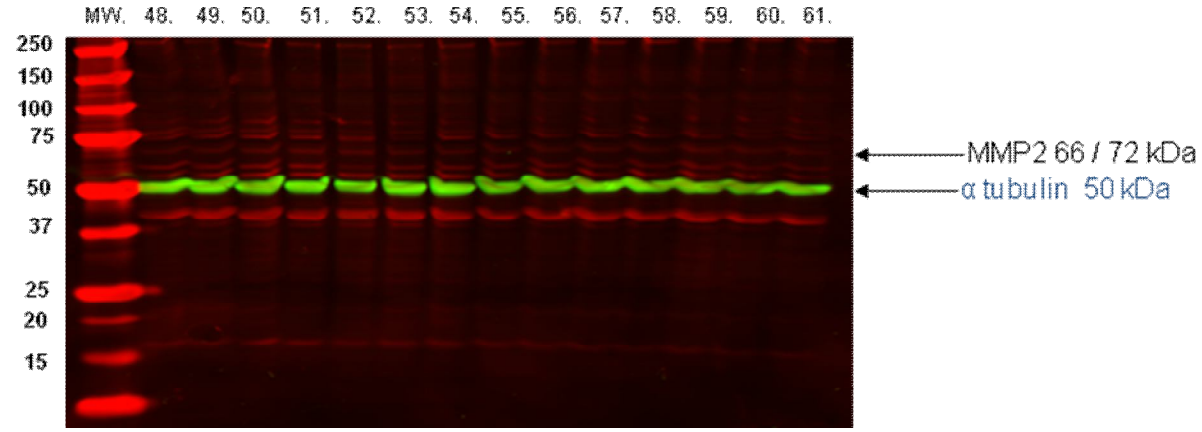

Levels of MMP-2 in the Corpus Callosum (full run) 7 days post BCCAo

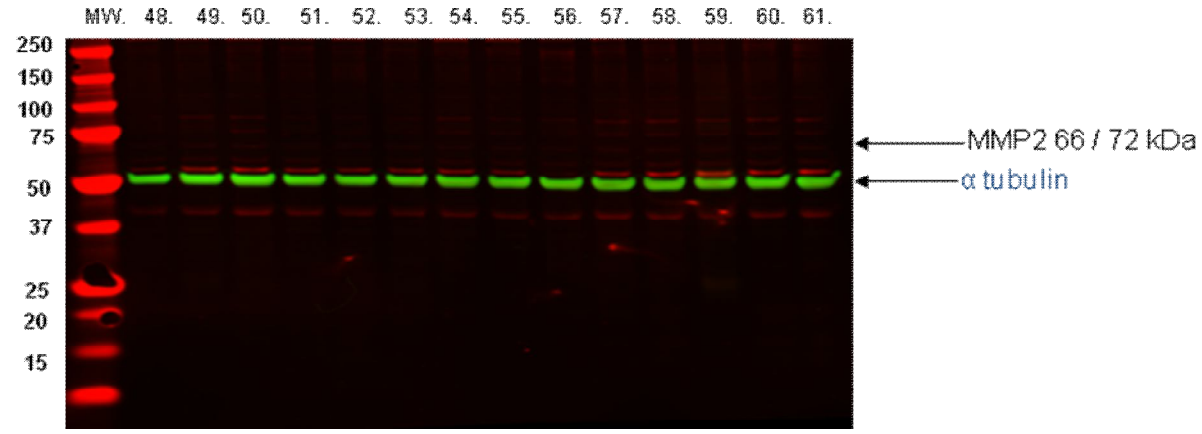

Levels of MMP-2 in the Caudatoputamen (full run) 7 days post BCCAo

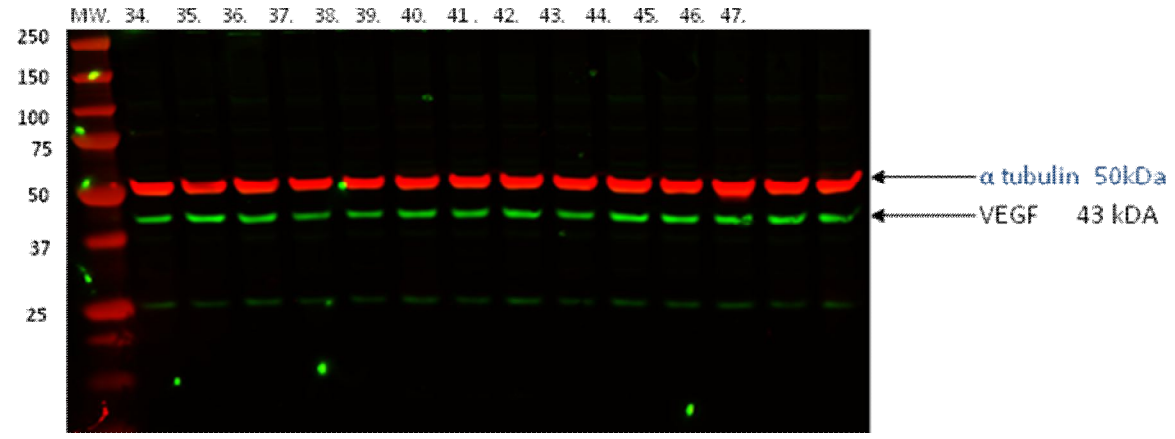

Levels of VEGF in the Cortex (full run) 3 hours post BCCAo

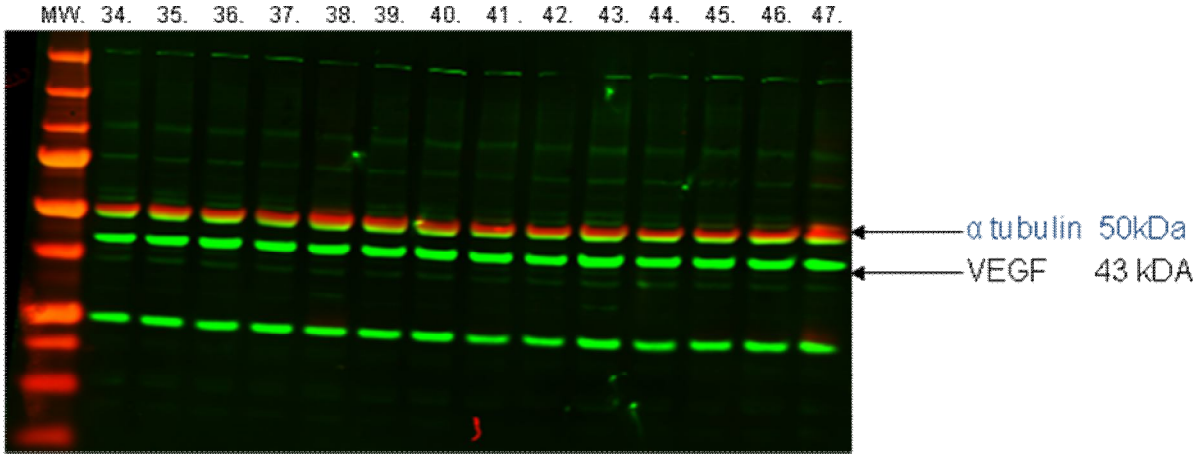

Levels of VEGF in the Corpus Callosum (full run) 3 hours post BCCAo

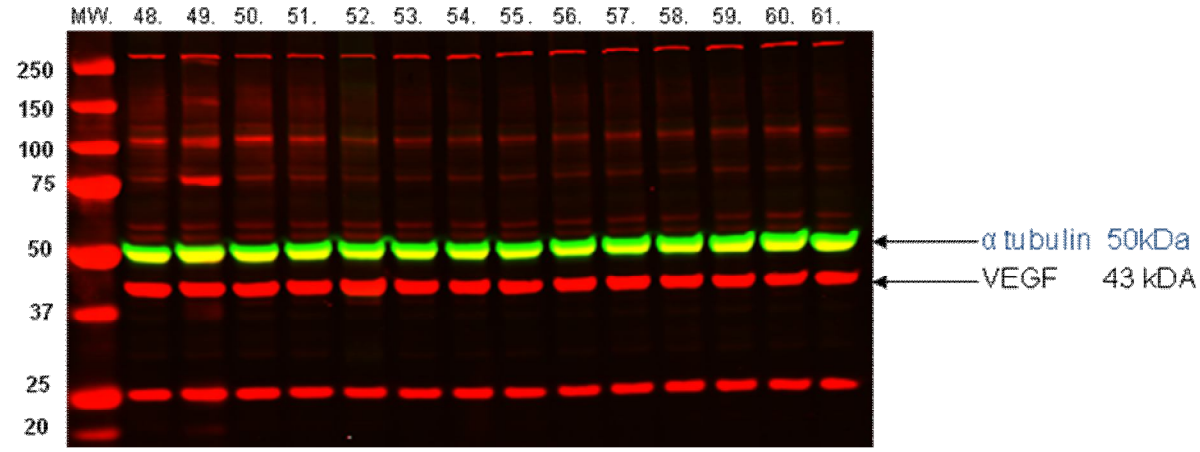

Levels of VEGF in the Cortex (full run) 7 days post BCCAo

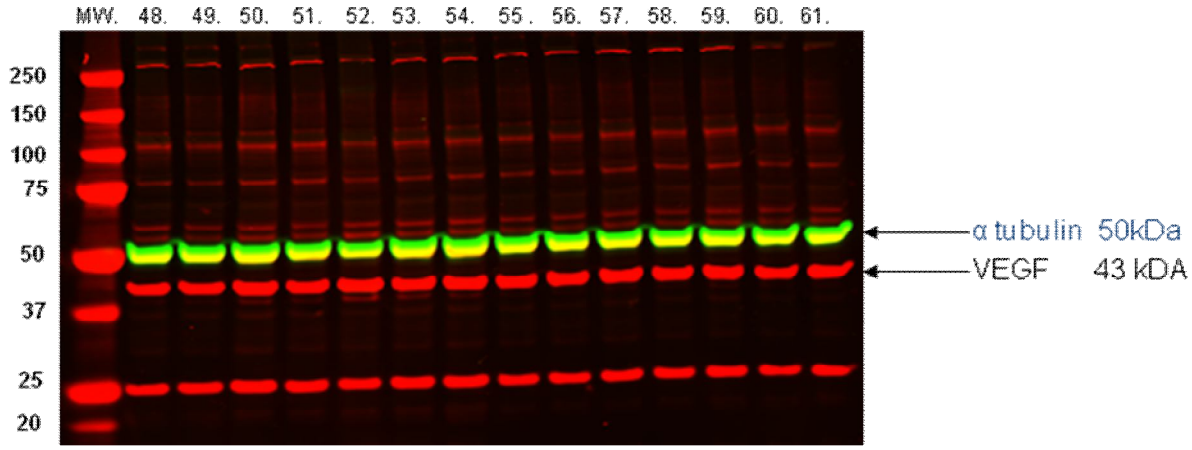

Levels of VEGF in the Corpus Callosum (full run) 7 days post BCCAo

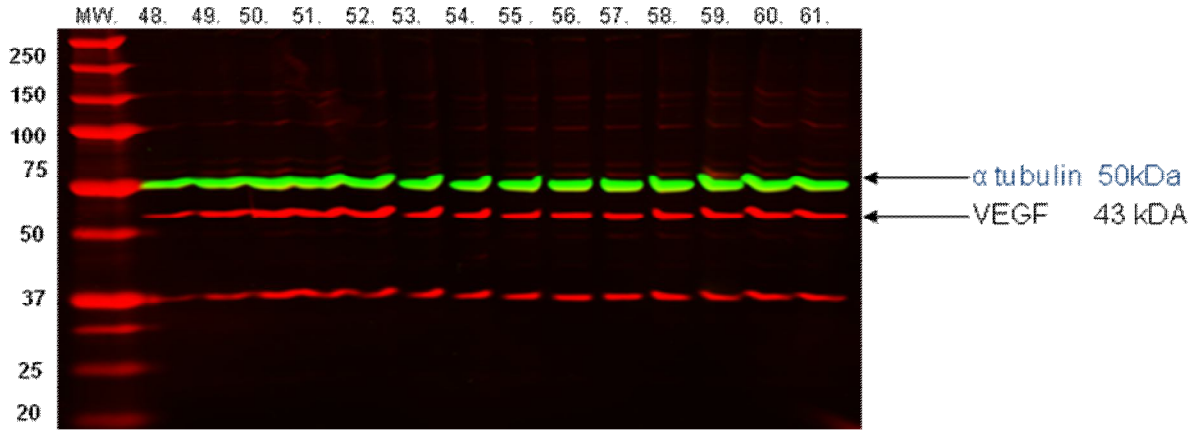

Levels of VEGF in the Caudatoputamen (full run) 7 days post BCCAo

Appendix F: Publications

Papers

Holland, P. R., Bastin, M. E., Jansen, M. A., Merrifield, G. D., Coltman, R., Scott, F., Nowers, H., **Khallout, K.**, Marshall, I., Wardlaw, J. M., Deary, I. J., McCulloch, J., Horsburgh, K. (2010). MRI is a sensitive marker of subtle white matter pathology in hypoperfused mice. Neurobiology of Aging.

Khallout K, Jansen M.A., Merrifield G.D., Bastin M.E, Launay S., Herrmann A., Holland P.R., Marshall I., Horsburgh K., McCulloch J. (2012).
Cerebral hypoperfusion causes white matter injury which precedes blood-brain barrier dysfunction with time. *In preparation for Stroke Journal*

Abstracts

Khallout K, Jansen M.A., Merrifield G.D., Bastin M.E, Launay S., Herrmann A., Holland P.R., Marshall I., Horsburgh K., McCulloch J. (2011).
Cerebral hypoperfusion causes white matter injury leading to blood-brain barrier dysfunction with time. International Congress of Vascular Dementia, Riga, Latvia, October. **Received 2nd Poster Prize**

Holland P.R., Bastin M.E., Jansen M.A., Merrifield G.D. , Coltman R.B., Scott F., **Khallout K.**, Nowers H., Marshall I., Wardlaw J. M., Deary I. J., McCulloch J. and Horsburgh K. (2011). Chronic cerebral hyoperfusion results in selective disruption of white matter; an in vivo MRI study with implications for post spreading depression hypoperfusion. International Headache Congress, Germany, June.

Khallout K, Jansen M.A., Merrifield G.D., Bastin M.E, Launay S., Herrmann A., Holland P.R., Marshall I., Horsburgh K., McCulloch J. (2011). Cerebral hypoperfusion causes white matter injury leading to blood-brain barrier dysfunction with time. Neuroscience Day, Edinburgh, UK, March.

Launay S, Deighton RF, **Khallout K**, Deary IJ, Horsburgh K, McCulloch J. (2010). Proteomic analysis of cell death in a rat hypoperfusion model (BCCAo). First Conference of the European Research Institute for Integrated Cellular Pathology (ERI-ICP), Institut Pasteur, Paris, France, April

Bastin M, Jansen MA, Holland H, Merrifield GD, **Khallout K**, Horsburgh K, Wardlaw JM, Deary, Marshall I, McCulloch J. (2010). Quantitative tractography and white matter integrity in the rat brain.

Launay S, Deighton RF, **Khallout K**, Deary IJ, Horsburgh K, McCulloch J. (2009) Proteomic analysis of cell death in a rat hypoperfusion model (BCCAO). Research into Ageing Grantholders' Conference. Birmingham, UK, September.
2nd Poster Prize

Holland, P. R., Bastin, M. E., Coltman, R., **Khallout, K**., Scott, F., Dingwall, T., Jansen, M. A., Merrifield, G. D., Marshall, I., McCulloch, J., Horsburgh, K. (2009). Imaging White Matter Pathology in a Mouse Model of Chronic Cerebral Hypoperfusion. Research into Ageing Grantholders' Conference. Birmingham, UK, September.